

UNIVERSITY OF MISSOURI, COLUMBIA
MISSOURI UNIVERSITY RESEARCH REACTOR
LICENSE NO. R-103
DOCKET NO. 50-186

LOW-ENRICHED URANIUM CONVERSION
PRELIMINARY SAFETY ANALYSIS REPORT
FOR THE
UNIVERSITY OF MISSOURI RESEARCH REACTOR
AUGUST 18, 2017

REDACTED VERSION*

SECURITY-RELATED INFORMATION REMOVED

*REDACTED TEXT AND FIGURES BLACKED OUT OR DENOTED BY BRACKETS

UNIVERSITY of MISSOURI

RESEARCH REACTOR CENTER

August 18, 2017

U.S. Nuclear Regulatory Commission
Attention: Document Control Desk
Mail Station P1-37
Washington, DC 20555-0001

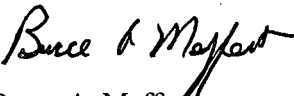
REFERENCE: Docket No. 50-186
University of Missouri-Columbia Research Reactor
Renewed Facility Operating License No. R-103

SUBJECT: Submission of a Highly Enriched to Low-Enriched Uranium Conversion Preliminary
Safety Analysis Report for the University of Missouri-Columbia Research Reactor

The University of Missouri Research Reactor (MURR) is submitting for review and comment the attached Preliminary Safety Analysis Report (PSAR) for the conversion of MURR from Highly Enriched Uranium (HEU) to Low-Enriched Uranium (LEU) fuel. Please note that MURR is not prepared to convert at this time. The proposed replacement LEU reactor fuel has not been qualified by the U.S. Department of Energy (DOE) or approved by the U.S. Nuclear Regulatory Commission (NRC) for use as a reactor fuel. This PSAR submittal follows the guidance provided in Chapter 18 of NUREG-1537, "Guidelines for Preparing and Reviewing Applications for the Licensing of Non-Power Reactors," – Part 1, "Format and Content," and Part 2, "Standard Review Plan and Acceptance Criteria." Included in the conversion PSAR is a description of the reactor, expected changes to the facility caused by fuel conversion, steady-state neutronic and thermal-hydraulic analyses, and detailed safety and accident analyses of the proposed MURR LEU core.

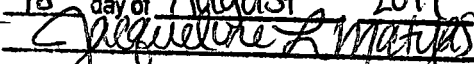
If there are any questions regarding this submittal, please contact me at (573) 882-5118 or MeffertB@missouri.edu. I declare under penalty of perjury that the foregoing is true and correct.

Sincerely,


Bruce A. Meffert
Reactor Manager

ENDORSEMENT:
Reviewed and Approved


Ralph A. Butler, P.E.
Director

State of Missouri
County of Boone
Subscribed and sworn to before me this
18 day of August, 2017

JACQUELINE L. MATYAS, Notary Public
My Commission Expires: March 26, 2019



JACQUELINE L. MATYAS
My Commission Expires
March 26, 2019
Howard County
Commission #15634309



xc: Reactor Advisory Committee
Reactor Safety Subcommittee
Dr. Mark McIntosh, Vice Chancellor for Research, Graduate Studies and Economic Development
Mr. Alexander Adams, U.S. Nuclear Regulatory Commission
Mr. Geoffrey Wertz, U.S. Nuclear Regulatory Commission
Mr. Johnny Eads, U.S. Nuclear Regulatory Commission

Attachments:

1. Low-Enriched Uranium Conversion Preliminary Safety Analysis Report for the University of Missouri Research Reactor



Low-Enriched Uranium Conversion Preliminary Safety Analysis Report for the University of Missouri Research Reactor

Prepared by:

Argonne National Laboratory – John Stillman, Earl Feldman, David Jaluvka, Cezary Bojanowski, Adrian Tentner, Thad Heltemes, Benoit Dionne, Mohammad Kalimullah, John Stevens, and Erik Wilson

University of Missouri Research Reactor – Wilson Cowherd, Benjamin Rickman, J. Charles McKibben, Kiratadas Kutikkad, Nickie Peters, and Les Foyto

**University of Missouri Research Reactor
1513 Research Park Drive
Columbia, Missouri 65211**

Preface

The University of Missouri Research Reactor (MURR®) is a multi-disciplinary research and education facility providing a broad range of analytical, materials science and irradiation services to the research community and the commercial sector. Scientific programs include research in archaeometry, epidemiology, health physics, human and animal nutrition, nuclear medicine, radiation effects, radioisotope studies, radiotherapy, boron neutron capture therapy, and nuclear engineering; and research techniques including neutron activation analysis, neutron and gamma-ray scattering, and neutron interferometry. The heart of this facility is a pressurized, reflected, open pool-type, light water moderated and cooled, heterogeneous reactor designed for operation at a maximum steady-state power level of 10 Megawatts thermal (MW_{th}) – the highest-powered university-operated research reactor in the United States. It accommodates an experimental position (flux trap) through the center of the core, which is external to the reactor pressure vessel. A flux trap-type reactor is characterized by a thin fuel region adjacent to a good moderator, which thermalizes the neutrons and causes the thermal flux to peak in a region (center test hole) accessible for experiments. It also provides relatively high beam tube currents resulting from the high power density.

Because of its compact core design (33 liters), which requires a very high loading density of ^{235}U , MURR could not perform its mission with any previously qualified low-enriched uranium (LEU) fuels. However, in 2006 with the prospect of the National Nuclear Security Administration (NNSA) Global Threat Reduction Initiative Reactor Conversion Program validating the performance of U-10Mo monolithic LEU foil fuels, MURR began actively collaborating with what is currently the NNSA Material Management and Minimization Office's Reactor Conversion Program, along with four other U.S. high-performance research and test reactors that use highly enriched uranium (HEU) fuel, to find a suitable LEU fuel replacement. It was concluded that the proposed LEU fuel assembly design, in conjunction with an increase in power level from 10 to 12 MW_{th} , will (1) maintain safety margins during steady-state and transient conditions, (2) allow operating fuel cycle lengths to be maintained for efficient and effective use of the facility, and (3) preserve an acceptable level and spectrum of key neutron fluxes to meet the scientific mission of the facility.

This report is a preliminary version of the Safety Analysis Report (SAR) that would be submitted to the U.S. Nuclear Regulatory Commission (NRC) for approval prior to conversion. The report follows the recommended format and content of NUREG-1537, "Guidelines for Preparing and Reviewing Applications for the Licensing of Non-Power Reactors," Chapter 18, "Highly Enriched to Low-Enriched Uranium Conversions." The emphasis in any conversion SAR is to explain the differences between the LEU and HEU cores and to show the acceptability of the new design; there is no need to repeat information regarding the current reactor that will not change upon conversion. Hence, as seen in the report, the bulk of the SAR is devoted to Chapter 4, Reactor Description, and Chapter 13, Safety Analysis.

Summary of Contents

(Detailed contents are given at the beginning of each chapter.)

Chapter

1.0	THE FACILITY	1-1
2.0	SITE CHARACTERISTICS	2-1
3.0	DESIGN OF STRUCTURES, SYSTEMS, AND COMPONENTS	3-1
4.0	REACTOR DESCRIPTION	4-1
5.0	REACTOR COOLANT SYSTEMS	5-1
6.0	ENGINEERED SAFETY FEATURES	6-1
7.0	INSTRUMENTATION AND CONTROL SYSTEMS	7-1
8.0	ELECTRICAL POWER SYSTEMS	8-1
9.0	AUXILIARY SYSTEMS	9-1
10.0	EXPERIMENTAL FACILITIES AND UTILIZATION	10-1
11.0	RADIATION PROTECTION PROGRAM AND WASTE MANAGEMENT	11-1
12.0	CONDUCT OF OPERATIONS	12-1
13.0	ACCIDENT ANALYSES	13-1
14.0	TECHNICAL SPECIFICATIONS	14-1
15.0	FINANCIAL QUALIFICATIONS	15-1
16.0	OTHER LICENSE CONSIDERATIONS	16-1
17.0	DECOMMISSIONING	17-1
	APPENDIX A.....	A-1
	APPENDIX B.....	B-1
	APPENDIX C.....	C-1

THIS PAGE INTENTIONALLY LEFT BLANK

CHAPTER 1

THE FACILITY

THIS PAGE INTENTIONALLY LEFT BLANK

TABLE OF CONTENTS

1.0	THE FACILITY.....	1-1
1.1	Introduction.....	1-1
1.2	General Description of the Facility.....	1-1
1.3	Comparison with Similar Facilities	1-1
1.4	Summary and Conclusions on Principal Safety Considerations.....	1-1
	1.4.1 Reactor	1-1
1.5	Summary of Operations	1-2
1.6	Compliance with the Nuclear Waste Policy Act of 1982	1-2
1.7	Facility Modifications and History	1-2

1.0 THE FACILITY

1.1 Introduction

No changes are expected for this section due to conversion.

1.2 General Description of the Facility

The low-enriched uranium (LEU) fueled University of Missouri Research Reactor (MURR) is planning to operate at 12.0 MW thermal, with a substantial safety margin as demonstrated in Chapters 4 and 13.

1.3 Comparison with Similar Facilities

The LEU fuel element remains of the Materials Test Reactor (MTR) plate-type fuel design. The LEU fuel element has been re-designed in the fuel plates from the MURR highly enriched uranium (HEU) fuel elements to allow for more uniform power peaking factors and to meet operational performance requirements. The LEU fuel element has 23 thinner fuel plates instead of the 24 HEU fuel plates. The side plates and end fitting geometry remain unchanged to be compatible with the existing support structure geometry.

The LEU fuel utilized will be monolithic U-Mo fuel with 10 wt. % molybdenum. This fuel is currently being qualified by the U.S. High Performance Research Reactor (USHPRR) program to demonstrate performance under conditions that are relevant to MURR and other reactors in the USHPRR program, including irradiation performance and flow tests. This section will be revised based on the irradiation and testing being conducted by the USHPRR Program. A summary of testing conducted for this fuel system thus far is found in Section 4.2.1.1.

1.4 Summary and Conclusions on Principal Safety Considerations

1.4.1 Reactor

Preliminary analysis of the LEU-fueled MURR core demonstrated that an up-rate of the core power level is needed to provide a neutron flux to experimental facilities equivalent to the HEU-fueled core operating at 10 MW (Section 4.5.4.1). Solely on the basis of experimental performance, the conversion of MURR using the proposed LEU fuel element is feasible at 12 MW. This power uprate provides a modest benefit to the experimental performance of the facility. Analyses have shown a substantial margin to safety for the LEU-fueled core under steady-state and accident conditions.

The average power density for the HEU core operating at 10 MW is 303 kW/l. For the LEU core operating at 12 MW, the average power density is 364 kW/l. The average heat flux in the HEU core at 10 MW is 1.75×10^5 BTU/ft²-h. For the LEU core at 12 MW, the average heat flux is 2.25×10^5 BTU/ft²-h.

The abnormal conditions or postulated accident events or categories analyzed in this preliminary Safety Analysis Report (SAR) include the following:

- (1) Maximum Hypothetical Accident (MHA);
- (2) Insertion of Excess Reactivity;
- (3) Loss of Primary Coolant;
- (4) Loss of Primary Coolant Flow;
- (5) Mishandling or Malfunction of Fuel;
- (6) Experiment Malfunction;
- (7) Loss of Electrical Power;
- (8) External Events; and
- (9) Mishandling or Malfunction of Equipment.

For the HEU core, the MHA is the failure of a fueled experiment that is loaded in the graphite reflector region with a maximum radioiodine inventory of 150 Curies. The radiological consequences of the fueled experiment failure do not change as a result of conversion. However, the LEU fuel handling accident results in a larger dose to members of the general public outside the exclusion zone, and will therefore be classified as the MHA for the LEU core. This accident is selected to postulate conditions which lead to consequences worse than those resulting from any other credible accident.

In all of the other proposed accident events or categories listed above, fuel and cladding temperatures remain at levels below those required to produce cladding failure, and thus, no release of fission products would occur. Chapter 13, Accident Analyses, contains a detailed discussion of each accident scenario listed above.

1.5 Summary of Operations

No changes to this section are expected due to conversion.

1.6 Compliance with the Nuclear Waste Policy Act of 1982

Contractual agreement with the U.S. Department of Energy (DOE) for fuel assistance and spent fuel return will be updated for the LEU fuel.

1.7 Facility Modifications and History

This section will be updated to incorporate all major facility modifications and any license amendments that have been completed and approved since the operating license renewal approved in 2017. There are currently no amendments since the January 4, 2017 license renewal that have been approved.

THIS PAGE INTENTIONALLY LEFT BLANK

CHAPTER 2

SITE CHARACTERISTICS

THIS PAGE INTENTIONALLY LEFT BLANK

2.0 SITE CHARACTERISTICS

This chapter describes the geography, demographics, meteorology, hydrology, and seismic characteristics of the MURR site. No changes to this chapter are expected as a result of conversion.

THIS PAGE INTENTIONALLY LEFT BLANK

CHAPTER 3

DESIGN OF STRUCTURES, SYSTEMS, AND COMPONENTS

THIS PAGE INTENTIONALLY LEFT BLANK

TABLE OF CONTENTS

3.0	DESIGN OF STRUCTURES, SYSTEMS, AND COMPONENTS.....	3-1
3.1	Conformance with NRC General Design Criteria	3-1
3.2	Meteorological Damage.....	3-1
3.3	Water Damage	3-1
3.4	Seismic Damage.....	3-1
3.5	Mechanical Systems and Components.....	3-1
	3.5.1 Fuel System.....	3-1
	3.5.2 Reactor Core Assembly Support Structure	3-2
	3.5.3 Anti-siphon System.....	3-2

3.0 DESIGN OF STRUCTURES, SYSTEMS, AND COMPONENTS

This chapter identifies and describes the principal architectural and engineering design criteria for the structures, systems, and components that are required to ensure reactor safety and the protection of the general public. None of these criteria are expected to change due to the fuel conversion.

3.1 Conformance with NRC General Design Criteria

No changes are expected to the NRC General Design Criteria that are applicable to the design, construction, and operation of the MURR facility. Only editorial revisions related to the power uprate from 10 to 12 MW are planned for this section.

The MURR is designed and licensed for operation at a maximum steady-state power level of 10 MW thermal with HEU fuel. For operation with LEU fuel, the maximum steady-state power level will be 12 MW. The fission product inventory is substantially less than that of conventional nuclear power plants for which the General Design Criteria were primarily developed. In addition, the MURR operates at relatively low temperatures and pressures. No active engineered safety features (ESFs) are required for reactor core protection after shutdown. A conservative upper limit of energy released for an entire year of operation would be about 3,270 Megawatt-Days (MWd) for HEU operation (average of 151 hours per week at 10 MW), and 3,925 MWd for LEU operation. These comparisons illustrate why the MURR is in a much lower risk category when reviewing for compliance with the General Design Criteria.

Neutronic analyses using already developed computer models will be performed for the final conversion analysis to ensure fuel storage of the new LEU monolithic fuel satisfies the criticality criteria.

3.2 Meteorological Damage

No changes to this section are expected due to conversion.

3.3 Water Damage

No changes to this section are expected due to conversion.

3.4 Seismic Damage

No changes to this section are expected due to conversion.

3.5 Mechanical Systems and Components

3.5.1 Fuel System

The LEU fuel utilized will be monolithic U-Mo fuel with 10 wt. % molybdenum. The fuel core is made by alloying uranium and molybdenum into a foil, onto which a zirconium interlayer is bonded to prevent materials interactions during irradiation. The fuel core and interlayers are then sealed with an AA6061 cladding via a hot isostatic press (HIP). The uranium will be nominally enriched to 19.75% in the isotope ^{235}U . The element loading of ^{235}U for the element will be

1,507 grams. This fuel is currently being qualified by the USHPRR program to demonstrate performance under conditions that are relevant to MURR and other reactors in the USHPRR program, including irradiation performance and flow tests. This section will be revised based on the irradiation and testing being conducted by the USHPRR Program. A summary of testing conducted for this fuel system thus far is found in Section 4.2.1.1.

To ensure that the validity of the operational limit curves is maintained, the reactor core will consist of eight fuel assemblies. However, operation to 100 watts above shutdown power on less than eight (8) assemblies is permitted for the purposes of reactor calibration or multiplication studies. Safe operation with fewer than eight (8) elements at 100 watts above shutdown power is covered by the Mode III natural convection operation with eight (8) elements, which is significantly more challenging. This analysis is described in Section 4.6.1.

3.5.2 Reactor Core Assembly Support Structure

The mass of eight (8) HEU elements on the fuel element support matrix (spider) is approximately 50 kg (6.25 kg each). For the LEU fuel, the element mass on the fuel element support matrix (spider) will be approximately 100 kg (12.5 kg each). The current fuel element support matrix (spider) will be able to accommodate the increased mass.

The load on the fuel element support matrix (spider) includes both the submerged weight of the elements and the pressure force of the coolant flowing through the elements. For a core coolant flow rate of 3,750 gpm (14,195 lpm), 120° F (49 °C) coolant inlet temperature, and the reactor at zero power, the friction pressure drop (without form losses) is 14.20 psi (97.9 kPa) for the HEU core and 10.36 psi (71.4 kPa) for the LEU core. These numbers are based on a fuel plate length of 25.5 inches (64.77 cm), a plate roughness of 63 microinches, HEU core flow area and hydraulic diameter of 0.34 ft² and 0.158 inches, respectively, and LEU core flow area and hydraulic diameter of 0.38 ft² and 0.176 inches, respectively. The equation for determining the friction pressure drop is $fL/D \rho V^2/2$, where f is friction factor, L is length, D is hydraulic diameter, ρ is density, and V is velocity. The friction factor is based on the Moody diagram, i.e., the Colebrook equation. Thus, the friction pressure drop across the LEU core is 3.84 psi (14.20 psi - 10.36 psi) less than that across the HEU core. Since the diameter of the inner wall of the outer pressure vessel is 11.80 inches (30 cm) and the diameter of the outer wall of the inner pressure vessel is 5.32 inches (13.5 cm), the annular area between these two diameters is 87.1 in². Hence, the reduction in friction pressure drop caused by replacing the HEU core with the LEU corresponds to a reduction in force on the core support structures of $3.84 \text{ psi} \times 87.1 \text{ in}^2 = 334 \text{ lbf} = 152 \text{ kg}$. Even though the submerged LEU core mass will be about 52 kg greater than the HEU core, the maximum force on the fuel element support matrix (spider) with (1) the LEU core installed and (2) full flow through the core, results in a reduction in the total force on the fuel element support matrix (spider) by $152 - 52 = 100 \text{ kg}$, compared with the HEU core installed.

3.5.3 Anti-siphon System

No changes are planned for this section due to conversion. However, Section 6.3.8 has been revised based on an improved RELAP thermal-hydraulic model of the MURR core.

THIS PAGE INTENTIONALLY LEFT BLANK

CHAPTER 4

REACTOR DESCRIPTION

THIS PAGE INTENTIONALLY LEFT BLANK

TABLE OF CONTENTS

4.0	REACTOR DESCRIPTION.....	4-1
4.1	Introduction.....	4-1
4.2	Reactor Core	4-1
4.2.1	Reactor Fuel.....	4-2
4.2.1.1	Reactor Fuel System	4-2
4.2.1.2	Fuel Element Description	4-4
4.2.1.3	Fuel Element Materials of Construction	4-10
4.2.1.4	Fuel Element Acceptance Criteria	4-10
4.2.1.5	Core Loadings.....	4-12
4.2.1.6	Surveillance.....	4-12
4.2.2	Control Blades	4-12
4.2.2.1	Description.....	4-12
4.2.2.2	Evaluation of the Control Blades.....	4-12
4.2.2.3	Evaluation of Control Blade Thermal Distortion.....	4-13
4.2.2.4	Surveillance.....	4-13
4.2.3	Neutron Moderator and Reflector.....	4-13
4.2.4	Neutron Startup Source.....	4-14
4.2.5	Reactor Core Assembly Support Structure	4-14
4.3	Reactor Pool.....	4-14
4.4	Biological Shield.....	4-14
4.5	Nuclear Design.....	4-15
4.5.1	Control Worth and Excess Reactivity.....	4-15
4.5.1.1	Methodology	4-15
4.5.1.2	Results.....	4-17
4.5.2	Shutdown Margin.....	4-21
4.5.3	Other Core Physics Parameters.....	4-21
4.5.4	Operating Conditions	4-24
4.5.4.1	Experimental Performance.....	4-26
4.5.4.2	Steady-State Power Distributions	4-33
4.6	Thermal-Hydraulic Characteristics.....	4-58
4.6.1	Natural Convection Analysis	4-58
4.6.2	Steady-State Forced Cooling Analysis	4-61
4.6.2.1	Thermal Criteria.....	4-61

4.6.2.2	Key Correlations	4-61
4.6.2.2.1	Correlation for Predicting Flow Instability Power (Whittle and Forgan)	4-61
4.6.2.2.2	Correlation for Predicting Critical Heat Flux (Extended Groenveld 2006)	4-62
4.6.2.2.3	Nusselt Number Correlation for Predicting Film Coefficient (Dittus- Boelter)	4-64
4.6.2.3	Core Configuration and Operating Conditions	4-64
4.6.2.4	Engineering Hot Channel Factors	4-65
4.6.2.4.1	Engineering Local Hot Channel Factor Contributors	4-65
4.6.2.4.2	Combining Local Hot Channel Uncertainty Factor Components....	4-68
4.6.2.4.3	Global Hot Channel Factors.....	4-70
4.6.2.5	Methodology for Calculating Pressure at Core Inlet	4-72
4.6.2.6	Channel Thickness Reduction Due to Fuel Plate Swelling and Oxide Buildup.....	4-77
4.6.2.7	PLTEMP/ANL Code	4-77
4.6.2.8	Application of the PLTEMP/ANL Code to the MURR Cores	4-79
4.6.2.9	Reactor Flow Instability and Critical Heat Flux Reactor Power Limits	4-80
4.6.2.10	Operational Limit Curves	4-82
4.6.3	Safety Limit	4-87
4.6.4	Limiting Safety System Settings.....	4-87
4.6.4.1	Introduction.....	4-87
4.6.4.2	Bases	4-88
4.6.4.3	Conclusions.....	4-89

LIST OF FIGURES

Figure 4.1	Reactor Assembly Section in Elevation View.....	4-2
Figure 4.2	Reactor Assembly Sections in Plan View	4-2
Figure 4.3	MURR LEU Fuel Element	4-5
Figure 4.4	Suite of Neutron Physics Codes Used for MURR Analyses.....	4-16
Figure 4.5	Comparison of MURR Fresh Core Reactivity vs. Burnup (Control Blades at 23-Inches Withdrawn; 2008 Core Flux Trap and Reflector Conditions)	4-17
Figure 4.6	MURR Control Bank Worth Curves (Calculated)	4-19
Figure 4.7	Comparison of LEU and HEU Beamport 'E' Outbound Current at Day 0.....	4-31
Figure 4.8	Comparison of LEU and HEU Beamport 'E' Outbound Current at Day 2.....	4-31
Figure 4.9	Comparison of LEU 10 MW to HEU 10 MW at Day 0.....	4-32
Figure 4.10	Comparison of LEU 12 MW to HEU 10 MW at Day 0.....	4-32
Figure 4.11	Comparison of LEU 10 MW to HEU 10 MW at Day 2.....	4-33
Figure 4.12	Comparison of LEU 12 MW to HEU 10 MW at Day 2.....	4-33
Figure 4.13	MURR Core Layout	4-34
Figure 4.14	Normalized Radial Power Factors in a Fresh Element (HEU Reference Core)...	4-37
Figure 4.15	Normalized Radial Power Factors in a Fresh Element (LEU Reference Core) ..	4-37
Figure 4.16	Hot-stripe Heat Flux Radial Peaking Factor in a Fresh Element (HEU Cores) ..	4-38
Figure 4.17	Hot-stripe Heat Flux Radial Peaking Factor in a Fresh Element (LEU Cores)...	4-39
Figure 4.18	Average Heat Flux in Each Plate of Each Fuel Element in Case 3B2 (HEU Week 58, Day 0, with Empty Flux Trap and Blades A and D at Depleted Composition). 4-45	
Figure 4.19	Average Heat Flux in Each Plate of Each Fuel Element in Case 8A2 (LEU Week 76, Day 2, with Loaded Flux Trap and Blades A and D at Depleted Composition) 4-46	
Figure 4.20	Azimuthal Peaking Factors for Each Plate of Each Element in Case 3B2 (HEU Week 58, Day 0, with Empty Flux Trap and Blades A and D at Depleted Composition)	4-47
Figure 4.21	Azimuthal Peaking Factors for Each Plate of Each Element in Case 8A2 (LEU Week 76, Day 2, with Loaded Flux Trap and Blades A and D at Depleted Composition)	4-48
Figure 4.22	Azimuthal Peaking Factors by Plate Averaged for All Elements (LEU Core)	4-49
Figure 4.23	Azimuthal Peaking Factors by Plate Averaged for All Elements (HEU Core)....	4-49
Figure 4.24	Hot-stripe Heat Flux for Each Plate of Each Element in Case 3B2 (HEU Week 58, Day 0, with Empty Flux Trap and Blades A and D at Depleted Composition). 4-50	
Figure 4.25	Hot-stripe Heat Flux for Each Plate of Each Element in Case 8A2 (LEU Week 76, Day 2, with Loaded Flux Trap and Blades A and D at Depleted Composition) 4-50	
Figure 4.26	Heat Flux Profile in HEU Plate 1 of Element 1 (0 MWd Burnup) In Case 3B2 (The power distribution is normalized to a core power of 10 MW).....	4-53
Figure 4.27	Heat Flux Profile in HEU Plate 2 of Element 1 (0 MWd Burnup) in Case 3B2 (The power distribution is normalized to a core power of 10 MW).....	4-53

Figure 4.28	Heat Flux Profile in LEU Plate 22 of Element 8 (174 MWd Burnup) in Case 8A1 (The power distribution is normalized to a core power of 12 MW)	4-54
Figure 4.29	Heat Flux Profile in LEU Plate 23 of Element 8 (174 MWd Burnup) in Case 8A1 (The power distribution is normalized to a core power of 12 MW)	4-54
Figure 4.30	Heat Flux Profile in HEU Plate 1 of Element 7 (0 MWd Burnup) in Case 1B1 (The power distribution is normalized to a core power of 10 MW).....	4-55
Figure 4.31	Heat Flux Profile in LEU Plate 23 of Element 1 (0 MWd Burnup) in Case 7A1 (The power distribution is normalized to a core power of 12 MW).....	4-55
Figure 4.32	Heat Flux Profile in HEU Plate 1 of Element 5 (0 MWd Burnup) in Case 3A (The power distribution is normalized to a core power of 10 MW).....	4-56
Figure 4.33	Heat Flux Profile in LEU Plate 23 of Element 8 (174 MWd Burnup) in Case 7A (The power distribution is normalized to a core power of 12 MW).....	4-56
Figure 4.34	Heat Flux Profile in HEU Plate 2 of Element 5 (0 MWD Burnup) in Case 3A (The power distribution is normalized to a core power of 10 MW).....	4-57
Figure 4.35	Heat Flux Profile in LEU Plate 22 of Element 8 (174 MWd Burnup) In Case 7A (The power distribution is normalized to a core power of 12 MW).....	4-57
Figure 4.36	Heat Flux Profile in LEU Plate 3 of Element 5 (0 MWd Burnup) in Case 7A (The power distribution is normalized to a core power of 12 MW).....	4-58
Figure 4.37	Schematic Representation of the Reactor Core Inlet Piping	4-73
Figure 4.38	LEU Core CD35 Flow Instability Power for Pressurizer Pressure at 60 psia	4-84
Figure 4.39	LEU Core CD35 Flow Instability Power for Pressurizer Pressure at 75 psia	4-85
Figure 4.40	LEU Core CD35 Flow Instability Power for Pressurizer Pressure at 85 psia	4-86

LIST OF TABLES

Table 4-1	Uranium Loading for the HEU and LEU Fuel Elements	4-7
Table 4-2	Summary Sheet for the HEU and LEU Fuel Elements	4-8
Table 4-3	Summary of Fuel Element Specifications	4-9
Table 4-4	Isotopic Composition of Uranium Metal for HEU and LEU Fuel Systems.....	4-10
Table 4-5	LEU Fuel Plate Nominal Values and Tolerances.....	4-11
Table 4-6	Comparison of MCNP and DIF3D Core k-effective for HEU and LEU Cores.....	4-18
Table 4-7	Summary of Core Excess Reactivity	4-19
Table 4-8	Summary of Control Blade Bank Worth Comparison	4-20
Table 4-9	Summary of Core Excess Reactivity with Depleted Control Blade Effects	4-20
Table 4-10	Minimum Shutdown Margins with Depleted Control Blade Effects	4-21
Table 4-11	Comparison of Temperature and Void Reactivity Coefficients Between HEU and LEU.....	4-23
Table 4-12	Comparison of Delayed Neutron Fractions and Prompt Neutron Lifetimes.....	4-24
Table 4-13	Discharge Isotopes in MURR HEU and LEU Fuel Cycle Simulations	4-25
Table 4-14	Current and Proposed MURR Fuel Cycle Operating Characteristics	4-26
Table 4-15	Comparison of Day 0 LEU Fluxes and Reaction Rates to HEU ⁴	4-29
Table 4-16	Comparison of Day 2 LEU Fluxes and Reaction Rates to HEU ⁴	4-30
Table 4-17	Summary of Power Distribution Evaluations – HEU Cores	4-41
Table 4-18	Summary of Power Distribution Evaluations – LEU Cores.....	4-42
Table 4-19	Summary of Key Hot-stripe and Local Heat Fluxes – (HEU Cores).....	4-43
Table 4-20	Summary of Key Hot-stripe and Local Heat Fluxes (LEU Cores)	4-44
Table 4-21	Mode III Peak Fuel Temperatures and Core Flow Rates	4-60
Table 4-22	LEU CD35 Plate Overload Tolerance Fractions, %.....	4-66
Table 4-23	Sample Hot Channel Factor Calculation for Channel 23 and Plate 23 of the LEU CD35 Core	4-71
Table 4-24	Hot Channel Factors for the LEU CD35 Core (No Fuel Plate Swelling or Oxide Growth).....	4-72
Table 4-25	Reference Hydraulic Conditions Used in Conjunction with Equations 10 and 11 to Determine Δ PHR	4-75
Table 4-26	Reference Pressure Drop Data.....	4-77
Table 4-27	Reactor Flow Instability Power (MW) For LEU Core CD35 ¹	4-81
Table 4-28	LEU Core CD35 Flow Instability Power (MW) with the Pressurizer Pressure at 60 psia	4-82
Table 4-29	LEU Core CD35 Flow Instability Power (MW) with the Pressurizer Pressure at 75 psia	4-83
Table 4-30	LEU Core CD35 Flow Instability Power (MW) with the Pressurizer Pressure at 85 psia	4-83
Table 4-31	Mode I Limiting Safety System Settings.....	4-87

Table 4-32	Mode III Limiting Safety System Settings.....	4-88
Table 4-33	LSSS Margins to Operational Limits for Four Anticipated Transients.....	4-89

LIST OF REFERENCES

- 4.1 Gibson, G.W., Graber, M.J., and Francis, W.C., *Annual Progress Report on Fuel Element Development for FY-1963*, IDO-16934, 1963.
- 4.2 Graber, M.J., et al., *Performance Evaluation of Core II and III Advanced Test Reactor Fuel Elements*, ANCR-1027, Aerojet Nuclear Company, 1971.
- 4.3 Martin, M.M., Richt, A.E., and Martin, W.R., *Irradiation Behavior of Aluminum-Base Fuel Dispersions*, ORNL-4856, 1973.
- 4.4 Graber, M.J., et al., *Results of ATR Sample Fuel Plate Irradiation Experiment*, IDO-16958, 1964.
- 4.5 Walker, W.A., Graber, M.J., and Gibson, G.W., *ATR Fuel Materials Development Irradiation Results-Part II*, IDO-17157, 1966.
- 4.6 Francis, W.C., *Metallurgy and Materials Science Branch Annual Report Fiscal Year 1970*, IN-1437, 1970.
- 4.7 US Nuclear Regulatory Commission, Safety Evaluation by the Office of Nuclear Reactor Regulation Supporting Amendment No. 20 to Facility License No. R-103, University of Missouri at Columbia, Docket No. 50-186, August 1, 1990.
- 4.8 Letter from MURR to NRC, "Slight Elevation of Fission Products Detected in Primary Coolant Water Analyses," December 15, 1997.
- 4.9 US Nuclear Regulatory Commission, *Safety Evaluation Report Related to the Evaluation of Low Enriched Uranium Silicide-Aluminum Dispersion Fuel for Use in Non-Power Reactors*, NUREG-1313, Washington, D.C, July 1988.
- 4.10 Wilson, E., Ravenhill, S., Rabin, B., Wight, J., and Dunn, K., "HEU to LEU Fuel Conversion of U.S. High Performance Research Reactors: An Overview of the Fuel Development Effort," Proc. of IAEA International Conference on Nuclear Security, Vienna, Austria, December 5-9, 2016.
- 4.11 Hayes, S. L., "Irradiation Testing of Intermediate and High-Density U-Mo Alloy Dispersion Fuels to High Burnup," Proc. 23rd International Meeting on Reduced Enrichment for Research and Test Reactors, Las Vegas, Nevada, October 2000.
- 4.12 Batelle Memorial Institute, *Progress Report on Metallurgy of Tuballoy to University of Chicago*, CT-2623, January 1945.
- 4.13 Robinson, A. B., et al., *Irradiation Performance of U-Mo Alloy Based 'Monolithic' Plate-Type-Design Selection Update*, INL/EXT-09-16807, Idaho National Laboratory, Idaho Falls, Idaho, July 2013.

- 4.14 Meyer, M., et al., "Irradiation Performance of U-Mo Monolithic Fuel," *Nuc. Eng. and Tech.* 46 (2014) 169.
- 4.15 Rabin, B., et al., "U.S. Progress in U-Mo Monolithic Fuel Development," Proc. 36th International Meeting on Reduced Enrichment for Research and Test Reactors, Seoul, Rep. of Korea, October 2015.
- 4.16 Tentner, A., et al., *Evaluation of Thin Plate Hydrodynamic Stability through a Combined Numerical Modeling and Experimental Effort*, ANL/RTR/TM-16/9 Argonne National Laboratory, May 2017.
- 4.17 Specification for Low Enriched Uranium Monolithic Fuel Plates, SPC-1635, Rev. 6, Idaho National Laboratory, Idaho Falls, Idaho, March 2017.
- 4.18 Specification for Assembly of Fuel Elements for the MURR, TRTR-4, EG&G Idaho, Inc., Idaho Falls, Idaho, May 1986.
- 4.19 American National Standards Institute/American Nuclear Society, ANSI/ANS-15.2-1999 (R2016), "Quality Control for Plate-Type Uranium-Aluminum Fuel Elements," 1999.
- 4.20 Foyto, L. and McKibben, J. C., "MURR[®] Boral[®] Control Blade Thermal-Mechanical Analysis," MURR Technical Data Report No. 133, June 2012.
- 4.21 Hoyer, A., "Lifetime Analysis of Irradiated Beryllium in Research Reactors," University of Missouri – Columbia, Missouri, 2017.
- 4.22 Feldman, E. E., et al., *Technical Basis in Support of the Conversion of the University of Missouri Research Reactor (MURR) Core from Highly-Enriched to Low-Enriched Uranium – Steady-State Thermal-Hydraulic Analysis*, ANL/RERTR/TM-12-37, Rev. 1, Argonne National Laboratory, January 2013.
- 4.23 Olson, A. P., *A User's Guide for the REBUS-PC Code, Version 1.4*, ANL/RERTR/TM-32, Argonne National Laboratory, 2001.
- 4.24 Deen, J. R., et al., "WIMS-ANL User Manual, Rev. 5," ANL/TD/TM99-07, Argonne National Laboratory, 2003.
- 4.25 Hanan, N.A., et al., "The Use of WIMS-ANL Lumped Fission Product Cross Sections for Burned Core Analysis with the MCNP Monte Carlo Code," Proc. 1998 International Meeting on Reduced Enrichment for Research and Test Reactors, São Paulo, Brazil, Oct. 18-23, 1998.
- 4.26 X-5 Monte Carlo Team, "MCNP-A General Monte Carlo N-Particle Transport Code, Version 5 Volume I, II and III," LA-UR-03-1987/LA-CP-03-0245/LA-CP-03-0284, Los Alamos National Laboratory, 2003.

- 4.27 Dionne, B., Stillman, J, and Stevens, J., "Applicability of WIMS-ANL to Generate Cross Sections for Very High Density UMo Fuel in Proposed LEU Fuel Assembly," Proc. 2008 International Meeting on Reduced Enrichment for Research and Test Reactors, Washington, D.C., Oct. 5-9, 2008.
- 4.28 Stillman, J., et al., *Technical Basis in Support of the Conversion of the University of Missouri Research Reactor (MURR) Core from Highly-Enriched to Low-Enriched Uranium – Core Neutron Physics*, ANL/RERTR/TM-12-30, Argonne National Laboratory, September 2012.
- 4.29 Julian, C., "Low power testing," MURR internal report, 1971.
- 4.30 Peters, N. and Kutikkad, K., "MURR Control Blade Depletion Study Report," MURR Technical Data Report No. 134, June 2012.
- 4.31 MacFarlane, R. E, "New Thermal Neutron Scattering Files for ENDF/VI Release 2," LANL report, LA-12639-MS (1994).
- 4.32 Peters, N. J, Brockman, J.D, Robertson, J. D, "Using Monte Carlo Transport to Accurately Predict Isotope Production and Activation Rates at the University of Missouri Research Reactor," *J. Radioanal Nucl Chem*, 282:255–259 (2009).
- 4.33 McKibben, J. C., et al., *Feasibility Analyses for HEU to LEU Fuel Conversion of the University of Missouri Research Reactor (MURR)*, MURR Technical Data Report No. 0125, September 2009.
- 4.34 Stillman, J. A., et al., *Accident Analyses for Conversion of the University of Missouri Research Reactor (MURR) from Highly-Enriched to Low-Enriched Uranium*, ANL/GTRI/TM-14/5, Revision 1, Argonne National Laboratory, Argonne, Illinois, February 2017.
- 4.35 The RELAP5/MOD3.3 Code Manual, Nuclear Systems Analysis Division, Information Systems Laboratories, Inc., Rockville, Maryland and Idaho Falls, Idaho, Prepared for the Division of Systems Research, Office of Nuclear Regulatory Research, U. S. Nuclear Regulatory Commission, Washington, DC, March 2006.
- 4.36 *University of Missouri Research Reactor Safety Analysis Report*, submitted to the U.S. Nuclear Regulatory Commission, August 2006.
- 4.37 Olson, A. P. and Kalimullah, M., *A User's Guide to the PLTEMP/ANL Code*, Version 4.1, ANL/RERTR/TM-11-22, Nuclear Engineering Division, Argonne National Laboratory, April 6, 2011.
- 4.38 Whittle, R. H. and Forgan, R., "A Correlation for the Minima in the Pressure Drop Versus Flow-Rate Curves for Sub-Cooled Water Flowing in Narrow Heated Channels," *Nuclear Engineering and Design*, 1967, pp. 89-99.

- 4.39 Olson, A. P., "Analysis of Flow Excursion Experiments Relevant to Research Reactors," Proc. 2006 International Meeting on Reduced Enrichment for Research and Test Reactors, Cape Town, South Africa, October 29-November 3, 2006, http://www.rertr.anl.gov/RERTR28/PDF/S7-2_Olson.pdf.
- 4.40 Bernath, L., "A Theory of Local-Boiling Burnout and Its Application to Existing Data," Chemical Engineering Progress Symposium, Series No. 30, Volume 56, pp. 95-116 (1960).
- 4.41 Croft, M. W., *Advanced Test Reactor Burnout Heat Transfer Tests*, USAEC Report IDO-24465, ATR-FE-102, Ca-2, Babcock & Wilcox Company, January 1964.
- 4.42 Waters, E. D., Heat Transfer Experiments for the Advanced Test Reactor, USAEC Report BNWL-216, UC-80, Reactor Technology (TID-4500) Pacific Northwest Laboratory, Richland, Washington, May 1966.
- 4.43 Feldman, E. E., *Comparison of the PLTEMP Code Flow Instability Predictions with Measurements Made with Electrically Heated Channels for the Advanced Test Reactor*, ANL/RERTR/TM-11-23, Nuclear Engineering Division, Argonne National Laboratory, June 9, 2011.
- 4.44 Groeneveld, D. C., Shan, J. Q., Vasic, A. Z., Leung, L. K. H., Durmayaz, A., Yang, J., Cheng, S. C., and Tanase, A., "The 2006 CHF Look-up Table," *Nucl. Eng. and Design*, Vol. 237, pp. 1909-1922 (2007).
- 4.45 Hall, D. D. and Mudwar, I., "Critical Heat Flux for Water Flow in Tubes – II. Subcooled CHF Correlations," *Intern. J. Heat and Mass Transfer*, Vol. 43, pp. 2605-2640 (2000).
- 4.46 Celata, G. P., Cumo, M., and Mariani, A., "The Effect of the Tube Diameter on the Critical Heat Flux in Subcooled Flow Boiling," *Intern. J. of Heat and Mass Transfer*, Vol. 39, pp. 1755-1757 (1996).
- 4.47 Tanase, A., Cheng, S. C., Groeneveld, D. C., and Shan, J. Q., "Diameter Effect on Critical Heat Flux," *Nucl. Eng. Des.* Vol. 239, pp. 289-294 (2009).
- 4.48 Stillman, J., et al., *Irradiation Experiment Conceptual Design Parameters for MURR LEU U-Mo Fuel Conversion*, ANL/RERTR/TM-13-1, Revision 1, Argonne National Laboratory, Argonne, Illinois, June 2013.
- 4.49 Woodruff, W. L., *Evaluation and Selection of Hot Channel (Peaking) Factors for Research Reactor Applications*, ANL/RERTR/TM-28, Argonne National Laboratory, Argonne, Illinois, February 1997, <http://www.rertr.anl.gov/METHODS/TM28.pdf>.

4.0 REACTOR DESCRIPTION

This chapter discusses and describes the principal design features, operating characteristics, and parameters of the low-enriched uranium (LEU) fueled reactor. The analysis in this chapter supports the conclusion that the reactor is conservatively designed for safe operation and can be shut down under all credible operating conditions. The information in this chapter provides the design bases for many systems, subsystems, and functions discussed elsewhere in the Safety Analysis Report (SAR) and for many of the Technical Specifications (TS).

4.1 Introduction

The University of Missouri Research Reactor (MURR) is a pressurized, reflected, heterogeneous, open pool-type, which is light-water moderated and cooled. The reactor is currently designed and licensed to operate at a maximum thermal power level of 10 MW with forced cooling, or up to 50 kW in the natural convection mode. A unique design feature provides an experimental position (flux trap) through the center of the core. A flux trap-type reactor is characterized by a thin fuel region adjacent to a good moderator which thermalizes the neutrons and causes the thermal neutron flux to peak in a region (center test hole) accessible for experiments. A relatively high neutron flux is provided for beamport experiments as well. For LEU operation, a power uprate to 12 MW will enable the facility to maintain its current experimental performance.

The reactor core assembly is located eccentrically within a cylindrically-shaped, aluminum-lined pool, approximately 10 feet (3.0 m) in diameter and 30 feet (9.1 m) deep. The reactor core consists of three major regions: fuel, control blade, and reflector. The fuel region has a fixed geometry consisting of eight (8) fuel elements having identical physical dimensions placed vertically around an annulus in between two cylindrical reactor pressure vessels. Changes to the fuel assembly as a result of conversion are described in detail in Section 4.2.1. The control blades and reflector will not change as a result of conversion. A control blade thermal distortion analysis will be completed as part of the final conversion safety analysis.

No changes to the nominal conditions for the primary coolant system are expected due to conversion. Changes to the Limiting Safety System Settings (LSSS) due to conversion are discussed in Section 4.6.4 and Appendix A. Cooling of the reflector region, the control blade region, and the center test hole will not be affected by conversion.

The experimental facilities will not be affected by conversion.

4.2 Reactor Core

The reactor core consists of the following components: the reactor fuel, the control blades, reflectors, and the reactor core support structure. The reactor core assembly, including the pressure vessels, the fuel element support matrix, and the reflector support assembly are supported from the bottom of the reactor pool in circular sections that also serve as part of the primary and pool coolant piping. Cross-sectional views of the reactor core assembly are shown in Figures 4.1 and 4.2.

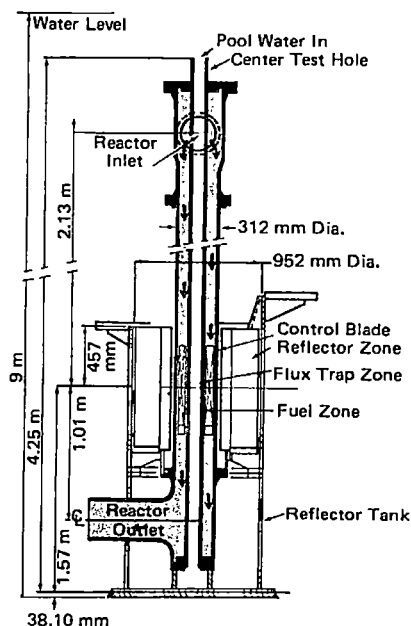


FIGURE 4.1
REACTOR ASSEMBLY SECTION IN
ELEVATION VIEW

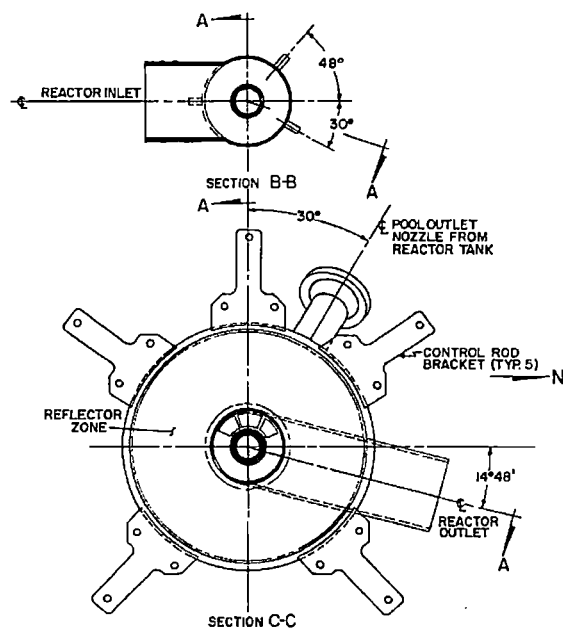


FIGURE 4.2
REACTOR ASSEMBLY SECTIONS IN
PLAN VIEW

Each of the reactor core components are described in greater detail in the subsequent sections.

4.2.1 Reactor Fuel

4.2.1.1 Reactor Fuel System

The fuel material at time of initial startup was a uranium-aluminum alloy with each fuel assembly loaded to a maximum of 650 grams of ^{235}U . This type of fuel system had performed very reliably in the Materials Test Reactor (MTR) and the Engineering Test Reactor (ETR) at the Idaho National Engineering Laboratory (INEL), as well as in other reactors throughout the world. However, in order to reduce the fuel cycle cost and the amount of ^{235}U needed per MWd of energy produced at the MURR, a conversion was performed in 1971 to switch to a uranium-aluminide UAl_x dispersion fuel material with a maximum loading of [REDACTED] grams of ^{235}U per assembly.

The MURR [REDACTED]-gram fuel element is a product of the UAl_x dispersion fuel system development. The UAl_x dispersion fuel system was developed at INEL for the high flux, high power Advanced Test Reactor (ATR) and subsequently used at the MTR and ETR prior to its use at the MURR (Refs. 4.1, 4.2). Several features of the UAl_x dispersion fuel system increase the fuel performance capability in high flux reactors (Refs. 4.3, 4.4, 4.5, 4.6). One of these features is that the powder dispersion fuel matrix provides some inherent void space, which helps reduce fission product swelling. The UAl_x structure has exceptional tolerance for fission gas retention and burnable

poisons can readily be dispersed in the fuel matrix. Due to the compact core size, the fuel uses HEU to obtain sufficient excess reactivity to be able to operate at 10 MW.

The excellent performance of UAl_x fuels has been consistently demonstrated over the past forty-one years in test and research reactors such as the ATR and the MURR. MURR has used more than 830 UAl_x fuel elements since 1971 with no failures. ATR has used more than 3,950 UAl_x fuel elements since 1972 with 24 possible leaking fuel elements. All ATR fuel leakage has been caused by pitting corrosion. ATR has had no other type of UAl_x fuel element failure and no failures have occurred since the early 1990's. There also have been no aluminide fuel element failures at the MURR due to pitting corrosion (Ref. 4.7), but one fuel element was retired early after it had been used for 126 MWd of its planned 150-MWd usage due to a slight increase in iodine-131 (^{131}I) level in the primary coolant (Ref. 4.8). A corrosion pit develops slowly and penetration of the aluminum cladding would be easily detected by the installed on-line fission product monitor.

As a continuation of the dispersion fuel development efforts, the U.S. Department of Energy (DOE) Reduced Enrichment for Research and Test Reactors (RERTR) program subsequently identified and qualified through the U.S. Nuclear Regulatory Commission (NRC) an intermetallic form of LEU uranium silicide (U_3Si_2) for use in the US (Ref. 4.9). This is presently the highest density fuel qualified for use in research and test reactors with substantial burnup.

Conversion of MURR from an HEU fuel system to an LEU fuel system has required redesign of the MURR fuel element. Reducing the enrichment to 19.75 wt. % ^{235}U led to changing the fuel-bearing region of the MURR plates from a dispersion fuel form to an alloy of uranium and 10 w% molybdenum, referred to as the U-10Mo monolithic fuel foil. This high-density U-10Mo monolithic alloy fuel is currently under development and qualification as described below (Ref. 4.10).

Subsequent to the intermediate density LEU U_3Si_2 fuel qualification, the need for higher density fuels led to further fuel qualification efforts. Approximately one dozen candidate alloys or intermetallic compounds were chosen for irradiation screening tests (Ref. 4.11). All fuels screened were capable of higher densities than U_3Si_2 . The outcome of the RERTR-1, -2, and -3 tests was that no other candidate of either dispersed intermetallic compounds or dispersed alloys showed the same promise as U-10Mo alloy (in this case still dispersed in an aluminum matrix). These tests provided high burnup up to 5×10^{21} fissions/cm³ at moderate temperatures up to 100 °C but with fuel loading limited to approximately 4 gU/cm³. It is notable that this is a return to qualification of the U-10Mo alloy where substantial data is available since the U-Mo alloy fuel form has been in development from the 1940's (Ref. 4.12) for several decades though this included significantly higher irradiation temperatures and lower burnups than MURR requires.

Therefore, upon confirming favorable swelling performance of UMo alloy (dispersed powder) after irradiation, the program selected U-Mo for further dispersion development, and as well tested two small monolithic disks in RERTR-4. The monolithic U-10Mo alloy testing continued to show favorable irradiation behavior, and therefore replaced dispersion fuel testing.

The monolithic U-10Mo alloy density of 15.3 gU/cm³ is adequate for all U.S. High Performance Research Reactors (USHPRR), including MURR, and is far above the 8 gU/cm³ expected from

the new dispersion fuel also under development for reactors in Europe or elsewhere. Thus, for the USHPRR the monolithic U-10Mo testing progressively increased the irradiation envelope in the RERTR-6 through RERTR-10 experiments. Through these tests a number of laboratory-scale fabrication methods were evaluated. Favorable irradiation performance across the parameter range of interest was found with U-10Mo fuel foils with a 0.001-inch thick zirconium diffusion barrier between the fuel and aluminum cladding (Ref. 4.13). Following down-selection to this fuel system, RERTR-12 was conducted as a comprehensive large-scale mini-plate test, and was accompanied by several full-size-plate tests (Refs. 4.14, 4.15). Prior to a conversion, full-size plate and full fuel element fabrication for irradiation and flow testing are planned for the MURR LEU fuel element design.

The change in fuel form also required adjustments to the fuel-bearing region thicknesses in the fuel plates and increased coolant channel thickness, resulting in the reduction of the number of fuel plates in an element from 24 to 23. Additionally, a reactor power uprate to 12 MW is sufficient to allow the reactor to continue to meet the facility's mission. The plate-specific calculated peak plate burnup in the 12 MW LEU fuel system is $< 3.4 \times 10^{21}$ fissions/cm³, compared to the $< 2.3 \times 10^{21}$ fissions/cm³ in the 10 MW HEU dispersion fuel system.

4.2.1.2 Fuel Element Description

A drawing of the MURR LEU fuel element and a schematic of the element cross-section are shown in Figure 4.3. Eight (8) such fuel elements comprise the fixed MURR core.

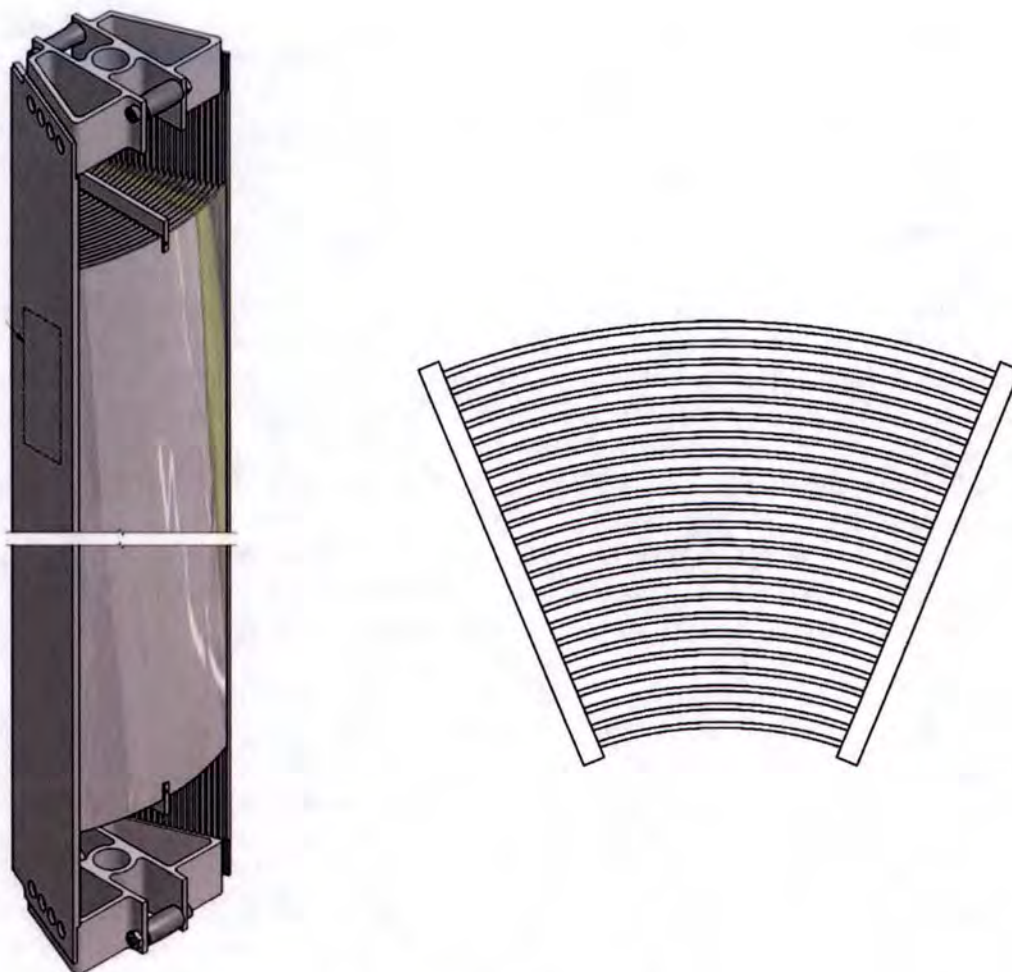


FIGURE 4.3
MURR LEU FUEL ELEMENT

The fuel elements have a radial dimension of 3.21 inches (8.15 cm)—as determined from radial length from the inside of the inner roller to the outside of the outer roller—and an overall length of 32.5 inches (82.55 cm). The LEU fuel element is designed to be similar to the HEU fuel element. The LEU element has identical side plates and end fitting geometry which is compatible with the existing support structure. As discussed below, the number of fuel plates in the element has been reduced from 24 plates in the HEU element to 23 plates in the LEU element. There will also be changes to the thickness and arc width of the fuel zone in the plates, the overall thickness of the fuel plates, the thickness of the coolant channels between plates, and the thickness of the coolant channels between the outermost plates and the pressure vessels.

The LEU fuel element design was developed through an extensive series of scoping studies, followed by optimization of a design that meets the conversion goals of reactor safety, fuel utilization, and experimental performance. The proposed fuel element has been designated “CD35,” and is constructed with 23 fuel plates (instead of 24 plates as in the HEU elements). The element uses various U-10Mo foil thicknesses to flatten the radial heat flux profile. The thinnest

nominal aluminum alloy AA6061 cladding is 0.011 inches (0.2794 mm) and the thinnest total plate thickness is 0.044 inches (1.1176 mm). There is a thin zirconium layer that is nominally 0.001 inches (0.0254 mm) on the largest surfaces of the fuel foil that serves as an interaction layer between the U-10Mo and AA6061 cladding. The other portions of the element construction (e.g., side plate length, width, and thickness; and end fittings) will be identical to the HEU fuel element.

The construction method of the LEU fuel plates is described in Section 4.2.1.3. The dimensions of the fuel plate components are described in Section 4.2.1.4. The fuel plates are supported along their vertical edges by slotted aluminum side plates. The side plates are 31.75 inches (80.65 cm) long by 3.16 inches (8.03 cm) wide and 0.15 inches (3.81 mm) thick. The fuel plates are permanently fastened into the side plates using a mechanical binding procedure that provides a tensile strength of greater than 150 pounds per linear inch of the side plate joint. This ensures a rigid assembly that is fully capable of withstanding the hydraulic forces imposed by the primary coolant flow velocity. For HEU this is 25.1 ft/s (7.65 m/s), and for LEU is 23.1 ft/s (7.04 m/s) at a total core flow rate of 3,850 gpm (14, 574 lpm), which is the high end of the normal operating band for core flow rate for both HEU and LEU. The core flow areas are 0.3419 ft² for HEU and 0.3715 ft² for LEU. HEU fuel assemblies of similar construction have withstood severe hydraulic tests at flow velocities up to 50 ft/s (15.24 m/s) without distortion.

For LEU fuel elements, the proposed design changes required a thinner fuel plate thickness and one fewer plate in order to provide adequate neutron moderation. Otherwise, the LEU fuel element design is of identical construction to the HEU fuel element without changes to the side plates, combs, or end fittings, except for changes to accommodate the number and thickness of the fuel plates and the thickness of the coolant channels. Experimentally benchmarked modeling has been conducted up to a maximum flow velocity of 8.7 m/s, which includes engineering uncertainty factors (Ref. 4.16). This work concluded that the effect of plate deflection due to fluid-structure interaction on the MURR LEU fuel element thermal-hydraulic and structural performance is insignificant, thus indicating an adequate design margin in this regard. As a part of the conversion, flow testing of a full LEU fuel element is also planned at a dedicated flow test facility that has been constructed for this purpose. Table 4-1 shows the ²³⁵U gram loading for each of the plates in the HEU and LEU elements. Table 4-2 shows a comparison of the summary data for the HEU and LEU elements. Table 4-3 shows a summary of the LEU fuel system nominal specifications alongside the prior HEU specifications for comparison.

TABLE 4-1
URANIUM LOADING FOR THE HEU AND LEU FUEL ELEMENTS

Plate Number	HEU Fuel Element	LEU Fuel Element
	²³⁵ U Content (grams)	
1		18.09
2		25.66
3		36.26
4		47.89
5		50.45
6		52.99
7		55.53
8		58.07
9		60.61
10		63.16
11		65.70
12		68.24
13		70.78
14		73.32
15		75.86
16		78.41
17		80.95
18		83.49
19		86.03
20		88.59
21		91.15
22		93.71
23		81.87
24		N/A
Total		1507

TABLE 4-2
SUMMARY SHEET FOR THE HEU AND LEU FUEL ELEMENTS

Description	HEU Nominal Value	LEU Nominal Value
Fuel Content (grams ²³⁵ U per element)	■	1507
Type of Fuel	Aluminide-UAl _x mostly UAl ₃ Phase	U-10Mo Monolithic Alloy
Fuel Density (grams of ²³⁵ U loaded per cubic centimeter)	1.43	3.03
Boron Content (natural boron per element)	Trace Impurities	Trace Impurities
Cold Excess Reactivity, Δk/k (clean core – control blades full out)	8.6%	7.0%
Control Blade Worth for Fresh / Mixed Cores (Δk/k)	20.3% / 21.5%	17.0% / 17.7%
Peak Burnup Density (fissions per cubic centimeter)	< 2.3 × 10 ²¹	< 3.4 × 10 ²¹
Energy per Element at Peak Fission Density (MWd per element)	≈ 150	180

TABLE 4-3
SUMMARY OF FUEL ELEMENT SPECIFICATIONS

Description	HEU Nominal Value	LEU Nominal Value
Fuel Material		
Enrichment ²³⁵ U		19.75%
Thickness		0.009 – 0.020 inches (0.2286 – 0.5080 mm)
Interlayer		
Material		Zirconium
Thickness		0.001 inches (0.0254 mm)
Cladding		
Material		Aluminum AA6061
Thickness		0.011 – 0.0165 inches (0.2794 – 0.4191 mm)
Fuel Assembly		
Number of Fuel Plates		23
Innermost Fuel Plate Center Radius		2.778 inches (7.056 cm)
Outermost Fuel Plate Center Radius		5.780 inches (14.681 cm)
Overall Fuel Assembly Length		32.5 inches (82.550 cm)
Overall Fuel Plate Length		25.5 inches (64.770 cm)
Overall Active Fuel Length		24.0 inches (60.960 cm)
Fuel Plate Thickness		0.044 – 0.049 inches (1.118 – 1.225 mm)
Distance Between Fuel Plates		0.092 – 0.093 inches (2.337 – 2.362 mm)
Nominal ²³⁵ U Loading		1507 grams
Element Weight		12.50 kg

4.2.1.3 Fuel Element Materials of Construction

The fuel material for the HEU UAl_x dispersion fuel system consists of a uranium powder enriched in the isotope ²³⁵U (93.0 ± 1.0%) dispersed in an aluminum powder (dispersion fuel meat). The fuel material for the LEU monolithic fuel system consists of an alloy of LEU with 10.0 ± 1.0 wt. % molybdenum (U-10Mo fuel foil). The isotopic composition of the uranium metal present in both fuel systems is listed in Table 4-4.

TABLE 4-4
ISOTOPIC COMPOSITION OF URANIUM METAL FOR HEU AND LEU FUEL SYSTEMS

Isotope	HEU Dispersion Fuel Limit (wt. % of Total)	LEU Monolithic Fuel Limit [4.17] (wt. % of Total)
²³² U	N/A	$\leq 2 \times 10^{-7}$
²³⁴ U	≤ 1.20	≤ 0.26
²³⁵ U	93.0 ± 1.0	19.75 ± 0.20
²³⁶ U	≤ 0.70	≤ 0.46
²³⁸ U	6.0 ± 1.0	Remainder

The HEU fuel system has ≤ 15.0 ppm equivalent boron content (EBC) in the fuel meat, whereas the LEU fuel system has an EBC of ≤ 5.0 ppm in the fuel foil.

The U-10Mo fuel foil is roll-bonded to two 0.001-inch zirconium interlayers that conform to the chemical requirements of ASTM B352-11 (UNS R60001) with less than 100 ppm oxygen. These interlayers serve as a diffusion barrier to prevent deleterious reactions from occurring between the U-10Mo fuel foil and the aluminum-based alloy cladding during fabrication or irradiation. The fuel foil and interlayers are clad in AA6061-T6 that is in conformance with the ASTM B 209 (UNS A96061) standard. The aluminum cladding is bonded to the fuel foil and interlayers using a hot isostatic press (HIP) process at 560 °C and 15 kpsi (105 MPa) with a 90-minute hold time. The cladding serves to isolate the fuel foil and fission products from the reactor coolant.

The handling and guide fixtures (end fittings) are aluminum alloy 6061-T6 or 6061-T651, ASTM B 209, or Alloy 356-T6, ASTM 221 if fabricated from solid bar stock, or Alloy 356-T71, ASTM B 618 or ASTM B 26 if a casting was used. The side plates are AA6061-T6 or AA6061-T651, ASTM B 209. The reactivity effect of all impurities in this alloy is less than the equivalent of 15.0 ppm of boron. The rollers on the end fittings are constructed of Type 304 stainless steel, ASTM A 276.

4.2.1.4 Fuel Element Acceptance Criteria

All fuel elements are inspected and tested after fabrication and prior to delivery to the reactor facility. The acceptable LEU fuel plate nominal dimensions and tolerances are shown in Table 4-5.

TABLE 4-5
LEU FUEL PLATE NOMINAL VALUES AND TOLERANCES

Fuel Plate Dimension	Location	Nominal Value and Tolerance
Fuel Foil Thickness	Plate 1	0.009 ± 0.001 inches (0.2286 ± 0.0254 mm)
	Plate 2	0.012 ± 0.001 inches (0.3048 ± 0.0254 mm)
	Plate 3	0.016 ± 0.001 inches (0.4064 ± 0.0254 mm)
	Plates 4–22	0.020 ± 0.001 inches (0.5080 ± 0.0254 mm)
	Plate 23	0.017 ± 0.001 inches (0.4318 ± 0.0254 mm)
U-235 Content	All Plates	19.75 ± 0.20 wt. %
Molybdenum Content	All Plates	10 ± 1 wt. %
Zirconium Interlayer	All Plates	0.001 ± 0.0005 inches (0.0254 ± 0.0127mm)
Zirconium Interlayer Minimum Thickness	All Plates	0.0005 inches (0.0127 mm)
AA6061 Cladding Thickness ¹	Plate 1	0.0165 ± 0.001 inches (0.4191 ± 0.0254 mm)
	Plate 2	0.015 ± 0.001 inches (0.3810 ± 0.0254 mm)
	Plate 3	0.013 ± 0.001 inches (0.3302 ± 0.0254 mm)
	Plates 4–22	0.011 ± 0.001 inches (0.2794 ± 0.0254 mm)
	Plate 23	0.015 ± 0.001 inches (0.3810 ± 0.0254 mm)
AA6061 Cladding Minimum Thickness ¹	All Plates	0.0095 inches (0.2286 mm)
Plate Thickness	Plate 1–22	0.044 ± 0.002 inches (1.1176 ± 0.0508 mm)
	Plate 23	0.049 ± 0.002 inches (1.2246 ± 0.0508 mm)
Distance Between Plates ²	Channel 1	0.0805 ± 0.007 inches (2.0447 ± 0.1778 mm)
	Channels 2–5	0.093 ± 0.008 inches (2.3622 ± 0.2032 mm)
	Channels 6–19	0.092 ± 0.008 inches (2.3368 ± 0.2032 mm)
	Channels 20–23	0.093 ± 0.008 inches (2.3622 ± 0.2032 mm)
	Channel 24	0.0805 ± 0.010 inches (2.0447 ± 0.2540 mm)

¹ The measured point minimum AA6061 cladding thickness ("point minclad") by ultrasonic probe inspection can be 0.0095 inches with a bulk minimum AA6061 cladding thickness ("bulk minclad") no less than 0.0107 inches. The terms "point minclad" and "bulk minclad" are defined in Reference 4.17.

² The nominal dimension is between the bounding edge of the inner and outer element rollers and the surface of the plate for Channel 1 and 24, respectively.

The acceptance criteria and quality control requirements, which reasonably assure proper performance of the MURR fuel elements, are described in References 4.18 and 4.19. The fuel elements are also inspected at the reactor facility prior to initial use in the reactor. Fuel element measurements and alignments are verified using a straight and curved plane and end fitting templates. Fabrication of elements will need to verify these preliminary assumed design parameters, including tolerances.

4.2.1.5 Core Loadings

There are no changes to this section as a result of LEU conversion.

4.2.1.6 Surveillance

Currently one out of every eight (8) HEU fuel elements that have reached their end-of-life are inspected for anomalies. After conversion, LEU fuel elements will have the element with the highest burnup from each pair of elements introduced into the core inspected for anomalies at the middle-of-life burnup (90 MWd) and when this element has reached the end-of-life. A startup plan as a separate appendix to the future full conversion SAR is expected to require additional inspection during the initial LEU startup cores. These inspections, coupled with continuous fission product monitoring and routine water analysis of the primary coolant, provide a means for detection of any possible defects resulting from reactor operation, thereby reducing the possibility of a fission product release to the primary coolant system. Inspection of some of the fuel elements at the end of their life allows for decay which results in a reduction in exposure to personnel.

4.2.2 Control Blades

4.2.2.1 Description

No changes to this section are expected due to conversion.

4.2.2.2 Evaluation of the Control Blades

The reactivity worth and speed of travel for the control blades are sufficient to allow complete control of the reactor system from a shutdown condition to full power operation. The insertion rate for the control blades is adequate to ensure prompt shutdown of the reactor in the event a scram signal is received.

The control blades have been configured to control the excess reactivity of the HEU fueled core needed for 10 MW continuous operation (including xenon override) and will provide a shutdown margin of at least $0.02 \Delta k$. This shutdown margin ensures that the reactor can be shut down from any operating condition even if the most reactive control blade and the regulating blade should remain in the fully withdrawn position. The loading of boron in the shim blades has been evaluated and allows continuous operation of LEU cores operating at 12 MW and ensures that the required shutdown margin is met for cores loaded with LEU (see Section 4.5.2).

The nominal speed of the shim blades is one inch per minute (2.54 cm/min) in the outward direction and two inches per minute (5.08 cm/min) in the inward direction. Speed of the regulating blade is 40 inches per minute (101.6 cm/min) in both directions. Overall travel of the shim blades

and the regulating blade is 26.0 inches (66.04 cm); centered slightly below the core vertical centerline.

The inward and outward speed of the control blades will remain the same for conversion to LEU fuel. Calculations of the differential control blade worths have been performed to confirm that the Technical Specification limit on the reactivity insertion rate from control blade withdrawal is met (see Section 4.5.1.2).

4.2.2.3 Evaluation of Control Blade Thermal Distortion

MURR has used the current style of control blades since before going to 10 MW power level in 1974 and has had no problem with thermal distortion of the control blades. An analysis of the control blade thermal distortion for the HEU core was completed in Reference 4.20. For the LEU core operating at 12 MW, a comparable analysis of the control blade thermal distortion will be completed as part of the submission of the complete safety analysis report.

4.2.2.4 Surveillance

No changes to this section are expected due to conversion.

4.2.3 Neutron Moderator and Reflector

Neutron reflection is provided by two concentric right circular annuli surrounding the reactor pressure vessels. The reflector materials have a rigid structure that retains size and shape, and supports all projected forces and weights. No changes would occur to the reflector materials that would interfere with safe reactor operation or safe shutdown of the reactor. The inner reflector annulus is a 2.71-inch (6.88-cm) thick solid cylindrical sleeve of beryllium metal which forms the outer wall of the control blade gap. Five (5) aluminum spacers ensure that the beryllium reflector is concentric with the outer pressure vessel, thus maintaining the required control blade gaps. The outer reflector annulus consists of canned vertical elements of graphite having a total thickness of 8.89 inches (22.58 cm).

The reactor is designed to allow the removal and/or replacement of both the beryllium reflector and any of the graphite reflector elements. Replacement of the beryllium reflector is performed approximately every 26,000 MWd, which corresponds to eight years of operation at the current operating schedule of approximately 150 hours per week. The replacement interval is based on approaching but not reaching the irradiation point that caused the first beryllium reflector to crack. The original beryllium reflector had two four-inch diameter beamport holes just below the vertical centerline for beamports 'A' and 'F.' Based on this past operational experience, the last four (4) beryllium reflector replacements have been completed with no additional in-service beryllium reflectors cracking. Replacement of the beryllium reflector requires the reactor to be shut down for approximately one week and includes the removal of all the fuel elements and control blades, the upper portion of the reactor pressure vessel and primary inlet piping.

Evaluation of the beryllium reflector lifetime for LEU fuel conversion has recently been completed (Ref. 4.21). The calculations indicate an increase in the overall lifetime, perhaps by 25%, with about half the gain coming from no longer having the beamport holes in the reflector. Furthermore,

with LEU fuel the 60 kg of U-238 in the core provides a reduction in the gamma heating of the beryllium, which contributes to the gain. With conversion to LEU fuel and increasing the power to 12 MW, the beryllium reflector lifetime can approach 12 years compared to the beryllium reflector lifetime of eight (8) years for a 10 MW HEU core based on the failure of the first beryllium reflector that had beamport holes.

4.2.4 Neutron Startup Source

There are no changes to this section as a result of LEU conversion.

4.2.5 Reactor Core Assembly Support Structure

The reactor core assembly support structure consists of the outer reactor pressure vessel, the island tube (inner reactor pressure vessel), the fuel element support matrix (spider), and the reflector tank. None of these components are expected to change as a result of conversion.

The fuel elements are supported and positioned within the reactor pressure vessels by a support matrix (spider). The spider is held in place by the open upper end of a pipe with a slightly smaller outer diameter than the inner diameter of the outer pressure vessel. This slightly smaller pipe extends up about 8 inches (20.3 cm) into the outer pressure vessel from the inner edge of the flange face to which the outer pressure vessel bottom flange attaches.

Due to changes in the element design, an evaluation of the loading on the fuel element spider was conducted. Appendix A of Reference 4.22 performed a detailed analysis of the load on the fuel element spider. This analysis shows that the load on the spider is the sum of: 1) the weight of the core in water, i.e., the weight of the core in air reduced by the weight of the volume of water that it displaces, and 2) the friction pressure drop force across the core due to coolant flow through the core. While the submerged weight of the HEU core is 73.9 lbf (33.5 kg), the LEU core weighs 187.9 lbf (85.2 kg) when fully submerged in water. The latter quantity affecting the load on the spider is the product of the friction pressure drop through the core and the total annular cross-sectional area between the inner and outer pressure vessels. The inner diameter of the outer pressure vessel is 11.80 inches (30 cm) and the outer diameter of the inner pressure vessel is 5.32 inches (13.5 cm), resulting in an annular area of 87.13 in² (562.13 cm²). For a total core flow rate of 3,750 gpm (14,195 lpm), a coolant inlet temperature of 120 °F (48.9 °C), and the reactor at zero power, the friction pressure drop is shown to be 14.20 psi (97.9 kPa) for the HEU core and 10.36 psi (71.4 kPa) for the LEU core. Thus, the friction pressure drop force is 1,237 lbf (= 14.20 psi × 87.13 in²) for the HEU core and 903.0 lbf (= 10.36 psi × 87.13 in²) for the LEU core. Hence, the total load on the spider is 1,311 (= 73.9 + 1237) lbf (594.7 kg) for the HEU core and 1,091 (= 187.9 + 903.0) lbf (494.9 kg) for the LEU core. Therefore, the load on the spider is reduced by 220 (1311 - 1091) lbf (99.8 kg) by replacing the HEU core with the LEU core.

4.3 Reactor Pool

There are no changes to this section as a result of LEU conversion.

4.4 Biological Shield

There are no changes to this section as a result of LEU conversion.

4.5 Nuclear Design

4.5.1 Control Worth and Excess Reactivity

4.5.1.1 Methodology

Reactor physics parameters, including core excess reactivity and control rod worths for the current HEU-fueled core and the proposed LEU core configurations were estimated by creating detailed core models and fuel depletion simulations. It was particularly important to demonstrate the ability to accurately predict safety margins. Furthermore, the current experimental flux levels and reaction rates for typical HEU weekly fuel cycles rather than for an all-fresh core configuration must be predicted so that confidence can be established for the models developed for the proposed LEU core analysis. Since the fuel depletion simulation scheme allows for the creation and tracking of all significant fission product inventories, core models with mixed-burnup fuel elements were used to evaluate the power distributions for critical states and calculate reactivity parameters.

The REBUS-DIF3D (Ref. 4.23) and WIMS-ANL (Ref. 4.24) reactor analysis programs, developed and maintained by the Argonne National Laboratory (ANL), as well as the standard Monte Carlo simulation program, MCNP, were used to perform neutronic calculations for fuel conversion analysis. A brief description of each computer code used is provided below.

WIMS-ANL: WIMS-ANL is a one-dimensional lattice physics code used to generate burnup dependent, multi-group cross sections. The code utilizes either 69- or 172-group libraries of cross-section data for 123 isotopes generated from ENDF-6. The 69-group library is typically used for research reactor analysis. A customized 10-group structure was developed based on the neutron spectrum that exists in the MURR core for collapsing cross-section data for actinides (Ref. 4.27), structural materials, explicit fission products, and a lumped fission product and stored in a library to be used by the REBUS-DIF3D code. The collapsed data were saved for several different regions within the fuel plates, as well as different structural regions because of the rapid spectrum changes. WIMS-ANL was also used to generate a 69-group lumped fission product library that represents fission products not explicitly represented in the MCNP libraries (Ref. 4.25). This multi-group data can be used in MCNP analyses of depleted cores.

REBUS-DIF3D: DIF3D is a three-dimensional, multi-group neutron diffusion code that can model systems in a number of geometries. REBUS is a depletion code that utilizes neutron fluxes from a neutronics solver (DIF3D) and cross-section data to solve isotopic transmutation calculations. A detailed Θ -R-Z diffusion MURR core model was developed for DIF3D (Ref. 4.23). The details of the DIF3D model were developed iteratively in order to match the diffusion calculations with MCNP analysis and with experiments. A REBUS model was created to perform extended single-cycle depletion ("straight rundown") of an all-fresh core, as well as a highly detailed simulation of the typical weekly operations at MURR with fuel shuffling between in-core and ex-core locations. The depleted core characteristics (such as plate-by-plate and axially-segmented atom densities) can be saved and passed on to MCNP for more detailed neutronics analyses.

MCNP: MCNP is a continuous energy Monte Carlo neutron transport code (Ref. 4.26). MCNP is capable of modeling the heterogeneous details of the MURR fuel elements, core structures, and

experimental facilities while capturing the rapidly changing spectra across these various regions. Using the 69-group lumped fission product library generated by WIMS-ANL, the code can be used to model cores of depleted as well as fresh elements. MCNP was used for all detailed calculations of core k-effective values, critical control blade positions and control blade worths, detailed power distributions, and experimental fluxes and reaction rates.

A summary of the code-suite scheme used for the analyses is shown in Figure 4.4; taken from Section 2.1 of Reference 4.28.

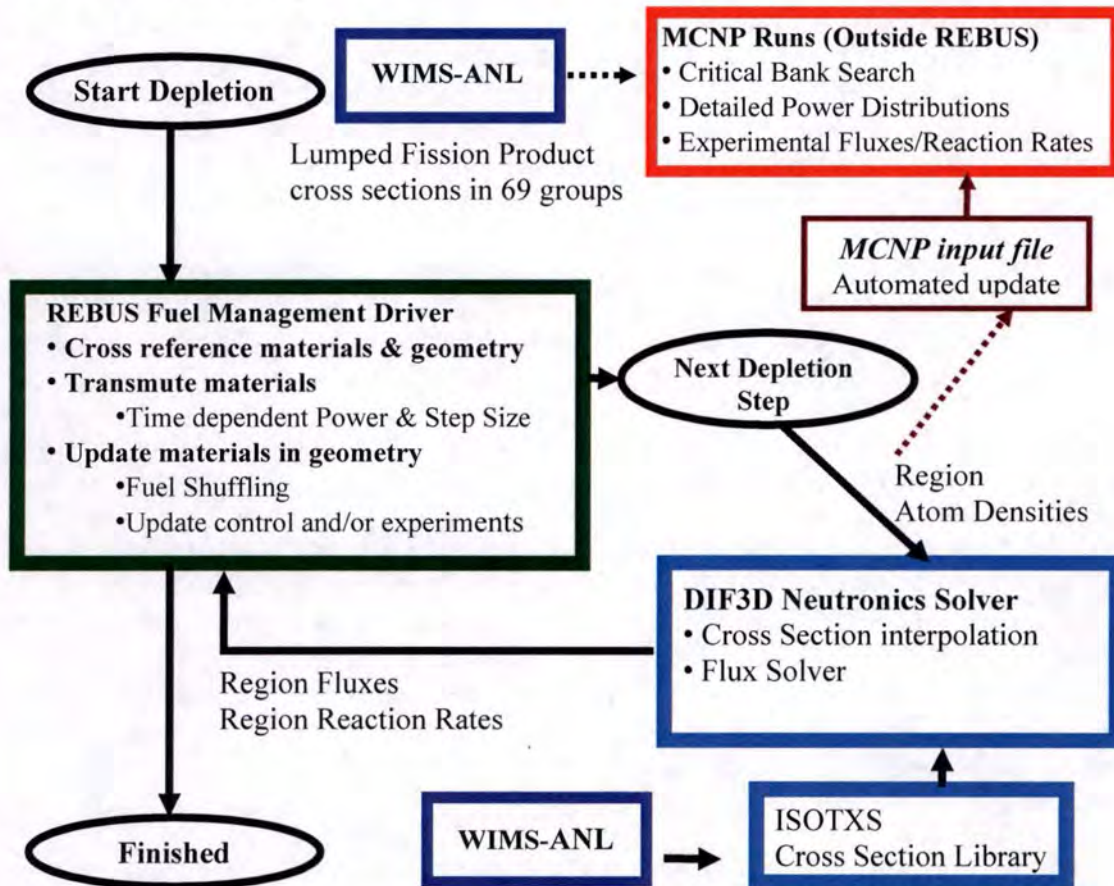


FIGURE 4.4
SUITE OF NEUTRON PHYSICS CODES USED FOR MURR ANALYSES

Extensive work was performed and documented in Section 2.2 of the Reference 4.28 to validate the neutron physics codes and models for application to the MURR. Experimental data for HEU fueled cores are available from two sources:

1. A 1971 report of startup physics tests was compiled by Caudle Julian for a core loaded with 8 fresh HEU fuel elements (Ref. 4.29). The report provided critical blade positions with several different flux trap configurations.

2. Measured “criticals” for the core loaded with mixed-burnup HEU fuel elements in the current reactor configuration are available. These critical measurements can be used to validate the models for cores with various total core fuel burnup and history of the shim blades.

The MCNP and REBUS-DIF3D models were benchmarked against these reference data. Results of the benchmark calculations are given in Reference 4.28.

4.5.1.2 Results

A comparison of the predicted straight run-down of core reactivity vs. fuel burnup, beginning with all-fresh fuel, is shown for the current MURR HEU and proposed LEU cores in Figure 4.5 below. The rundown results were calculated with REBUS-DIF3D. The figure shows that the beginning-of-cycle (BOC) excess reactivity for the HEU core is larger than the LEU core by ~2%. However, after the xenon-135 (^{135}Xe) saturation, an effectively slower loss of reactivity in the LEU core can be observed due to the approximately two times greater total ^{235}U loading and subsequent buildup of other fissile materials (notably ^{239}Pu) during operation. The HEU model bias based on a critical case reported in Reference 4.29 is $-0.5\% \Delta k/k$. Assuming this model bias at EOC, the EOC core burnup for the HEU and LEU cores is estimated from the curves to be 640 MWd and 770 MWd, respectively. The approximately 20% larger fuel burnup per LEU element, coupled with a 20% higher operating power for the LEU core, results in about the same number of fuel elements being used per year for the LEU core as with the current HEU core, assuming the same total operating hours per year. However, changes in core and experiment loading can affect the overall reactivity, which can also slightly affect the total number of fuel elements consumed per year.

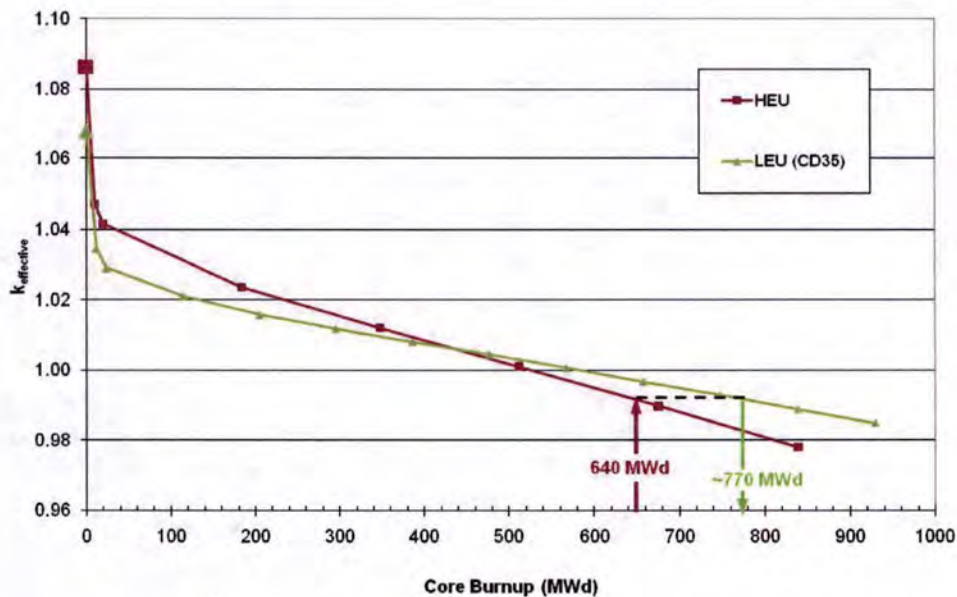


FIGURE 4.5
COMPARISON OF MURR FRESH CORE REACTIVITY VS. BURNUP
(CONTROL BLADES AT 23-INCHES WITHDRAWN; 2008 CORE FLUX TRAP AND
REFLECTOR CONDITIONS)

Depletion calculations are very important for the MURR fuel conversion analysis. A depletion capability was developed and benchmarked to MCNP and measurements using REBUS-DIF3D for both the current HEU core and the LEU CD35 core. Modeling the complex MURR fuel-shuffling sequence for a typical ("pseudo-equilibrium") core requires the evaluation of hundreds of state points. Afterwards, MCNP models were updated to include the depleted materials from REBUS-DIF3D to allow evaluations of measured critical states and demonstrate the overall accuracy of the fuel cycle simulations. Details of the REBUS-DIF3D HEU and LEU "pseudo-equilibrium" cycles are described in Section 2.2.3 of Reference 4.28.

Table 4-6 provides a comparison of core k-effective calculated by MCNP and DIF3D for fresh and depleted cores from the "pseudo-equilibrium" cycles. The results show very close agreement between the two codes for predicting the core k-effective, increasing confidence in the DIF3D diffusion theory model which is the basis for determining the depleted core compositions and demonstrating that the composition data can be correctly transferred from one model to the other.

TABLE 4-6
COMPARISON OF MCNP AND DIF3D CORE K-EFFECTIVE FOR HEU AND LEU CORES

Fuel	Condition		Blade Position (inches withdrawn)		MCNP k_{eff}	DIF3D k_{eff}	Difference ($\Delta k/k$)
			Shim blade	Regulating blade			
HEU	All Fresh	No Xe	23.0	13.4 ¹	1.08360 ± 12 pcm	1.08630	0.23%
HEU	Mixed ²	No Xe	17.8	10	1.00022 ± 10 pcm	1.00002	-0.02%
HEU	Mixed ²	Eq Xe	24.0	15	0.99983 ± 10 pcm	1.00019	0.04%
LEU	All Fresh	No Xe	23.0	13.4 ¹	1.06689 ± 11 pcm	1.06793	0.09%
LEU	Mixed ³	No Xe	17.6	10	1.00008 ± 8 pcm	1.00010	0.002%
LEU	Mixed ³	Eq Xe	24.3	15	1.00001 ± 10 pcm	0.99918	-0.08%

¹ Regulating blade position for all fresh core calculations is at core mid-plane.

² Week 58 of HEU fuel cycle simulation.

³ Week 76 of LEU (CD35) fuel cycle simulation.

Summary results of the excess reactivity and differential and integral blade worths for fresh and depleted HEU and LEU cores calculated by MCNP with non-depleted control blade models are given in Tables 4-7 and 4-8, and Figure 4.6, below. Table 4-7 compares the hot and cold Core Excess Reactivities. Here it can be seen that the excess reactivity of the LEU core is smaller than the HEU core, as was expected due to the presence of a significant amount of non-fissile ²³⁸U in the LEU core.

TABLE 4-7
SUMMARY OF CORE EXCESS REACTIVITY

Simulated Core Excess Reactivity:	HEU Fresh Core	HEU Mixed Core	LEU Fresh Core	LEU Mixed Core
¹ Hot Excess Reactivity (% $\Delta k/k$)	8.5	4.0	7.0	3.6
² Cold Excess Reactivity (% $\Delta k/k$)	8.6	4.1	7.0	3.6
Cold Reactivity with All Blades In (% $\Delta k/k$)	-11.6	-17.2	-10.0	-14.0

¹Hot conditions are for 10 MW operations with HEU fuel, 12 MW operations with LEU fuel.

²Cold conditions are isothermal after forced convection pumps are running (increased pressure in coolant channels increases moderator density relative to stagnant state).

The reactivity worth of the entire control bank was calculated with MCNP for HEU-fueled and LEU-fueled cores under different core burnup conditions. The calculated control bank differential worth curves for fresh control blades are provided in Figure 4.6. The control blade withdrawal rate in MURR is 1 inch/minute. Using the control bank worth curves in Figure 4.6 and the blade withdrawal rate, the calculated maximum reactivity insertion from control bank withdrawal is 0.00027 $\Delta k/k/s$ for HEU-fueled cores and 0.00023 $\Delta k/k/s$ for LEU-fueled cores. These values meet the MURR Technical Specification requirement that the total reactivity insertion rate from blade withdrawal is less than 0.00030 $\Delta k/k/s$.

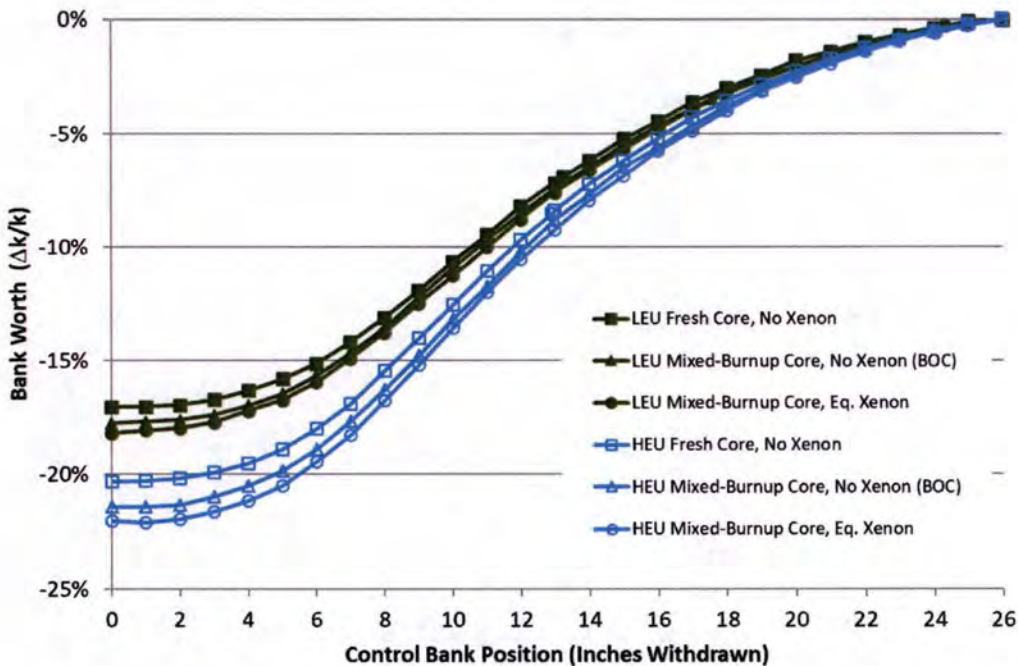


FIGURE 4.6
MURR CONTROL BANK WORTH CURVES (CALCULATED)

Integral control blade worths for fresh (non-depleted) control blades for all-fresh and typical mixed-burnup HEU cores and for the proposed LEU cores are given in Table 4-8 below. As with the core excess reactivity values, the total control rod worth for the LEU core configurations are also smaller than those for similar HEU configurations. The control bank worth for the LEU-fueled cores is about 3.5% $\Delta k/k$ lower than for the HEU-fueled cores. The smaller control rod worth can be directly attributed to the harder neutron spectrum in the LEU core due to the presence of the larger amount of ^{238}U . The excess reactivity, however, is also smaller for the LEU core, as was shown in Table 4-7. It is shown in Section 4.5.2 that the reduced control rod worth in the LEU cores is sufficient to meet the minimum shutdown margin requirement for MURR. Likewise, the total bank worth is sufficiently large to compensate for any credible reactivity insertion accidents postulated for MURR.

TABLE 4-8
SUMMARY OF CONTROL BLADE BANK WORTH COMPARISON

Simulated Core Rod Worth:	HEU Fresh Core	HEU Mixed Core No Xe	HEU Mixed Core Eq. Xe	LEU Fresh Core	LEU Mixed Core No Xe	LEU Mixed Core Eq. Xe
Total Bank Worth at Cold Conditions ($\Delta k/k$)	-20.3%	-21.5%	-22.1%	-17.0%	-17.7%	-18.2%

The previous results are based on models which utilized only non-depleted (fresh) control blades. Additional improvements were made to the MURR MCNP model by factoring in the effect of control blade depletion on typical HEU critical states. Depleted control blade models, reported in References 4.28 and 4.30, were incorporated in the HEU critical state models to predict the critical blade heights. The results were then compared against measured critical blade heights for a number of startup experiments with control blades with different in-cycle histories of up to 1,850 in-cycle days. It is observed that the computed k-effectives for actual critical blade heights are predicted within 0.5% $\Delta k/k$. This adds further credibility to the models used for studying the feasibility of the LEU core.

The MCNP predictions of core excess reactivity with the effect of depleted control blades are presented in Table 4-9.

TABLE 4-9
SUMMARY OF CORE EXCESS REACTIVITY WITH DEPLETED CONTROL BLADE EFFECTS

Simulated Core Cold Excess Reactivity ($\% \Delta k/k$)	HEU Fresh Core	HEU Mixed Core	LEU Fresh Core	LEU Mixed Core
Blades B&C Fresh; Blades A&D 8-years depleted	8.7%	4.2%	7.2%	3.7%
All Blades 8-years depleted	8.8%	4.4%	7.3%	3.8%

4.5.2 Shutdown Margin

The Technical Specifications for the present HEU-fueled MURR core requires a shutdown margin of $> 2\% \Delta k/k$ with the most reactive control blade and regulating blade fully withdrawn.

To ensure the safe shutdown of the proposed MURR LEU core, comparison studies were done for the present HEU and the proposed LEU core. MCNP calculations were performed to estimate the shutdown margins of both the HEU and the LEU cores with fresh BORAL[®] in each control blade model. However, the worst-case fuel power peaking conditions where control blade depletion is concerned, is one where there is a pair of depleted blades and a pair of fresh blades surrounding the core. Consequently, the MCNP predictions of shutdown margin with the effect of depleted control blades are also presented in Table 4-10.

For the predictions with all-fresh control blades, the shutdown margins for the LEU cores are less than the HEU cores. However, it can be seen from Table 4-10 with the current reflector elements and utilization that the shutdown margin even for the limiting LEU case, i.e., all-fresh core, is still larger than the minimum value required by the Technical Specifications by 1.9%. Significant changes in the reflector utilization could make this not true. Fuel burnup and poison buildup during reactor operation will decrease the core excess reactivity and increase the shutdown margins.

For the shutdown margin predictions which include the effect of control blade depletion, a decrease in its value is consistent with increasing the average runtime on the control blades. This is shown in Table 4-10. Similar trends are observed both for the HEU and LEU cores. The smallest shutdown margin of 3.1% is seen for the fresh LEU case with all control blades at the end of their useable cycle. Even in this case, the shutdown margin requirement for MURR is met. Lastly, since the sum of the magnitudes of the reactivity worths of all unsecured experiments in the reactor must be less than $0.6\% \Delta k/k$, the above shutdown margin is enough to ensure safe reactor shutdown even in the case of simultaneous ejection of all unsecured experiments in the reactor.

TABLE 4-10
MINIMUM SHUTDOWN MARGINS WITH DEPLETED CONTROL BLADE EFFECTS

Simulated Core Cold Minimum Shutdown Margin (%$\Delta k/k$)	HEU Fresh Core	HEU Mixed Core	LEU Fresh Core	LEU Mixed Core
All Blades Fresh	4.2%	9.3%	3.9%	7.6%
Blades B&C Fresh; Blades A&D 8-years Depleted	3.8%	8.8%	3.4%	7.2%
All Blades 8-years Depleted	3.4%	8.5%	3.1%	6.9%

4.5.3 Other Core Physics Parameters

The void and temperature reactivity feedback coefficients for the typical HEU cores were derived from measurements in Reference 4.29 and detailed MCNP calculations. A detailed study and validation of the MCNP methodology for calculating the feedback coefficients was conducted in Reference 4.28. Experiments reported in Reference 4.29 measured the primary coolant isothermal

temperature coefficient for an all-fresh HEU core at conditions which existed in the MURR in 1971. The values were reported as a range between -4.4×10^{-5} to $-11.9 \times 10^{-5} \Delta k/k/^\circ F$. This configuration was modeled in MCNP to include changes in the moderator/coolant density and temperature, as well as flux trap and reflector sample loadings at the time of the experiment. Based on this effort to replicate the experiment with an MCNP calculation, the isothermal coolant temperature coefficient was calculated to be $-13.4 \times 10^{-5} \Delta k/k/^\circ F$. The temperature mesh of the ENDF/B VI.0 $S(\alpha, \beta)$ data sets used to adjust neutron scattering behavior in the MCNP models are quite coarse (Refs. 4.31, 4.26) and could be refined to improve the results of the calculations relative to the measurements. Nonetheless, the calculated value is near the range of the experimentally measured values.

A similar approach in MCNP was used to calculate and validate the HEU and LEU primary coolant and fuel temperature coefficients and coolant void coefficient. The reactivity coefficients were calculated by making small perturbations to the appropriate reactor conditions in MCNP. Reactivity coefficients were calculated for three different core states for each fuel type (HEU and LEU): 1) all fresh fuel, 2) a typical mixed-burnup core loading at beginning-of-cycle (BOC) with no xenon, and 3) a typical mixed-burnup core loading at equilibrium xenon conditions. The comparison between the HEU and LEU is shown in Table 4-11.

The reactivity coefficient for a range of percent coolant void from 0% - 5% were calculated. Benchmarks for the HEU cases were made to the MURR 1971 measurements and reported in Reference 4.29. For the largest void fraction range studied (i.e., up to 5%), it is observed that the calculated void coefficient for the HEU core has slightly more negative values than the LEU core by $\sim 10\%$ for the all-fresh core and 5% - 7% for the mixed-fuel cores. The smallest magnitude for the coolant void coefficient is -2.36×10^{-3} and $-2.33 \times 10^{-3} \Delta k/k/\% \text{-void}$ for the HEU and LEU cores, respectively. These values are more negative than the Technical Specification requirement for MURR of $-2.0 \times 10^{-3} \Delta k/k/\% \text{-void}$.

The calculated coolant temperature coefficient is much less negative (about 60% smaller) for LEU fuel. However, the values reported for the LEU cores show an increase in negative reactivity (i.e., more negative reactivity feedback) with fuel temperature increase, which will provide an inherent feedback mechanism in the event of reactor transients.

The MURR Technical Specifications require that the reactor temperature coefficient be more negative than $-6 \times 10^{-5} \Delta k/k/^\circ F$. The reactor temperature coefficient accounts for the core operating conditions that simultaneously affect fuel temperature, coolant temperature, and coolant density. The reactor temperature coefficient defined in this manner was calculated by combining the reactivity effect of an isothermal coolant and fuel temperature increase of $1^\circ F$ and the reactivity effect of the coolant density reduction associated with the same temperature increase. The temperature coefficients in Table 4-11 were calculated for changes to the coolant or fuel temperature only. The coolant void coefficients in Table 4-11 were calculated assuming a perturbation of the coolant density only. The reactivity effect contributed by coolant voiding under isothermal conditions was computed based on the inversely proportional relationship between coolant temperature and density. At the pressure and temperature conditions that are typical of the coolant in the MURR primary system, a temperature increase of $1^\circ F$ will result in a 0.026% reduction in the coolant density. Consequently, the reactivity effect of the coolant voiding

associated with a 1 °F increase in the coolant temperature can be computed by multiplying the coolant void fractions in Table 4-11 by 0.026. This reactivity effect was added to the summation of the coolant and fuel temperature coefficients. The worst-case combination of all these effects which yields the smallest magnitude reactivity effect was assumed in the computation. The minimum isothermal temperature coefficient calculated in this manner is -9.7×10^{-5} and $-7.8 \times 10^{-5} \Delta k/k/^\circ F$ for the HEU and LEU fuel, respectively. The HEU and LEU fuel are both found to meet the Technical Specification requirement.

TABLE 4-11
COMPARISON OF TEMPERATURE AND VOID REACTIVITY COEFFICIENTS
BETWEEN HEU AND LEU

Simulated Core	HEU			LEU		
	Fresh	Mixed-Burnup Core		Fresh	Mixed-Burnup Core	
	No Xe	No Xe	Eq. Xe	No Xe	No Xe	Eq. Xe
Coolant Void Coefficient ($\Delta k/k/\%$ void)						
0 to 0.5% void	-3.18E-03	-2.76E-03	-2.36E-03	-3.04E-03	-2.76E-03	-2.42E-03
0.5 to 1.0% void	-3.23E-03	-2.88E-03	-2.42E-03	-2.93E-03	-2.65E-03	-2.33E-03
1.0 to 5.0% void	-3.33E-03	-2.91E-03	-2.58E-03	-3.04E-03	-2.77E-03	-2.41E-03
Coolant Temperature Coefficient ($\Delta k/k/^\circ F$)						
69 to 170 °F	-2.33E-05	-3.30E-05	-3.55E-03	-0.72E-05	-1.19E-05	-1.35E-05
Fuel Temperature Coefficient ($\Delta k/k/^\circ F$)						
69 to 260 °F				-4.43E-06	-3.91E-06	-4.22E-06
260 to 440 °F				-1.15E-05	-1.13E-05	-1.07E-05
440 to 620 °F				-1.10E-05	-1.07E-05	-1.05E-05

The reactor kinetics parameters were calculated using the kinetics option in MCNP. As shown in the Table 4-12 below, the delayed neutron fraction (β_{eff}) is a slightly smaller value for the LEU-fueled core relative to HEU (i.e., less than 0.02% change), while the neutron lifetime (Λ) is shorter by about 25% in the harder spectrum of LEU fuel.

The core physics parameters presented in this section change with LEU conversion due to several factors. These changes are due to the different fraction of fissions occurring in uranium or plutonium, and to a lesser extent the difference in discharge burnup due to the higher operating power. All the core physics parameters were calculated based on fuel cycle simulations and so therefore include the impacts of all actinides produced.

TABLE 4-12
COMPARISON OF DELAYED NEUTRON FRACTIONS AND PROMPT NEUTRON
LIFETIMES

	HEU Fresh	HEU Mixed Core No Xe	HEU Mixed Core Eq. Xe	LEU Fresh	LEU Mixed Core No Xe	LEU Mixed Core Eq. Xe
Effective Delayed Neutron Fraction ¹	0.80%	0.79%	0.78%	0.79%	0.77%	0.77%
Prompt Neutron Lifetime (μ s) ¹	49.5	57.8	62.1	38.7	43.8	47.9

¹No Xe, I, or Sm for fresh cores; Sm per prior depletion history for mixed cores. Typical samples loaded in flux trap; k_{eff} for MCNP calculations had $\sigma \leq 4$ pcm; consequently, reactivity coefficients reported have $\sigma < 6\%$.

Actinide isotopic inventories from REBUS-DIF3D fuel cycle simulations for both HEU and LEU cores list the plutonium inventory for an element about to be discharged at end-of-life. The plutonium inventory includes ^{238}Pu , ^{239}Pu , ^{240}Pu , ^{241}Pu and ^{242}Pu . Since the ^{238}U isotopic loading is significantly higher in LEU cores, this impacts the plutonium inventory. An LEU fuel element that is at the discharge burnup (i.e., at 180 MWd) with no decay is shown to have approximately 26 grams of plutonium of various isotopes. In comparison, for an HEU fuel element at the discharge burnup (i.e., 150 MWd), with no decay, 1 gram of plutonium is produced. Approximately 91 wt. % of the plutonium mass is ^{239}Pu for the LEU fuel element as compared to 83 wt. % for the HEU. Table 4-13 shows a detailed comparison of the plutonium inventory between the HEU and LEU fuel elements at the discharge burnup.

The effect of the changes to the above reactor physics parameters on the stability and safety of the reactor operation and the behavior of the reactor during anticipated transients are studied and reported in Chapter 13.

4.5.4 Operating Conditions

The goal of the proposed MURR LEU fuel conversion is to design and build a LEU core that can be operated safely and at the same time maintain the experimental and irradiation performance of the present HEU core. Analyses have shown that this can be achieved with the proposed LEU core design provided the reactor power level is uprated from the current 10 MW. A power uprate to 12 MW is sufficient to meet the current HEU experimental performance levels while using the same number of fuel elements needed per year to maintain the reactor's weekly operating schedule. The dynamic design is expected to leave the MURR with minimal changes in the overall reactor operations compared to the present HEU core.

REBUS-DIF3D (Ref. 4.23) simulations of the operational fuel cycle for the proposed LEU core were validated against similar models done for the current MURR HEU fuel cycle. The HEU fuel cycle simulations were benchmarked against data collected from the current HEU fuel cycle. In the current scheme, the typical targeted discharge burnup for the HEU fuel elements is 150 MWd. About 22 elements are consumed every year. Results from the HEU fuel cycle simulation predicted a discharge burnup of 149 MWd and about 22.1 elements per year. Using the same

approach, the predictions for the LEU core at 12 MW has a discharge burnup of 180 MWd and uses 21.9 elements per year. A summary of the important fuel cycle characteristics for HEU and LEU cores are provided in Table 4-14.

TABLE 4-13
DISCHARGE ISOTOPES IN MURR HEU AND LEU FUEL CYCLE SIMULATIONS
(DATA ARE AT END OF IRRADIATION AND DO NOT INCLUDE ANY POST-IRRADIATION DECAY)

	HEU	LEU (CD35)
Element State	Maximum HEU Discharge Burnup in Fuel Cycle	Maximum LEU Discharge Burnup in Fuel Cycle
Burnup (MWd)	149.94	180.26
Mass (g)		
All HM	675.6	7440.8
U	673.9	7412.9
Pu	1.003	26.437
U-235	586.7	1285.3
Pu-238	0.046	0.091
Pu-239	0.834	24.065
Pu-240	0.090	1.752
Pu-241	0.031	0.508
Pu-242	0.002	0.022
Fraction in Pu (wt. %)		
Pu-238	4.60%	0.34%
Pu-239	83.14%	91.03%
Pu-240	8.98%	6.63%
Pu-241	3.09%	1.92%
Pu-242	0.20%	0.08%

TABLE 4-14
CURRENT AND PROPOSED MURR FUEL CYCLE OPERATING CHARACTERISTICS

Parameter	Current HEU Fuel	Proposed LEU Fuel (CD35)
Maximum burnup:	150 MWd/element due to insufficient excess reactivity < 1.6E+21 peak fissions/cc burnup (i.e., < 43 at% U5 peak burnup) HEU Technical Specification limit is 2.3E+21 peak fissions/cc	180 MWd/element due to insufficient excess reactivity < 3.4E+21 peak fissions/cc burnup (i.e., < 44 at% U5 peak burnup)
EOC Core MWd (control blades full out):	~640 MWd core with equilibrium xenon	~765 MWd core with equilibrium xenon
Refuelings:	Weekly – replace all eight fuel elements; fuel elements are used in 18-20 core loadings to achieve 145 to 150 MWd burnup at 10 MW	Weekly – replace all eight fuel elements; fuel elements are used in about 18-20 core loadings to achieve ~180 MWd burnup at 12 MW
Fuel Cycle:	22 elements used per year at 10 MW 32 fuel elements in active fuel cycle	22 elements used per year at 12 MW 32 fuel elements in active fuel cycle

The peak fission density burnup of the HEU fuel is limited by the TS at 2.3×10^{21} fissions/cm³. The peak local HEU burnup estimated from the fuel cycle simulation is 1.54×10^{21} fissions/cm³ – well below the TS limit. In the REBUS-DIF3D depletion modeling, the fuel was depleted plate-by-plate in 12 axial segments. The fuel was not subdivided azimuthally for the depletion calculations. In order to account for the influence of the azimuthal power shape on the burnup, the azimuthal peaking factors by plate calculated by the detailed MCNP power distribution calculations were applied to the fission density. For the U-10Mo fuel form that will be utilized for the LEU fuel elements, the calculated plate-specific peak fission density in the MURR fuel cycle is 3.37×10^{21} fissions/cm³, corresponding to 43.5 atom-percent burnup relative to the initial ²³⁵U in the fuel. The calculated fission density includes fissions from all fissionable species.

4.5.4.1 Experimental Performance

The conversion of the MURR from HEU to LEU fuel will affect experimental fluxes. The effects were examined by calculating flux and reaction rate predictions in a number of important experimental locations for several core states. For a detailed comparison of neutron flux spectra and spatial distribution performances in various irradiation positions, 'typical' mixed-fuel core configurations were chosen from the simulated HEU fuel cycle to be benchmarked. For the typical HEU core case at 10 MW, the reaction rates for various isotopes and fluxes are benchmarked and reported to be within 5% of measurements by Peters et al. (Ref. 4.32).

To compare the experimental performance of the LEU core, a typical core was chosen to be a case at a similar stage to that of the HEU. Based on current and projected MURR utilization, the following three experimental locations were selected for comparing the effect of an HEU to LEU fuel conversion.

- Center Test Hole (Flux Trap) Irradiation Positions:

The current unperturbed peak thermal flux in the flux trap region is 6×10^{14} n/cm²-sec, whereas the peak fast flux (> 1.0 MeV) is 6×10^{13} n/cm²-sec. Detailed 2 group and 69 group tallies in MCNP were used to compare HEU and LEU values of:

- Flux in Flux Trap (FT) tube B, 18-21 inches above bottom of holder, where a sulfur bearing sample can was modeled for P-33 production;
- Flux and S-32 (n,p) P-32 reaction rate in FT tube B, 13-15 inches above bottom of holder, where a sulfur bearing sample can was modeled for P-32 production via the fast threshold reaction;
- Flux and reaction rates of Ir-191 (n, γ) and Ir-193 (n, γ) in FT tube C, 17-20 inches above bottom of holder, where Ir wires were explicitly modeled in an aluminum holder; and
- Flux in FT tube B, 6-8 inches above bottom of holder, where a BaCO sample was modeled for Cs production.

- Graphite Reflector Region Irradiation Positions:

The graphite reflector region has a number of sample positions that are used to irradiate various sample materials. The average measured value of thermal flux can vary from approximately 1×10^{13} n/cm²-sec to 1×10^{14} n/cm²-sec. Detailed 2 group and 69 group tallies in MCNP were used to compare HEU and LEU values of:

- Flux in the bottom three (3) inches of Graphite Reflector Element No. 3, Row 1 Pneumatic Tube (P-tube); and
- Flux and Si-30 (n, γ) reaction rate in the Green 5 irradiation location, where a 5-inch diameter silicon sample was modeled.

- Beamports:

There are four (4) radial and two (2) radial-tangential beamports. The measured thermal and epithermal beams emerging from the beam tubes at the outside surface of the biological shield are approximately 9×10^9 n/cm²-sec and 2.7×10^8 n/cm²-sec, respectively. Detailed tallies in MCNP were used to compare HEU and LEU values of:

- The 47 group outbound current at a plane bisecting beam tube 'E' at the radius of the inner wall of the reflector tank (i.e., beyond the outer edge of the graphite reflector). Outbound current was defined as current in a direction within the outbound half-space.

The 69 group tallies were made for the energy group structure of the WIMS-ANL libraries. The 47 group spectrum of the beam tube 'E' currents was specified by a key experimentalist.

Neutron fluxes and reaction rates were calculated for the reference cores described in Section 4.5.4.2. The cores were Week 58 of the HEU simulation and Week 76 of the LEU simulation. Both the beginning-of-week core at Day 0 (i.e., no Xe, lower control blades) and the same core depleted to Day 2 (equilibrium Xe, higher control blades) were examined.

Table 4-15 summarizes the ratio of LEU fluxes and reaction rates at 10 MW and 12 MW to HEU at 10 MW for the critical state at the beginning of the week, labeled Day 0. Table 4-16 presents the same comparisons after equilibrium Xe, at Day 2, of the week. Figures 4.7 and 4.8 illustrate the ratio of LEU 47 group outbound currents in beam tube 'E' at 10 MW and 12 MW to HEU at 10 MW for Day 0 and Day 2. Figures 4.9 through 4.12 show the 69-group comparison of fluxes and reaction rates.

The thermal neutron flux (< 1 eV neutron energy) is most important for the mission of a research reactor like MURR. It is clear from the tables and figures that the flux and reaction rate losses would exceed 10% if the power level of 10 MW is maintained for LEU operation. However, an uprate to 12 MW would provide modest benefit for all of the fluxes and reaction rates tallied. In the same irradiation channels, the thermal neutron fluxes (i.e., ≤ 1.0 eV) generally range from 5% - 7% larger than the HEU case, while the fast neutron fluxes range from 9% - 13% larger. As expected, there is less softening of the spectra as flux distributions extends from the core out into the reflector regions for the LEU core.

Solely based on experimental performance, the conversion of MURR using the proposed LEU fuel element is feasible at 12 MW.

TABLE 4-15
COMPARISON OF DAY 0 LEU FLUXES AND REACTION RATES TO HEU⁴

Metric	Neutron Energy Range		
	≤ 1 eV	> 1 eV	Sum
LEU 10 MW Week 76 Day 0 (no Xe), Critical Bank 17.567 inches withdrawn, Reg. Blade 10 inches withdrawn			
Flux ¹ in FT Tube B ² 18-21 inches	87% $\pm 0.1\%$	93% $\pm 0.1\%$	90% $\pm 0.1\%$
S-32 (n,p) Reactions ³ in FT Tube B 13-15 inches	N/A	94% $\pm 0.2\%$	94% $\pm 0.2\%$
Flux in FT Tube B 13-15 inches	88% $\pm 0.1\%$	94% $\pm 0.1\%$	91% $\pm 0.1\%$
Ir-191 (n, γ) Reactions in FT Tube C 17-20 inches	88% $\pm 0.3\%$	93% $\pm 1.5\%$	88% $\pm 0.3\%$
Ir-193 (n, γ) Reactions in FT Tube C 17-20 inches	88% $\pm 0.3\%$	98% $\pm 2.1\%$	90% $\pm 0.6\%$
Flux in Ir Wires of FT Tube C 17-20 inches	88% $\pm 0.3\%$	94% $\pm 0.4\%$	92% $\pm 0.3\%$
Flux in FT Tube B 6-8 inches	88% $\pm 0.1\%$	93% $\pm 0.1\%$	90% $\pm 0.1\%$
Flux in Reflector Element No. 3, Row 1, P- Tube Bottom 3 inches	87% $\pm 0.1\%$	93% $\pm 0.2\%$	89% $\pm 0.1\%$
Si-30 (n, γ) Reactions in Green 5 Position	89% $\pm 0.0\%$	93% $\pm 1.5\%$	89% $\pm 0.2\%$
Flux in Green 5 Sample Position	89% $\pm 0.0\%$	92% $\pm 0.1\%$	90% $\pm 0.0\%$
LEU 12 MW Week 76 Day 0 (no Xe), Critical Bank 17.567 inches withdrawn, Reg. Blade 10 inches withdrawn			
Flux ¹ in FT Tube B ² 18-21 inches	105% $\pm 0.1\%$	110% $\pm 0.1\%$	106% $\pm 0.1\%$
S-32(n,p) Reactions ³ in FT Tube B 13-15 inches	N/A	114% $\pm 0.3\%$	114% $\pm 0.3\%$
Flux in FT Tube B 13-15 inches	105% $\pm 0.1\%$	113% $\pm 0.1\%$	109% $\pm 0.1\%$
Ir-191(n, γ) Reactions in FT Tube C 17-20 inches	106% $\pm 0.4\%$	111% $\pm 1.8\%$	105% $\pm 0.4\%$
Ir-193 (n, γ) Reactions in FT Tube C 17-20 inches	106% $\pm 0.4\%$	112% $\pm 2.4\%$	106% $\pm 0.7\%$
Flux in Ir Wires of FT Tube C 17-20 inches	106% $\pm 0.4\%$	111% $\pm 0.5\%$	108% $\pm 0.3\%$
Flux in FT Tube B 6-8 inches	106% $\pm 0.1\%$	113% $\pm 0.1\%$	110% $\pm 0.1\%$
Flux in Reflector Element No. 3, Row 1, P- Tube Bottom 3 inches	105% $\pm 0.1\%$	109% $\pm 0.2\%$	104% $\pm 0.1\%$
Si-30 (n, γ) Reactions in Green 5 Position	106% $\pm 0.1\%$	110% $\pm 1.7\%$	105% $\pm 0.2\%$
Flux in Green 5 Sample Position	107% $\pm 0.0\%$	109% $\pm 0.1\%$	106% $\pm 0.0\%$

¹ Fluxes were compared as n/s/cm².

² Axial positions noted as inches above bottom of flux trap sample holder.

³ Reaction rates were compared as Reactions/s.

⁴ HEU is 10 MW Week 58 Day 0 (no Xe); Critical Bank height: 17.809" withdrawn; Regulating Blade height: 10 inches withdrawn.

TABLE 4-16
COMPARISON OF DAY 2 LEU FLUXES AND REACTION RATES TO HEU⁴

Metric	Neutron Energy Range		
	≤ 1 eV	> 1 eV	Sum
LEU 10 MW Week 76 Day 2 (eq. Xe), Critical Bank 24.314 inches withdrawn, Reg. Blade 15 inches withdrawn			
Flux ¹ in FT Tube B ² 18-21 inches	87% \pm 0.1%	93% \pm 0.1%	90% \pm 0.1%
S-32 (n,p) Reactions ³ in FT Tube B 13-15 inches	N/A	93% \pm 0.3%	93% \pm 0.3%
Flux in FT Tube B 13-15 inches	86% \pm 0.1%	93% \pm 0.1%	90% \pm 0.1%
Ir-191(n, γ) Reactions in FT Tube C 17-20 inches	87% \pm 0.3%	94% \pm 1.5%	87% \pm 0.3%
Ir-193 (n, γ) Reactions in FT Tube C 17-20 inches	87% \pm 0.3%	94% \pm 2.0%	89% \pm 0.6%
Flux in Ir Wires of FT Tube C 17-20 inches	87% \pm 0.3%	92% \pm 0.4%	91% \pm 0.3%
Flux in FT Tube B 6-8 inches	87% \pm 0.1%	91% \pm 0.1%	88% \pm 0.1%
Flux in Reflector Element No. 3, Row 1, P- Tube Bottom 3 inches	88% \pm 0.1%	93% \pm 0.2%	89% \pm 0.1%
Si-30(n, γ) Reactions in Green 5 Position	89% \pm 0.0%	92% \pm 1.4%	89% \pm 0.1%
Flux in Green 5 Sample Position	89% \pm 0.0%	92% \pm 0.1%	90% \pm 0.0%
LEU 12 MW Week 76 Day 2 (eq. Xe), Critical Bank 24.314 inches withdrawn, Reg. Blade 15 inches withdrawn			
Flux ¹ in FT Tube B ² 18-21 inches	105% \pm 0.1%	112% \pm 0.1%	108% \pm 0.1%
S-32 (n,p) Reactions ³ in FT Tube B 13-15 inches	N/A	112% \pm 0.3%	112% \pm 0.3%
Flux in FT Tube B 13-15 inches	104% \pm 0.1%	111% \pm 0.1%	107% \pm 0.1%
Ir-191(n, γ) Reactions in FT Tube C 17-20 inches	105% \pm 0.4%	112% \pm 1.8%	105% \pm 0.4%
Ir-193(n, γ) Reactions in FT Tube C 17-20 inches	105% \pm 0.4%	113% \pm 2.4%	107% \pm 0.7%
Flux in Ir Wires of FT Tube C 17-20 inches	105% \pm 0.4%	111% \pm 0.5%	109% \pm 0.3%
Flux in FT Tube B 6-8 inches	104% \pm 0.1%	110% \pm 0.1%	106% \pm 0.1%
Flux in Reflector Element No. 3, Row 1, P- Tube Bottom 3 inches	105% \pm 0.1%	111% \pm 0.2%	107% \pm 0.1%
Si-30 (n, γ) Reactions in Green 5 Position	107% \pm 0.0%	111% \pm 1.7%	107% \pm 0.2%
Flux in Green 5 Sample Position	107% \pm 0.0%	111% \pm 0.1%	108% \pm 0.0%

¹ Fluxes were compared as n/s/cm².

² Axial positions noted as inches above bottom of flux trap sample holder.

³ Reaction rates were compared as Reactions/s.

⁴ HEU is 10 MW Week 58 Day 0 (no Xe); Critical Bank height: 17.809 inches withdrawn; Regulating Blade height: 10 inches withdrawn.

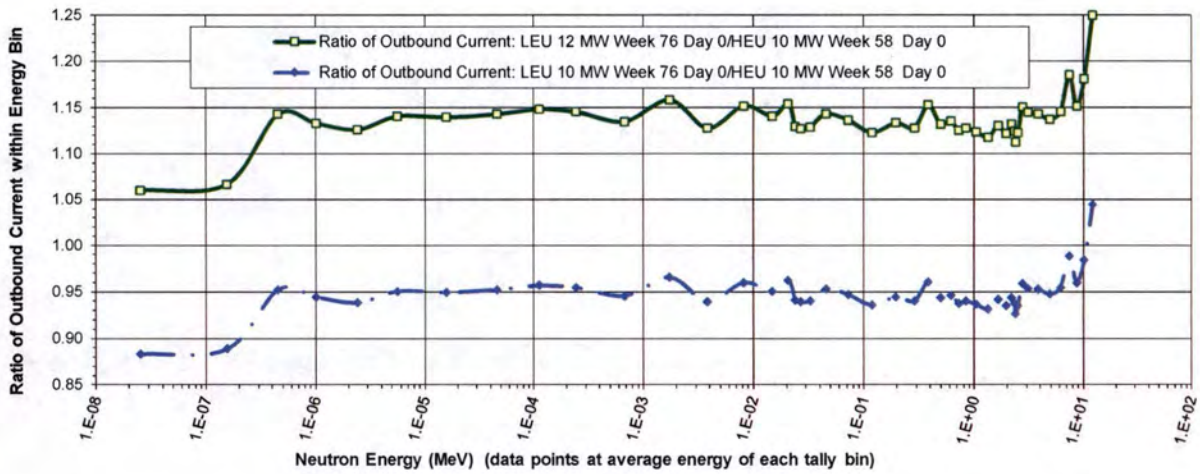


FIGURE 4.7
COMPARISON OF LEU AND HEU BEAMPORT 'E' OUTBOUND CURRENT AT DAY 0

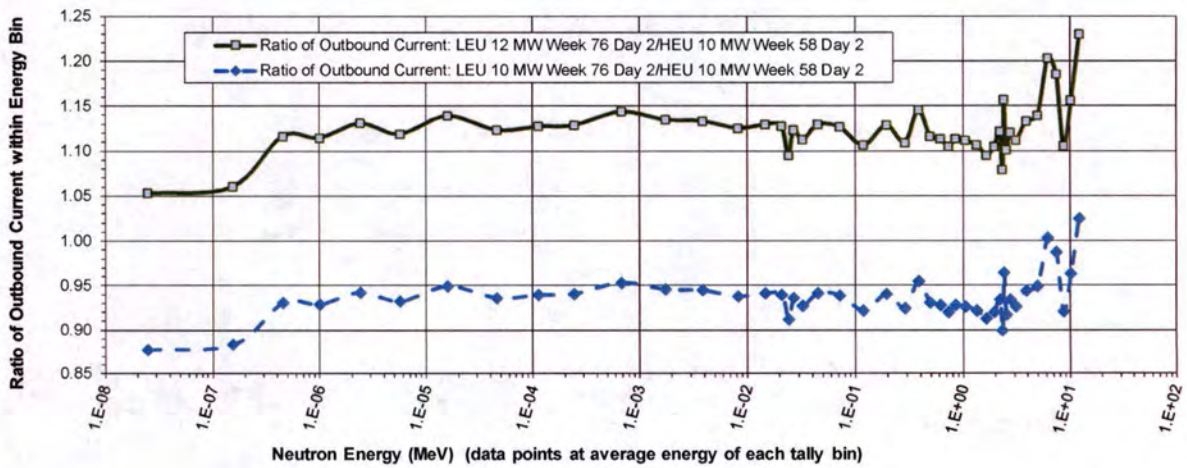


FIGURE 4.8
COMPARISON OF LEU AND HEU BEAMPORT 'E' OUTBOUND CURRENT AT DAY 2

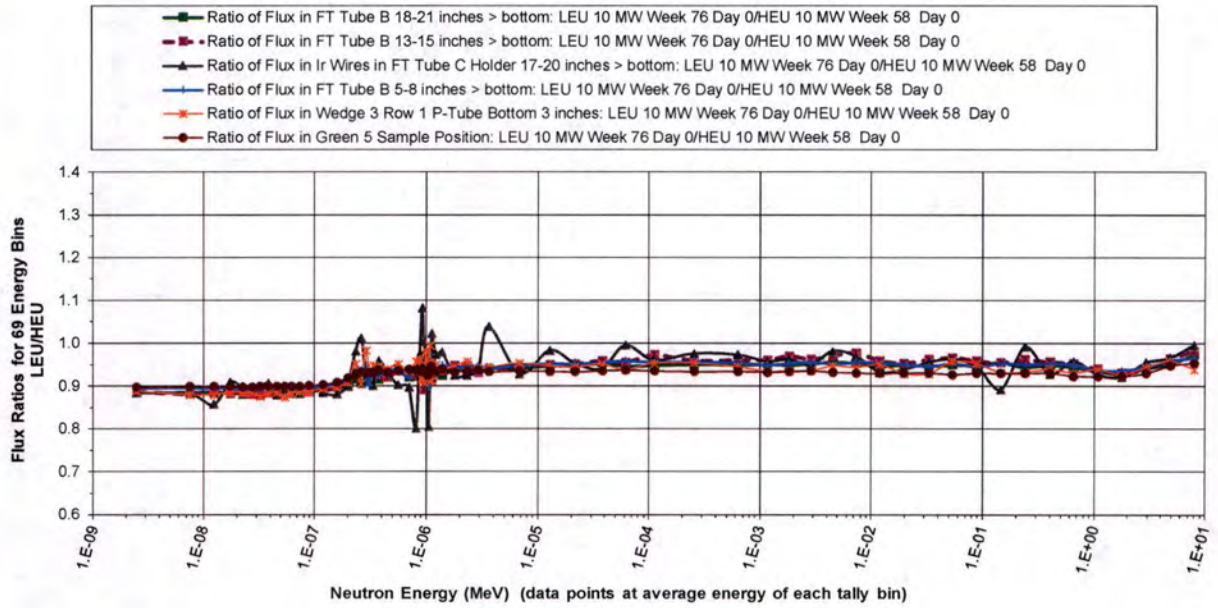


FIGURE 4.9
COMPARISON OF LEU 10 MW TO HEU 10 MW AT DAY 0

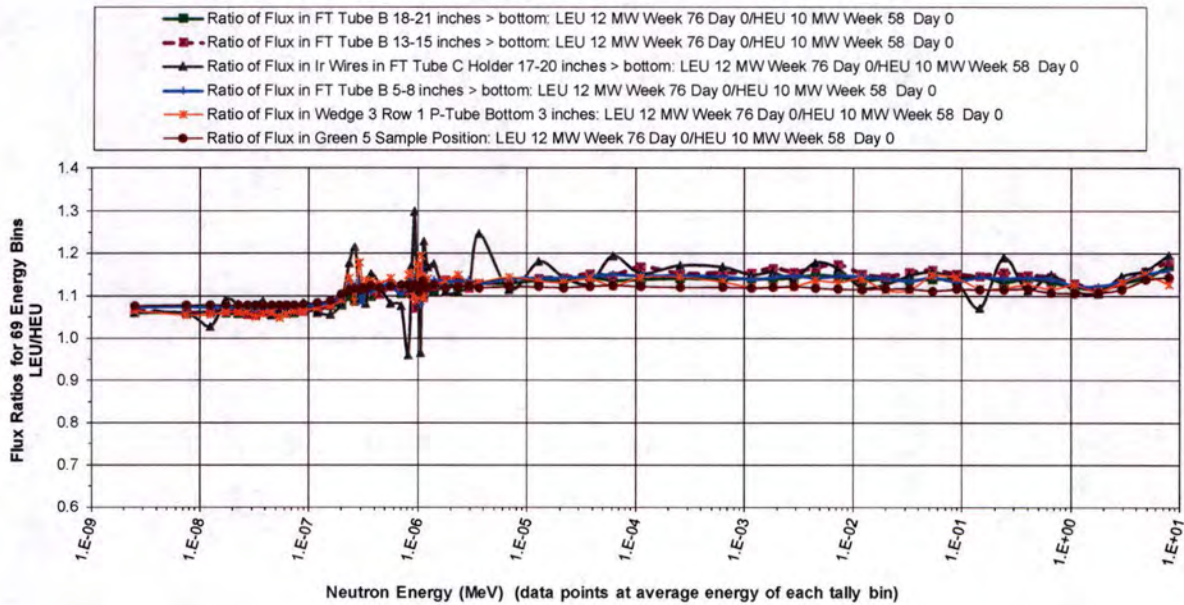


FIGURE 4.10
COMPARISON OF LEU 12 MW TO HEU 10 MW AT DAY 0

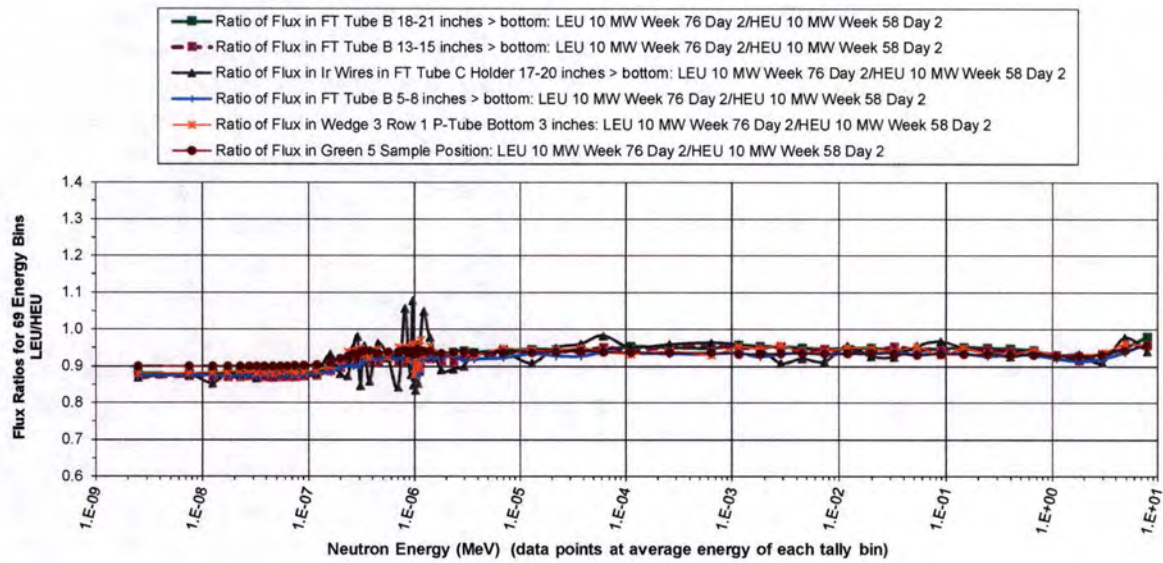


FIGURE 4.11
COMPARISON OF LEU 10 MW TO HEU 10 MW AT DAY 2

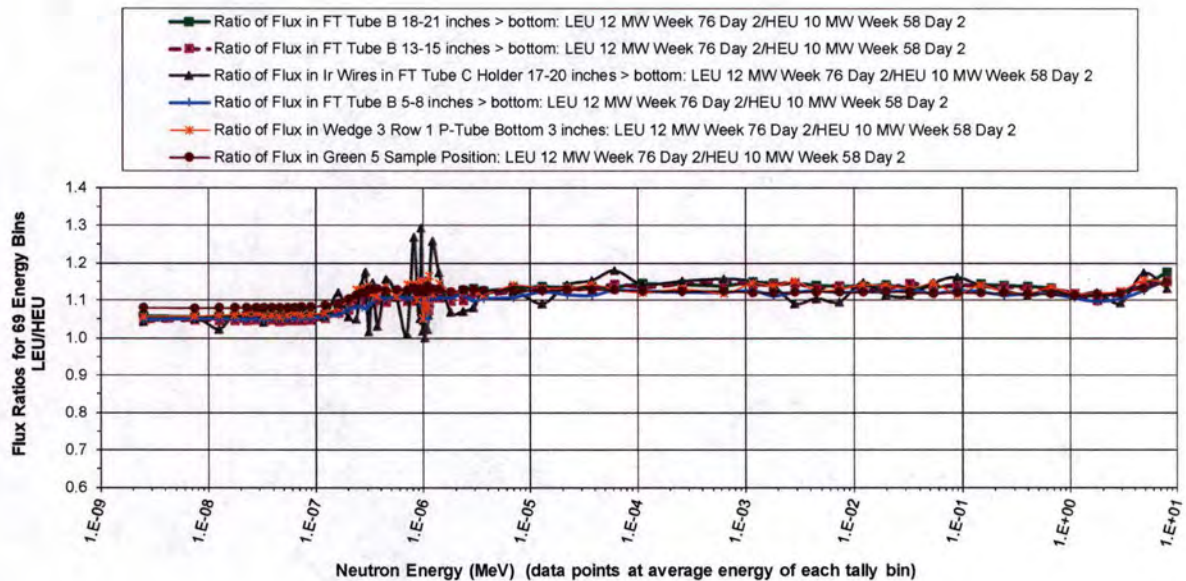


FIGURE 4.12
COMPARISON OF LEU 12 MW TO HEU 10 MW AT DAY 2

4.5.4.2 Steady-State Power Distributions

Extensive analysis of the power distributions for MURR HEU and LEU cores were reported in References 4.33 and 4.28. The power distributions were calculated with MCNP by tallying the fission power (f7 tally) (Ref. 4.26) within 24 axial, 9 azimuthal, and either 24 (HEU) or 23 (LEU)

radial segments (plate-by-plate) of the fuel meat in the entire core of eight elements (i.e., either 5,184 (HEU) or 4,968 (LEU) segments per element). Power distributions were calculated for a variety of critical configurations of various cores in order to identify the highest peaking factors that might limit the margin to onset of flow instability (FI) and/or critical heat flux (CHF) during steady-state operations. The MCNP tallies were normalized by a post-processor to facilitate studies of different core power levels and different levels of tally detail. It should be noted that credit for power deposition outside the fuel is not modeled here, but is taken into account in the steady-state thermal-hydraulic safety margin calculations. The power distributions calculated by MCNP were also employed in the accident analyses performed in Chapter 13.

Figure 4.13 identifies the fuel element positions and control blades in the MURR core. Power peaking is dependent upon the mix of burnup states among the elements in the core, upon the core xenon buildup state, upon critical control blade compositions and positions, and upon the experiment/sample loadings, particularly in the flux trap. A number of cases that covered the range of expected variations in these conditions were examined. In the results presented on the following pages, cases are labeled with a nomenclature CFb, where C indicates the fuel type and its burnup condition, F indicates the flux trap loading, and b indicates the control blade conditions.

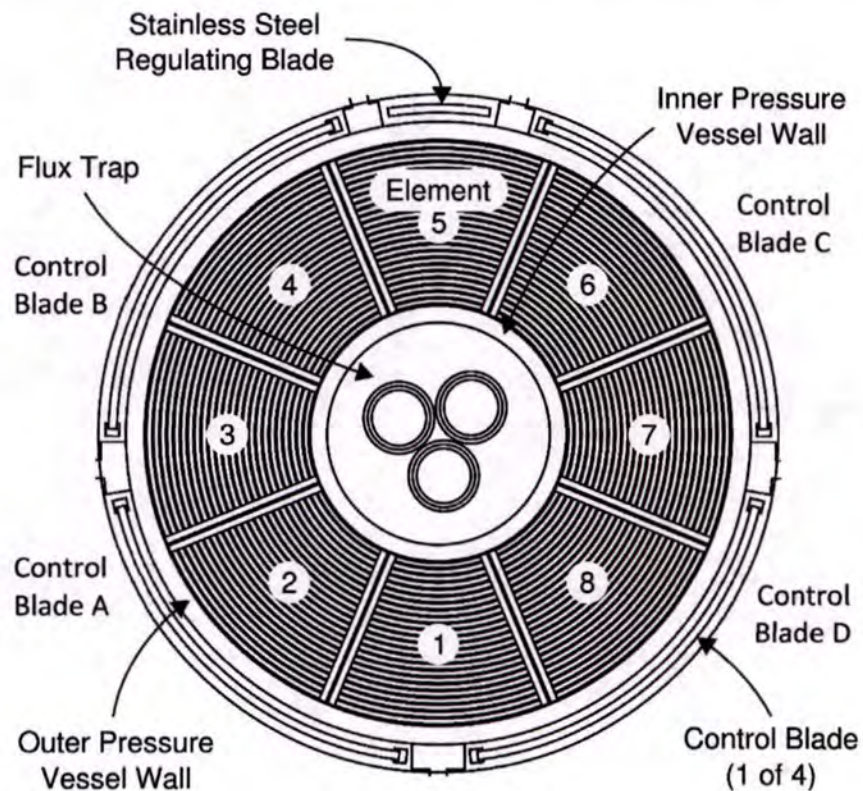


FIGURE 4.13
MURR CORE LAYOUT

The core fuel type and burnup conditions ("C" in the case name label) examined are as follows:

HEU		LEU	
C=1	All elements fresh, BOC (no Xe)	C=5	All elements fresh, BOC (no Xe)
C=2	All elements fresh, day 2 (eq. Xe)	C=6	All elements fresh, day 2 (eq. Xe)
C=3	Reference mixed core, BOC (no Xe)	C=7	Reference mixed core, BOC (no Xe)
C=4	Reference mixed core, day 2 (eq. Xe)	C=8	Reference mixed core, day 2 (eq. Xe)

Low-power physics testing will be conducted for initial LEU cores loaded with all fresh elements. So, in addition to evaluating the power distribution for the reference mixed cores, cores loaded with eight fresh elements of either HEU or LEU were also evaluated. For actual initial operations with all fresh LEU fuel, it has been proposed that some of the elements could be constructed with side plates that have a borated aluminum alloy or some other means to reduce overall reactivity and provide control rod heights of typical mixed core operations. The structural integrity of this proposed alloy to be developed remains to be evaluated. Alternatives which could be more readily shown to not impact the structural integrity of the side plate may be pursued. The borated side plates should reduce the azimuthal power peaking factors, while the radial and axial peaking factors should be reduced due to less difference in burnup among the fuel elements, so that the overall peaking will be within the range of the cases analyzed here. Thus, it is expected that the first all fresh operating cores of MURR with LEU fuel will be bounded by the present analysis.

Two flux trap loading conditions were considered. The nominal case, indicated by F=A in the case name label, has the flux trap region containing the sample holder loaded with typical samples for MURR operations. An off-nominal "empty trap" case, in which the flux trap region contains only water since no sample holder or samples are installed, is indicated by F=B.

The control blade condition assumed in the fuel cycle simulation was that all blades were at their fresh composition and banked in position. The effect of perturbations of the effective control blade ^{10}B concentration due to depletion and mismatched positioning of the blades on the core power distribution was examined since variations of this sort can exist in MURR. Shim blades in the MURR will be at different points in their lifetime, and as discussed in Section 2.2.4 of Reference 4.28 and Reference 4.30, the ^{10}B concentration depletes significantly in the bottom four inches of a given blade towards the end of its eight (8) years of utilization. The differences in the ^{10}B concentration at the tip of the shim blades can create a tilt in the core power distribution. Furthermore, a MURR TS limits the height of the blade tips to be mismatched up to one inch when operating above 100 kW. As an extreme scenario, perturbed heat flux profiles were calculated with two of the blades at their end-of-life (8 years) and positioned one inch above the other two blades, which were assumed to be fresh. The four shim blades were identified as A through D, as shown in Figure 4.13.

Calculations for the reference LEU core found that the power peaks in the fresh element in position 1 near its interface with the element in position 8 that is near its discharge burnup. The largest perturbation of the peak heat flux will occur under conditions where two blades (e.g., A and D) in that region of the core are highly depleted and the remaining blades (e.g., B and C) are fresh, pushing the power even more to that region of the core. Allowing the depleted blades to be further

withdrawn up to the Technical Specification limit creates an even greater power tilt. The cores for each fuel type (HEU and LEU) were evaluated under three conditions with regard to blade depletion and positioning, which is indicated by the character "b" in the case name.

- | | |
|---------|---|
| b=Blank | All blades fresh and banked. |
| b=1 | Blades C and D at 8 years depletion, blades A and B fresh. Blades C and D positioned 1 inch higher than A and B, per Technical Specification. |
| b=2 | Blades A and D at 8 years depletion, blades B and C fresh. Blades A and D positioned 1 inch higher than B and C, per Technical Specification. |

In the results presented below, the heat flux will be treated as the figure-of-merit for comparing the core states and predicting the potential impact on safety margins. The reason for this can be understood from Figures 4.14 and 4.15 which illustrate the radial (plate-by-plate) shapes of plate power (W), fuel foil power density (W/cm^3), and plate surface heat flux (W/cm^2) for a fresh element in one of the reference cores of the HEU and LEU design, respectively (mixed burnup + BOC + loaded flux trap + control blades all fresh and banked = Case 3A and Case 7A). Power within a segment of an outboard plate is higher than power within the equivalent segment of an inboard plate because of the greater fuel volume. However, since the volume of coolant being heated increases at the same rate as the volume of fuel in which power is tallied (i.e., the longer the arc length of the plate, the longer the arc length of the coolant channel), the higher power in outboard plates does not imply a more challenging case for thermal margin. While there is a much higher radial power density peaking factor in the fuel plates nearest the more moderated outer edges of the fuel element, the safety limits are based on heat flux. Therefore, the LEU fuel plates with the highest power densities have thinner fuel foils to reduce the heat flux transferred to the coolant and increase the safety margins. In the case of the HEU, identical fuel thicknesses in all plates causes the radial peaking factors and heat flux to share the same radial peak to average ratio.

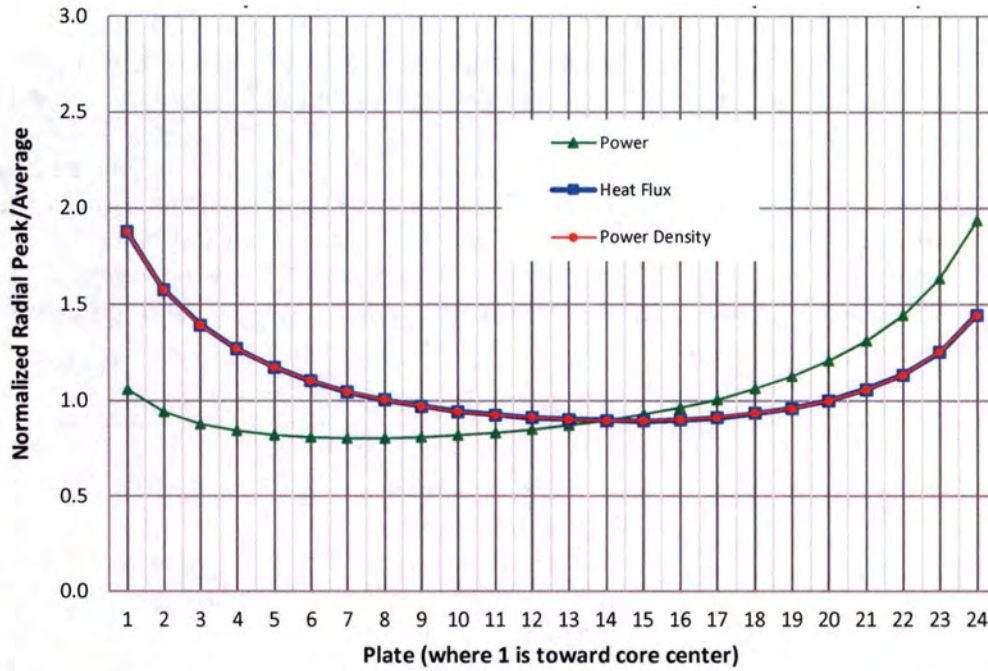


FIGURE 4.14
 NORMALIZED RADIAL POWER FACTORS IN A FRESH ELEMENT
 (HEU REFERENCE CORE)

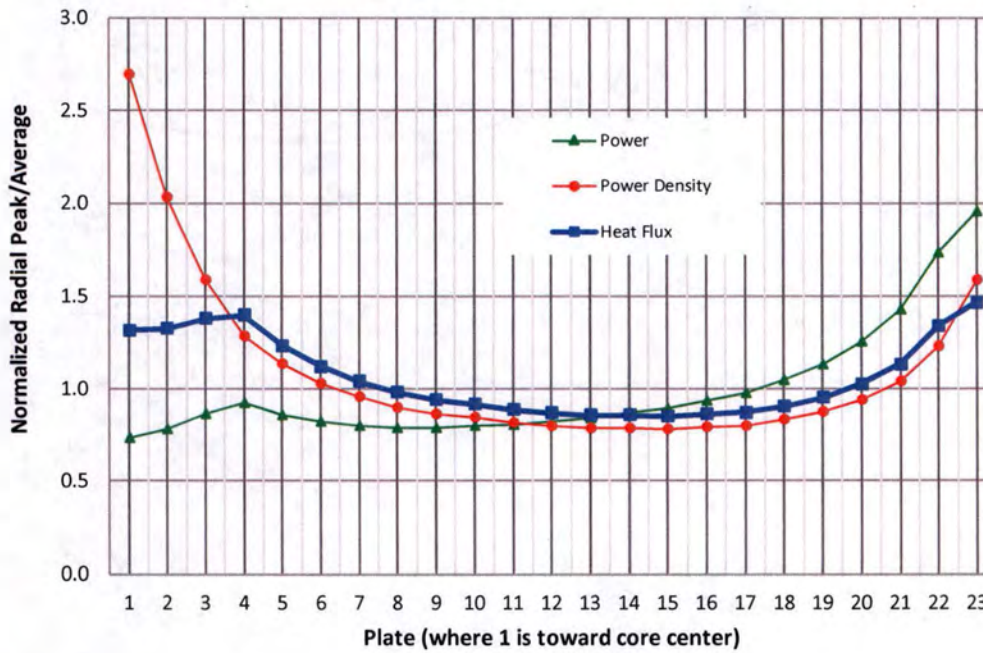


FIGURE 4.15
 NORMALIZED RADIAL POWER FACTORS IN A FRESH ELEMENT
 (LEU REFERENCE CORE)

Figures 4.16 and 4.17 show the hot-stripe heat flux in a fresh element in HEU and LEU cores for several conditions of total core burnup, day in the cycle, flux trap loading, and control blade configuration. The details of the core conditions are elaborated in Tables 4-17 and 4-18 for the HEU and LEU fuel, respectively. These figures illustrate some of the factors that influence the heat flux profile in the core. First, the *mix of burnup states* of the elements within the core largely determines the power sharing between elements. A core with fresh elements alongside elements that will be discharged at the EOC is expected to have the highest element peaking factor since the fresh elements will produce a greater fraction of the total power. For the reference mixed burnup LEU core at BOC, the fresh elements produce about 7% more power than all previously burned elements, and about 10% more than the previously burned elements at the EOC.

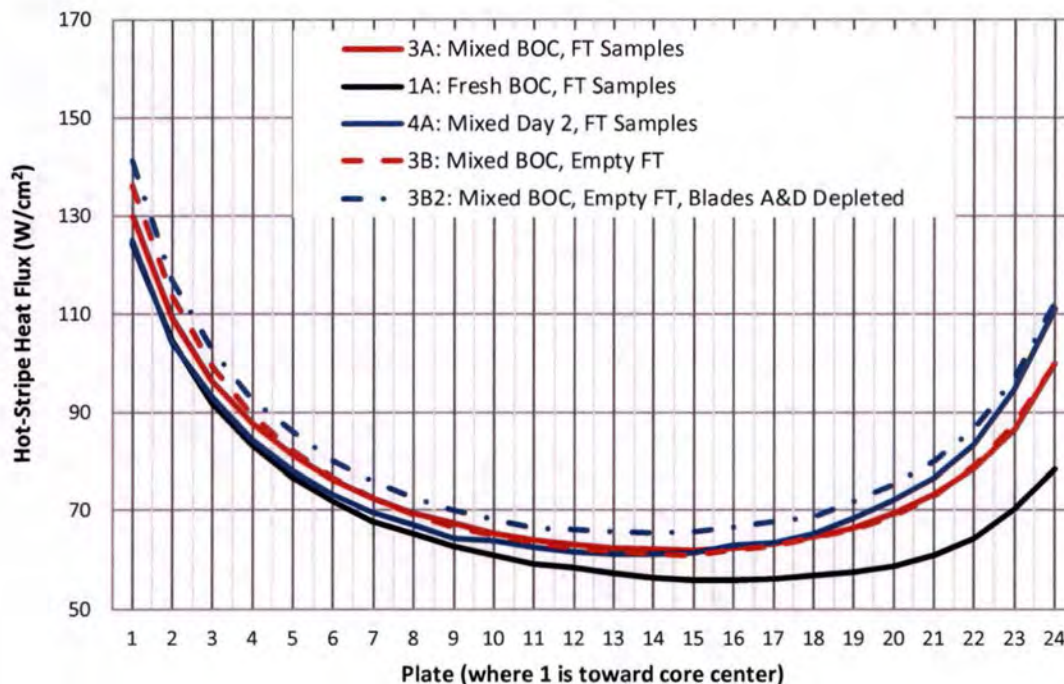


FIGURE 4.16
HOT-STRIPE HEAT FLUX RADIAL PEAKING FACTOR IN A FRESH ELEMENT
(HEU CORES)

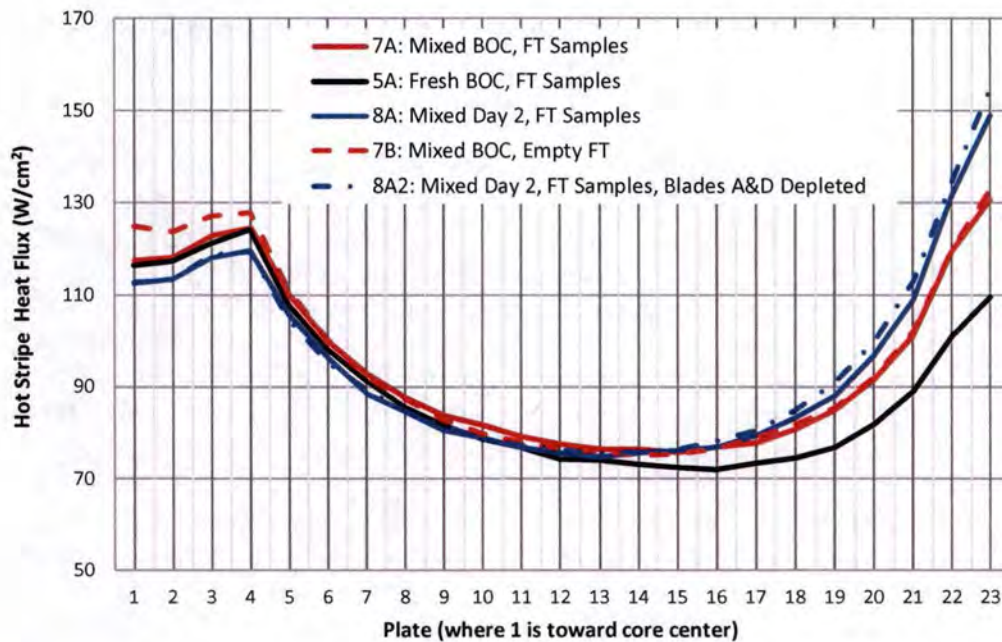


FIGURE 4.17
HOT-STRIPE HEAT FLUX RADIAL PEAKING FACTOR IN A FRESH ELEMENT
(LEU CORES)

The LEU Case 5A, which is comparable to HEU Case 1A, is loaded with all fresh elements. The critical blade position is more deeply inserted for Case 5A (13.3 inches withdrawn) than for the reference mixed core (Case 7A, 17.6 inches withdrawn) to compensate for the higher excess reactivity at BOC. This is similar to the Case 1A and 3A for the HEU cores. Figures 4.16 and 4.17 illustrate the effect that the *critical control blade position* has on heat flux profile for fresh HEU and LEU cores. For the LEU cores, the hot-stripe heat flux for plate 23 is 15% lower in the all-fresh core because the radial power profile is suppressed in the outer plate(s) when the blades are more deeply inserted. This effect is important for margin to FI, which is largely driven by the axially averaged heat-flux, which contributes to the total coolant temperature rise in the channel adjacent to the plate. The deeper blade insertion would naturally cause a shift in the power profile towards the innermost plates, but because the overall power share of the fresh element is reduced due to the more even power sharing in the all-fresh core, no increase in the hot-stripe heat flux in the innermost plates is observed.

The lower blade position also increases axial peaking, particularly in the outer plates. The change in axial peaking is not important for margin to FI, but this effect is important to CHF since the local axial clad temperature is proportional to the local heat flux. From preliminary calculations, it appears that the steady-state safety limits in MURR will be limited by FI, but a CHF analysis will be included in the detailed safety analysis to verify this.

A third factor affecting the heat flux profile is the *time in the cycle*, and is illustrated by the Case 4A and 8A results in Figures 4.16 and 4.17, respectively. As xenon builds up to equilibrium during operation, the control blades are withdrawn to compensate for the negative reactivity effect of the

xenon. The change in control blade position shifts the power radially outward and axially upward, as discussed above. The xenon may also alter the power shape directly since it builds up in the regions of highest power.

Fourth, the *flux trap contents* can affect the heat flux profile. Having no samples or sample holder in the flux trap region is an off-normal condition for the MURR, but is one that will be evaluated for its effect on the power distribution and safety limits, nonetheless. When the sample holder is not inserted in the flux trap region, the core reactivity decreases due to the positive void coefficient of this region, and removing the sample holder and samples increases the amount of water in the flux trap. This decrease in core reactivity means the critical blade position is slightly higher when only water is in the flux trap region. However, increasing the amount of moderation from the flux trap region has a direct effect on the power in the interior plates, as can be seen in the curves for Cases 3B and 7B in Figures 4.16 and 4.17, respectively.

The final factor affecting the heat flux profile is the *control blade history and positioning*. As discussed above, accounting for the depletion of the control blades being different for each blade, as well as the mismatch of the blade heights up to the TS limit, will introduce a power tilt in the core. This can be seen in the Case 3B2 and 8A2 curve in Figures 4.16 and 4.17, which show that the hot-stripe heat flux increases in the outer plates (and decreases in the inner plates) relative to Case 3B and 8A.

After considering all of the various contributors to power peaking discussed above, power distributions were calculated for 24 cases that enveloped the distinct combinations of effects for each fuel type. The atom densities of the fuel compositions for each core state were read from REBUS-DIF3D depletion results to automatically update an MCNP input file. A search was then performed with MCNP to find the critical blade position for the core (i.e., blades moved until MCNP predicted a k-effective of 1.0). The 24 cases for the HEU fuel are summarized in Table 4-17, showing the core conditions and the calculated critical blade height for each case. The 24 cases for the LEU core are summarized in Table 4-18.

Finally, a post-processor was applied to read the metal file and produce power distribution edits suitable for the thermal-hydraulics analyses of FI and CHF. The peak hot-stripe and local heat fluxes for each case are summarized in Tables 4-19 and 4-20 for the HEU and LEU cores, respectively. The location of the peak in terms of element position, azimuthal stripe, plate, and axial position (for local heat flux) is also indicated. Consequently, the details of the power distribution will be explored for these two cases for illustrative purposes.

TABLE 4-17
SUMMARY OF POWER DISTRIBUTION EVALUATIONS – HEU CORES

Core state that may bound power peaking				Element Burnup (MWd) at Beginning of Week				Fresh Blades	Depleted Blades	Critical Blade Position (Inches withdrawn)			MCNP k-eff
Case	Burnup State	Time (Days)	Flux Trap	X1 X5	X2 X6	X3 X7	X4 X8			Fresh Blades	Depleted Blades	Reg Blade	
1A	Fresh	0	Samples	0	0	0	0	A, B, C, D		12.911		10	0.99983
1A1	Fresh	0	Samples	0	0	0	0	A, B	C, D	10.307	11.307	10	1.00020
1A2	Fresh	0	Samples	0	0	0	0	B, C	A, D	10.466	11.466	10	1.00009
2A	Fresh	2	Samples	0	0	0	0	A, B, C, D		16.782		15	1.00017
2A1	Fresh	2	Samples	0	0	0	0	A, B	C, D	14.423	15.423	15	1.00002
2A2	Fresh	2	Samples	0	0	0	0	B, C	A, D	14.556	15.556	15	1.00014
3A	"Week 58"	0	Samples	0	81	65	142	A, B, C, D		17.809		10	1.00044
3A1	"Week 58"	0	Samples	0	81	65	142	A, B	C, D	15.473	16.473	10	0.99999
3A2	"Week 58"	0	Samples	0	81	65	142	B, C	A, D	15.536	16.536	10	0.99985
4A	"Week 58"	2	Samples	0	81	65	142	A, B, C, D		24.031		15	1.00020
4A1	"Week 58"	2	Samples	0	81	65	142	A, B	C, D	22.394	23.394	15	1.00014
4A2	"Week 58"	2	Samples	0	81	65	142	B, C	A, D	22.373	23.373	15	0.99993
1B	Fresh	0	Empty	0	0	0	0	A, B, C, D		13.295		10	0.99974
1B1	Fresh	0	Empty	0	0	0	0	A, B	C, D	10.694	11.694	10	1.00000
1B2	Fresh	0	Empty	0	0	0	0	B, C	A, D	10.873	11.873	10	1.00006
2B	Fresh	2	Empty	0	0	0	0	A, B, C, D		17.367		15	0.99985
2B1	Fresh	2	Empty	0	0	0	0	A, B	C, D	15.041	16.041	15	0.99993
2B2	Fresh	2	Empty	0	0	0	0	B, C	A, D	15.187	16.187	15	1.00006
3B	"Week 58"	0	Empty	0	81	65	142	A, B, C, D		18.380		10	0.99969
3B1	"Week 58"	0	Empty	0	81	65	142	A, B	C, D	16.125	17.125	10	1.00010
3B2	"Week 58"	0	Empty	0	81	65	142	B, C	A, D	16.216	17.216	10	0.99998
4B	"Week 58"	2	Empty	0	81	65	142	A, B, C, D		26.000		15	1.00029
4B1	"Week 58"	2	Empty	0	81	65	142	A, B	C, D	24.569	25.569	15	0.99988
4B2	"Week 58"	2	Empty	0	81	65	142	B, C	A, D	24.664	25.664	15	1.00016

"Samples" indicates a typical loading of samples in all three flux trap tubes.

"Empty" indicates neither samples nor tubes in the flux trap (i.e., "empty island" configuration).

Full blade withdrawal is 26 inches.

TABLE 4-18
SUMMARY OF POWER DISTRIBUTION EVALUATIONS – LEU CORES

Core state that may bound power peaking				Element Burnup (MWd) at Beginning of Week				Fresh Blades	Depleted Blades	Critical Blade Position (Inches withdrawn)			MCNP k-eff
Case	Burnup State	Time (Days)	Flux Trap	X1 X5	X2 X6	X3 X7	X4 X8			Fresh Blades	Depleted Blades	Reg Blade	
5A	Fresh	0	Samples	0	0	0	0	A, B, C, D		13.259		10	1.00016
5A1	Fresh	0	Samples	0	0	0	0	A, B	C, D	10.656	11.656	10	0.99993
5A2	Fresh	0	Samples	0	0	0	0	B, C	A, D	10.814	11.814	10	0.99999
6A	Fresh	2	Samples	0	0	0	0	A, B, C, D		17.193		15	0.99985
6A1	Fresh	2	Samples	0	0	0	0	A, B	C, D	14.912	15.912	15	1.00001
6A2	Fresh	2	Samples	0	0	0	0	B, C	A, D	15.027	16.027	15	0.99990
7A	"Week 76"	0	Samples	0	96	77	170	A, B, C, D		17.567		10	1.00008
7A1	"Week 76"	0	Samples	0	96	77	170	A, B	C, D	15.209	16.209	10	0.99975
7A2	"Week 76"	0	Samples	0	96	77	170	B, C	A, D	15.351	16.351	10	1.00014
8A	"Week 76"	2	Samples	0	96	77	170	A, B, C, D		24.314		15	1.00001
8A1	"Week 76"	2	Samples	0	96	77	170	A, B	C, D	22.765	23.765	15	1.00004
8A2	"Week 76"	2	Samples	0	96	77	170	B, C	A, D	22.698	23.698	15	0.99986
5B	Fresh	0	Empty	0	0	0	0	A, B, C, D		13.650		10	0.99998
5B1	Fresh	0	Empty	0	0	0	0	A, B	C, D	11.080	12.080	10	1.00003
5B2	Fresh	0	Empty	0	0	0	0	B, C	A, D	11.258	12.258	10	1.00009
6B	Fresh	2	Empty	0	0	0	0	A, B, C, D		17.891		15	0.99997
6B1	Fresh	2	Empty	0	0	0	0	A, B	C, D	15.580	16.580	15	0.99988
6B2	Fresh	2	Empty	0	0	0	0	B, C	A, D	15.741	16.741	15	1.00017
7B	"Week 76"	0	Empty	0	96	77	170	A, B, C, D		18.193		10	1.00013
7B1	"Week 76"	0	Empty	0	96	77	170	A, B	C, D	15.933	16.933	10	1.00012
7B2	"Week 76"	0	Empty	0	96	77	170	B, C	A, D	16.030	17.030	10	1.00003
8B	"Week 76"	2	Empty	0	96	77	170	A, B, C, D		26.000		15	0.99917
8B1	"Week 76"	2	Empty	0	96	77	170	A, B	C, D	25.621	26.000	15	0.99998
8B2	"Week 76"	2	Empty	0	96	77	170	B, C	A, D	25.312	26.000	15	0.99986

"Samples" indicates a typical loading of samples in all three flux trap tubes.

"Empty" indicates neither samples nor tubes in the flux trap (i.e., "empty island" configuration).

Full blade withdrawal is 26 inches.

TABLE 4-19
SUMMARY OF KEY HOT-STRIPE AND LOCAL HEAT FLUXES – (HEU CORES)

Case	Hot-Stripe Heat Flux (W/cm ²)		Local Heat Flux (W/cm ²)	
	Peak	Location ¹	Peak	Location ²
1A	126.8	X2 S9 P1	181.4	X4 A15 S9 P1
1A1	132.1	X7 S9 P1	187.8	X7 A15 S9 P1
1A2	130.7	X1 S9 P1	184.0	X2 A16 S1 P1
2A	122.4	X5 S1 P1	173.4	X7 A14 S9 P1
2A1	126.5	X7 S9 P1	176.2	X7 A14 S9 P1
2A2	124.9	X1 S9 P1	173.0	X7 A15 S9 P1
3A	131.3	X5 S1 P1	185.3	X5 A14 S1 P1
3A1	131.5	X1 S1 P1	180.9	X5 A15 S9 P1
3A2	134.0	X1 S1 P1	181.3	X1 A14 S1 P1
4A	125.5	X5 S1 P1	168.0	X5 A13 S1 P1
4A1	125.4	X1 S1 P1	165.6	X5 A13 S1 P1
4A2	126.2	X1 S1 P1	165.6	X5 A13 S1 P1
1B	133.3	X5 S1 P1	194.4	X2 A17 S1 P1
1B1	139.2	X7 S1 P1	197.6	X7 A16 S1 P1
1B2	137.0	X1 S9 P1	195.0	X1 A17 S9 P1
2B	128.4	X5 S1 P1	178.6	X6 A15 S9 P1
2B1	131.9	X7 S9 P1	180.2	X6 A15 S9 P1
2B2	131.4	X1 S1 P1	180.3	X7 A15 S9 P1
3B	137.0	X5 S1 P1	188.8	X1 A15 S1 P1
3B1	138.6	X1 S1 P1	187.5	X1 A14 S1 P1
3B2	141.3	X1 S1 P1	189.9	X1 A14 S1 P1
4B	131.0	X1 S1 P1	166.4	X1 A13 S1 P1
4B1	131.9	X1 S1 P1	167.3	X1 A13 S1 P1
4B2	131.9	X1 S1 P1	166.6	X1 A12 S1 P1

¹ Xi Sj Pkk. i is element number. j is azimuthal stripe in plate, numbered 1-9 moving clockwise. kk is plate, numbered 1-24 moving from inner pressure vessel to outer pressure vessel.

² Xi Azz Sj Pkk. i is element number. zz is axial level, numbered 1-24 from top of fuel meat. j is azimuthal stripe in plate, numbered 1-9 moving clockwise. kk is plate, numbered 1-24 moving from inner pressure vessel to outer pressure vessel.

TABLE 4-20
SUMMARY OF KEY HOT-STRIPE AND LOCAL HEAT FLUXES (LEU CORES)

Case	Hot-Stripe Heat Flux (W/cm ²)		Local Heat Flux (W/cm ²)	
	Peak	Location ¹	Peak	Location ²
5A	125.3	X5 S1 P4	222.2	X8 A18 S9 P23
5A1	129.6	X8 S1 P4	233.3	X6 A17 S9 P23
5A2	129.8	X1 S9 P4	229.5	X8 A17 S9 P23
6A	125.8	X7 S1 P23	211.9	X6 A16 S9 P23
6A1	143.2	X6 S9 P23	222.2	X6 A15 S9 P23
6A2	141.0	X8 S9 P23	216.4	X7 A15 S9 P23
7A	130.6	X1 S1 P23	210.8	X1 A16 S1 P23
7A1	142.0	X1 S1 P23	228.1	X1 A16 S1 P23
7A2	148.1	X1 S1 P23	218.1	X1 A16 S1 P23
8A	149.0	X1 S1 P23	193.0	X1 A12 S1 P23
8A1	155.0	X1 S1 P23	201.9	X1 A13 S1 P23
8A2	156.8	X1 S1 P23	196.7	X1 A12 S1 P23
5B	126.9	X5 S9 P4	220.3	X6 A17 S1 P23
5B1	133.8	X7 S1 P4	234.0	X6 A17 S9 P23
5B2	132.2	X8 S9 P4	229.9	X8 A17 S9 P23
6B	127.3	X6 S9 P23	210.2	X6 A15 S9 P23
6B1	144.0	X7 S1 P23	217.2	X6 A14 S9 P23
6B2	142.0	X8 S9 P23	213.5	X7 A15 S9 P23
7B	133.1	X1 S1 P23	208.9	X1 A15 S1 P23
7B1	144.1	X1 S1 P23	226.4	X1 A15 S1 P23
7B2	150.0	X1 S1 P23	217.0	X1 A14 S1 P23
8B	151.3	X1 S1 P23	190.7	X1 A12 S1 P23
8B1	152.5	X1 S1 P23	191.3	X1 A13 S1 P23
8B2	154.6	X1 S1 P23	191.6	X1 A12 S1 P23

¹ Xi Sj Pkk. i is element number. j is azimuthal stripe in plate, numbered 1-9 moving clockwise. kk is plate, numbered 1-23 moving from inner pressure vessel to outer pressure vessel.

² Xi Azz Sj Pkk. i is element number. zz is axial level, numbered 1-24 from top of fuel meat. j is azimuthal stripe in plate, numbered 1-9 moving clockwise. kk is plate, numbered 1-23 moving from inner pressure vessel to outer pressure vessel.

The margin to FI is primarily dependent upon total heat transferred to a coolant channel rather than the axial shape of the heat flux. The largest hot-stripe heat flux calculated for the HEU cores is 141.3 W/cm² in Case 3B2, while the largest hot-stripe heat flux for the LEU cores is 156.8 W/cm² in Case 8A2.

Figures 4.18 and 4.19 plot the average heat flux for each plate of each element for Case 3B2 and Case 8A2, respectively. For Case 8A2, the peak axial average heat fluxes is in plate 23 (outermost plate) of the element in core position 1 (fresh element). For Case 3B2, the peak axial average heat flux is in plate 1 (innermost plate) of the element in core position 1 (fresh element). The radial shape of the heat flux in the figure for Case 8A2 illustrates the important effect of moderation and fissile material self-shielding, as well as the choice of fuel foil thickness for reducing the heat flux peaking in comparison to that of Case 3B2. The innermost and outermost plates in the MURR

tend to have a much higher heat flux (i.e., fission rate) due to their proximity to the heavily-moderated flux trap (plate 1) and reflectors (plate 23 for the LEU design). The interior plates have a lower heat flux due to both less moderation from the coolant channels and the self-shielding effect of outboard plates consuming thermal neutrons coming from the flux trap and reflector. As indicated in Figure 4.19, the fuel foils in the innermost and outermost plates are thinned relative to the interior plates in order to prevent extremely high heat flux peaking which would reduce the margin to FI (as well as the margin to CHF).

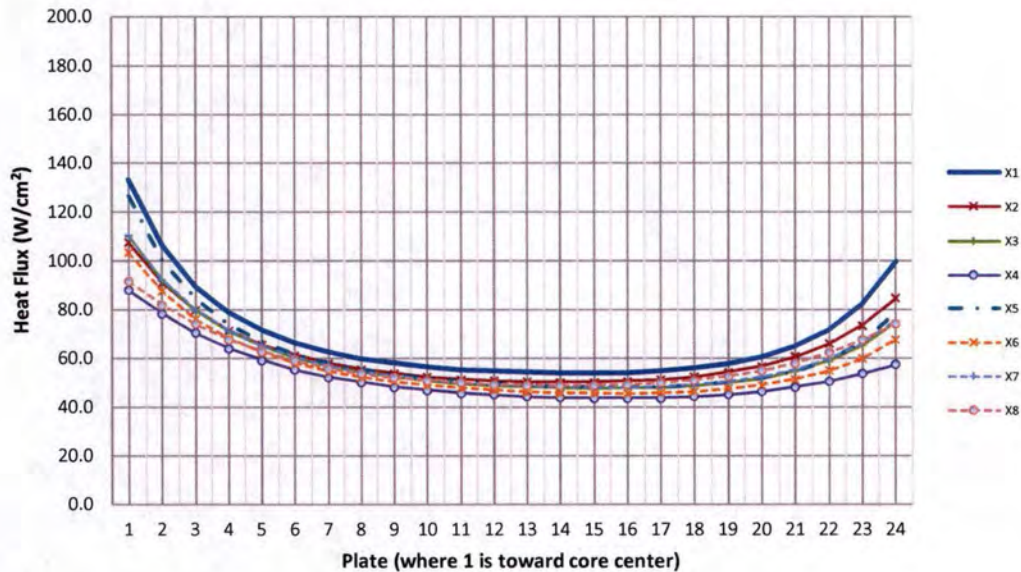


FIGURE 4.18
 AVERAGE HEAT FLUX IN EACH PLATE OF EACH FUEL ELEMENT IN CASE 3B2
 (HEU WEEK 58, DAY 0, WITH EMPTY FLUX TRAP AND BLADES A AND D AT
 DEPLETED COMPOSITION)

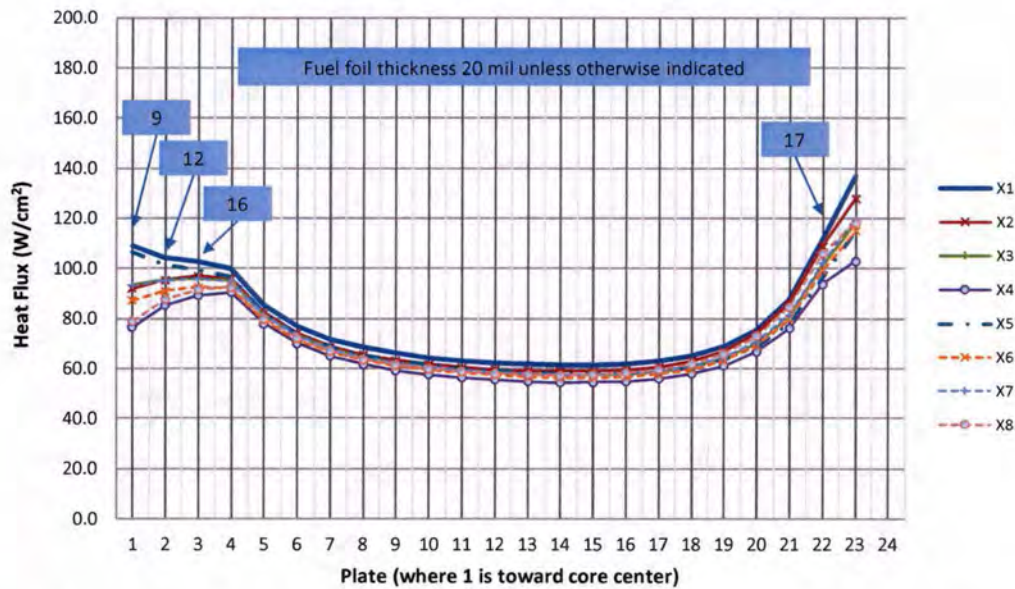


FIGURE 4.19
AVERAGE HEAT FLUX IN EACH PLATE OF EACH FUEL ELEMENT IN CASE 8A2
(LEU WEEK 76, DAY 2, WITH LOADED FLUX TRAP AND BLADES A AND D AT
DEPLETED COMPOSITION)

The effects of moderation and self-shielding are also important in the azimuthal power profile of the MURR elements. There is a 70 mil wide unfueled region of the plates adjacent to the side plates. Consequently, the fuel near the side plates sees relatively more moderation and less self-shielding than the azimuthal interior region. As discussed in Section 2.2.5 of Reference 4.28, the details of the MCNP fission power were tallied with three azimuthal stripes of 5 mm width (~200 mil) along the edge of the fueled region of each plate. The remainder of each plate in the azimuthal interior of the plate was subdivided into three tally regions of equal angle, so that the entire meat width was included in the detailed power distribution.

Figures 4.20 and 4.21 illustrate the azimuthal peaking factor for each plate of each element for Cases 3B2 and 8A2, respectively. For the LEU case, the moderation effect on the power peaking along the fueled edge is clearly pronounced for the interior plates, which have azimuthal peaking factors of 1.15 to 1.35. The corresponding values of the azimuthal peaking factor for HEU Case 3B2 are 1.10 to 1.30. The effect is most pronounced for the elements in positions 1, 3 and 7 in these cases due to uneven burnup and positioning of the shim blades assumed in Case 8A2. For example, as can be seen in the inset chart for Case 8A with the blades at their fresh composition and banked, the azimuthal power peaking is less skewed in these elements. The azimuthal effect is somewhat smaller for the outboard plates since there is significant moderator and little self-shielding already, as discussed above. For plate 1, the azimuthal peaking factor is < 1.05, while for plate 23 the peaking factor is < 1.20 (< 1.15 when the blades are uniform and banked).

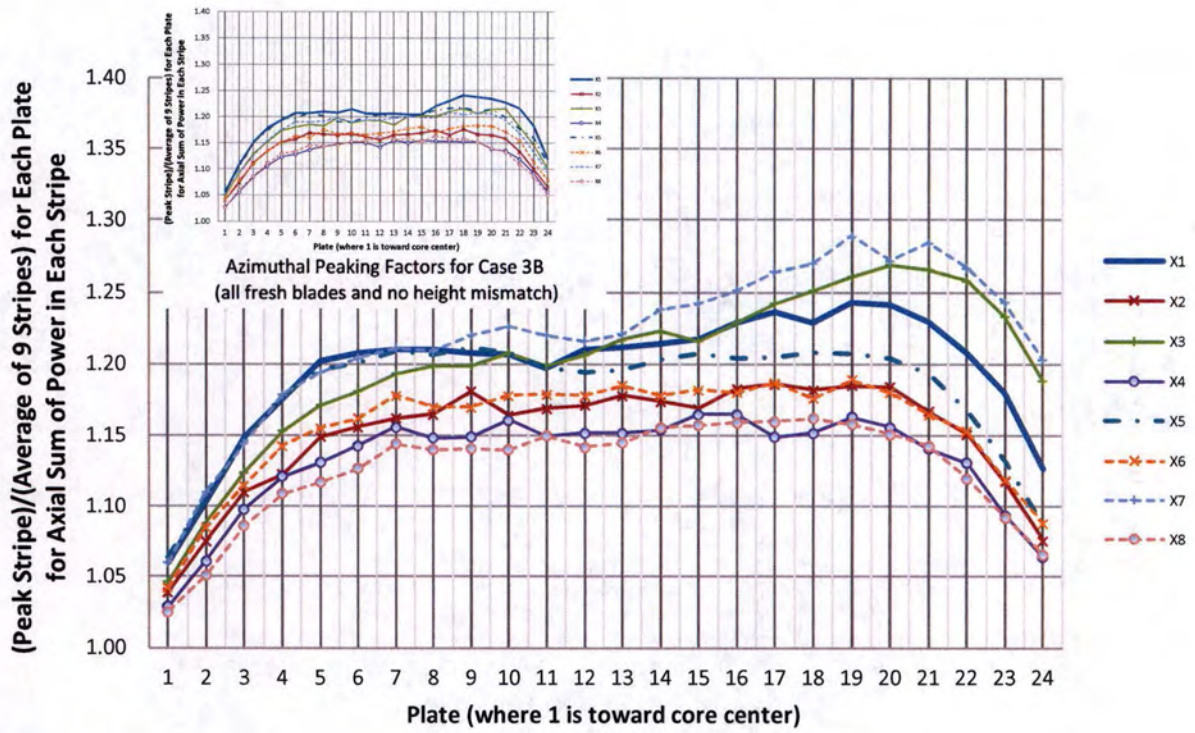


FIGURE 4.20
 AZIMUTHAL PEAKING FACTORS FOR EACH PLATE OF EACH ELEMENT IN CASE 3B2 (HEU WEEK 58, DAY 0, WITH EMPTY FLUX TRAP AND BLADES A AND D AT DEPLETED COMPOSITION)

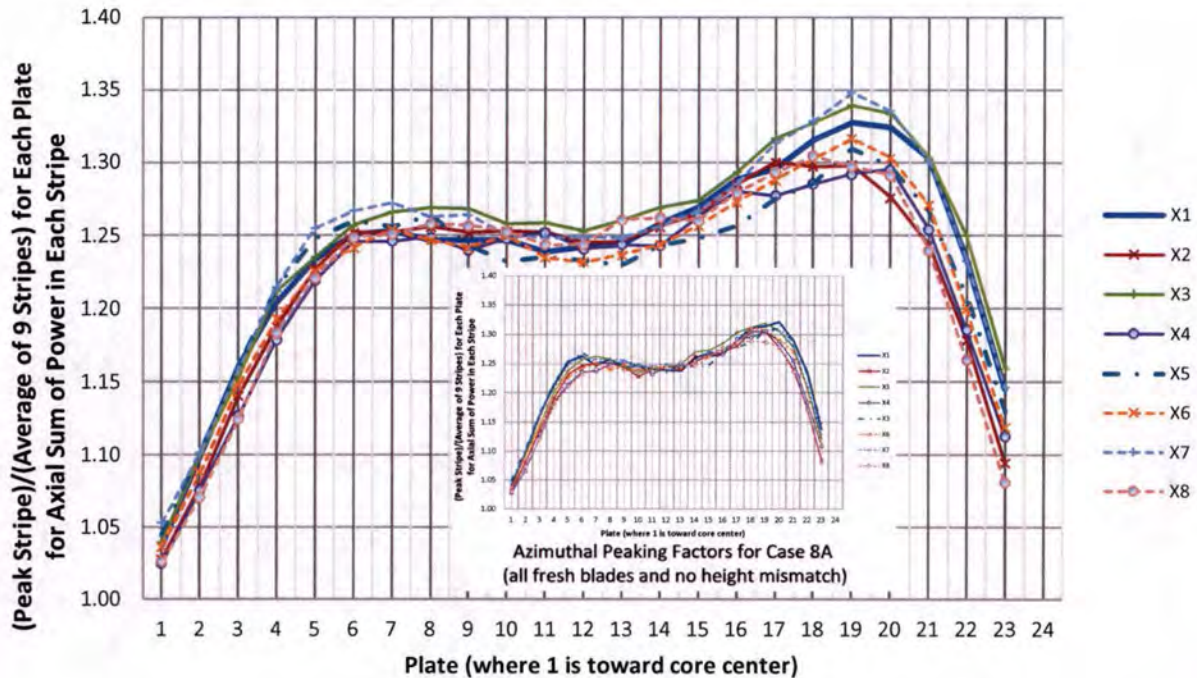


FIGURE 4.21

AZIMUTHAL PEAKING FACTORS FOR EACH PLATE OF EACH ELEMENT IN CASE 8A2 (LEU WEEK 76, DAY 2, WITH LOADED FLUX TRAP AND BLADES A AND D AT DEPLETED COMPOSITION)

Another trend in the azimuthal peaking factor for the LEU cores is illustrated in Figure 4.22, which plots the average azimuthal peaking factor for all elements in a given core by fuel plate. For the all fresh core (Case 5A), the shim blades are more deeply inserted, which pushes the power more towards the innermost plates. Consequently, the azimuthal peaking factor which tends to be greatest for plate 20 is smaller than in the mixed burnup reference cores. Cases 7A and 7B are for the same mixed burnup state of the fuel, but with and without samples loaded in the flux trap region, respectively. Since the blades are slightly more withdrawn in Case 7B, the azimuthal peaking factor in plate 20 is slightly greater. As xenon builds to equilibrium (Cases 8A and 8B), the critical position for the control blades moves upward to nearly fully withdrawn, which shifts the power radially outward, increasing the importance of the edge effect for those plates that are closer to the reflector. For comparison, a similar illustration is presented in Figure 4.23 for the HEU fueled cores.

The average heat flux in the interior plates is lower than in the outboard plates, so the largest azimuthal peaking factors do not correspond to a "hot stripe" for the entire element. Figures 4.24 and 4.25 illustrate the hot-stripe heat flux for each plate of each element in Case 3B2 and Case 8A2, respectively. The hot-stripe heat flux can be thought of as the multiplication of the plate average heat flux (Figures 4.18 and 4.19 for the HEU and LEU, respectively) by the azimuthal peaking factor (Figures 4.20 and 4.21 for the HEU and LEU, respectively).

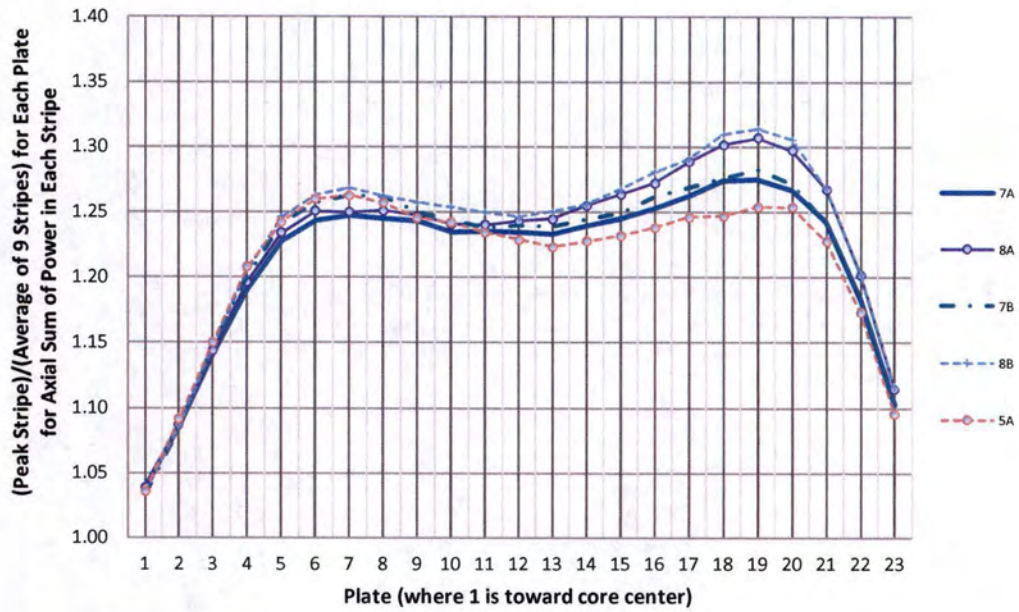


FIGURE 4.22
AZIMUTHAL PEAKING FACTORS BY PLATE AVERAGED FOR ALL ELEMENTS (LEU CORE)

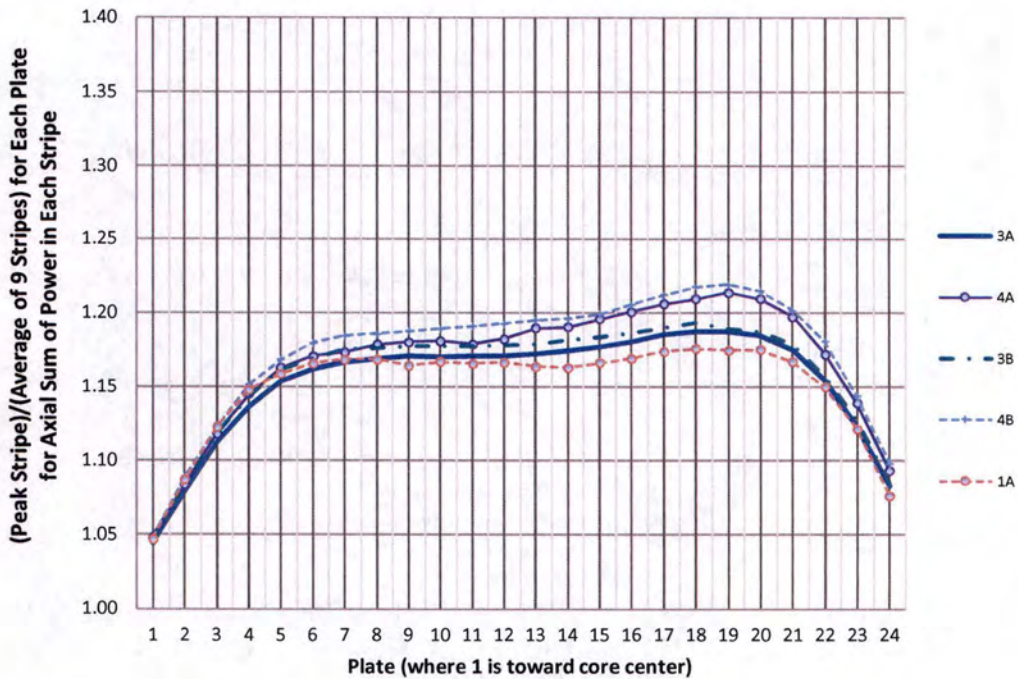


FIGURE 4.23
AZIMUTHAL PEAKING FACTORS BY PLATE AVERAGED FOR ALL ELEMENTS (HEU CORE)

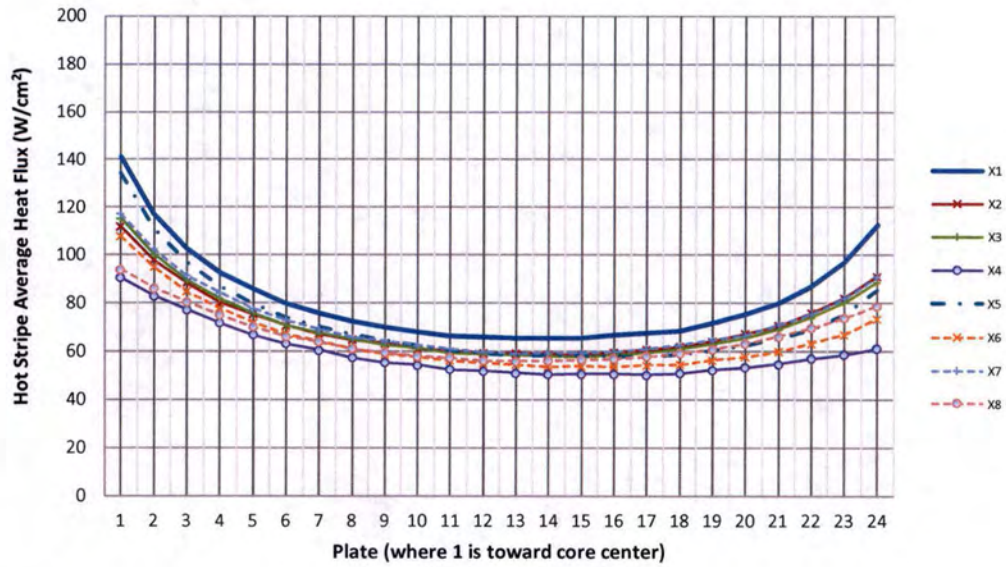


FIGURE 4.24
HOT-STRIP HEAT FLUX FOR EACH PLATE OF EACH ELEMENT IN CASE 3B2
(HEU WEEK 58, DAY 0, WITH EMPTY FLUX TRAP AND BLADES A AND D AT
DEPLETED COMPOSITION)

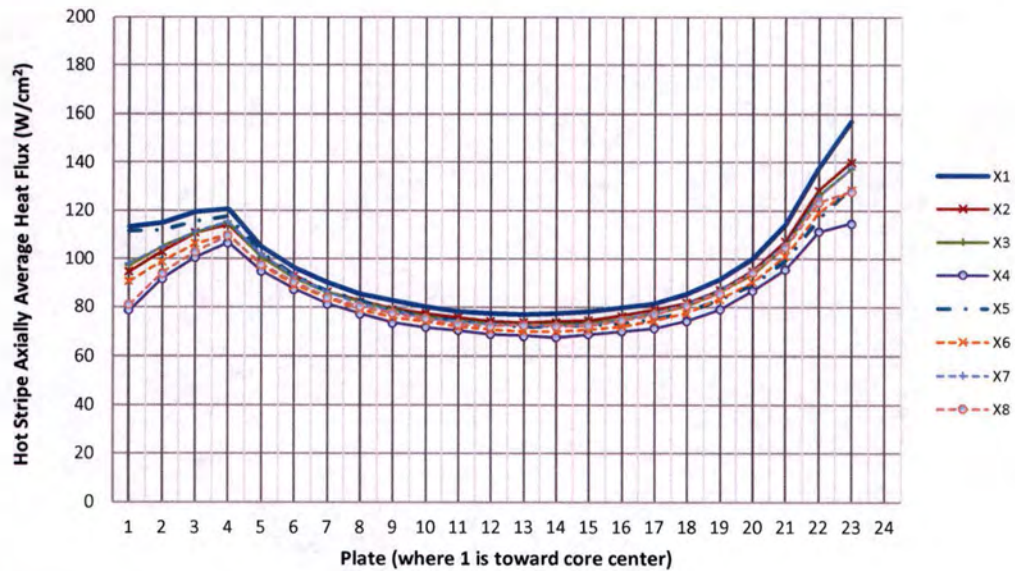


FIGURE 4.25
HOT-STRIP HEAT FLUX FOR EACH PLATE OF EACH ELEMENT IN CASE 8A2
(LEU WEEK 76, DAY 2, WITH LOADED FLUX TRAP AND BLADES A AND D AT
DEPLETED COMPOSITION)

Also, the hot-stripe heat flux in the first 4 plates in Case 8A2 is relatively flat (~5% variation) as compared to Case 3B2; achieving as flat a power distribution as possible was a design goal. Also, as the elements reach the end-of-life, the outboard plates deplete more than the interior plates, so that the power profile becomes less peaked.

The prior discussion provides an illustration how the various core components in MURR (e.g., fuel and control blade burnup, experiment loading, etc.) affect the power distribution during steady-state operations. The Case 3B2 will have the highest "hot-stripe" heat flux for a given steady-state reactor power among all cores loaded with HEU. Likewise for LEU, the Case 8A2 will have the highest hot-stripe heat flux. These cases would be expected to have the smallest margin to FI during steady-state operations. However, as previously stated, 24 different core states were modeled in the neutronics analysis, as summarized in Tables 4-17 and 4-18 for the HEU and LEU cores, respectively. Thermal-hydraulic margins at steady-state operating conditions were evaluated for each of these core states to determine the smallest margins to FI and CHF expected for MURR with the current HEU and proposed LEU fuel. The steady-state thermal-hydraulic analysis (discussed in Section 4.6, below) is based on the detailed power distributions calculated by the MCNP neutronics model. Likewise, the transient analyses described in Chapter 13 assume the reactor initially operating at steady-state followed by some postulated accident condition. Therefore, the transient analyses also utilize the detailed power distributions calculated by MCNP.

The axial and azimuthal heat flux profiles for 11 select cores/fuel plates are provided in Figures 4.26 through 4.36. These core/fuel plates were selected based on those which yield the smallest margin to steady-state FI, smallest margin to steady-state CHF, the smallest margin to the fuel temperature safety limit for reactivity insertion accidents, and the smallest margin to the fuel temperature safety limit for loss of coolant accidents. The heat flux profiles in Figures 4.26 through 4.36 are normalized to a core power of either 10 MW or 12 MW for HEU and LEU cores, respectively. Also, the calculated heat flux profiles presented in these figures assume an even power split between the two radial surfaces (concave and convex) of the fuel plate with 50% of the power emanating from each surface. The actual power split between these two surfaces during operation is modeled in the steady-state thermal-hydraulics and transient accident calculations.

Figures 4.26 and 4.27 provide the detailed heat flux profiles in plates 1 and 2 of the fresh element in core position 1 in Case 3B2. These plates are adjacent to coolant channel 2, which is the location of the smallest margin to FI at steady-state in all of the HEU cores evaluated. The peak heat flux values for these plates for a normalized core power of 10 MW are 189.9 and 157.6 W/cm² for plates 1 and 2, respectively. Figures 4.28 and 4.29 provide the heat flux profiles in plates 22 and 23, respectively, in the depleted element in position 8 (174 MWd element burnup) for Case 8A1. Channel 23 of this element (which is between plates 22 and 23) has the smallest margin to FI at steady-state for all of the LEU cores evaluated. For a normalized core power of 12 MW, the peak heat flux values for plates 22 and 23 are 153.0 and 154.0 W/cm², respectively.

The smallest margin to CHF occurs in fresh fuel elements in Cases 1B1 and 7A1 for cores loaded with HEU and LEU fuel, respectively. Figure 4.30 provides the detailed heat flux profile in plate 1 of the fresh HEU element in core position 7 in Case 1B1, while Figure 4.31 provides the heat flux in plate 23 of the fresh LEU element in core position 1 in Case 7A1. The effect of the blade depletion and mismatched blade heights on the power distribution is more pronounced in the case

of LEU. This is attributable to the proximity of the limiting plate to the control blade. The HEU outer plate would exhibit similar shape. The HEU has a single fuel thickness, and thus peak heat flux peak occurs in plate 1. Since the LEU fuel thicknesses were varied by plate in order to optimize power peaking, the overall peak heat flux increase from HEU to LEU is therefore modest despite the 20% power uprate. The peak heat flux values in these cases are 197.6 W/cm^2 in Case 1B1 and 228.1 W/cm^2 in Case 7A1 for normalized core power levels of 10 and 12 MW, respectively.

Transient analyses for reactivity insertion accidents (RIA) and loss of coolant accidents (LOCA) are evaluated in Chapter 13. Cores that are typical for normal MURR operations with a mixed-burnup loading of fuel, experimental samples in the center flux trap, and banked control blades were considered for these accidents. For the HEU core (Case 3A), the smallest margin to the fuel temperature safety limit in a RIA occurs in plate 1 of the fresh element in core position 5. The steady-state heat flux profile for this plate is provided in Figure 4.32, with a peak heat flux of 185.3 W/cm^2 for a core at 10 MW and assuming an even power split between the two radial surfaces of the fuel plate. However, less than half of the heat generated within the fuel plate is conducted toward the plate surface that is adjacent to the limiting coolant channel (the convex surface of the plate), which is taken into account in the transient analysis. For the typical core loaded with LEU (Case 7A), the smallest margin to the fuel temperature safety limit occurs in plate 23 of the most depleted element in core position 8 (174 MWd), with a peak heat flux of 170.5 W/cm^2 for a normalized core power of 12 MW. The steady-state heat flux profile for this plate is provided in Figure 4.33.

For the class of plant transients caused by loss of coolant (LOCA) or loss of coolant flow (LOFA), the accident with the smallest margin to the fuel temperature safety limit is the double-ended cold-leg break LOCA for both HEU and LEU fueled cores. For Case 3A with HEU fuel, the peak fuel temperature occurs in plate 2 of the fresh element in core position 5. The detailed heat flux profile for this fuel plate with normalized core power of 10 MW is shown in Figure 4.34, with a peak heat flux of 155.1 W/cm^2 . The effect of the double-ended cold leg break LOCA in a typical core loaded with LEU (Case 7A) was evaluated both with and without the assumption of coolant flow redistribution due to burnup among the elements in the core. When there is flow redistribution, the peak fuel temperature during the LOCA occurs in plate 22 of the most depleted element in core position 8. The heat flux profile in this plate for a normalized core power of 12 MW is provided in Figure 4.35, with a peak heat flux of 169.7 W/cm^2 . When there is assumed to be no flow redistribution among the elements due to burnup in the LEU core, the peak fuel temperature is calculated to occur in plate 3 of the fresh element in core position 5. The detailed heat flux profile for this plate is provided in Figure 4.36, which has a peak heat flux of 175.9 W/cm^2 .

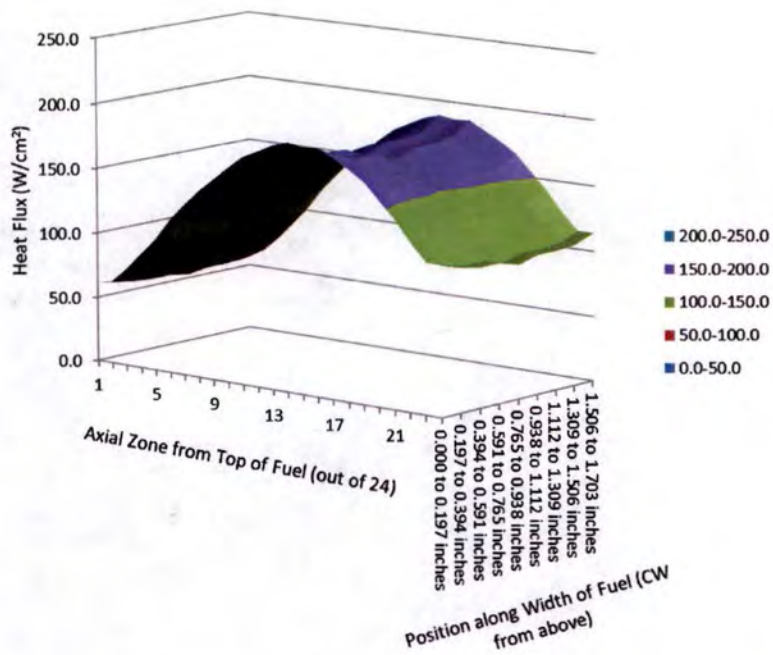


FIGURE 4.26
HEAT FLUX PROFILE IN HEU PLATE 1 OF ELEMENT 1 (0 MWD BURNUP) IN CASE 3B2 (THE POWER DISTRIBUTION IS NORMALIZED TO A CORE POWER OF 10 MW)

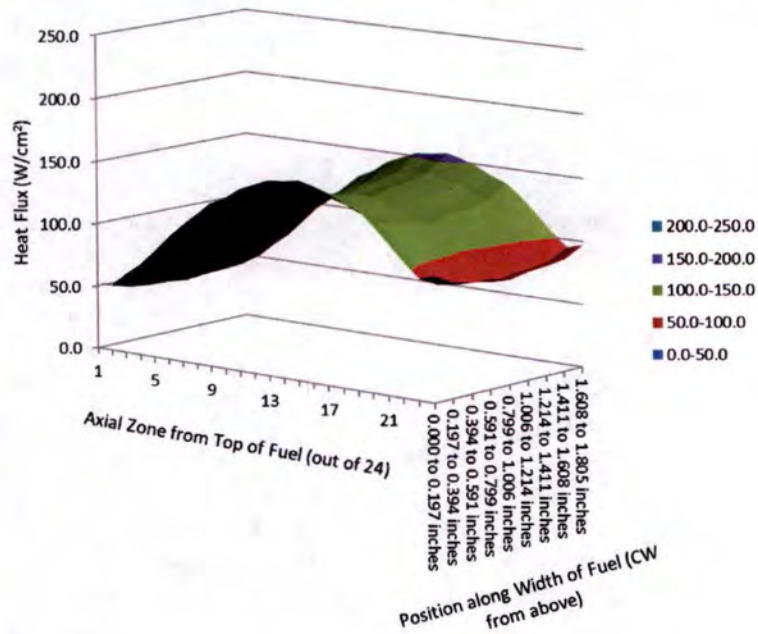


FIGURE 4.27
HEAT FLUX PROFILE IN HEU PLATE 2 OF ELEMENT 1 (0 MWD BURNUP) IN CASE 3B2 (THE POWER DISTRIBUTION IS NORMALIZED TO A CORE POWER OF 10 MW)

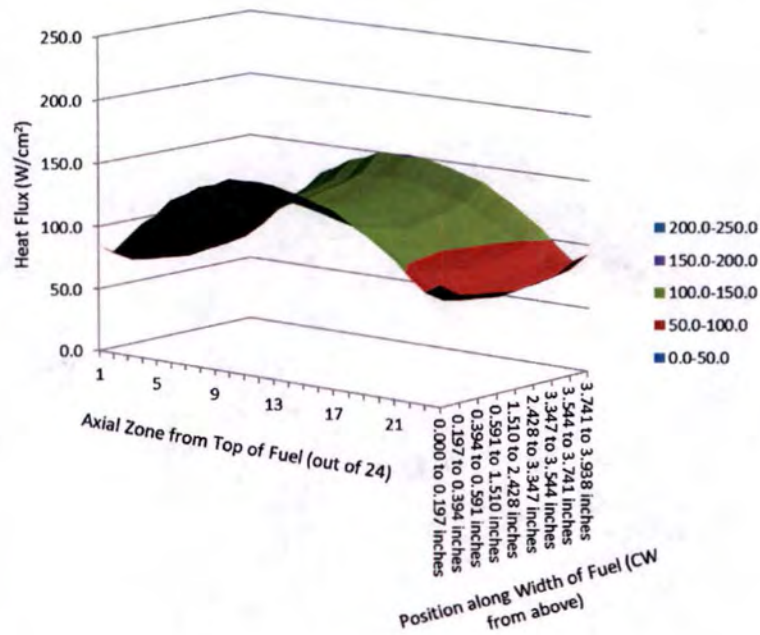


FIGURE 4.28
HEAT FLUX PROFILE IN LEU PLATE 22 OF ELEMENT 8 (174 MWD BURNUP) IN CASE 8A1 (THE POWER DISTRIBUTION IS NORMALIZED TO A CORE POWER OF 12 MW)

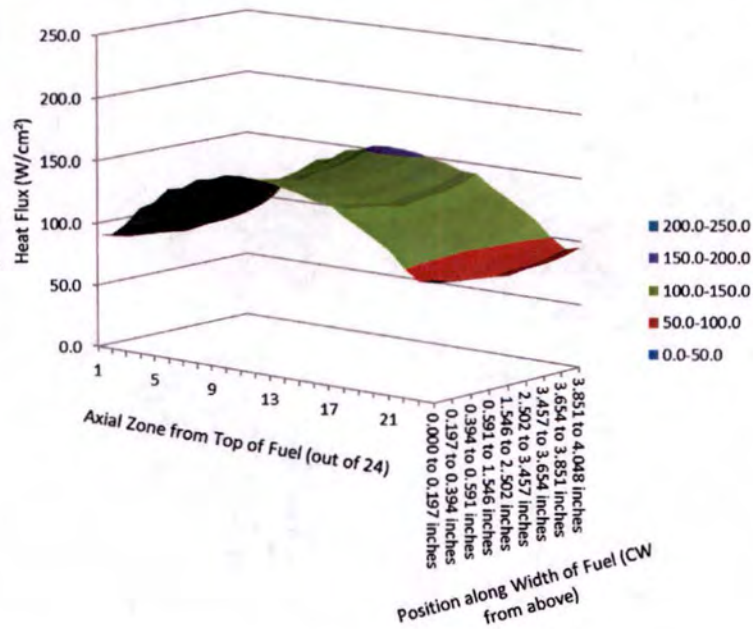


FIGURE 4.29
HEAT FLUX PROFILE IN LEU PLATE 23 OF ELEMENT 8 (174 MWD BURNUP) IN CASE 8A1 (THE POWER DISTRIBUTION IS NORMALIZED TO A CORE POWER OF 12 MW)

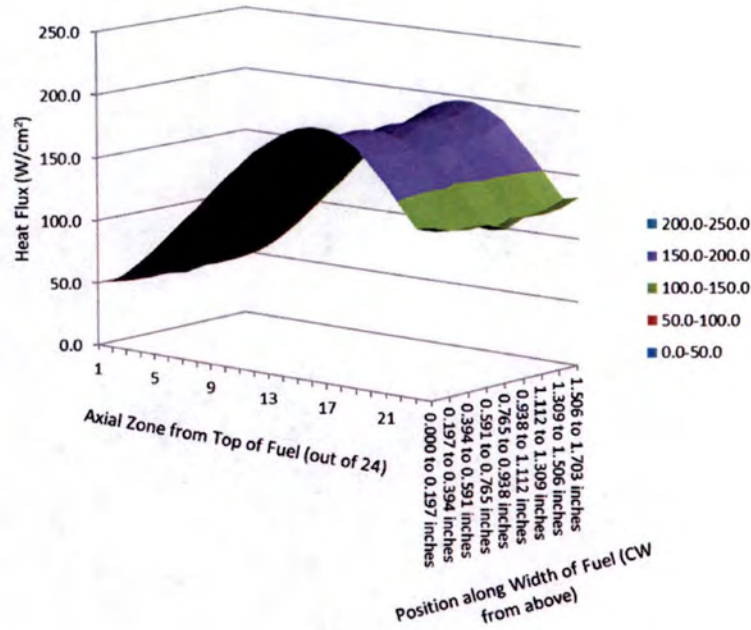


FIGURE 4.30
HEAT FLUX PROFILE IN HEU PLATE 1 OF ELEMENT 7 (0 MWD BURNUP) IN CASE 1B1 (THE POWER DISTRIBUTION IS NORMALIZED TO A CORE POWER OF 10 MW)

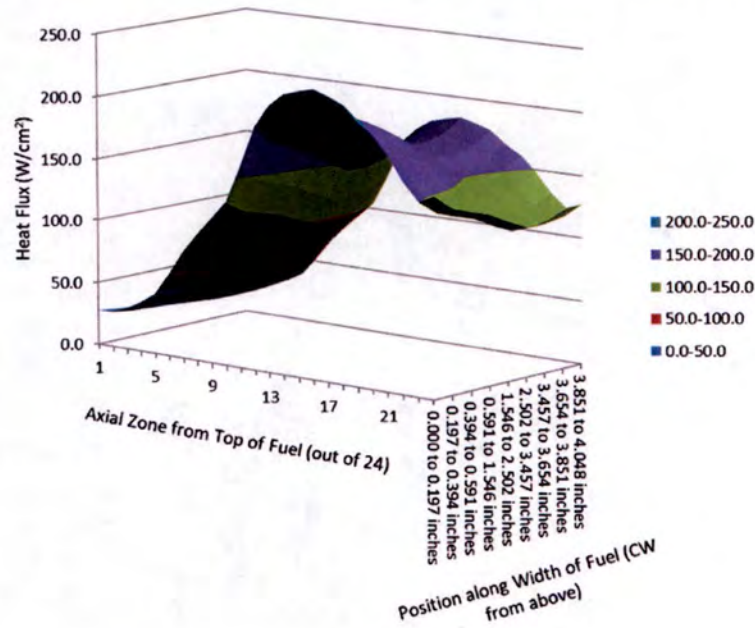


FIGURE 4.31
HEAT FLUX PROFILE IN LEU PLATE 23 OF ELEMENT 1 (0 MWD BURNUP) IN CASE 7A1 (THE POWER DISTRIBUTION IS NORMALIZED TO A CORE POWER OF 12 MW)

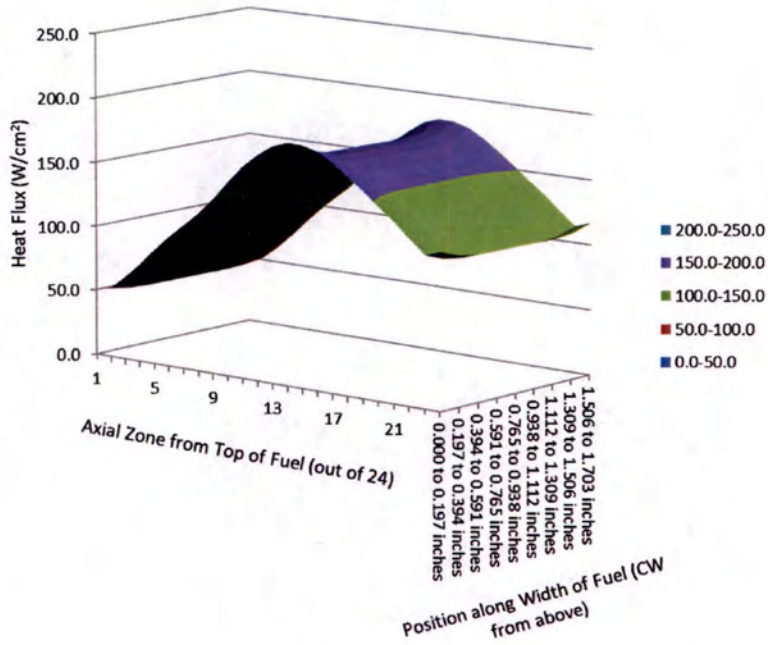


FIGURE 4.32
HEAT FLUX PROFILE IN HEU PLATE 1 OF ELEMENT 5 (0 MWD BURNUP) IN CASE 3A
(THE POWER DISTRIBUTION IS NORMALIZED TO A CORE POWER OF 10 MW)

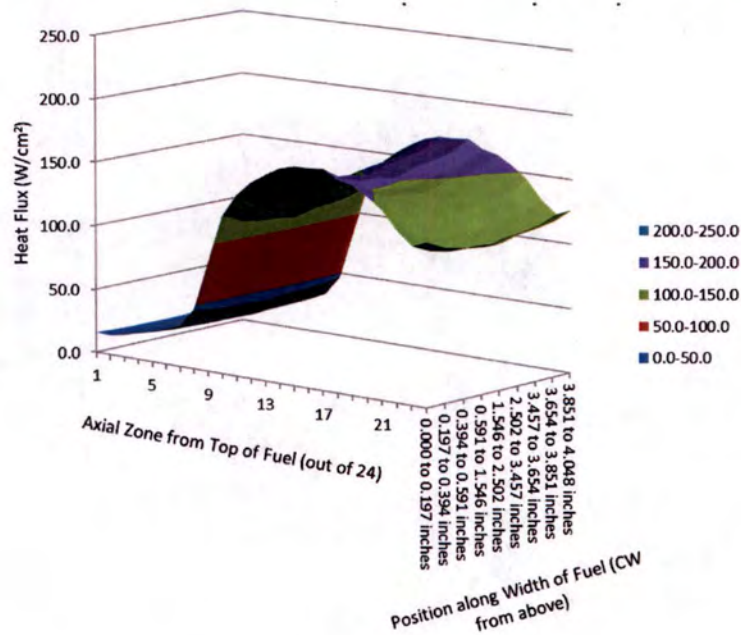


FIGURE 4.33
HEAT FLUX PROFILE IN LEU PLATE 23 OF ELEMENT 8 (174 MWD BURNUP) IN CASE 7A
(THE POWER DISTRIBUTION IS NORMALIZED TO A CORE POWER OF 12 MW)

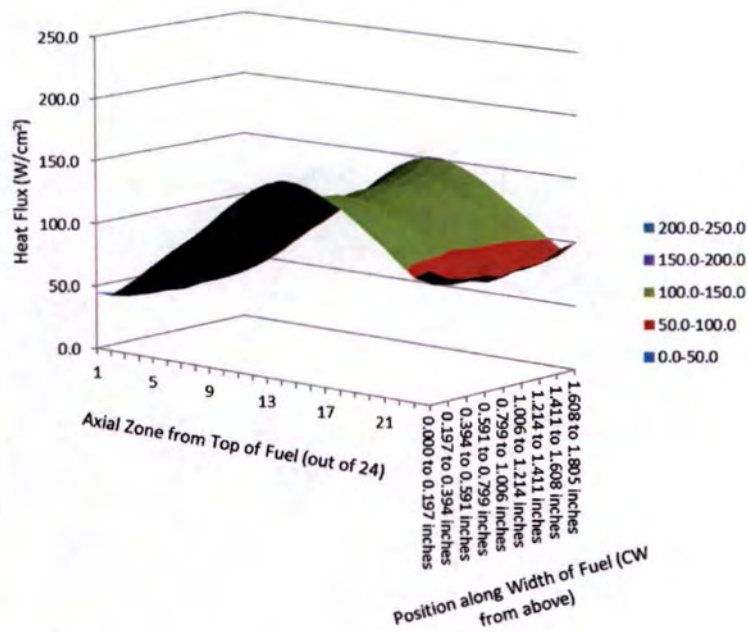


FIGURE 4.34
HEAT FLUX PROFILE IN HEU PLATE 2 OF ELEMENT 5 (0 MWD BURNUP) IN CASE 3A
(THE POWER DISTRIBUTION IS NORMALIZED TO A CORE POWER OF 10 MW)

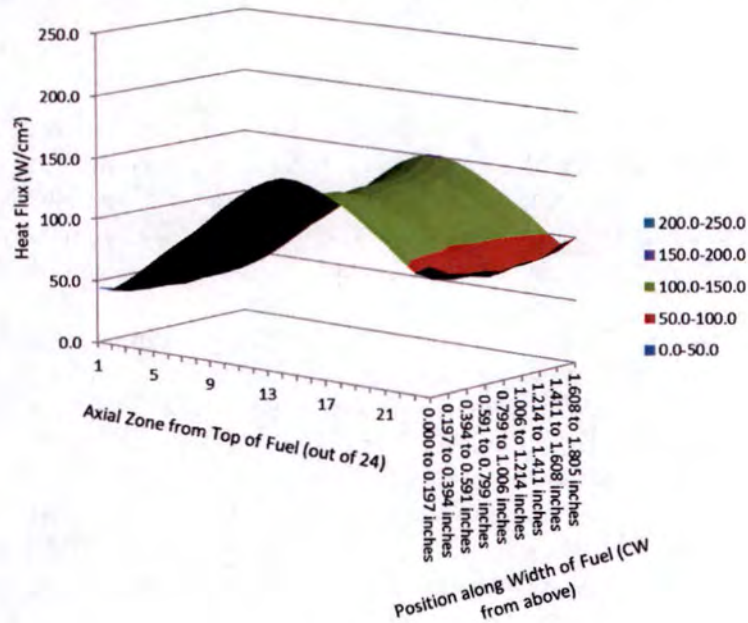


FIGURE 4.35
HEAT FLUX PROFILE IN LEU PLATE 22 OF ELEMENT 8 (174 MWD BURNUP) IN CASE
7A (THE POWER DISTRIBUTION IS NORMALIZED TO A CORE POWER OF 12 MW)

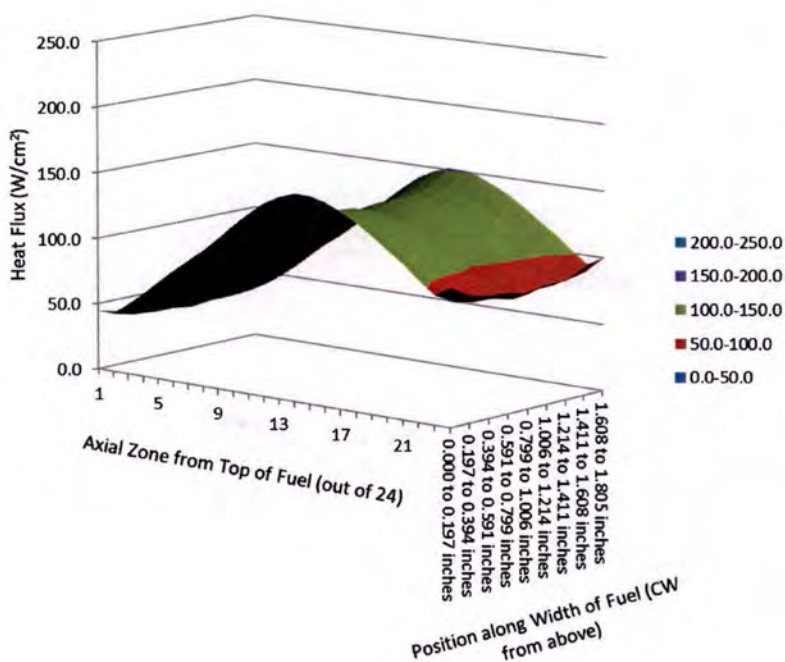


FIGURE 4.36

HEAT FLUX PROFILE IN LEU PLATE 3 OF ELEMENT 5 (0 MWD BURNUP) IN CASE 7A
(THE POWER DISTRIBUTION IS NORMALIZED TO A CORE POWER OF 12 MW)

4.6 Thermal-Hydraulic Characteristics

The MURR is a pressurized, closed-loop, water-cooled system that is situated at the bottom of an open pool. Because of this unique design, there are separate primary and pool coolant systems. A single secondary coolant system removes the heat from the primary and pool coolant loops through heat exchangers and dissipates the heat to the atmosphere via a cooling tower. The components of the MURR coolant systems are described in detail in Chapter 5, Reactor Coolant Systems.

During the design phase of MURR, three separate operating regimes were defined: low-power mode with natural convection cooling, which has only been used for initial physics testing of new fuel elements for MURR; 5 MW operation with forced cooling; and 10 MW operation, also with forced cooling. MURR initially started operating with a single primary coolant pump and heat exchanger at a maximum licensed power level of 5 MW. After upgrading the primary, pool and the secondary coolant systems and associated instrumentation, the NRC in 1974 approved operation up to 10 MW. For the conversion of MURR to LEU U-10Mo monolithic fuel, the thermal-hydraulic design analysis was completed by working with the Nuclear Engineering Division at Argonne National Laboratory. This section of Chapter 4 presents the safety analysis with the operational limit curves.

4.6.1 Natural Convection Analysis

The model used to analyze natural convective cooling of the core is provided in Section C.2.2.11 of Appendix C. More specifics of this model and detailed analytical results for both the HEU and

LEU cores can be found in Appendix C of Reference 4.34. The analysis was performed with the aid of the RELAP5/MOD3.3 code (Ref. 4.35). The reactor core is cooled by natural convection during low-power operation, Mode III operation. To accomplish this, a flanged opening is provided in the invert loop. By removing this flange and the pressure vessel head, an open path is provided between the pool and the core thereby allowing natural circulation to take place. The object of the analysis was to determine the natural convection flow rate and the corresponding maximum fuel plate temperature for the initial low-power operation.

During natural convection operation, the reactor core is cooled by pool water flowing in through the open flange, down through the 12-inch (30.48-cm) pipe, up through the pressure vessel and core, and out again into the pool. In concept, the flow rate is determined by equating the total pressure drop due to friction and form-losses to the pressure rise due to the buoyancy head resulting from the heating of the water in the core and exiting out the open pressure vessel. The flow is turbulent in the piping and in the pressure vessel and is laminar in the coolant channels of the core.

For the analysis, a power for Mode III operation of 150 kW, as indicated on page 4-44 of the MURR SAR (Ref. 4.36), was assumed for the power generated by the eight elements in the core. This page also indicates that the LSSS power is 125% of 50 kW, or 62.5 kW.

Figure C.18 of Appendix C provides a schematic view of the model used in conjunction with the RELAP5 code. In this analysis a single HEU or LEU fuel element was scaled up to represent all eight elements in the core. In this representation of the core, all fuel plates and coolant channels of the assumed limiting element were explicitly represented. For the HEU core, the assumed limiting element is element 5, which is a fresh element. For the LEU core, the assumed limiting element is element 8, which is an end-of-life element. These elements were selected because they were found to be most limiting in both the most limiting Loss of Coolant Accident (LOCA) and in the most limiting Loss of Flow Accident (LOFA) transients for their respective fuel types.

In the physics analysis the power per unit volume of fuel meat varies azimuthally along the arc length of the fuel meat. In the RELAP5 model there is only one azimuthal stripe of fuel meat per fuel plate. Therefore, in order to be conservative and to represent the maximum heat flux along the arc length of each fuel plate, the average power of each plate was multiplied by the azimuthal peak-to-average volumetric power generation rate as determined in the physics analysis. This caused the power generated by the element in the model to be greater than it would be in a core that is generating 150 kW.

In the analysis, uncertainties due to calculation and due to manufacturing tolerances were taken into account by obtaining six RELAP5 solutions for the HEU core and the analogous set of six for the LEU core. Each set started with a base case (Case 1). Each successive case added one more conservatism to the analysis, as described in Appendix C of Reference 4.34. An abbreviated version of the six cases is:

Case 1: Base Case.

Case 2: Add 5 to the K-loss at the inlet to the 12-inch diameter pipe at the inlet to the model.

- Case 3: Make all coolant channels as thin as possible by assuming the maximum tolerances for coolant channel gap thicknesses and the maximum channel reduction due to maximum burnup, even in the fresh element.
- Case 4: Increase the hydraulic resistance at the inlet and at the outlet of the core.
- Case 5: Divide the heat transfer coefficient at the each fuel plate surface by 1.2.
- Case 6: Increase the core power by a factor of 1.24 in the HEU core and by a factor of 1.22 in the LEU core.

In all six (6) cases the peak fuel temperature occurred in the node 2 of plate 2, which is near the flux trap, for the HEU fuel and in node 3 of plate 22, which is near the control blades, for the LEU fuel (The top fuel node is node 1 and the bottom is node 4). The peak fuel temperatures and core flow rates for all six cases for both fuels are shown in Table 4-21. All of these temperatures are extremely low compared to blister temperature of either fuel. Because the power level is nearly two orders of magnitude lower than normal, the temperature rise from the surface of the fuel plate – or oxide surface in the case of the LEU core – to the fuel plate centerline is extremely small. For Case 6, which has the highest power of all six (6) cases, the HEU temperature rise is 0.2 °F (0.1 °C) and the LEU temperature rise is about 1.1 °F (0.6 °C). The larger temperature rise in the LEU case is largely due to the lower LEU thermal conductivity and the presence of the oxide layer for the LEU case. The important point to be made here is that the fuel plate surface temperatures are essentially the centerline temperatures provided in Table 4-21. For a depth of 17 feet of 120 °F water and an atmospheric pressure of 14.3 psi, the local pressure is 21.6 psia. This corresponds to a saturation temperature of 232 °F (111 °C). Thus, it can also be concluded that all of the fuel plate surface temperatures in both the HEU and the LEU core during Mode III operation are far below boiling. Hence, both fuels are equally safe during Mode III operation.

TABLE 4-21
MODE III PEAK FUEL TEMPERATURES AND CORE FLOW RATES

Case	HEU				LEU			
	Temperature		Core Flow		Temperature		Core Flow	
	°C	°F	kg/s	lbm/s	°C	°F	kg/s	lbm/s
1 (base)	73.5	164	3.87	8.54	71.7	161	3.82	8.43
2 (add K-loss of 5)	74.0	165	3.77	8.31	72.2	162	3.72	8.19
3 (reduce channel gaps to minimum)	77.3	171	2.81	6.20	72.6	163	3.30	7.27
4 (add abrupt area change)	77.7	172	2.78	6.13	72.9	163	3.26	7.18
5 (divide film coefficient by 1.20)	80.0	176	2.78	6.13	75.5	168	3.26	7.18
6 (increase power by more than 20%)	83.4	182	3.12	6.87	78.6	173	3.60	7.94

4.6.2 Steady-State Forced Cooling Analysis

The optimum LEU core design for conversion of MURR to LEU is designated as CD35 and is described in Section 4.2.1, Reactor Fuel. Section 4.6.2.1 describes the thermal criteria that the fuel must meet for safe operation in MURR. Section 4.6.2.2 describes the analytical correlations used to predict the onsets of flow instability (FI) and critical heat flux (CHF), and to predict the film coefficient at the surface of the fuel. Section 4.6.2.3 covers the different core configurations and operating conditions that are analyzed. Section 4.6.2.4 provides the engineering hot channel factors used in the analysis. Section 4.6.2.5 provides the analytical model that is used to determine the pressure drop from the pressurizer to the core inlet. Section 4.6.2.6 considers the reduction in coolant channel thickness due to fuel plate swelling and oxide buildup. Section 4.6.2.7 provides a description of the key analytical tool used in the analysis, the PLTEMP/ANL code¹ (Ref. 4.37). Section 4.6.2.8 describes the modeling of the MURR core with the PLTEMP/ANL code. Based on the PLTEMP/ANL code model, Section 4.6.2.9 provides the reactor powers at which the onset of FI is predicted to occur for each of the 24 core states. Lastly, for the most limiting FI core state, the power level at which FI is predicted to occur is provided in Section 4.6.2.10 as a function of the following three LSSS parameters: pressurizer pressure, reactor coolant inlet temperature, and core flow rate. In every instance where the FI power was predicted, the margin to CHF was also assessed and found to be substantially greater. Consequently, the parametric FI curves are taken to be the operational limit curves.

4.6.2.1 Thermal Criteria

The two principal thermal criteria to be met are that of FI and CHF must be avoided by maintaining a realistic margin to safety under all operating conditions. Either of these abnormal events can lead to a rapid increase in temperature and thereby cause fuel failure. The mechanism for FI is that subcooled boiling increases the hydraulic resistance in the channel, which diverts flow to the other parallel channels. The reduced flow leads to more boiling and hydraulic resistance and thereby causes a rapid reduction in channel flow. This flow reduction excursion usually leads to CHF. When CHF occurs in this manner, the event is classified as an FI event rather than a CHF event. A CHF event is one where CHF occurs without a flow excursion. Correlations for predicting CHF are based on measurement in channels in which the channel flow rate is maintained. Typically, this would require taking measurements in a stiff single-channel system. The distinction between an FI event and a CHF event is important because, generally the power level at which an FI event occurs is significantly lower and with less uncertainty in the prediction of the channel power level than that at which a CHF event occurs.

4.6.2.2 Key Correlations

4.6.2.2.1 Correlation for Predicting Flow Instability Power (Whittle and Forgan)

The Whittle and Forgan correlation will be used to predict the margin to FI (Ref. 4.38). The form of the correlation used in the analysis is as follows:

¹ See Reference 4.22 for further details.

$$\frac{T_{\text{allowed}} - T_{\text{inlet}}}{T_{\text{sat}} - T_{\text{inlet}}} = \frac{1}{1 + \eta \frac{D_h}{L_h}} \quad (1)$$

Where:

T_{allowed} is the bulk coolant exit temperature at which FI is predicted to be initiated;

T_{sat} is the coolant saturation temperature at the exit;

T_{inlet} is the coolant inlet temperature;

D_h and L_h are the heated diameter (4 times the flow area divided by the heated perimeter) and heated length of the channel, respectively; and

η is an adjustable parameter, for which a value of 32.5 is used.

As shown in Reference 4.39 a statistical analysis of the 74 applicable experiments in Reference 4.38 was performed and found that there is a 95% confidence interval that 95% of the rectangular channel data of future measurements of the Reference 4.38 type will not exceed an η value of 31.09. Thus, the 32.5 value of η is conservative due to being slightly larger than it needs to be to achieve these statistical parameters. The reactor power used in the thermal-hydraulic analysis is adjusted until the lowest power that achieves FI in at least one coolant channel is found.

In the MURR Hazards Summary Report it is assumed that FI will not occur in a coolant channel if bulk boiling at the channel exit is avoided and each local value of heat flux is less than half of the corresponding value of CHF as predicted by the Bernath correlation (Ref. 4.40). This two-part criterion is based on measured data reported by Croft (Ref. 4.41) in 1964 for electrically-heated channels that were designed to simulate ATR channels. Croft observed that in 0.094-inch (2.39 mm) thick rectangular channels, FI occurred when the heat flux at any axial location in the heated channel reached about 60% of the value of CHF as predicted by the Bernath correlation for that location or bulk boiling occurred at the exit. Croft postulated that burnout occurred by a process referred to as "hydraulic instability or autocatalytic vapor binding" which was seen as a form of CHF that occurred prematurely. MURR chose to use a more restrictive value of 50% instead of 60%. Requiring a heat flux that is 50% of the CHF is the same as requiring a CHF ratio, i.e., ratio of CHF to heat flux, of 2.0.

Waters (Ref. 4.42) also used tests in electrically heated channels to measure the onset of fuel burnout caused by FI in the ATR. The ATR fuel elements are thermal-hydraulically similar to those in the MURR reactor. However, the ATR heated length is 48 inches (121.9 cm), which is twice that of the MURR. Reference 4.43 showed that equation 1 with a value of η of 32.5 accurately predicts FI in the Croft and the Waters experiments.

4.6.2.2.2 Correlation for Predicting Critical Heat Flux (Extended Groeneveld 2006)

If FI is prevented or is assumed not to occur, the MURR core potentially could experience a subcooled CHF (critical quality $X < 0$). The calculations that follow explore this scenario. The recent subcooled CHF literature was searched and evaluated, and the Groeneveld 2006 CHF Table (Ref. 4.44) with a new diameter correction (Ref. 4.45) was selected as the most reliable for

predicting CHF in the MURR steady-state thermal-hydraulic analysis. This correlation is reproduced in equation 2, below.

$$q_c(D, P, G, X_o) = \begin{cases} q_c(0.008, P, G, X_o) \left(\frac{0.008}{D}\right)^n & \text{if } G \leq 8000 \\ q_c(0.008, P, 8000, X_o) \left(\frac{0.008}{D}\right)^n \left(\frac{G}{8000}\right)^{0.376} & \text{if } G > 8000 \end{cases} \quad (2)$$

Where:

q_c = CHF (kW/m²);

n = 0.312;

D = Diameter of the tube (m). As discussed below, it is in general the heated diameter of the channel, given by $(4 \times \text{flow area}/\text{heated perimeter})$. Note that the heated diameter equals the tube diameter for a circular tube heated over the whole perimeter;

P = Coolant pressure (bar);

G = Coolant mass flux in the channel (kg/m²-s); and

X_o = Equilibrium quality at the CHF location (critical quality).

Range of application:

$3 < D < 25$ mm;

$1000 < G < 30,000$ kg/m²-s;

$1.0 \leq P \leq 210$ bar;

(heated length)/ $D > 25$ for subcooled CHF;

(heated length)/ $D > 50$ for saturated CHF;

inlet temperature > 0.01 °C; and

$-0.5 < X_o < 1.0$.

The diameter correction in equation 2 ($n = 0.312$) was recommended by Celata (Ref. 4.46), Hall and Mudawar (Ref. 4.45), and finally by the exhaustive review of Tanase et al. (Ref. 4.47) with Groeneveld as co-author. The first term in equation 2, $q_c(0.008, P, G, X)$, is obtained from a look-up table that is basically a normalized data bank of CHF for a vertical water-cooled tube of 0.3150-inch (0.008 m) diameter. The 2006 table provides CHF values at 24 pressures, 20 mass fluxes, and 23 qualities, covering the ranges 14.5 to 3,046 psia (1 to 210 bars) pressure, 0 to 1,638.5 lb/ft²-s (0 to 8,000 kg/m²-s) mass flux, and -0.5 to 1.0 critical quality. The 2006 table is derived from a world-class database containing 33,175 measured CHF data points, out of which 8,394 "bad" data points due to FI or poorly performed experiments were not used. It is the combined database (Ref. 4.44) created by the Atomic Energy of Canada, Limited (AECL), Canada, and the Institute of Physics and Power Engineering (IPPE), Russia. The root-mean-square error reported by Groeneveld et al. (Ref. 4.44) for subcooled CHF is 14.7%, if the 2006 table is used with the direct

substitution method, and 7.1%, if the 2006 table is used with the heat balance method. The direct substitution method was used in the analysis. The factor $(G/8000)^{0.376}$ in equation 2 uses $q_c(0.008, P, 8000, X_0)$ and extends the application of the 2006 table to mass fluxes greater than $8000 \text{ kg/m}^2\text{-s}$, using the same mass flux-dependence of CHF as in the Hall-Mudawar subcooled correlation (Ref. 4.45).

4.6.2.2.3 Nusselt Number Correlation for Predicting Film Coefficient (Dittus-Boelter)

The Dittus-Boelter Nusselt number correlation with an added factor of $(\mu_b/\mu_w)^{0.11}$, where μ_b is the viscosity of the coolant evaluated at the bulk coolant temperature and μ_w is the viscosity of the coolant evaluated at the wall temperature, was used in the analysis. The viscosity ratio factor is to account for the potentially large variation in coolant viscosity over the coolant channel cross section at a specific axial level. Thus, the Nusselt number, Nu, used in the analysis is:

$$\text{Nu} = 0.023 \text{Re}^{0.8} \text{Pr}^{0.4} \left(\frac{\mu_b}{\mu_w} \right)^{0.11} \quad (3)$$

Where:

Nusselt Number, Nu = $h D_e / k$;

Reynolds number, Re = $\rho V D_e / \mu_b$; and

Prandtl number, Pr = $\mu_b c_p / k$.

With:

h = film coefficient (BTU/hr-ft²-°F);

ρ = bulk coolant density (lbm/ft³);

V = mean coolant velocity over the flow cross section (ft/s);

D_e = hydraulic diameter (ft);

c_p = specific heat capacity of the bulk coolant (BTU/lbm-°F); and

k = the thermal conductivity of the bulk coolant (BTU/hr-ft-°F).

Although the film coefficient has a substantial effect on the temperatures within the fuel plate, it has only a second-order effect on FI and CHF. This is because it only affects how the power generated within a fuel plate is split between the two channels on either side of the fuel plate.

4.6.2.3 Core Configuration and Operating Conditions

As covered in Section 4.5.4.2, based on the two possible extremes for each of three operating condition variables (fuel element burnup state, ¹³⁵Xe status, and flux trap region status) the neutron physics analysis considered eight general cases that together bound the worst thermal-hydraulic state for the proposed LEU CD35 reactor cores for the radial, axial, and azimuthal plate peaking factors. Within each of these cases there are the three control blade arrangements that bracket the control blades possibilities, resulting in a total of 24 core states. Table 4-18 describes this set of 24 cases for LEU CD35 core.

4.6.2.4 Engineering Hot Channel Factors

Hot channel factors are used in the thermal-hydraulic analyses in order to take into account the potential adverse effects of manufacturing tolerances and uncertainties in modeling on the quantities being predicted for safety analysis purposes. For example, a coolant channel may be thinner than its nominal value. A thinner channel would result in a lower coolant velocity than in a nominal channel. It would also have a lower flow rate due to both the lower velocity and the smaller flow area. The lower flow rate, in turn, would increase the channel bulk coolant temperature rise and could also reduce the film coefficient at the bounding fuel plate surfaces. In the analysis, separate hot channel factors are introduced for the effect on coolant channel flow rate, for the effect on bulk coolant temperature rise, and for the effect on film coefficient. Each of these hot channel factors would have values greater than 1.0. The bulk coolant temperature rise and the film temperature rise would each be multiplied by their hot channel factors. The coolant channel flow rate would be divided by its hot channel factor. The hot channel factor is always used as a multiplicative factor or a divisor, depending on which choice represents an adverse effect.

Typically, a nominal analysis is performed first. Then the hot channel factors are applied to each channel individually. If instead, all of the channels were assumed to be simultaneously at the minimum thickness that their tolerances permit, much of the effect on flow would be masked. Since the total reactor flow rate is assumed to be a known value, narrowing all of the channels at the same time would not redirect flow away from any one channel. Much of the effect would appear as a greater core pressure drop and no change in channel flow rate. First, a nominal analysis is performed in which the individual channel flow rates are determined with all channels assumed to be at their nominal thicknesses. Then the adverse effects on coolant channel flow rate, bulk coolant temperature, and fuel plate surface temperature are captured via three separate hot channel factors, which are applied to the channel coolant flow rate, bulk coolant temperature rises, and fuel plate surface temperature rises that are obtained in the nominal analysis.

4.6.2.4.1 Engineering Local Hot Channel Factor Contributors

The five local contributors to hot channel factor that were considered in the analysis are:

- Fuel meat thickness and ^{235}U homogeneity (Local);
- ^{235}U fuel plate loading;
- Power peaking;
- Channel spacing (or gap thickness); and
- Flow distribution.

Each of these five contributors is a random effect that can affect one fuel plate or channel, without affecting another. This is to be contrasted with a global factor such as an uncertainty in film coefficient due to the choice of Nusselt number correlation, discussed later, which can adversely affect the film temperature rise at all fuel plate surfaces simultaneously. The first three contributors affect heat flux. The remaining two contributors affect channel flow rate.

Fuel Meat Thickness and ^{235}U Homogeneity (Local)

The combined effect of the local fuel meat thickness and ^{235}U homogeneity are measured together by the fuel plate manufacturer. Radiographs of every fuel plate are taken by sending gamma rays through the thickness of the entire fuel plate. The relative amount of uranium within a specified area is detected by how dark the area appears on the radiograph for the plate. The darkness of the area is compared to a standard, which is an absolute standard that is the same for each plate of the same nominal fuel meat thickness. This method of measurement combines the local effects of fuel meat thickness and uranium density. A tolerance value of $\pm 20\%$ is provided for the HEU fuel and $\pm 15\%$ for the LEU fuel in Reference 4.48. Both of these tolerance values are over a 0.50-inch (1.27 cm) diameter area. In the thermal analysis, this tolerance has a direct effect on local heat flux, but essentially no effect on channel bulk coolant temperature rise.

^{235}U Fuel Plate Loading

There is a tolerance on the total ^{235}U fuel plate loading within a fuel plate, which is not a local or spot tolerance. Table 2.2 in Reference 4.48 indicates that for the HEU fuel this tolerance is $\pm 1\%$. Reference 4.48 also provides tolerance values for the LEU design, which differ plate-by-plate. The basis for these LEU values is a ± 0.001 inch tolerance on the thickness of the fuel meat. Thus, the fuel meat can be as much as 1 mil thicker than its nominal value over the entire fuel length. Hence, the fuel meat of plate 1 of the LEU CD35 design, which is nominally 9 mils thick, can be between 8 and 10 mils thick. This represents a tolerance of $\pm 1/9 = \pm 11\%$. Due to self-shielding effects, a tolerance of $\pm 11\%$ will cause less than $\pm 11\%$ variation in plate heat flux. This was studied with the MCNP code (Ref. 4.26). The results are provided in Table 4-22 for the LEU CD35 design. In the thermal analysis, the power overload fraction in percent was rounded up to the nearest whole percent, as indicated in the table. The results for plates 4 through 22 of the CD35 design are based on MCNP analysis of plate 4. In the thermal analysis this tolerance has a direct effect on bulk coolant temperature rise. It has no effect on local heat flux, which is a local effect that is fully taken into account in the combined tolerance of the local fuel meat thickness and uranium homogeneity that is measured by radiography.

TABLE 4-22
LEU CD35 PLATE OVERLOAD TOLERANCE FRACTIONS, %

Plate	Meat Thickness (mils)	Overload Tolerance Fraction, %	
		Calculated	Used
1	9	8.5	9.0
2	12	6.2	7.0
3	16	5.4	6.0
4 - 22	20	3.4	4.0
23	17	3.9	4.0

Power Density

In spite of the considerable geometric and analytical detail that goes into determining the three-dimensional distribution of power throughout the core with the aid of the MCNP code (Ref. 4.28), there is some uncertainty in the calculated power density distribution. For both the HEU and the LEU cores, the power density tolerance is assumed to affect the values of heat flux by $\pm 10\%$. This value is based on a combination of judgment and analysis. Part of this uncertainty is due to potential variations in the distribution of the fuel as allowed by fuel element manufacturing tolerances and clearances in the core to facilitate fuel element insertion and removal. In the MURR conversion feasibility study report (Ref. 4.33) the effects of 0.008-inch (0.203 mm) changes in channel thicknesses and 0.015-inch (3.81 mm) movements of entire elements on individual fuel plate powers were studied for a preliminary LEU element design and were found to be no more than about $\pm 2\%$, which is well within the $\pm 10\%$ tolerance assumed.

Channel Spacing (or Gap Thickness)

Variations in channel thickness can be due to tolerance in the as-built fuel plate thickness, to fuel swelling and clad oxidation, and to variations in the fuel plate spacing during fuel element manufacture. For thin rectangular channels for which the hydraulic diameter is approximately twice the channel thickness and where the flow is turbulent with friction factor approximated as, $f = Re^{-\alpha}$, where Re is Reynolds number, Reference 4.49 shows that the hot channel factor component for velocity, F_v , is:

$$F_v = \left(\frac{t_{\text{nom_chan}}}{t_{\text{hot_chan}}} \right)^{\frac{1+\alpha}{2-\alpha}} \quad (4)$$

where $t_{\text{nom_chan}}$ is the nominal thickness of the channel and $t_{\text{hot_chan}}$ is the minimum thickness of the channel. The Reynolds number exponent, α , is normally between 0.20 and 0.25 for turbulent flow. In the hydraulic analysis, 0.25 is used. Equation 4 is based on the perturbation in the flow rate of a single channel due to a decrease in channel thickness from $t_{\text{nom_chan}}$ to $t_{\text{hot_chan}}$ with no change in pressure drop between the inlet and outlet of the channel. F_v is the ratio of the velocity through the channel when the channel thickness is at its nominal value to the velocity through the channel when the channel thickness is at its minimum value.

Similarly, the ratio of the nominal channel flow rate to the hot channel flow rate, F_w , which is a hot channel factor component for flow rate, is the product of F_v and the ratio of the nominal channel flow area to the hot channel flow area, i.e., $t_{\text{nom_chan}} / t_{\text{hot_chan}}$. Hence,

$$F_w = \left(\frac{t_{\text{nom_chan}}}{t_{\text{hot_chan}}} \right)^{\frac{3}{2-\alpha}} \quad (5)$$

Reference 4.49 shows that the hot channel factor component for film coefficient, F_h , is:

$$F_h = \left(\frac{t_{\text{nom_chan}}}{t_{\text{hot_chan}}} \right)^{\frac{0.4+\alpha}{2-\alpha}} \quad (6)$$

This relationship is based on the Dittus-Boelter Nusselt number correlation.

Table 4-3 and Table 4-5 provide the nominal distances between fuel plates, which is the nominal coolant channel gap thickness, of all of the internal channels for the HEU and LEU cores. All of the channels that are not end channels have a channel thickness tolerance of ± 8 mils. The minimum channel thickness for the end channel nearest the flux trap (channel 1) is 0.088 (2.235 mm) and 0.0735 (1.867 mm) inches for the HEU and LEU cores, respectively. The minimum channel thickness for the end channel furthest from the flux trap is 0.065 (1.651 mm) and 0.0705 (1.791) inches for the HEU and LEU cores, respectively. For both the HEU and the LEU cores, the minimum value of the end channel nearest the flux trap is always 22 mils less than its nominal value and the minimum value of the end channel furthest from the flux trap is always 25 mils less than its nominal value. The minimum value for each end channel is based on the fuel element rollers nearest the channel being pressed against the nearest pressure vessel wall.

Flow Distribution

For a series of parallel channels all of equal thickness, slight variations in manufacturing that are not captured by the tolerances and other effects that are not captured by the analytical methods can lead to variations in flow among the channels. For example, the hydraulic analysis uses Moody friction factors that are obtained from the Colebrook equation and are a function of Reynolds number and relative roughness. The surface roughness is an empirically determined quantity and the Colebrook equation is a fit to empirical data. For both the HEU and the LEU cores the uncertainty in element flow rate due to uncertainty in flow distribution is assumed to be $\pm 15\%$. This is based on judgment.

4.6.2.4.2 Combining Local Hot Channel Uncertainty Factor Components

Table 4-23 provides a sample hot channel factor calculation for channel 23 and plate 23 of the LEU CD35 core. Channel 23 is between fuel plates 22 and 23.

The table layout is by columns:

- Lists the local hot channel factor contributors;
- Lists the tolerance fractions;
- Gives the effect that the contributor has on the bulk coolant temperature rise. In the hot channel factor calculation, where there are two fuel plates bounding a channel, each is assumed to contribute equally to the channel bulk coolant temperature rise. This is to be contrasted with an end channel for which the single bounding fuel plate contributes 100% to the channel bulk coolant temperature rise;
- Contribution to Plate 22 convex side film temperature rise;
- Contribution to channel 23 bulk coolant temperature rise;

- Contribution to Plate 23 concave side film temperature rise;
- Contribution to Plate 23 heat flux; and
- Contribution to Channel 23 velocity.

In the first column each of the first three contributors listed above, which are fuel meat thickness and ^{235}U homogeneity (local), ^{235}U fuel plate loading, and power density, appears twice, once for each of the two fuel plates that bound channel 23. A 15% increase in the power generated at a particular location of the fuel plate is assumed to cause a 15% increase in the local heat flux exiting both surfaces of the fuel plate. This will cause a 15% increase in the local film temperature rise on each side of the fuel plate. This explains the three 1.15 factors shown in the second and third rows of the table. Since local variations in heat flux should have a negligible effect on the overall bulk coolant temperature rise, F_{BULK} is not impacted by this local 15% tolerance.

The ^{235}U loading and the power density contributors each increase the total power produced by each fuel plate. Therefore, they both increase the bulk coolant temperature rise. A 4% ^{235}U loading tolerance from one of two fuel plates that heat a channel causes a 2% increase in the coolant temperature rise. Hence, it contributes a factor of 1.02 to F_{BULK} . Similarly, a 10% power density tolerance contributes a factor of 1.05 to F_{BULK} . The power density increases the local heat flux in the same manner that the fuel meat thickness and ^{235}U homogeneity does and similarly affects F_{FILM} and F_{FLUX} . However, the ^{235}U loading does not contribute to F_{FILM} and F_{FLUX} . The reason is, as explained earlier, that in the radiography measurements fuel meat thickness and uranium homogeneity is measured against an absolute standard that includes the effect of uranium loading. Thus, if a ^{235}U loading factor were included here, the effect of this tolerance would be included twice.

As shown in the small subsection at the bottom of Table 4-23, the nominal thickness of channel 23 is 93 mils and the tolerance is 8 mils. In this example, there is no reduction in channel thickness due to fuel swelling or oxide buildup. Thus, the hot channel thickness is 93 – 8 mils, or 85 mils, and the ratio of the nominal channel thickness to the hot channel thickness is 93/85, or 1.094. This ratio is used in equations 4, 5, and 6 with an α of 0.25 to obtain components of F_{VELOCITY} , F_{BULK} , and F_{FILM} , respectively. As shown in the “Channel Thickness” row in the table, the component for F_{VELOCITY} , which is based on the equation for F_v , is 1.066, the one for F_{BULK} , which is based on the equation for F_w , is 1.167, and both of the ones for F_{FILM} , which is based on the equation for F_h , are 1.034.

Taken by itself, the flow distribution tolerance of 15% would cause the nominal values of velocity and flow rate to each be divided by a factor of 1.15. Dividing the flow rate by a factor of 1.15 increases the bulk coolant temperature rise by the same factor. Hence, in the “Flow Distribution” row of Table 4-23, F_{BULK} and F_{VELOCITY} are each 1.15. The 1.118 factor in the same row for the two values of F_{FILM} is $1.15^{0.8}$. This is because in the Dittus-Boelter correlation for Nusselt number, the film coefficient is proportional to flow rate raised to the 0.8 power.

For LEU core CD35, the combined components of: F_{FILM} for the convex side of plates 22, F_{FILM} for the concave side of plate 23, F_{BULK} and F_{VELOCITY} for channel 23, and F_{FLUX} for plate 23 are shown near the bottom of Table 4-23 for both the multiplicative and statistical combination

methods described Reference 4.22. The same methods were repeated for all of the fuel plates and all of the coolant channels of all three cores. Table 4-24 provides values of combined hot channel factors for the LEU CD35 core for the case of no fuel plate swelling or oxide growth.

The multiplicative combination of hot channel factor components is employed in the MURR SAR (Ref. 4.36). Using the multiplicative combination of hot channel factor components in the current analysis facilitates more direct comparisons between the earlier analysis and the current one. An important acceptance criterion for the LEU core that is to replace the HEU core is that the thermal safety margins for the replacement core must be comparable to or greater than those of the HEU core. The acceptability of the replacement core essentially would not be affected by the larger power margins that the statistical combination of hot channel factor components for the LEU core would predict, since the HEU core, which is the standard to be achieved, would also display larger power margins.

4.6.2.4.3 Global Hot Channel Factors

In contrast to the just considered local hot channel factors, which are assumed to occur randomly, this section considers global, or systematic, hot channel factors. A prime example of a global hot channel factor is the one that arises in the film coefficient at the surface of the fuel plate. The uncertainty in the equation 3 Nusselt number correlation being employed to obtain the film coefficient can affect all fuel plate surfaces simultaneously. In the analysis, based on judgment, an uncertainty factor of 1.20 is applied to the film coefficient. Hence, the values of film coefficient, h , used in the analysis are obtained by dividing the value of h (predicted via equation 3) by 1.20.

The safety limiting values of power, flow rate, inlet temperature, and pressurizer pressure are additional examples of global factors. In the operation of the MURR, the uncertainty in the measurement of these quantities is taken into consideration. For example, because the uncertainty in the inlet temperature is 5 °F, the trip setting on inlet temperature is set at least 5 °F lower than it would be if there was no uncertainty in the measurement of the inlet temperature. Hence, no uncertainty factors associated with these measured quantities are included in the analysis.

TABLE 4-23
 SAMPLE HOT CHANNEL FACTOR CALCULATION FOR CHANNEL 23 AND PLATE 23
 OF THE LEU CD35 CORE

Local Contributor	Tolerance, Fraction	Effect on Bulk ΔT , Fraction	Plate 22 Film ΔT , F_{FILM}	Channel 23 Bulk ΔT , F_{BULK}	Plate 23 Film ΔT , F_{FILM}	Plate 23 Heat Flux, F_{FLUX}	Channel 23 Velocity, $F_{VELOCITY}$
Fuel Meat Thickness & ^{235}U Homogeneity (Local) for Plate 22	0.15		1.15				
Fuel Meat Thickness & ^{235}U Homogeneity (Local) for Plate 23	0.15				1.15	1.15	
^{235}U Loading for Plate 22	0.04	0.50		1.020			
^{235}U Loading for Plate 23	0.04	0.50		1.020			
Power Density for Plate 22	0.10	0.50	1.10	1.050			
Power Density for Plate 23	0.10	0.50		1.050	1.10	1.10	
Channel Thickness (See below.)			1.034	1.167	1.034		1.066
Flow Distribution	0.15		1.118	1.15	1.118		1.15
Uncertainties Combined Multiplicatively			1.46	1.54	1.46	1.27	1.23
Uncertainties Combined Statistically			1.22	1.24	1.22	1.18	1.16

Channel Thickness, mils	
Nominal Channel	93
Tolerance	8
Swelling & Oxide	0
Hot Channel	85
Thickness Ratio, Nominal/Hot	1.094

TABLE 4-24
HOT CHANNEL FACTORS FOR THE LEU CD35 CORE
(NO FUEL PLATE SWELLING OR OXIDE GROWTH)

Chan nel (or Plate*)	Multiplicative Combination					Statistical Combination					Thick ness Ratio
	F _{FIL} M Left	F _{BUL} K	F _{FILM} Right	F _{FLUX}	F _{VELO} CITY	F _{FILM} Left	F _{BUL} K	F _{FILM} Right	F _{FLUX}	F _{VELO} CITY	
1	-	2.16	1.56	1.27	1.39	-	1.60	1.24	1.18	1.25	1.30
2	1.46	1.60	1.46	1.27	1.23	1.22	1.24	1.22	1.18	1.16	1.09
3	1.46	1.58	1.46	1.27	1.23	1.22	1.24	1.22	1.18	1.16	1.09
4	1.46	1.55	1.46	1.27	1.23	1.22	1.24	1.22	1.18	1.16	1.09
5	1.46	1.54	1.46	1.27	1.23	1.22	1.24	1.22	1.18	1.16	1.09
6	1.46	1.54	1.46	1.27	1.23	1.22	1.24	1.22	1.18	1.16	1.10
7	1.46	1.54	1.46	1.27	1.23	1.22	1.24	1.22	1.18	1.16	1.10
8	1.46	1.54	1.46	1.27	1.23	1.22	1.24	1.22	1.18	1.16	1.10
9	1.46	1.54	1.46	1.27	1.23	1.22	1.24	1.22	1.18	1.16	1.10
10	1.46	1.54	1.46	1.27	1.23	1.22	1.24	1.22	1.18	1.16	1.10
11	1.46	1.54	1.46	1.27	1.23	1.22	1.24	1.22	1.18	1.16	1.10
12	1.46	1.54	1.46	1.27	1.23	1.22	1.24	1.22	1.18	1.16	1.10
13	1.46	1.54	1.46	1.27	1.23	1.22	1.24	1.22	1.18	1.16	1.10
14	1.46	1.54	1.46	1.27	1.23	1.22	1.24	1.22	1.18	1.16	1.10
15	1.46	1.54	1.46	1.27	1.23	1.22	1.24	1.22	1.18	1.16	1.10
16	1.46	1.54	1.46	1.27	1.23	1.22	1.24	1.22	1.18	1.16	1.10
17	1.46	1.54	1.46	1.27	1.23	1.22	1.24	1.22	1.18	1.16	1.10
18	1.46	1.54	1.46	1.27	1.23	1.22	1.24	1.22	1.18	1.16	1.10
19	1.46	1.54	1.46	1.27	1.23	1.22	1.24	1.22	1.18	1.16	1.10
20	1.46	1.54	1.46	1.27	1.23	1.22	1.24	1.22	1.18	1.16	1.09
21	1.46	1.54	1.46	1.27	1.23	1.22	1.24	1.22	1.18	1.16	1.09
22	1.46	1.54	1.46	1.27	1.23	1.22	1.24	1.22	1.18	1.16	1.09
23	1.46	1.54	1.46	1.27	1.23	1.22	1.24	1.22	1.18	1.16	1.09
24	1.58	2.21	-	-	1.43	1.25	1.71	-	-	1.28	1.35

*"Plate" applies only to F_{FLUX}. ("Channel" applies to all other entries.)

4.6.2.5 Methodology for Calculating Pressure at Core Inlet

Figure 4.37 shows a schematic representation of the reactor core inlet piping. The measured pressurizer pressure used in the operation of the reactor is the pressure of the nitrogen gas above the liquid surface in the pressurizer. This pressure is controlled and has a minimum LSSS value of 75 psia (517 kPa). Point 1 in Figure 4.37 is 608 feet and 6 inches (185.5 m) above sea level. The flow in Loop 'A' and the flow in Loop 'B' are each always 25 gpm (94.6 lpm) more than half of the core flow. Thus, in the figure where the total core flow rate is 3,600 gpm (13,627 lpm), 1,825 gpm (6,908 lpm) enters from the left through Loop 'A' and another 1,825 gpm (6,908 lpm) enters through Loop 'B'. At point 2, 50 gpm (189 lpm) is extracted from the Loop 'A' flow and

goes to the deionizer. The deionizer flow remains constant at 50 gpm (189 lpm) regardless of the core flow. At point 3, the remaining 1,775 gpm (6,719 lpm) of the Loop 'A' flow merges with the 1,825 gpm (6,908 lpm) flow of Loop 'B' to form the combined flow of 3,600 gpm (13,627 lpm) that goes through the core. Hence, the flow rate between points 2 and 3 is always 25 gpm (94.6 lpm), less than half of the total core flow rate. The flow rate between points 3 and 4 is always the total core flow rate.

As shown in Figure 4.37, the pressurizer is attached to a stagnant leg below Loop 'A.' For the thermal-hydraulic analysis of the reactor core, the pressure at point 4, which is between the fuel plates and at the inlet to them, is needed. The pressure at point 1 is the pressurizer pressure reduced by the gravity head, ΔP_P , from the surface of the liquid water in the pressurizer to point 1, which is along Loop 'A.' The Bernoulli equation, modified to include the hydraulic resistance from point 1 to 4, is used to determine the pressure drop from point 1 to point 4.

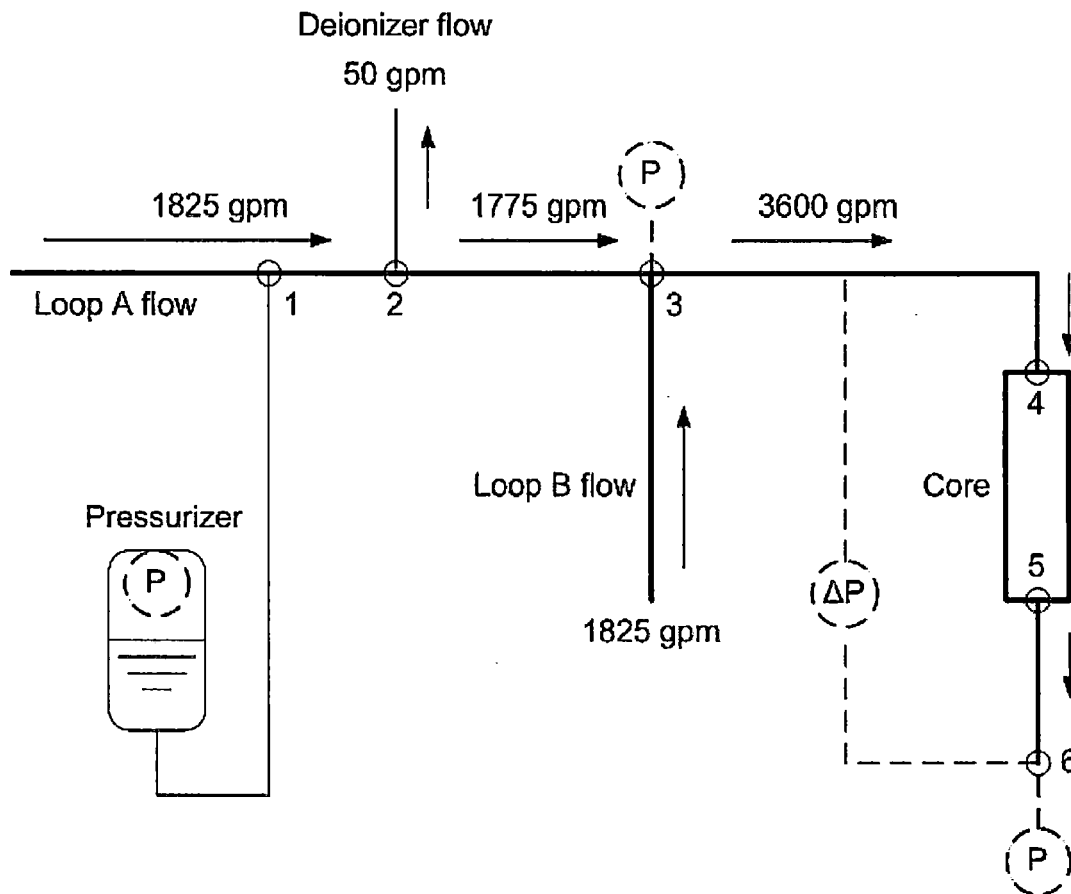


FIGURE 4.37
SCHEMATIC REPRESENTATION OF THE REACTOR CORE INLET PIPING

A zero-inch reading for the pressurizer liquid water level corresponds to 48 inches (1.22 m) below point 1. L is the water level in the pressurizer in inches above the zero reading, then:

$$\Delta P_P = P_P - P_1 = \rho_P \times g \times (48 - L) \quad (7)$$

where P_P and P_1 are the pressure at the pressurizer water surface and point 1, respectively, ρ_P is the density of the liquid in the pressurizer and also in the pressurizer pipe leg leading to point 1, g is the acceleration due to gravity, 9.80665 m/s^2 . Since the water in the stagnant leg leading from the pressurizer to Loop 'A' is at $85 \text{ }^\circ\text{F}$ ($29.4 \text{ }^\circ\text{C}$), the density is 995.97 kg/m^3 . The nominal value of L is zero inches. The primary coolant charging pump starts adding water to the pressurizer when the pressurizer water level lowers to 6 inches (15.2 cm) below its nominal value. A low water-level scram is initiated at -16 inches (-40.6 cm).

The Bernoulli equation, modified to include the hydraulic resistance from point 1 to 4 is:

$$P_1 + \frac{\rho V_1^2}{2} + \rho g Z_1 = P_4 + \frac{\rho V_4^2}{2} + \rho g Z_4 + \Delta P_{HR} \quad (8)$$

where P is pressure, ρ is the density of the fluid between points 1 and 4, V is velocity, Z is elevation, ΔP_{HR} is the pressure drop due to the hydraulic resistance between points 1 and 4, and subscripts 1 and 4, of course, refer to points 1 and 4. The pressure drop due to the hydraulic resistance is an irrecoverable pressure loss caused by the pipes and fittings between points 1 and 4.

Equations 7 and 8 may be combined to eliminate P_1 and obtain:

$$P_4 = P_P - \rho_P g (48 - L) + \rho g (Z_1 - Z_4) - \frac{\rho(V_4^2 - V_1^2)}{2} - \Delta P_{HR} \quad (9)$$

$Z_1 - Z_4$ is 15.25 inches (38.74 cm). The velocity at any point is the local volumetric flow rate in the pipe, divided by the local pipe flow area. Point 1 is in an 8-inch pipe that has a flow area of 0.34741 ft^2 (0.10589 m^2). The flow rate at point 4 is always the total core flow rate. The flow area at point 4 is the flow area inside the fueled region, which is 0.3419 ft^2 (0.10421 m^2) and 0.3715 ft^2 (0.11323 m^2), for the HEU and LEU CD35 cores, respectively.

A set of relationships that define ΔP_{HR} were obtained by MURR staff during March through May of 2011. They used hydraulic handbook data and analytical models that were calibrated with measurements on the MURR. Measurements were made on March 27, 2011 with the eight core fuel elements in the reactor vessel and the reactor operating at 10 MW. Measurements were also taken on March 28, 2011 with the eight core fuel elements out of the reactor vessel while the primary coolant system was operating. The locations where pressure measurements were made are indicated in Figure 4.37 by the letter "P" inside a dashed circle. The pressure difference, which is indicated in Figure 4.37 by " ΔP " inside a dashed circle, was also measured, along with coolant flow rates and temperatures.

The pressure drop ΔP_{HR} can be divided into three pressure drops, one from point 1 to point 2 of Figure 4.37, one from point 2 to point 3, and one from point 3 to point 4. Each of these three pressure drops is the sum of a pressure drop component that is characterized by friction, ΔP_f , at the walls of the pipes and another component, ΔP_K , which is characterized by form losses (often called "K-losses"). The value of ΔP_{HR} is the sum of these six (6) pressure drop components.

From well-known hydraulic relationships for turbulent flow through pipes and fittings, one can derive the relationship for the pressure drop portion along each pipe segment that is characterized by friction at the walls of the pipes as:

$$\Delta P_f = \Delta P_{f0} \left(\frac{\rho}{\rho_0} \right)^{0.8} \left(\frac{Q}{Q_0} \right)^{1.8} \left(\frac{\mu}{\mu_0} \right)^{0.2} \quad (10)$$

where ΔP_{f0} , ρ_0 , Q_0 , and μ_0 are the pressure drop portion, density, volumetric flow rate, and viscosity for a reference temperature T_0 ; and ΔP_f , ρ , Q , and μ are the corresponding quantities at any temperature T . In a similar manner, one can derive the relationship for the pressure drop portion along each pipe segment that is characterized by form losses as:

$$\Delta P_K = \Delta P_{K0} \left(\frac{\rho}{\rho_0} \right)^{1.0} \left(\frac{Q}{Q_0} \right)^{2.0} \quad (11)$$

where ΔP_{K0} , ρ_0 , and Q_0 are the pressure drop portion, density, and volumetric flow rate for a reference temperature T_0 ; and ΔP_K , ρ , and Q are the corresponding quantities at any temperature T .

In equations 10 and 11, Q and Q_0 always correspond to the flow rate and reference flow rate, respectively, along the particular path. In the derivation of equation 10 it was assumed that friction factor is inversely proportional to the Reynolds raised to the 0.20 power. The data in Table 4-25 provide the frictional and non-frictional portions of ΔP_{HR} for each of the three path segments between points 1 and 4 for a reference temperature of 120 °F (48.9 °C) and the reference flow rate indicated for each path segment in the table and in Figure 4.37. As shown in the table, the frictional value of ΔP_f from point 2 to point 3 is 0. The values of density and viscosity at the reference temperature are 988.69 kg/m³ and 5.5725E-4 Pa-s, respectively. Density and viscosity are essentially independent of pressure over the range of pressures of interest to the operation of the MURR. A pressure of 4.5 bar (65 psi) was assumed in obtaining ρ_0 and μ_0 and ρ_P in equation 7. Equation 9, with ΔP_{HR} obtained from equations 10 and 11 and data from Table 4-25, can be used to obtain P_4 .

TABLE 4-25
REFERENCE HYDRAULIC CONDITIONS USED IN
CONJUNCTION WITH EQUATIONS 10 AND 11 TO
DETERMINE ΔP_{HR}

The six individual pressure drops provided in Table 4-25 are often the sum of the pressure drops of several hydraulic components. The total list of component groups and their associated components are listed below. The path from the pressurizer to the core outlet is divided into 24 component pressure drops that are categorized into seven distinct groups. Within each group all of the pressured drops are considered to be either frictional,

Path Segment	T_0 , °F	Q_0 , gpm	Pressure Drop at T_0 , psi	
			Frictional, ΔP_{f0} (Equation 10)	Non-frictional, ΔP_{K0} (Equation 11)
Point 1 to 2	120	1825	0.0913	4.500
Point 2 to 3	120	1775	0.0	0.2640
Point 3 to 4	120	3600	4.5551	0.8008

i.e., a result of pipe-wall friction, or non-frictional, i.e., a result of some type of form-loss. The list of seven component groups is as follows:

List of Component Groups:

1. 8-inch fine mesh strainer before the expander (1)
2. Primary coolant loop 'A' between pressurizer to expander:
 - a. Pressurizer surge line to primary coolant loop 'A' centerline (2)
 - b. 4.5 feet of 8-inch pipe (3)
3. Primary coolant loop 'A' 8-inch/12-inch expander (4)
4. From expander through pressure vessel entrance:
 - a. 1 foot of 12-inch pipe (5)
 - b. Tee combining primary coolant loop 'A' & loop 'B' (6)
 - c. 65.5 feet of 12-inch pipe (7)
 - d. Two 12-inch 90° elbows (8)
 - e. 12-inch butterfly valve (9)
 - f. 31.575 feet of 12-inch pipe (10)
 - g. Two 12-inch 90° elbows (11)
 - h. Three 12-inch 45° elbows (12)
 - i. 12-inch swing check valve (13)
 - j. Entrance Tee to pressure vessel annulus (14)
5. In pressure vessel up to reactor core:
 - a. Junction of 12-inch inlet pipe through fuel element upper end fitting (15)
 - b. 17.75-inch long annulus (16)
 - c. 34.25-inch long annulus (17)
 - d. 3.75-inch long annulus (18)
 - e. Flow in fuel element upper end fitting (19)
6. Step changes in pressure vessel:
 - a. Gentle reduction in annulus (20)
 - b. Two step changes in annulus (21)
7. Entrance into fuel element channels:
 - a. Entrance to fuel element end fitting (22)
 - b. Exit from fuel element end fitting (23)
 - c. Entrance into fuel element channels (24)

Table 4-26 provides the reference pressure drop assigned to them as a result of hydraulic measurements and analysis with the corresponding flow rate, and coolant temperature for each of the seven groups. The last column of this table indicates whether the pressure drop is frictional or

non-frictional. By comparing Table 4-25 with Table 4-26, one can observe that first three non-zero pressure drops in Table 4-25 were obtained from Component Groups 1, 2, and 3 in Table 4-26, that the last frictional pressure drop in Table 4-25 was obtained from the sum of the two pressure drops for Component Groups 4 and 5 in Table 4-26, and that the last non-frictional pressure drop in Table 4-25 was obtained from the sum of the two pressure drops for Component Groups 6 and 7 in Table 4-26.

TABLE 4-26
REFERENCE PRESSURE DROP DATA

Component Group	ΔP_0 (PSI)	Q_0 (GPM)	T_0 (°F)	Frictional
1. 8-inch fine mesh strainer before expander (1)	4.5000	1825	120	No
2. Loop 'A' between pressurizer to expander (2-3)	0.0913	1825	120	Yes
3. Loop 'A' 8-inch/12-inch expander (4)	0.2640	1775	120	No
4. Expander through pressure vessel entrance (5-14)	3.3961	3600	120	Yes
5. In pressure vessel up to reactor core (15-19)	1.1590	3600	120	Yes
6. Step changes in pressure vessel (20-21)	0.0439	3600	120	No
7. Entrance into fuel element & channels (22-24)	0.7569	3600	120	No

4.6.2.6 Channel Thickness Reduction Due to Fuel Plate Swelling and Oxide Buildup

The reduction in channel thickness due to fuel plate swelling and oxide buildup reduces the flow through the channel. This adversely affects the bulk coolant temperature rise and the film temperature rise at the surface of the fuel plate. Since the total core flow rate is controlled, the flow that is diverted from one channel must go to another channel. A bounding approach to the flow reduction in one channel could cause an overly optimistic assessment of the flow in the other channels. This problem is avoided by treating the channel thickness reduction as if it were the result of a local manufacturing tolerance, as described in Section 4.6.2.4.

For the HEU core the maximum reduction in channel thickness due to fuel plate swelling and oxide buildup for channels bounded by two fuel plates is assumed to be 10 mils. For the LEU core this value was reduce to 8 mils to reflect expected fuel swelling and oxide growth. The reduction in end channel thickness is taken to be half of the internal channel values, i.e., 5 mils for the HEU and 4 mils for the LEU core. For the fresh fuel, the channel thickness reduction due to fuel plate swelling and oxidation buildup is assumed to be zero. The channel thickness reduction is assumed to be linearly proportional to burnup.

4.6.2.7 PLTEMP/ANL Code

The PLTEMP/ANL code (Ref. 4.37) is the primary thermal-hydraulic computational tool that is used in evaluating the margins to FI and CHF during steady-state operation. It is capable of modeling all of the MURR fuel elements at one time and considering all of the fuel plates and

coolant channels of each element simultaneously. In the PLTEMP/ANL code, the only coupling between parallel elements is hydraulic.

The code divides the axial length of the core into a series of 24 parallel axial layers and predicts the temperatures and heat fluxes of each layer. The code considers the thermal boundary conditions in the channel on each side of a fuel plate in determining the fraction of the power emanating from each face of the fuel plate. This can be particularly important when the channel on one side of a fuel plate is much cooler than the channel on the other side, such as may occur in the end channels of an element.

The code includes a hot channel factor on bulk coolant temperature rise for each channel of each element. It also includes a hot channel factor on film temperature rise, i.e., from bulk coolant to fuel plate surface, for each heated surface of each fuel plate. There is also a hot channel factor on heat flux for each fuel plate in the core. A global hot channel factor on the Nusselt correlation, which is used in determining the local values of film coefficient, is also included. The code does not include a hot channel factor on coolant velocity, $F_{VELOCITY}$, for the CHF models used in the analysis.

The code can explicitly represent the axial power distribution of each fuel plate. Although not used in the current analysis, the code also allows the fuel meat of each fuel plate to be subdivided into vertical strips, so that the axial power distribution for each strip can be explicitly represented. Since the MURR LEU core has thin rectangular channels with large aspect ratios, the strip-wise variations in power can be extremely significant to the thermal-hydraulic performance of the core. The code does not include thermal conduction from one axial layer to the next or one vertical strip to the next. Within each axial level of each strip, the heat transfer from the fuel meat to the bulk coolant is assumed to be one dimensional with the thermal conductance from the fuel plate surface to the adjacent bulk coolant represented by a film coefficient. Equation 3 is the Nusselt number (or film coefficient) correlation used of those included in the code. An unheated vertical strip can also be included at the ends of the channel, before the first and after the last heated vertical strip of each channel. The adjustable user-input parameter that allows for coolant mixing between adjacent strips to be set to no mixing, complete mixing, or anything in between—was set to no mixing.

The code has a hydraulic model that predicts the coolant flow rate of each channel in the core. The pressure drop, ΔP , across the length of each coolant channel is the same for all of the channels and is represented as:

$$\Delta P = (f_i L/D_i + K) \times \rho_i V_i^2/2; \quad (12)$$

Where:

- f_i = the Moody friction factor for channel I;
- L = the length of the channel (ft);
- D_i = the hydraulic diameter of channel I (ft);
- ρ_i = the coolant density of channel I (lbm/ft³);

- V_i = the bulk coolant velocity of channel i based on ρ_i (ft/s); and
- K = a single value used to represent the sum of the inlet and outlet form-loss values and is applied to all coolant channels in the element.

The ρ_i , V_i , and Reynolds number are evaluated at the average of the coolant channel inlet and outlet temperatures. If ΔP is known, then a value of V_i can be determined using equation 12 for each coolant channel in the core. Because the flow area of each channel is known, the total core flow rate for a given value of ΔP can be determined. The code has a search capability which allows the assumed pressure drop across the reactor to be adjusted until the total flow rate through the reactor is predicted to be the desired value. This, in effect, allows the total core flow rate to be a user-specified input.

The flow rate of each strip of a channel is assumed to be linearly proportional to the arc length of the strip. For each vertical strip of each heated coolant channel in the core, the PLTEMP/ANL code can calculate the flow instability ratio (FIR), which is the ratio of the allowed bulk coolant temperature rise based on equation 1 to the calculated bulk coolant temperature rise. The code has a search capability to automatically adjust the reactor power until the minimum FIR value of the strips in the core is a particular value that is specified by code input. Similarly, the code has the ability to calculate the CHF ratio for each of the two heat transfer surfaces of each axial level of each strip of each plate of each element in the core and to adjust the core power until a specified value of minimum CHF ratio is achieved. A beta version of PLTEMP v 4.2 of October 30, 2013 (SVN revision 65) which includes speedup improvements, extended Groeneveld 2006 CHF table, channel-dependent hot channel factors, and an improved double search algorithm was used in the analysis.

4.6.2.8 Application of the PLTEMP/ANL Code to the MURR Cores

A PLTEMP/ANL model was developed for the HEU core and another was developed for the LEU CD35 core. Each model explicitly and simultaneously represented all coolant channels and all fuel plates of all eight elements of each core. The heated width of each fuel plate was represented as a single vertical strip and was not subdivided into smaller strips. However, a single unheated strip on each side of the heated strip was modeled. Thus, each coolant channel was represented as three adjoining subchannels. In the model, it was assumed that there is no mixing among these three subchannels. Hence, it was assumed that none of the power that is deposited in the fuel meat is shared with either of the two unheated edge subchannels.

The heated length of the core was subdivided into 24 horizontal sublayers. This was done to match the axial power distributions provided by the core neutron physics analysis (Ref. 4.28). The core neutron physics analysis also subdivided each fuel meat into nine vertical strips. Although the code can explicitly represent this fine structure, it assumes that there is no heat conduction between adjacent strips.

Rather than represent each strip, the PLTEMP/ANL model for each MURR core used multipliers on the local hot channel factor to account for the more severe thermal conditions of the limiting strip. For each of the nine heated strips of each fuel plate, the ratio of the average heat flux in a strip to the average heat flux for the entire heated width of the fuel plate was determined. (Here,

in the determination of average heat fluxes in a strip, half of the power of each fuel plate strip was assumed to exit each strip face.) The largest ratio for each plate was identified and incorporated into the three local hot channel factors: F_{FLUX} , F_{FILM} , and F_{BULK} . Thus, the value of F_{FLUX} , and the two values of F_{FILM} for each fuel plate was multiplied by the largest of the fuel plate's nine heat flux ratios. For each internal coolant channel, the value of F_{BULK} was multiplied by the average of the ratios for the two bounding fuel plates. For each end channel, F_{BULK} was multiplied by this ratio for the one bounding fuel plate. The hot channel factors listed in Table 4-24 do not include these heat-flux ratio multipliers. Thus, in the PLTEMP/ANL model, the multiplicatively-combined channel-by-channel and plate-by-plate hot channel factors provided in Table 4-24 were multiplied by these ratios to predict an upper bound for the thermal conditions of the most limiting strip of each channel and to also include the reductions in channel thickness due to fuel plate swelling and clad surface oxidation, as described in Section 4.6.2.6.

Because the code does not include a hot channel factor on coolant velocity ($F_{VELOCITY}$), this effect is investigated separately, as described in Section 16f of Reference 4.22. This factor has no effect on the margin to FI that is predicted by equation 1 because velocity does not appear in this equation. However, it does have an effect on CHF as predicted by equation 2 because mass flux, G , is the product of density and velocity. A reduction in velocity will reduce the predicted CHF value.

Core neutron physics calculations showed that 6.0% of the reactor power generated by the HEU core is deposited outside of the primary coolant system. Therefore, the power represented in the PLTEMP/ANL model is only the 94% of the reactor power deposited in the core. So, for the HEU core, all PLTEMP/ANL values of power obtained by the code were divided by 0.940 to calculate the total power to be inserted in the tables of results provided later. Similarly, for the LEU CD35 cores, 3.6% of the reactor power is deposited outside the primary coolant system. According, the PLTEMP/ANL powers for the CD35 cores were divided by 0.964 to obtain total power.

4.6.2.9 Reactor Flow Instability and Critical Heat Flux Reactor Power Limits

Each of the 24 core states for the LEU CD35 cores were analyzed to determine the limiting power level for the selected FI and CHF criteria. Since the limiting power level is being calculated, the pressurizer water level was assumed at the low SCRAM set point of -16 inches (40.6 cm) and the three non-power Limiting Safety System Setting (LSSS) variables were set at the LSSS values:

<u>Fuel Type</u>	<u>Pressurizer Pressure</u>	<u>Core Inlet Flow Rate</u>	<u>Core Inlet Temperature</u>
LEU CD35 core	75 psia	3,300 gpm	145 °F

The results are given in Table 4-27. The bases for the LSSS values are given in Section 4.6.4.

For the LEU CD35 core, the most limiting FI occurs in core case 8A1 at a power level of 17.10 MW, which is margin of 2.1 MW above the LSSS power of 15.0 MW (See Section 4.6.4). For the HEU this margin also is 2.1 MW above the HEU LSSS power of 12.5 MW. This case has fuel elements with equilibrium xenon and a mix of fuel power histories ranging from 0 to 170 MWd. The reactor has samples loaded in the flux trap, and control blades are two each with the two extreme utilization histories. The two fresh control blades are one-inch lower than the two with high burn up. The limiting coolant channel is channel 23 between fuel plates 22 and 23 in fuel

element 8, with 170 MWd of previous power history. The steady-state heat flux profiles for these plates normalized to a core power of 12 MW are provided in Figures 4.28 and 4.29.

TABLE 4-27
REACTOR FLOW INSTABILITY POWER (MW) FOR LEU CORE CD35¹

Case	Power	Element	Coolant Channel
5A	19.63	5	4
5A1	18.91	8	4
5A2	18.86	1	4
6A	20.57	2	4
6A1	18.79	6	23
6A2	19.05	8	23
7A	18.57	8	4
7A1	17.99	6	23
7A2	17.95	8	23
8A	17.87	8	23
8A1	17.10	8	23
8A2	17.15	8	23
5B	19.19	4	3
5B1	18.32	7	4
5B2	18.56	2	4
6B	19.99	5	3
6B1	18.73	6	23
6B2	18.94	8	23
7B	18.17	4	4
7B1	17.65	8	4
7B2	17.58	8	4
8B	17.56	8	23
8B1	17.37	6	23
8B2	17.25	8	23
Min. Ratio	1.140		
Margin, MW	2.10		

¹ All other reactor operating conditions are at the safety limit – 145 °F inlet temperature, 3,300 gpm based on the inlet density, and 75 psia at the pressurizer. The pressurizer level is at –16 inches.

For each of the 24 core states the CHF ratio was calculated at a core power that was greater than 15 MW. In every instance, the predicted CHF ratio was greater than 2.0 (See Table 18 of Reference 4.22).

4.6.2.10 Operational Limit Curves

Because core case 8A1 of Table 4-27 is the most limiting state with regard to FI, the PLTEMP/ANL code was used to perform a parametric study in which the three LSSS parameters – pressurizer pressure, core inlet temperature, and core inlet flow rate – were varied. The pressurizer water level was set to the low level SCRAM set point at 16 inches (40.6 cm) below centerline because this provides the lowest core inlet pressure for a given pressurizer pressure.

The FI power limits were determined for various possible combinations of six different core inlet temperatures and eleven different core inlet flow rates at the following three different pressurizer pressures: 60, 75 and 85 psia (413.7, 517.1 and 586.1 kPa). The power limits for the 66 cases at each of the three pressurizer pressures are given in Tables 4-28 through 4-30. These values are graphed in Figures 4.38 through 4.40 where curves of allowed power versus coolant flow rate are provided for parametric values of inlet coolant temperature. While the fuel temperature safety limit in the TS provides a not-to-exceed value for the fuel temperature, Figures 4.38 through 4.40 provide operational limit curves where temperatures are known without further analysis to not exceed the fuel temperature safety limit. Because in every instance the flow instability power is lower than the critical heat flux power (Ref. 4.22), the flow instability limit results of Tables 4-28 through 4-30 are the operational limit curves.

TABLE 4-28
LEU CORE CD35 FLOW INSTABILITY POWER (MW)
WITH THE PRESSURIZER PRESSURE AT 60 PSIA

Reactor Inlet Water Conditions											
Temp	Flow Rate (GPM)										
°F	400	800	1200	1600	2000	2400	2800	3200	3300	3600	4000
120	2.57	5.05	7.45	9.75	11.93	13.96	15.79	17.39	17.74	18.68	19.57
140	2.27	4.45	6.55	8.56	10.46	12.20	13.76	15.09	15.38	16.13	16.78
145	2.19	4.30	6.33	8.27	10.09	11.76	13.25	14.51	14.79	15.49	16.09
160	1.96	3.84	5.66	7.38	8.98	10.45	11.73	12.79	13.02	13.57	13.99
180	1.66	3.24	4.77	6.20	7.52	8.70	9.71	10.50	10.65	11.01	11.18
200	1.36	2.65	3.88	5.02	6.06	6.96	7.69	8.22	8.31	8.47	8.39

TABLE 4-29
LEU CORE CD35 FLOW INSTABILITY POWER (MW)
WITH THE PRESSURIZER PRESSURE AT 75 PSIA

Reactor Inlet Water Conditions											
Temp	Flow Rate (GPM)										
°F	400	800	1200	1600	2000	2400	2800	3200	3300	3600	4000
120	2.80	5.50	8.14	10.69	13.14	15.47	17.64	19.63	20.09	21.39	22.87
140	2.49	4.90	7.24	9.50	11.66	13.70	15.59	17.30	17.70	18.80	20.02
145	2.42	4.75	7.02	9.20	11.29	13.26	15.08	16.72	17.10	18.15	19.31
160	2.19	4.30	6.34	8.31	10.18	11.93	13.55	14.98	15.31	16.21	17.17
180	1.88	3.70	5.45	7.12	8.71	10.18	11.51	12.67	12.93	13.63	14.33
200	1.58	3.10	4.56	5.95	7.24	8.43	9.48	10.37	10.56	11.05	11.50

Table 4-30
LEU Core CD35 Flow Instability Power (MW)
with the Pressurizer Pressure at 85 psia

Reactor Inlet Water Conditions											
Temp	Flow Rate (GPM)										
°F	400	800	1200	1600	2000	2400	2800	3200	3300	3600	4000
120	2.93	5.77	8.54	11.23	13.83	16.32	18.68	20.87	21.38	22.87	24.62
140	2.63	5.17	7.64	10.04	12.35	14.55	16.62	18.53	18.98	20.26	21.75
145	2.55	5.01	7.41	9.74	11.98	14.11	16.10	17.95	18.38	19.61	21.03
160	2.32	4.56	6.74	8.84	10.86	12.78	14.57	16.20	16.58	17.65	18.88
180	2.02	3.96	5.84	7.66	9.39	11.01	12.52	13.87	14.19	15.05	16.02
200	1.71	3.36	4.95	6.47	7.92	9.26	10.48	11.56	11.81	12.47	13.17

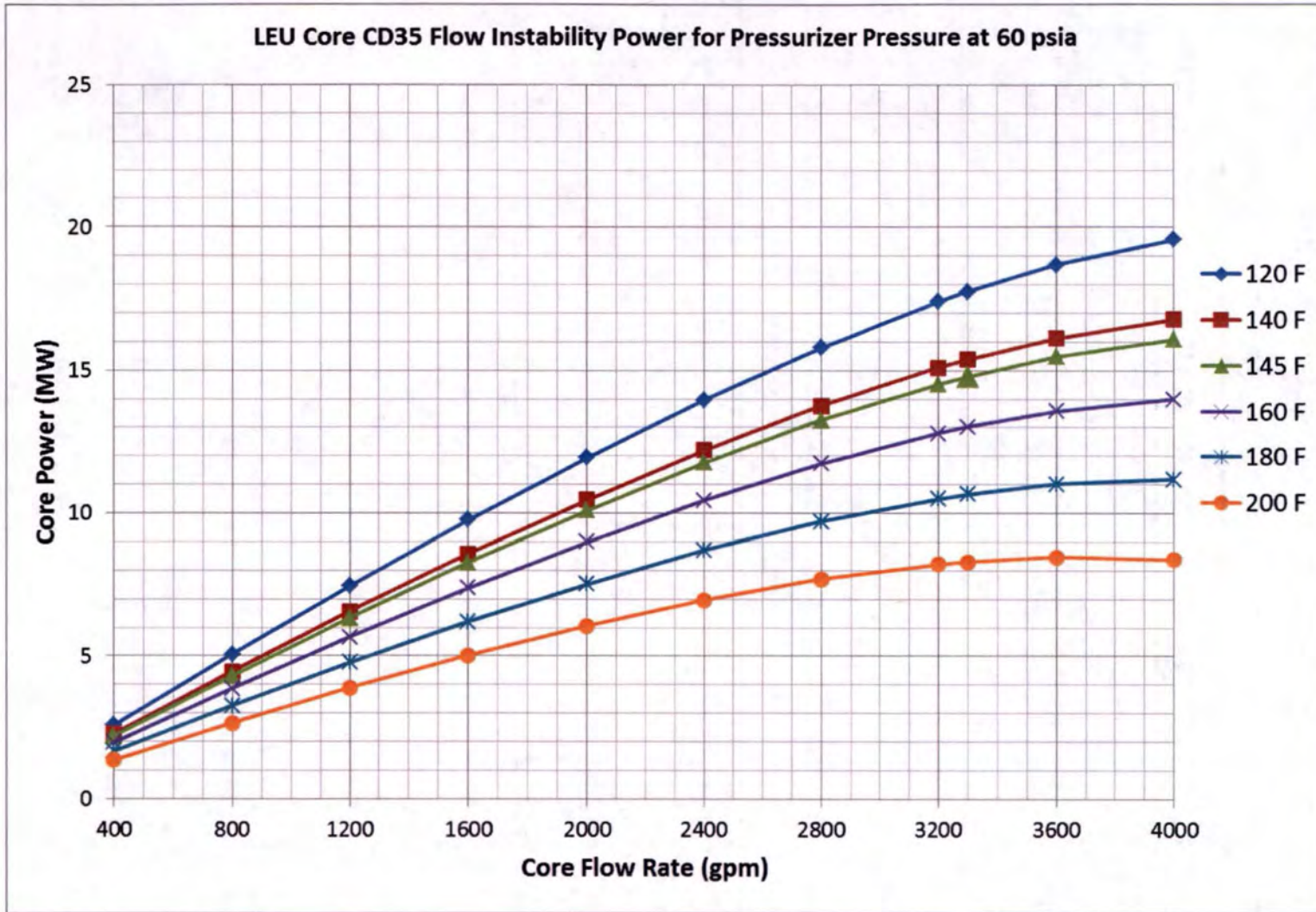


FIGURE 4.38
LEU CORE CD35 FLOW INSTABILITY POWER FOR PRESSURIZER PRESSURE AT 60 PSIA

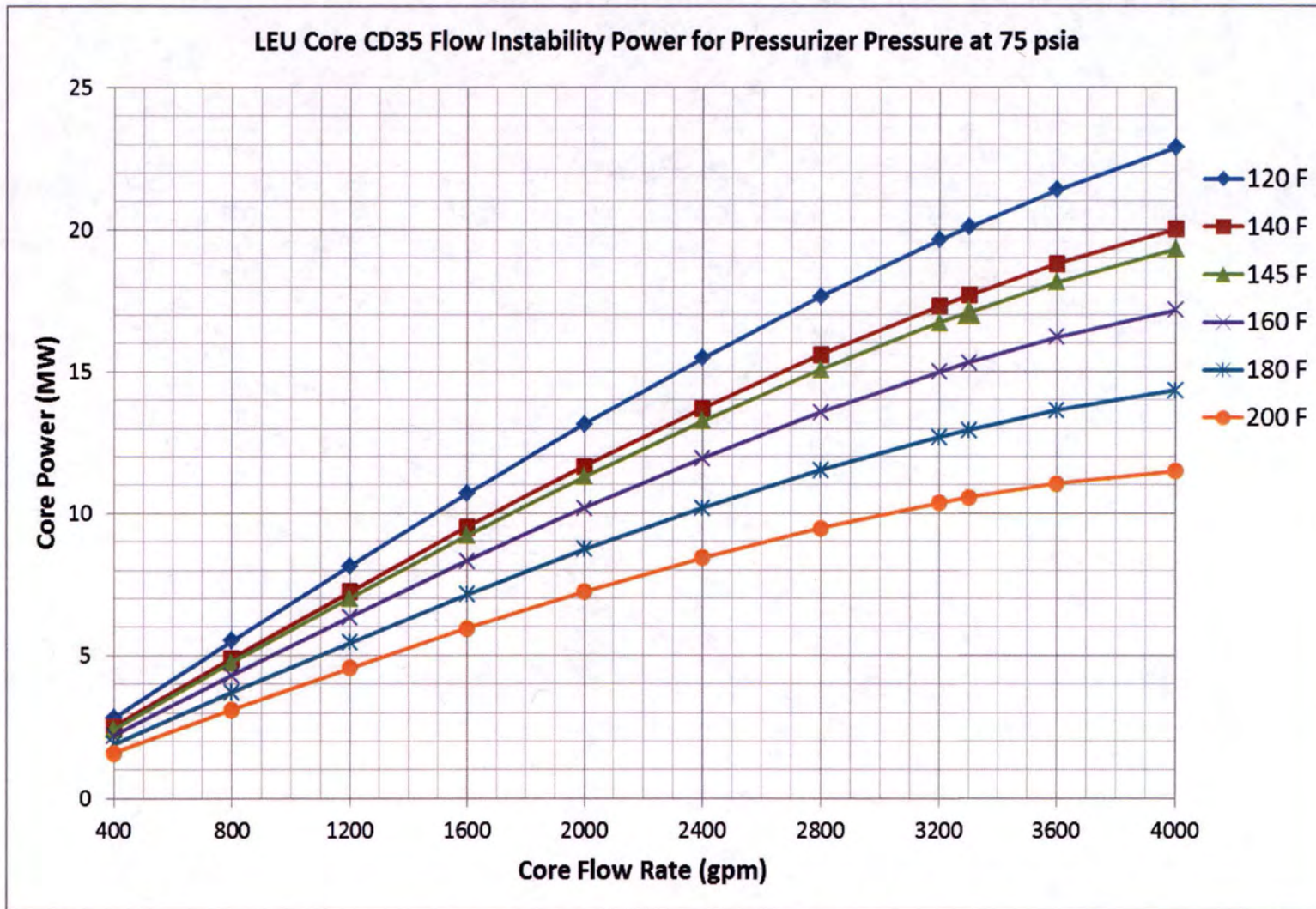


FIGURE 4.39
LEU CORE CD35 FLOW INSTABILITY POWER FOR PRESSURIZER PRESSURE AT 75 PSIA



FIGURE 4.40
LEU CORE CD35 FLOW INSTABILITY POWER FOR PRESSURIZER PRESSURE AT 85 PSIA

4.6.3 Safety Limit

The safety limit defines the maximum reactor fuel element temperature that can be permitted to ensure that the integrity of the fuel cladding is maintained to guard against an uncontrolled release of radioactivity. Maintaining the integrity of the fuel cladding requires that the fuel remain below the blistering temperature. A burnup-dependent fuel temperature safety for U-10Mo monolithic fuel is formulated based on blister threshold temperature data. For all operating conditions that avoid either a Departure from Nucleate Boiling (DNB) by not exceeding the Critical Heat Flux (CHF), or the Onset of Flow Instability (OFI), fuel temperatures remain substantially below the fuel temperature safety limit.

4.6.4 Limiting Safety System Settings

4.6.4.1 Introduction

Limiting Safety System Settings (LSSS) were established from the results of the operational limit analysis presented in Section 4.6.2.10. The LSSSs are settings for automatic protection devices that prevent the MURR operational limits from being exceeded. The settings for Mode I operation are given in Table 4-31. For reactor power, the LSSS is 125% of full power operation. Thus, the highest power obtainable before a reactor scram occurs would be 15 MW [1.25×12 MW] for Mode I. The LSSS on primary pressure is a minimum of 75 psia (517 kPa) in the pressurizer, and the LSSS on reactor inlet water temperature is a maximum of 145 °F (62.8 °C). The LSSS on primary coolant flow for Mode I operation is a minimum of 1,675 gpm (6,340.6 lpm) in either of the parallel primary coolant loops [total of 3,350 gpm (12,681.1 lpm)]. Since 50 gpm (189 lpm) of the primary coolant flow is diverted to the reactor coolant cleanup system, the actual reactor core flow rate at the LSSS is 3,300 gpm (12,491.9 lpm) in Mode I. The core differential pressure scram has a set point corresponding to a flow value of 3,300 gpm (12,491.9 lpm), which provides a backup to the primary coolant low flow scram. The setting for Mode III operation is given in Table 4-32. The LSSS for reactor power in this mode is 125% of full power. Thus, the highest power obtainable before a reactor scram occurs would be 62.5 kW [1.25×50 kW].

TABLE 4-31
MODE I LIMITING SAFETY SYSTEM SETTINGS

Parameter	Limiting Safety System Setting
Reactor Power	15.0 MW (125% of Full Power of 12 MW) (Maximum)
Primary Coolant Flow	1,675 gpm each loop (Minimum) 3,300 gpm total through core (Minimum)
Reactor Inlet Water Temperature	145 °F (Maximum)
Primary Coolant Pressurizer Pressure	75 psia (Minimum)

TABLE 4-32
MODE III LIMITING SAFETY SYSTEM SETTINGS

Parameter	Limiting Safety System Setting
Reactor Power	62.5 kW (125% of Full Power of 50 kW) (Maximum)

4.6.4.2 Bases

The operational limit analysis as described in Section 4.6.2.10 presents three (3) parametric curves which together define a four-dimensional safety limit envelope prescribing limiting combinations of values for reactor power, primary coolant flow, reactor inlet water temperature, and pressurizer pressure. Operation within this safety envelope will prevent fuel plate meltdown or clad damage as a result of FI. The LSSSs were chosen such that the true value of any of the four safety-related variables will not exceed the operation limit envelope under the most severe anticipated transient.

Figure 4.39 depicts the FI conditions for the LSSS for a pressurizer pressure of 75 psia (517 kPa). From this curve, the operational margin to FI for three (3) of four (4) anticipated transients may be assessed. The four anticipated transients are on reactor power, coolant inlet temperature, core coolant flow rate, and pressurizer pressure. The margins to FI were determined using the PLTEMP/ANL code using the Whittle and Forgan correlation, and are described in detail below.

- Case 1 postulates a power transient with the primary coolant flow rate, inlet temperature, and pressure are set at their respective LSSS values in Mode I operation. Figure 4.39 confirms that the highest power that does not exceed the operational limit curve is 17.10 MW, or 2.10 MW above the reactor power LSSS scram set point. Thus, an operational margin exists for safety system reaction time required to prevent reaching the FI threshold under these conditions.
- Case 2 postulates a transient on the reactor inlet water temperature for steady-state Mode I operation of the reactor with flow and pressure set at their LSSS and reactor power at the LSSS of 15.0 MW. One could verify from Figure 4.39 that FI would not occur until a reactor inlet water temperature of 162.6 °F (72.56 °C) was reached. The safety margin is thus 17.6 °F above the LSSS of 145 °F (62.8 °C) on reactor inlet water temperature. Any increase of the primary coolant inlet temperature would be slow, thus the reactor safety system would have more than adequate time to terminate the transient before FI occurs. Periodic compliance checks and past operating history provide confidence that the primary coolant temperature measurement error is no greater than ± 2 °F. Therefore, there is sufficient operational margin for a temperature transient of this type.
- Case 3 postulates a transient on the primary coolant flow rate for Mode I operation with pressurizer pressure at the LSSS of 75 psia (517 kPa), reactor power at the LSSS power of 15.0 MW, and reactor water inlet temperature at the LSSS of 145 °F (62.8 °C). Figure 4.39 predicts that the primary coolant flow rate could be reduced to 2,780 gpm (10,523 lpm) before FI would occur, implying a safety margin of 520 gpm (1,968 lpm) below the LSSS

of 3,300 gpm (12,492 lpm) on coolant flow through the core. Operating history has shown that the true value of primary coolant flow does not vary from the measured value by more than ± 50 gpm. Thus, there is sufficient margin for the reactor safety system to terminate the transient before FI occurs. Chapter 13 provides a detailed analysis of the results of the most severe loss of flow accident for the MURR.

- Case 4 postulates a coolant pressure transient for Mode I operation with reactor power, core inlet flow rate, and reactor water inlet temperature set to their LSSS of 15.0 MW, 3,300 gpm (12,492 lpm), and 145 °F (62.8 °C), respectively. Based on the PLTEMP/ANL code model used to produce Figures 4.38 and 4.39, a calculated pressurizer pressure of 61.20 psia (421.96 kPa) corresponds to the limiting pressure at which the FI starts to occur, implying a safety margin of 13.80 psia (95.15 kPa) below the LSSS of 75 psia (517 kPa) on pressurizer pressure. Operating history has shown that the true value of pressurizer pressure does not vary from the measured value by more than ± 2 psi, thus there is sufficient margin for the reactor safety system to terminate the transient before FI occurs. The HEU SAR Chapter 13 provides a detailed analysis of the results of the most severe loss of flow accident for the MURR HEU core, which is the loss of pressurizer pressure.

The Whittle and Forgan correlation combined with the additional uncertainty assumptions for power densities and coolant flow rates used for the LEU CD35 FI operational limit analysis provide more conservative operational limit values than those calculated for the operational limits in the most recent MURR HEU SAR (Ref. 4.36). Therefore, to more accurately compare the operational limit margins between the MURR HEU cores and the proposed LEU CD35 cores, the limits for the four cases for the MURR HEU cores were calculated using the Whittle and Forgan correlation. These results were previously summarized in Table 28 of Reference 4.22. Table 4-33 compares the PLTEMP/ANL calculated FI margins using the Whittle and Forgan correlation for both HEU and LEU CD35 cores.

TABLE 4-33
LSSS MARGINS TO OPERATIONAL LIMITS FOR FOUR ANTICIPATED TRANSIENTS

	HEU	LEU CD35
Case 1 (Reactor Power)	2.11 MW	2.10 MW
Case 2 (Core Coolant Inlet Temperature)	19.1 °F	17.6 °F
Case 3 (Core Coolant Flow Rate)	620 gpm	520 gpm
Case 4 (Pressurizer Pressure)	14.30 psia	13.80 psia

4.6.4.3 Conclusions

The LSSSs on the four important parameters of reactor power, primary coolant flow, reactor inlet water temperature, and primary coolant pressurizer pressure provide sufficient margins for the automatic devices to scram the reactor and prevent a violation of the operational limit envelope.

THIS PAGE INTENTIONALLY LEFT BLANK

CHAPTER 5

REACTOR COOLANT SYSTEMS

THIS PAGE INTENTIONALLY LEFT BLANK

TABLE OF CONTENTS

5.0	REACTOR COOLANT SYSTEMS.....	5-1
5.1	Introduction.....	5-1
5.2	Primary Coolant System	5-1
5.3	Pool Coolant System.....	5-1
	5.3.1 Reflector Plenum Natural Convection Valve	5-2
5.4	Secondary Coolant System	5-2
5.5	Reactor Coolant Cleanup System	5-2
5.6	Primary Coolant Make-Up Water System	5-2
5.7	Nitrogen-16 Control System	5-2
5.8	Decay Heat Removal System.....	5-2

5.0 REACTOR COOLANT SYSTEMS

This chapter provides the design bases, description, and functional analyses of the reactor coolant systems. With the power uprate to 12 MW, flow rates, pumps, heat exchangers, cooling tower specifications, and other related parameters will change. Analyses related to these changes are described in various other chapters.

5.1 Introduction

Editorial changes will be made to reflect the changes in power level for three modes of operation.

The University of Missouri Research Reactor (MURR) utilizes three coolant systems: Primary, Pool, and Secondary. The primary and pool coolant systems are designed for two modes of operation:

- (1) Mode I – For HEU-fueled cores at power levels of up to 10 MW with the primary coolant system pressurized and at a flow rate of approximately 3,750 gpm (14,195 lpm), and a pool coolant flow rate of approximately 1,200 gpm (4,542 lpm); used when all heat exchange and pumping capacity is available; For LEU-fueled cores the operating power level is up to 12 MW.
- (2) Mode III – At power levels of up to 50 kW with the primary coolant system open to the reactor pool, the reactor pressure vessel head removed, the flanged port open, and the pool water level at the elevation of either the upper or lower reactor bridge; used for core flux calibrations following the loading of a new core, or after a fuel rearrangement; Mode III operating conditions are not affected by conversion.

5.2 Primary Coolant System

The primary coolant system is designed to remove heat from the reactor core. The HEU core operates at a power level of 10 MW. For the LEU core, the operating power level will be 12 MW. No changes to the circulation pumps are expected due to conversion. Each of the two (2) primary coolant system heat exchangers are currently capable of removing 17×10^6 BTU/h (5 MW) of heat from 1,800 gpm (6,814 lpm) of primary coolant water, which is sufficient for HEU operation. While the cooling tower is adequate to discharge 15 MW, the capacity of the plate-type heat exchanger will require an upgrade for LEU operations.

5.3 Pool Coolant System

The pool coolant system consists of two (2) main circulating pumps, a heat exchanger, an automatic isolation valve, a reflector plenum natural convection valve, a hold-up tank, a return diffuser, a bypass loop for water clean-up, and associated valves and piping. The system is designed to transfer 3.6×10^6 BTU/h at a flow rate of 1,200 gpm (4,542 lpm). This allows for LEU reactor operation at a maximum thermal power of 12 MW.

5.3.1 Reflector Plenum Natural Convection Valve

No changes are expected to this section due to conversion.

5.4 Secondary Coolant System

Editorial changes will be made to reflect the changes in the reactor power level, the flow rates, heat exchangers, and cooling tower specifications.

5.5 Reactor Coolant Cleanup System

No changes are expected to this section due to conversion.

5.6 Primary Coolant Make-Up Water System

No changes are expected to this section due to conversion.

5.7 Nitrogen-16 Control System

No changes are expected to this section due to conversion.

5.8 Decay Heat Removal System

The decay removal system will transfer decay heat from the core to the reactor pool with no net formation of steam in the loop. The current HEU analysis is based on 30 days of continuous operation at 10 MW, an inlet coolant temperature of 140 °F (60 °C), and a pool temperature of 100 °F (38 °C). For LEU conversion under the same or more conservative conditions as HEU, except for the reactor power uprate to 12 MW, analysis of decay heat removal has shown that there is no formation of steam predicted in the in-pool heat exchanger. The in-pool heat exchanger is activated during reactor shutdown or transient conditions that have been analyzed in Chapter 13 loss of flow accidents (LOFAs) with acceptable results.

THIS PAGE INTENTIONALLY LEFT BLANK

CHAPTER 6

ENGINEERED SAFETY FEATURES

THIS PAGE INTENTIONALLY LEFT BLANK

TABLE OF CONTENTS

6.0	ENGINEERED SAFETY FEATURES.....	6-1
6.1	Introduction.....	6-1
6.2	Containment System	6-2
6.2.1	Introduction.....	6-2
6.2.2	Reactor Containment Building	6-2
6.2.2.1	Description.....	6-2
6.2.2.2	Design Basis.....	6-2
6.2.3	Penetrations and Closures	6-4
6.2.3.1	Utility Entry Water Seal.....	6-4
6.2.3.2	Pedestrian Entry	6-4
6.2.3.3	Heavy Equipment Entry.....	6-4
6.2.3.4	Supply and Exhaust Air Ducts	6-4
6.2.3.5	Supply and Exhaust Backup Doors.....	6-4
6.2.3.6	Electrical Entry	6-4
6.2.3.7	Pneumatic Tube System Entry	6-5
6.2.3.8	Building Leak Rate Test Penetrations.....	6-5
6.2.3.9	Exhaust Line for Potentially Contaminated Air.....	6-5
6.2.4	Compressed Air and Inflatable Gaskets.....	6-5
6.2.5	Description of Operation.....	6-5
6.2.6	System Redundancy and Reliability	6-5
6.2.7	Limiting Conditions for Operation	6-5
6.2.8	Surveillance.....	6-5
6.2.9	Design Features.....	6-5
6.3	Anti-Siphon System	6-5
6.3.1	Introduction.....	6-5
6.3.2	Design Criteria.....	6-5
6.3.3	Pressure Tank.....	6-6
6.3.4	Anti-Siphon Isolation Valves.....	6-6
6.3.5	Level Controller.....	6-6
6.3.6	Description of Operation.....	6-6
6.3.7	System Redundancy and Reliability	6-6

6.3.8	Design Analysis	6-7
6.3.9	Limiting Conditions for Operations.....	6-8
6.3.9.1	Surveillance.....	6-9

REFERENCES

- 6.1 Preliminary Hazards Report, University of Missouri Research Reactor, University of Missouri, Columbia, Missouri, March 1961.
- 6.2 Hazards Summary Report, University of Missouri Research Reactor, University of Missouri, Columbia, Missouri, July 1965.
- 6.3 Hazards Summary Report, Addendum 1, University of Missouri Research Reactor, University of Missouri, Columbia, Missouri, February 1966.
- 6.4 Hazards Summary Report, Addendum 2, University of Missouri Research Reactor, University of Missouri, Columbia, Missouri, May 1966.
- 6.5 Hazards Summary Report, Addendum 3, University of Missouri Research Reactor, University of Missouri, Columbia, Missouri, August 1972.
- 6.6 Hazards Summary Report, Addendum 4, University of Missouri Research Reactor, University of Missouri, Columbia, Missouri, October 1973.
- 6.7 Hazards Summary Report, Addendum 5, University of Missouri Research Reactor, University of Missouri, Columbia, Missouri, January 1974.
- 6.8 Design Data, Vol. 1, University of Missouri Research Reactor, University of Missouri, Columbia, Missouri, September 1962.
- 6.9 Safety Analyses Report, University of Missouri Research Reactor, University of Missouri, Columbia, Missouri, submitted August 2006.

6.0 ENGINEERED SAFETY FEATURES

This chapter discusses and describes the Engineered Safety Features (ESFs) for the reactor facility. The ESFs are active or passive features designed to mitigate the consequences of accidents and to keep radiological exposures to the public, the facility staff, and the environment within federal limits. The concept for ESFs evolved from the defense-in-depth philosophy of multiple layers of design features to prevent or mitigate the release of radioactive materials to the environment during accident conditions. The need for ESFs is determined by analyzing accidents that could occur, even though prudent and conservative design of the reactor facility has made the incidence of an accident very unlikely.

6.1 Introduction

During the design and the subsequent safety evaluation of the University of Missouri Research Reactor (MURR),² two systems were identified as required ESFs: the containment system and the anti-siphon system. These systems are designed to mitigate the consequences of certain identifiable accidents and to keep radiological exposures to the operating staff and the general public within the limits of Title 10, Chapter I, of the Code of Federal Regulations, Part 20 (10 CFR 20). The two accident scenarios which require an engineered safety feature are the Fuel Failure during operation Accident (FFA) and the Loss of Coolant Accident (LOCA).

The FFA is an accident condition which postulates the melting of four (4) fuel plates in the reactor core and the subsequent release of fission products to the primary coolant system.¹ While this accident does not result in conditions which lead to consequences to the public outside of the facility worse than those resulting from any other anticipated accident (i.e., the maximum hypothetical accident, or MHA), it is only in the FFA that it is possible that there will be energy released and steam formation that will result in increased pressure in the containment building. The circumstances that lead to the FFA are immaterial to the analysis. While the cladding of the fuel element is the first barrier of protection against the release of fission products to the atmosphere, it is hypothetically assumed in this accident that the cladding is completely consumed in an Al-water reaction. Should this barrier fail, the containment system will perform a complete isolation of the reactor containment building, thus providing a second barrier against an uncontrolled release of radioactive materials to the environment.

For the LOCA, the anti-siphon system functions as a backup system to the various safety instrumentation and equipment (e. g., pressure sensors, pump and valve interlocks, etc.) all of which ensures that the reactor core does not become uncovered during a LOCA. A rupture of the primary coolant system, followed by a loss of pressure, causes the anti-siphon system to admit a fixed volume of air to the high point of the reactor outlet piping, the inverted loop, thus breaking

¹The original safety evaluation of the MURR is documented in the Preliminary Hazards Report (Ref. 6.1), the Hazards Summary Report (Ref. 6.2), and Hazards Summary Report, Addenda 1-5 (Ref. 6.3-6.7).

any potential siphon that may have been created by the pipe rupture. The FFA and LOCA are discussed in detail in Chapter 13, Accident Analyses.

6.2 Containment System

6.2.1 Introduction

No changes to this section are expected due to conversion.

6.2.2 Reactor Containment Building

6.2.2.1 Description

No changes to this section are expected due to conversion.

6.2.2.2 Design Basis

The reinforced concrete walls of the reactor containment building have been designed to withstand a peak internal pressure of 2.0 psig (13.8 kPa above atmosphere). This design pressure was not predicated on any one accident scenario, rather the pressure was selected to envelope all postulated accident scenarios. It is difficult to envision a pressure buildup within the containment structure to 2.0 psig (13.8 kPa above atmosphere) because the primary coolant system coolant temperatures under normal operating conditions for the LEU core are an inlet temperature of 120 °F (49 °C) and outlet temperature of 141 °F (61 °C). The Technical Specification (TS) maximum reactor inlet water temperature is 145 °F (63 °C) (TS 2.2.a) for the LEU core. The maximum reactor pool coolant temperature limit is 120 °F (49 °C). Lastly, the maximum design temperature of the bulk water in the reactor is only 160 °F (71 °C) (Ref. 6.8). Thus, in the event of a rupture in the primary coolant system piping, the coolant in the reactor core region would remain sub-cooled relative to atmospheric pressure and the water would not flash to steam as in the case of a highly pressurized water reactor. In addition, the one foot (0.3 m) diameter column of water immediately above the one foot (0.3 m) diameter reactor pressure vessel is calculated to absorb 108 MW-sec of energy before reaching 212 °F (100 °C). (Ref. 6.2) Therefore, any large, positive reactivity insertion leading to an uncontrolled power excursion, which results in the formation of steam in the reactor pressure vessel and a rupture in the primary coolant system within the reactor pool volume, would be quickly quenched by the pool water.

The energy release necessary to cause a 2.0-psig (13.8-kPa above atmosphere) equilibrium loading within the reactor containment building has been calculated. (Ref. 6.2) The calculation includes the following assumptions:

1. No heat sinks;
2. Initial containment building air temperature: 75.2 °F (24.0 °C) with 50% relative humidity;
3. Initial pool water temperature: 100 °F (38 °C);
4. Containment building volume: 240,000 ft³ (6,796 m³); and

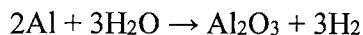
5. Final condition of 100% saturated air at 113 °F (45 °C) in the containment building.

The amount of energy needed to be released in the reactor pool to provide the steam to cause a 2.0-psig (13.8-kPa above atmosphere) increase within the containment structure corresponds to 1,040 MW-sec of energy release. Under the above conditions, the final equilibrium temperature within the containment building would be 113 °F (45 °C). This amount of energy release is considerably greater than would be expected as a result of any accident to this type of reactor.¹ The actual required energy would be even greater due to the actual heat sinks present in containment. All of the surfaces in contact with the air in containment are heat sinks and would be absorbing heat due to the steam condensing on them until the surface reaches 113 °F (45 °C) and the containment differential pressure is 2 psi. Additionally, the components in the pool and the pool surfaces would also serve as heat sinks.

However, the possibility that a severe fuel meltdown causing a molten aluminum water (Al-H₂O) reaction, which releases a considerable amount of energy, does exist. The specific conditions under which such a reaction might occur are widely discussed in literature pertaining to reactor hazards. It is currently believed that the occurrence of an Al-H₂O reaction requires:

1. That the aluminum be present in a finely divided form such as droplets or particles of less than 500 microns; and
2. That the temperature of the aluminum be greater than its melting point of 1,220 °F (933.3 °K).

The chemical formula for the aluminum-water reaction is:



The mass of aluminum in the HEU fuel plates of eight (8) fuel assemblies (complete core loading) is 32.3 kg, of which more than 70% is cladding. The amount of aluminum in the LEU fuel plates of eight (8) fuel assemblies (complete core loading) is 17.2 kg, which is all cladding. If all of the aluminum in the fueled portion of the fuel plates were to react completely with water, it would produce 490 and 260 MW-sec in the HEU and LEU cores, respectively. While the LEU fuel plates also have a zirconium interaction barrier between the U-10Mo and AA6061 cladding which could react with water, it is not considered credible that this reaction could occur since the melting temperature of Zr is significantly higher than that of aluminum, 3,371 °F (2128 °K). Furthermore, due the relatively small mass of Zr in the LEU fuel plates, even if the Zr-water reaction were to occur, it would increase the energy release by less than 6%.

In addition to the energy produced from the aluminum-water reaction, hydrogen gas would be formed. The amount of hydrogen produced by the reactions would be 1,422 and 755 ft³ at standard conditions in the HEU and LEU cores, respectively. If the hydrogen were to completely recombine with oxygen to form water, an additional 514 MW-sec would be released in the HEU core and an additional 273 MW-sec would be released in the LEU core. Thus, the total energy release for the HEU and LEU cores would be 1,004 and 533 MW-sec, respectively. This is less than the 1,040

MW-sec of corresponding energy in steam, which would have to be released to cause a 2.0-psig (13.8-kPa above atmosphere) equilibrium, overpressure in the reactor containment building.

To postulate that the total reaction of the aluminum in all fuel plates, along with the recombination of the evolved hydrogen, would occur is an excessively conservative and unrealistic assumption. A more realistic, but still exceedingly conservative, approach would be to assume that only the aluminum in four number-1 fuel plates would melt and react with the primary coolant system water. This assumption is consistent with the FFA, which is evaluated in Chapter 13. The four number-1 fuel plates in the HEU fuel assembly contain 426 grams of aluminum. In the LEU fuel assembly, the mass of aluminum in the four number-1 plates is 314 grams. This would equate to an energy release of only 6.5 MW-sec in the HEU core, and 4.8 MW-sec in the LEU core. If the hydrogen that is produced from the reactions were to completely recombine, the total energy release in the HEU and LEU cores would be 13.2 and 9.8 MW-sec, respectively.

In conclusion, the reactor containment building design pressure of 2.0 psig (13.8 kPa above atmosphere), based on the previous calculations, is completely adequate for all postulated accident scenarios. The design of the containment engineered safety feature gives reasonable assurance that it will not interfere with reactor operation or shutdown.

6.2.3 Penetrations and Closures

No changes to this section are expected due to conversion.

6.2.3.1 Utility Entry Water Seal

No changes to this section are expected due to conversion.

6.2.3.2 Pedestrian Entry

No changes to this section are expected due to conversion.

6.2.3.3 Heavy Equipment Entry

No changes to this section are expected due to conversion.

6.2.3.4 Supply and Exhaust Air Ducts

No changes to this section are expected due to conversion.

6.2.3.5 Supply and Exhaust Backup Doors

No changes to this section are expected due to conversion.

6.2.3.6 Electrical Entry

No changes to this section are expected due to conversion.

6.2.3.7 Pneumatic Tube System Entry

No changes to this section are expected due to conversion.

6.2.3.8 Building Leak Rate Test Penetrations

No changes to this section are expected due to conversion.

6.2.3.9 Exhaust Line for Potentially Contaminated Air

No changes to this section are expected due to conversion.

6.2.4 Compressed Air and Inflatable Gaskets

No changes to this section are expected due to conversion.

6.2.5 Description of Operation

No changes to this section are expected due to conversion.

6.2.6 System Redundancy and Reliability

No changes to this section are expected due to conversion.

6.2.7 Limiting Conditions for Operation

No changes to this section are expected due to conversion.

6.2.8 Surveillance

No changes to this section are expected due to conversion.

6.2.9 Design Features

No changes to this section are expected due to conversion.

6.3 Anti-Siphon System

6.3.1 Introduction

No changes to this section are expected due to conversion.

6.3.2 Design Criteria

No changes to this section are expected due to conversion.

6.3.3 Pressure Tank

The anti-siphon pressure tank is a 25-gallon (95-l), 0.105-inch (2.7-mm) thick stainless steel tank located on the lower bridge level of the reactor pool. The tank is cylindrically-shaped with nominal dimensions of 16 inches (41 cm) in diameter and 30 inches (76 cm) in length, and a design pressure of 150 psig (1.03 MPa above atmosphere).

The anti-siphon system volume consists primarily of the following:

- A 25-gallon (95-l) pressure tank with a section of ¾-inch piping and a section of ½-inch tubing with a combined volume of 3.358 ft³.
- The 4-inch (10.2-cm) diameter anti-siphon vertical line running up from the anti-siphon isolation valves and the lower end splits into two (2) 4-inch lines, which connect to the two (2) anti-siphon isolation valves with a total volume of 1.503 ft³.
- The dry well for the anti-siphon system level controller has an air volume of 0.518 ft³ and the bottom connects via a 2-inch pipe to the 4-inch pipes bolted to the two (2) anti-siphon isolation valves.

The combined anti-siphon system air volume is 5.379 ft³ (40.24 gal). A relief valve set at 100 psig (0.69 MPa above atmosphere) is connected to the pressure tank air supply line to protect the anti-siphon system from over-pressure.

6.3.4 Anti-Siphon Isolation Valves

No changes to this section are expected due to conversion.

6.3.5 Level Controller

No changes to this section are expected due to conversion.

6.3.6 Description of Operation

During normal reactor plant operation, the anti-siphon system is maintained dry and pressurized to 36 psig (248 kPa above atmosphere) for HEU operations. The anti-siphon system pressure may need to be increased for the LEU core because of the smaller pressure drop through the LEU core. This will be assessed during initial criticality testing of the LEU core. The range of the low- and high-end anti-siphon tank pressure values are 27 and 45 psig, respectively.

6.3.7 System Redundancy and Reliability

There are no changes to this section due to conversion.

6.3.8 Design Analysis

A potential mechanism for siphoning water out of the primary pressure vessel is a break in the 12-inch hot leg pipe immediately upstream of primary coolant isolation valve V507A. The MURR primary coolant loop represented in Figure C.1 of Appendix C was used in the simulation of the MURR facility with the aid of the RELAP5 computer code, which is briefly described in Section C.2.1 of Appendix C. Consider a double-ended break at primary coolant isolation valve V507A, as indicated in Figure C.1 by the light green arrows on either side of the valve. One could conceive of water being siphoned from the upstream portion of the double-ended break and gradually being displaced by air entering the downstream portion of the break. In theory, this could continue until the reactor pressure vessel is virtually empty. In practice, this may be rather difficult to achieve. There is a very long, highly resistive flow path that would have to empty before the incoming air could reach the top of the reactor vessel. Primary coolant isolation valve V507B will fully close within 10 seconds of the initial break; thereby block the source of air needed for the siphon to function. Moreover, core inlet check valve V502 may close even sooner and block the source of air.

In spite of these obstacles to uncovering the fuel by siphoning water from the hot leg, prudent design has dictated the inclusion of an anti-siphon system to evacuate the water in the downward flow portion of the hot leg and thereby absolutely preclude siphoning via the hot leg. The depressurization in the hot leg of the reactor causes the two parallel redundant anti-siphon isolation valves, indicated as V543 in Figure C.1 of Appendix C, to open, which, in turn, connects the 40-gallon volume of compressed air in the anti-siphon system to the top of the core outlet header.

In the simulations to demonstrate the effectiveness of the anti-siphon system, conditions most conducive to siphoning were selected. Hot water at atmospheric pressure is closer to boiling than is cold water. Any steam that is produced in the hot leg downcomer by boiling can serve the same function as injected air at the same location in preventing siphoning. Therefore, the reactor was assumed to be at zero power with the coolant at a very low temperature of 86° F (30 °C). In the same spirit, the initial mass in the anti-siphon system was minimized to limit its effectiveness, by assuming a low initial air pressure of 26 psig (40.3 psia) and a high initial gas temperature of 120° F (49 °C), the maximum allowed temperature for the pool coolant by the TS. MURR TS 3.4.b requires the minimum anti-siphon system tank pressure to be 27 psig, and by procedure, the pressure is kept at 36 psig when the reactor is operating; thus, the pressure assumed in the simulations is 1 psi below the allowed minimum.

In the simulation, the transient was initiated by a double-ended break at primary coolant isolation valve V507A. In order to simulate an overly optimistic source of air to facilitate siphoning, a double-ended break is assumed to simultaneously occur at primary coolant isolation valve V507B. Thus, the air needed to promote siphoning does not need to travel from the hot leg break, through the primary coolant circulation pumps and the primary coolant heat exchangers to reach the reactor inlet, but instead is introduced very close to the reactor inlet and at the same very low elevation as the hot leg break.

For the simulation, no channel reduction due to burnup was assumed. The reason is that the assumption of no channel reduction implies lower core resistance, which should facilitate more siphoning. Also as a conservatism, the initial flow rate was taken to be the maximum of 3,850 gpm (14,574 lpm), because a higher initial flow rate increases the inertia of the fluid.

The Limiting Safety System Settings (LSSS) pressurizer pressure of 75 psia and the scram set point pressurizer level of -16 inches were used for the anti-siphon system analysis. The pressurizer temperature was set to 86 °F to be consistent with the primary inlet coolant temperature.

The RELAP5 simulation was performed twice with the HEU core – once with the anti-siphon system active and once with it inactive – so that the contribution of the anti-siphon system could be discerned. Similarly, these two (2) simulations were performed with the LEU core.

The following four criteria were evaluated in assessing the propensity for siphoning in each of the four simulations:

1. Time for core coolant inlet check valve V502 to permanently close;
2. Minimum liquid fraction in the inlet plenum (which is located immediately above the core);
3. Time required for the hot leg (exit pipe) to empty; and
4. Time required for the flow at the exit to the hot leg (exit pipe) to go to zero.

A more detailed explanation and the results of these four simulations can be found in Section B-5.12 of Ref. 6.9. The conclusion is that the simulations predict that there is no siphoning for either the HEU or the LEU core with the anti-siphon system activated or with it not activated. An earlier version of this analysis performed with an earlier version of the RELAP5 model and similar, but not the same, assumptions, is described in Section 5.6 of Ref. 6.9, with results provided in Section 5.7.5 of Ref. 6.9. This analysis reached the same conclusion, i.e., that in none of the four (4) simulations siphoning occurs. The prediction of no siphoning, even with the anti-siphon system not activated, could almost be anticipated given that the water exit, which is located at the primary coolant outlet isolation valve, and the source of air needed for siphoning, which is located at the primary coolant inlet isolation valve, are both at the same elevation. The design of MURR with a large pool surrounding the pressure vessel and portions of the primary coolant loop provides excellent protection against siphoning. The pool limits the available sources of air from a break from occurring at any location except remote to the vessel region. These types of breaks outside of the pool were modeled above and did not induce siphoning.

6.3.9 Limiting Conditions for Operations

No changes to this section are expected due to conversion.

6.3.9.1 Surveillance

No changes to this section are expected due to conversion from either the SAR as submitted for HEU relicensing in 2006 or subsequent requests for additional information during the HEU relicensing review.

CHAPTER 7

**INSTRUMENTATION AND
CONTROL SYSTEMS**

THIS PAGE INTENTIONALLY LEFT BLANK

7.0 INSTRUMENTATION AND CONTROL SYSTEMS

Some set points or actuating values for the reactor safety system are expected to change due to the power uprate to 12 MW. However, no major changes to the MURR Instrumentation and Control (I&C) Systems' operating philosophies or methodologies are expected due to the fuel conversion. No new analysis is necessary for the I&C Systems due to the fuel conversion.

THIS PAGE INTENTIONALLY LEFT BLANK

CHAPTER 8

ELECTRICAL POWER SYSTEMS

THIS PAGE INTENTIONALLY LEFT BLANK

8.0 ELECTRICAL POWER SYSTEMS

No new analysis or system changes are planned for the electrical power systems as part of the LEU fuel conversion.

THIS PAGE INTENTIONALLY LEFT BLANK

CHAPTER 9

AUXILLIARY SYSTEMS

THIS PAGE INTENTIONALLY LEFT BLANK

TABLE OF CONTENTS

9.0	AUXILIARY SYSTEMS.....	9-1
9.1	Heating, Ventilation and Air-Conditioning Systems	9-1
9.2	Handling and Storage of Reactor Fuel.....	9-1
9.3	Fire Protection Systems and Programs	9-1
9.4	Communication System.....	9-2
9.5	Possession and Use of Byproduct, Source and Special Nuclear Material	9-2
9.6	Nitrogen Supply System	9-2
9.7	Emergency Pool Fill System.....	9-2
9.8	Pool Skimmer System.....	9-2
9.9	Closed Circuit Television System.....	9-2
9.10	Battery Operated Emergency Lights.....	9-2
9.11	Radioactive Waste Disposal Systems	9-2
9.12	Demineralized Water Supply System	9-2
9.13	Reactor Loop Vent System	9-2
9.14	Compressed Air System.....	9-2

9.0 AUXILIARY SYSTEMS

This chapter discusses and describes the auxiliary systems that support the operation of the MURR facility. These auxiliary systems are important to the safe operation and shutdown of the reactor.

9.1 Heating, Ventilation and Air-Conditioning Systems

No changes are expected to this section due to conversion.

9.2 Handling and Storage of Reactor Fuel

The fuel handling and storage system provides a safe, effective and reliable means of transporting, handling and storing reactor fuel from the time it enters the facility until it leaves. Fuel, new or irradiated, is stored in any one of the 88 [REDACTED] storage locations (not including the core). These storage locations need to meet, among other shielding and thermal (cooling) considerations, the following criterion:

- a) A fuel storage geometry such that the calculated k_{eff} is less than 0.9 under all conditions of moderation and fuel burn up combinations.

Due to the lowering of fuel enrichment, the amount of total uranium will be considerably higher in the LEU fuel compared to the current HEU fuel. The loading of ^{235}U in a single fuel element will be 1,507 grams compared to [REDACTED] grams for the HEU fuel, and the weight of the individual element will go from approximately 6.25 kg to roughly 12.5 kg. This will require a redesign and fabrication of a new buoyant assist fuel handling tool. However, the 50 kg additional weight of the core will present no problem to the structural support in the pressure vessel. This is because the pressure drop across the LEU fuel elements with the 92- and 93-mil coolant channels will be significantly reduced compared to the HEU fuel elements with 80-mil HEU coolant channels, so that the overall structural force required to support the core will be less with LEU than with the current HEU when the reactor is operating (see Section 4.2.5).

The additional weight of the LEU fuel elements necessitates a future reanalysis of the fuel storage and handling issues in order to ensure the fuel elements can be safely supported by the fuel storage racks and handling tools. Additionally, future analysis of both the fresh fuel, as well as the spent fuel transport casks, is required and planned with the new LEU fuel type.

Criticality calculations have to be redone in the future for both fresh as well as irradiated/spent LEU fuel under the most limiting conditions to ensure safe storage and transport. The storage includes fuel elements in the fuel vault as well as storage of fuel elements in the pool.

9.3 Fire Protection Systems and Programs

No changes are expected to this section due to conversion.

9.4 Communication System

No changes are expected to this section due to conversion.

9.5 Possession and Use of Byproduct, Source and Special Nuclear Material

While no changes are expected to the byproduct and source material possession and use due to conversion, the transition from HEU to LEU fuel will require some changes to the facility Special Nuclear Material (SNM) control and accounting procedures to account for the different uranium enrichment and accompanying change in possession limits.

9.6 Nitrogen Supply System

No changes are expected to this section due to conversion.

9.7 Emergency Pool Fill System

No changes are expected to this section due to conversion.

9.8 Pool Skimmer System

No changes are expected to this section due to conversion.

9.9 Closed Circuit Television System

No changes are expected to this section due to conversion.

9.10 Battery Operated Emergency Lights

No changes are expected to this section due to conversion.

9.11 Radioactive Waste Disposal Systems

No changes are expected to this section due to conversion.

9.12 Demineralized Water Supply System

No changes are expected to this section due to conversion.

9.13 Reactor Loop Vent System

No changes are expected to this section due to conversion.

9.14 Compressed Air System

No changes are expected to this section due to conversion.

THIS PAGE INTENTIONALLY LEFT BLANK

CHAPTER 10

**EXPERIMENTAL FACILITIES
AND UTILIZATION**

THIS PAGE INTENTIONALLY LEFT BLANK

10.0 EXPERIMENTAL FACILITIES AND UTILIZATION

No changes to this section are expected due to conversion. Experiments are individually analyzed prior to insertion into any experimental facility of LEU-fueled cores. Impacts to experimental flux levels are expected to be minimal when the LEU-fueled core operates at 12 MW.

THIS PAGE INTENTIONALLY LEFT BLANK

CHAPTER 11

RADIATION PROTECTION PROGRAM AND WASTE MANAGEMENT

THIS PAGE INTENTIONALLY LEFT BLANK

11.0 RADIATION PROTECTION PROGRAM AND WASTE MANAGEMENT

No changes to this section are expected due to conversion.

THIS PAGE INTENTIONALLY LEFT BLANK

CHAPTER 12

CONDUCT OF OPERATIONS

THIS PAGE INTENTIONALLY LEFT BLANK

TABLE OF CONTENTS

12.0	CONDUCT OF OPERATIONS	12-1
12.1	Organization.....	12-1
12.2	Review and Audit Activities.....	12-1
12.3	Procedures.....	12-1
12.4	Reportable Events and Required Actions	12-1
12.5	Records	12-1
12.6	Emergency Planning	12-1
12.7	Security Planning.....	12-1
12.8	Quality Assurance.....	12-1
12.9	Operator Training and Requalification	12-1
12.10	Environmental Reports	12-1
12.11	Startup Plan.....	12-2

12.0 CONDUCT OF OPERATIONS

This chapter discusses and describes the conduct of operations at the reactor facility. This covers administrative aspects, details of the emergency preparedness and security protocols, quality assurance programs, and reactor operator requalification plan, all of which ensures a safe and reliable facility operation.

12.1 Organization

No changes are expected to this section due to conversion.

12.2 Review and Audit Activities

No changes are expected to this section due to conversion.

12.3 Procedures

No changes are expected to this section due to conversion.

12.4 Reportable Events and Required Actions

No changes are expected to this section due to conversion.

12.5 Records

No changes are expected to this section due to conversion.

12.6 Emergency Planning

No changes are expected to this section due to conversion.

12.7 Security Planning

No changes are expected to this section due to conversion.

12.8 Quality Assurance

No changes are expected to this section due to conversion.

12.9 Operator Training and Requalification

No changes are expected to this section due to conversion.

12.10 Environmental Reports

NUREG-1537, "Guidelines for Preparing and Reviewing Applications for the Licensing of Non-Power Nuclear Reactors," specifies that issuance of an operating license for a research reactor is an action that requires an Environmental Assessment (EA). An Environmental Report (ER) will be prepared by the MURR staff to aid the NRC in preparing the EA to meet the requirements of

the National Environmental Protection Act of 1969, as amended. MURR will update the ER that was submitted to the NRC in 2006 as a part of relicensing as part of the anticipated LEU conversion SAR submittal in the future.

12.11 Startup Plan

The startup plan section will need to be written to define the reactor physics tests to be completed to address all the items included in NUREG-1537 Part 1 Section 12.11. The Startup test procedures for the current [REDACTED] gram ^{235}U aluminide fuel elements performed in 1971 can serve as a guide in drafting this section.

The transitional use of LEU fuel elements with absorber in the side plates will need to be addressed as an extended startup phase prior to LEU operation with typical LEU fuel elements (where the equilibrium core does not have any burnable absorbers).

The startup plan covering zero or low-power testing and transitional cores will be submitted to the NRC as an appendix in the future conversion SAR.

THIS PAGE INTENTIONALLY LEFT BLANK

CHAPTER 13

ACCIDENT ANALYSIS

THIS PAGE INTENTIONALLY LEFT BLANK

TABLE OF CONTENTS

13.0	ACCIDENT ANALYSES.....	13-1
13.1	Introduction.....	13-1
13.2	Accident-Initiating Events and Scenarios, Accident Analyses and the Determination of Consequences.....	13-1
13.2.1	Maximum Hypothetical Accident - LEU Fuel Handling Accident	13-1
13.2.1.1	Accident Initiating Events and Scenarios	13-2
13.2.1.2	Accident Analysis and Consequences	13-2
13.2.1.2.1	Occupational Dose.....	13-6
13.2.1.2.2	Public Dose	13-7
13.2.1.2.3	Additional Analysis	13-9
13.2.2	Insertion of Excess Reactivity	13-9
13.2.2.1	Introduction.....	13-9
13.2.2.2	Changes to Modeling Relative to Prior SAR Analysis.....	13-10
13.2.2.3	Accident Initiating Events and Scenarios	13-18
13.2.2.4	Accident Analysis and Consequences	13-22
13.2.2.4.1	HEU Core Step Reactivity Insertion Accident Results.....	13-23
13.2.2.4.2	LEU Core Step Reactivity Insertion Accident Results	13-28
13.2.2.4.3	LEU Core Blade Withdrawal Accident	13-36
13.2.2.4.4	LEU Core Startup Accident.....	13-38
13.2.2.5	Conclusions.....	13-42
13.2.3	Loss of Primary Coolant.....	13-43
13.2.3.1	Accident Initiating Events and Scenarios	13-43
13.2.3.2	Accident Analysis and Consequences	13-45
13.2.3.3	Cold Leg Double-Ended LOCA Analysis Used for Recent HEU Relicensing.....	13-50
13.2.3.4	Conclusions.....	13-50
13.2.4	Loss of Primary Coolant Flow.....	13-53
13.2.4.1	Accident Initiating Events and Scenarios	13-53
13.2.4.2	Accident Analysis and Consequences	13-55
13.2.4.3	Limiting LOFA Analysis Used in Recent HEU Relicensing	13-56
13.2.4.4	Conclusions.....	13-57
13.2.5	Fuel Failure During Operation Accident	13-58
13.2.5.1	Occupational Dose	13-61

13.2.5.2 Public Dose	13-64
13.2.6 Experiment Malfunction	13-66
13.2.7 Loss of Electrical Power	13-66
13.2.8 External Events	13-66
13.2.9 Mishandling or Malfunction of Equipment	13-66

LIST OF FIGURES

Figure 13.1	PARET/ANL Fuel Plate/Coolant Channel.....	13-15
Figure 13.2	Heat Transfer Coefficient from Mol Plate Surface to Primary Coolant Channel 70 MS After 0.6% $\Delta K/K$ Step Reactivity Insertion in LEU Reference Core Initiated from LSSS Conditions on Temperature and Flow Rate	13-26
Figure 13.3	Reactor Power and Maximum Fuel Temperatures.....	13-30
Figure 13.4	Peak Local Heat Flux Calculated By MCNP5 for Plates in Bol, Mol, and Eol Element in LEU Reference Core Operating at 12 MW	13-33
Figure 13.5	Reactor Startup Accident in LEU Core 7A	13-41
Figure 13.6	Reactor Startup Accident in LEU Core 5B1 in Natural Circulation Mode.....	13-42
Figure 13.7	HEU Element 5 Double-Ended Cold-Leg LOCA Results	13-48
Figure 13.8	LEU Element 8 Double-Ended Cold-Leg LOCA Results (With Flow Redistribution Due to Burnup)	13-52
Figure 13.9	HEU Core Peak Fuel Centerline Temperature at Limiting Location for Loss-of-Site Power (No Flow Redistribution Due to Burnup).....	13-56
Figure 13.10	LEU Core Peak Fuel Centerline Temperature at Peak Temperature Location for Seizure of One Pump (No Flow Redistribution Due to Burnup).....	13-58
Figure 13.11	Airborne Concentration of Radionuclides.....	13-63

LIST OF TABLES

Table 13-1	Whole-Core Activity of Radioiodines and Noble Gases (Curies).....	13-4
Table 13-2	Specific Activity of Radioiodines and Noble Gases in LEU Fuel (CI/GM- ²³⁵ U).....	13-5
Table 13-3	Data for Calculating Fission Product Source Term.....	13-6
Table 13-4	Key Reactor Parameters for Reactivity Insertion Accidents	13-11
Table 13-5	Initial Steady-State Conditions for RIA Analyses Based On Regulatory Request During HEU Relicensing	13-11
Table 13-6	Reactivity Feedback Coefficients and Kinetics Parameters for MURR Calculated With Mcnp5	13-12
Table 13-7	Nominal HEU and LEU Fuel Plate Dimensions	13-14
Table 13-8	Fuel Plate/Channel Dimensions in PARET/ANL Model.....	13-16
Table 13-9	Peak Steady-State Heat Flux (W/CM ²) in HEU and LEU Cores.....	13-18
Table 13-10	Conditions for Base and Branch Cases for Reactivity Insertion Accidents	13-20
Table 13-11	Peak Reactor Power And Peak Fuel Temperature For 0.6% Δ K/K Step Insertion of Reactivity in HEU Reference Core.....	13-24
Table 13-12	Peak Fuel Temperature (°C) for 0.6% Δ k/K Step Insertion of Reactivity in HEU Reference Core Operating at the Most Extreme License Conditions	13-27
Table 13-13	Peak Reactor Power and Peak Fuel Temperature.....	13-29
Table 13-14	Peak Fuel Temperature (°C) For 0.6% Δ k/K Step Insertion of Reactivity in LEU Reference Core Operating at the Most Extreme License Conditions	13-32
Table 13-15	Results for Selected Plates in 0.6% Δ k/K Step Reactivity Insertion Accident in LEU Reference Core Operating at the Most Extreme License Conditions	13-34
Table 13-16	Peak Fuel Temperature for 0.25% Δ k/K and 0.10% Δ k/K Step Reactivity Insertions in LEU Reference Core at the Most Extreme License Conditions .	13-35
Table 13-17	Peak Reactor Power and Peak Fuel Temperature for Blade Withdrawal Accident in LEU Reference Core.....	13-37
Table 13-18	Peak Reactor Power and Peak Fuel Temperature.....	13-39
Table 13-19	Initial Conditions Assumed in the RELAP5 Simulations	13-45
Table 13-20	Fractional Release of Whole-Core Radioactive Source From Fuel Failure Accident in HEU And LEU Cores.	13-61
Table 13-21	10-Minute Occupational Dose from Radioiodines and Noble Gases in Containment from FFA	13-64
Table 13-22	Maximum Dose in the Unrestricted Area.....	13-65

REFERENCES

- 13.1 *University of Missouri Research Reactor Safety Analysis Report*, submitted to the U.S. Nuclear Regulatory Commission, August 2006.
- 13.2 B. Rickman, *HEU to LEU Conversion: Fuel Handling Accident*, MURR-TDR-0139, University of Missouri, December 2014.
- 13.3 The RELAP5/MOD3.3 Code Manual, Nuclear Systems Analysis Division, Information Systems Laboratories, Inc., Rockville, Maryland and Idaho Falls, Idaho, Prepared for the Division of Systems Research, Office of Nuclear Regulatory Research, U. S. Nuclear Regulatory Commission, Washington, DC 20555, March 2006.
- 13.4 J. A. Stillman, et al., *Accident Analyses for Conversion of the University of Missouri Research Reactor (MURR) from Highly-Enriched to Low-Enriched Uranium*, ANL/GTRI/TM-14/5, Revision 1, Argonne National Laboratory, Argonne, IL, February 2017.
- 13.5 Letter to U.S. Nuclear Regulatory Commission from Ralph A. Butler, P.E, October 1, 2015. [Docket 50-186, University of Missouri-Columbia Research Reactor, Amended Facility Operating License R-103; Subject: Written communication as specified by 10 CFR 50.4(b)(1) regarding responses to the "University of Missouri at Columbia - Request for Additional Information Regarding the Renewal of Facility Operating License No. R-103 for the University of Missouri at Columbia Research Reactor (TAC No. ME1580)," dated April 17, 2015.]
- 13.6 J. M. Beeston, R. R. Hobbins, G. W. Gibson, and W. C. Francis, "Development and Irradiation of Uranium Aluminide Fuels in Test Reactors," *Nucl. Tech.*, Vol. 49, p. 136-149 (June 1980).
- 13.7 F. J. Rice, et. al., *Preliminary Blister Anneal Testing Results for U-Mo Monolithic Fuel Plates*, INL/LTD-14-33608, Revision 1, Idaho National Laboratory, March 2015.
- 13.8 Guidelines for Preparing and Reviewing Applications for the Licensing of Non-Power Reactors, Standard Format and Content, NUREG-1537, Part 1, United States Nuclear Regulatory Commission, February 1996.
- 13.9 Guidelines for Preparing and Reviewing Applications for the Licensing of Non-Power Reactors, Standard Review Plan and Acceptance Criteria, NUREG-1537, Part 2, United States Nuclear Regulatory Commission, February 1996.
- 13.10 A. P. Olson, *A Users Guide to the PARET/ANL Code*, ANL/RERTR/TM-11-38, Version 7.5, Argonne National Laboratory, August 14, 2012.

- 13.11 J. A. Stillman, et al., *Accident Analyses for Conversion of the University of Missouri Research Reactor (MURR) from Highly-Enriched to Low-Enriched Uranium*, ANL/GTRI/TM-14/5, Revision 1, Argonne National Laboratory, February 2017.
- 13.12 J. Stillman, et al., *Technical Basis in Support of the Conversion of the University of Missouri Research Reactor (MURR) Core from High-Enriched to Low-Enriched Uranium – Core Neutron Physics*, ANL/RERTR/TM-12-30, Argonne National Laboratory, September 2012.
- 13.13 J. C. Griess, H. C. Savage, and J. L. English, *Effect of Heat Flux on the Corrosion of Aluminum by Water. Part IV. Tests Relative to the Advanced Test Reactor and Correlation with Previous Results*, ORNL-3541, Oak Ridge National Laboratory, February 1964.
- 13.14 J. A. Stillman, et al., *Irradiation Experiment Conceptual Design Parameters for MURR LEU U-Mo Fuel Conversion*, ANL/RERTR/TM-13-1, Rev. 1, Argonne National Laboratory, June 2013.
- 13.15 X-5 Monte Carlo Team, “MCNP-A General Monte Carlo N-Particle Transport Code, Version 5 Volume I, II and III,” LA-UR-03-1987/LA-CP-03-0245/LA-CP-03-0284, Los Alamos National Laboratory, 2003.
- 13.16 E. E. Feldman, et al., Preliminary Accident Analyses for Conversion of the University of Missouri Research Reactor (MURR) from Highly-Enriched to Low-Enriched Uranium, ANL/GTRI/TM-13/7, Argonne National Laboratory, June 2013.
- 13.17 D. E. Burkes, et al., *Fuel Thermo-Physical Characterization Project: Fiscal Year 2013 Final Report*, PNNL-22981, November 2013.
- 13.18 N. J. Peters and K. Kutikkad, “Spatial Distribution of the Effective Fission Energy Deposition within the MURR Core: HEU vs. LEU Fuel Comparison,” MURR-TDR-0140, University of Missouri, December 2014.
- 13.19 L. Foyto, et al., *CD35 Low-Enriched Uranium Transition Fuel Cycle Report*, MURR-TDR-0138, University of Missouri, September 2013.
- 13.20 W. M. Cowherd, “Maximum Hypothetical Accident Analysis for HEU to LEU Fuel Conversion at the University of Missouri Research Reactor,” University of Missouri-Columbia thesis, Columbia, Missouri, December 2014.
- 13.21 N. G. Hogue, 16-01: Determination of Derived Air Concentrations for Kr-89, Kr-90, Xe-137, and Xe-139, MURR Health and Safety Technical Basis Report, March 20, 2016.
- 13.22 Letter from MURR to NRC, “Written communication as specified by 10 CFR 50.4(b)(1) regarding responses to the ‘University of Missouri at Columbia – Clarifications needed to Nuclear Regulatory Commission Staff Request for Additional Information Regarding the

- Renewal of Facility Operating License No. R-103 for the University of Missouri at Columbia Research Reactor (TAC no. ME1580),’ dated March 23, 2016,” April 15, 2016.
- 13.23 Bell, M. J., ORIGEN – *The ORNL Isotope Generation and Depletion Code*, ORNL-4628, Oak Ridge National Laboratory, May 1973.
- 13.24 D. L. Poston, and H. R. Trellue, *User’s Manual, Version 2.0 for MONTEBURNS Version 2.0*, LA-UR-99-4999, Los Alamos National Laboratory, September 2002.
- 13.25 NRC Regulations - Title 10, Code of Federal Regulations; Part 20: Standards for Protection Against Radiation, Nuclear Regulatory Commission.
- 13.26 Letter from NRC to MURR, “University of Missouri at Columbia – Request for Additional Information RE: License Renewal, Safety Analysis Report, 45-Day Response Question (TAC NO. MD3034)”, dated June 1, 2010.
- 13.27 *MURR Hazards Summary Report*, University of Missouri Research Reactor Facility, July 1965.
- 13.28 *MURR Hazards Summary Report*, Addendum 4, University of Missouri, Research Reactor Facility, October 1973.

13.0 ACCIDENT ANALYSES

This chapter demonstrates that various facility design features, safety limits, limiting safety system settings (LSSSs), and limiting conditions for operation have been selected to ensure that no credible accident can lead to unacceptable radiological consequences to people or the environment.

13.1 Introduction

Operational records have shown that light-water moderated, open pool-type reactors are extremely safe in design and construction. This safety is predicated upon the demonstrated ability of these water-moderated reactors to absorb reactivity additions by slight changes in their moderator. Negative void and temperature coefficients are intrinsic features of this type of reactor. Numerous experiments performed by the BORAX and SPERT programs have repeatedly demonstrated the inherent safety characteristics of water-moderated/cooled reactors.

The University of Missouri Research Reactor (MURR) described in this document, though more complex than the ordinary open pool-type research reactor, still possesses these same inherent safety characteristics as demonstrated by over 50 years of safe operation. Although the inherent safety of the MURR can be adequately shown, this inherent safety serves solely as a fail-safe or back-up mechanism in case of the failure of other control provisions. An extensive system of sensing devices, electronic circuits, signal conditioning equipment, and electro-mechanical devices are provided to protect the reactor against all credible postulated accident scenarios. The MURR Reactor Protective System has been designed to (1) initiate automatic actions to assure that reactor safety limits are not exceeded as a result of anticipated operational occurrences, and (2) sense accident conditions and to initiate the operation of systems and components important to safety.

13.2 Accident-Initiating Events and Scenarios, Accident Analyses and the Determination of Consequences

13.2.1 Maximum Hypothetical Accident - LEU Fuel Handling Accident

The Maximum Hypothetical Accident (MHA) postulates conditions leading to consequences worse than those from any credible accident. For the HEU core, the failure of a fueled experiment results in the greatest dose to a member of the general public outside the exclusion zone. For the LEU core, it has been found that the dose to a member of the general public is greatest for a postulated fuel handling accident (FHA).

FHAs cover a class of accident caused by events or scenarios that could cause a breach in the fuel cladding that results in the release of radioactive fission products. Events, which could cause an accident in this category, include a fuel handling event where a fuel plate is damaged or scratched severely enough to breach the cladding or the simple failure of the fuel cladding due to a manufacturing defect or corrosion. A summary description of the accident scenario, analysis, and consequences of the FHA is provided here. Previous modeling and analyses of the FHA for HEU and LEU fuel are described in detail in References 13.1 and 13.2, respectively.

13.2.1.1 Accident Initiating Events and Scenarios

All fuel handling is performed in accordance with Special Nuclear Material (SNM) Control and Accounting Procedures as outlined in the Operations Procedures. Irradiated fuel is handled with a specially designed remote tool that provides a positive indication of latching prior to movement of a fuel element. This feature is tested prior to any fuel handling sequence. Fuel elements are always handled one at a time so that they are maintained in a criticality-safe configuration.

New or irradiated fuel may be stored in any one of the 88 [REDACTED] storage locations (not including the core). These storage locations are designed to ensure a geometry such that the calculated k_{eff} is less than 0.9 under all conditions of moderation, thus allowing sufficient convection cooling and providing sufficient radiation shielding. This analysis for LEU fuel will be completed as part of a future activity and results will be reported in the final conversion safety analysis submission.

Irradiated fuel does not leave the facility until it is loaded into a U.S. Nuclear Regulatory Commission (NRC) approved cask for shipment. An irradiated fuel element is not loaded into a shipping cask until a predetermined cooling period has elapsed. The cooling time ensures that a fuel element has decayed to a level where air cooling is adequate to maintain the fuel temperature below the design limits. Thus, in the event of a dropped cask or a loss of coolant water from the cask, the fuel element would not release fission products by a meltdown.

The possibility of dropping a fuel element while underwater and damaging it severely enough to breach the fuel cladding was considered. In greater than 50 years of operating history, MURR Operations personnel have completed greater than 35,000 fuel element handling moves. Only once has a fuel element been miss handled so as to result in the outermost fuel plate (plate 24 of an HEU element) being bent. There was no measurable release of radioactive material from that event but the element was no longer used.

Based on that experience, it is conservatively assumed that the cladding on a fuel plate is damaged and a section of fuel meat that is one-inch square and 5 mils thick is exposed. The mass of fuel contained in this volume is 0.117 and 0.248 grams of ^{235}U for the HEU and LEU fuel element, respectively. Only the innermost and outermost plates of a fuel element are likely to receive any potential damage in the FHA. The innermost plate of the element (plate 1) is assumed to be damaged in the FHA analysis, and it is assumed that the damage occurs at the location of the peak power density. While the outermost plate of a fuel element has the most surface area, and therefore a greater likelihood of being damaged, it has a lower peak power density, and consequently, will have a lower inventory of fission products per gram of fuel than the innermost plate.

13.2.1.2 Accident Analysis and Consequences

The whole-core radioactive material source term was calculated by assuming full-power operation of the MURR core in twelve 10-day cycles over a 300-day period to simulate multiple cycles of fuel irradiation. The total irradiation time in the calculation of the source term was 120 full-power days, which is comparable to the typical number of full-power days for a MURR HEU element prior to discharge (19 cycles of operation at 6.3 full-power days per cycle). The HEU core power level is 10 MW, so that the fission product inventory assumed in the accident analysis corresponds

to a total core burnup of 1,200 MWd. This gives a conservative radioactive source term, since the total burnup of all elements in a typical HEU core is about 650 MWd.

A fuel cycle simulation for the MURR operating with the proposed LEU fuel demonstrated that the weekly operations cycle for the converted core would be the same as for the current HEU fuel (Ref. 13.12). Therefore, the radioactive source term in the LEU core is also computed based on twelve 10-day cycles, although the core power level in the calculation is increased to 12 MW, which is the uprated power necessary to maintain the MURR experimental performance with the LEU fuel. Consequently, the fission product inventory for the accident analysis corresponds to a core burnup of 1,440 MWd, while the anticipated total burnup of all elements in the LEU core in typical weekly operations will be approximately 750 MWd (Ref. 13.12).

The whole-core fission product inventory for the HEU core analysis in the SAR (Ref. 13.1) was calculated using the ORIGEN code (Ref. 13.23). ORIGEN is a zero-dimensional isotope generation and depletion analysis code. The code is provided with several one-group cross-section libraries that are applicable to a variety of reactor types, including light-water moderated reactors, but none of these prepared libraries were generated specifically for the MURR. However, the user does have the option of providing replacement cross-sections for any nuclides that are considered important for properly calculating reaction rates.

For the current HEU and LEU core FHA analysis, the whole-core fission product inventory is calculated using the MONTEBURNS code (Ref. 13.24). MONTEBURNS uses the space- and energy-dependent neutron flux calculated by a detailed MCNP model of the reactor to generate a one-group cross-section library needed by the ORIGEN depletion module. In this way, the one-group cross-sections used in the ORIGEN model are computed based on the neutron spectrum in the core at each depletion state point, so that the user does not need to compute a set of replacement cross-sections in advance. After each depletion step, the MCNP model is updated with a set of material cards that reflect the depleted fuel compositions.

Selected nuclides from the calculated whole-core fission product inventories for the HEU and LEU cores used for the FHA analysis are presented in Table 13-1. For the HEU core, the inventory used in the SAR analysis and the inventory calculated by MONTEBURNS for the current analysis are both provided. The calculated HEU-core inventories agree within a few percent for most nuclides. Larger inventory differences are observed for I-131, Kr-85m, Xe-135, and Xe-135m, and are due to differing basic cross section data or fission product yields in the ORIGEN and MONTEBURNS libraries. However, less than 15% of the total occupational dose, and less than 17% of the public dose in the unrestricted area comes from these four nuclides. The fission product inventory is higher in the LEU core for all radioisotopes considered in the accident analysis due to the 20% higher power level and fuel burnup, differences in the neutron spectrum in LEU vs. HEU fuel, and cross-section data.

TABLE 13-1
WHOLE-CORE ACTIVITY OF RADIOIODINES AND NOBLE GASES (CURIES)

		HEU (SAR [13.1])	HEU	LEU
Iodines	¹³¹ I	1.7E+05	2.20E+05	2.70E+05
	¹³² I	3.3E+05	3.08E+05	3.77E+05
	¹³³ I	5.1E+05	5.42E+05	6.60E+05
	¹³⁴ I	6.3E+05	6.11E+05	7.42E+05
	¹³⁵ I	5.2E+05	5.06E+05	6.16E+05
Noble Gases	⁸⁵ Kr	4.7E+02	4.63E+02	5.46E+02
	⁸⁵ Kr _m	1.1E+05	1.31E+05	1.54E+05
	⁸⁷ Kr	2.1E+05	2.05E+05	2.43E+05
	⁸⁸ Kr	3.0E+05	2.91E+05	3.44E+05
	⁸⁹ Kr	3.8E+05	3.69E+05	4.36E+05
	⁹⁰ Kr	3.8E+05	3.68E+05	4.34E+05
	¹³³ Xe	4.2E+05	3.85E+05	4.67E+05
	¹³⁵ Xe	9.6E+04	7.56E+04	1.64E+05
	¹³⁵ Xe _m	9.4E+04	3.62E+04	1.03E+05
	¹³⁷ Xe	4.9E+05	4.81E+05	5.84E+05
	¹³⁸ Xe	5.2E+05	5.01E+05	6.04E+05
	¹³⁹ Xe	4.2E+05	4.07E+05	4.89E+05

Table 13-2 provides a comparison of the radioiodine and noble gas activities per gram ²³⁵U in high-burnup HEU and LEU fuel elements at the end of irradiation, and after 30 minutes and 60 days of post-irradiation decay. The end of irradiation specific activities were calculated using the data in Table 13-1 and dividing by the core ²³⁵U inventories of 5,468 and 11,204 grams in the HEU and LEU cores, respectively. The fission product inventory following a decay period of 30 minutes was obtained from the same MONTEBURNS model used to generate the inventory for the FHA with an additional cooling period of 30 minutes following the last irradiation interval. The quickest time a fuel element can be brought to the reactor pool is about an hour (60 minutes) after reactor shutdown. To be conservative, the inventory after 30 minutes of post-irradiation decay was used in the FHA analysis. Finally, a spreadsheet model and confirmatory hand calculations were used to compute the radioisotope concentrations following 60 days of decay. These data were used for an analysis to confirm that containment integrity is not required when handling irradiated fuel with a decay time of greater than 60 days.

TABLE 13-2
 SPECIFIC ACTIVITY OF RADIOIODINES AND NOBLE GASES
 IN LEU FUEL (CI/GM-²³⁵U)

		HEU			LEU		
		End of Irradiation	30 Minutes Post-Irradiation Cooling	60 Days Post-Irradiation Cooling	End of Irradiation	30 Minutes Post-Irradiation Cooling	60 Days Post-Irradiation Cooling
Iodines	¹³¹ I	40.23	40.23	0.23	24.10	24.04	0.13
	¹³² I	56.33	56.14	0.00	33.65	33.61	0.00
	¹³³ I	99.12	98.57	0.00	58.91	58.55	0.00
	¹³⁴ I	111.74	100.40	0.00	66.23	59.38	0.00
	¹³⁵ I	92.54	87.78	0.00	54.98	52.14	0.00
Noble Gases	⁸⁵ Kr	0.0847	0.0847	0.0838	0.0487	0.0487	0.0482
	⁸⁵ Kr _m	23.96	22.49	0.00	13.75	12.89	0.00
	⁸⁷ Kr	37.49	28.90	0.00	21.69	16.70	0.00
	⁸⁸ Kr	53.22	47.18	0.00	30.70	27.22	0.00
	⁸⁹ Kr	67.48	0.10	0.00	38.91	0.06	0.00
	⁹⁰ Kr	67.30	0.00	0.00	38.74	0.00	0.00
	¹³³ Xe	70.41	70.41	0.03	41.68	41.72	0.02
	¹³⁵ Xe	13.83	16.66	0.00	14.64	16.12	0.00
	¹³⁵ Xe _m	6.62	6.62	0.00	9.19	9.18	0.00
	¹³⁷ Xe	87.97	0.41	0.00	52.12	0.24	0.00
	¹³⁸ Xe	91.62	21.21	0.00	53.91	12.45	0.00
¹³⁹ Xe	74.43	0.00	0.00	43.65	0.00	0.00	

The source term for the FHA can be calculated from the specific activity data in Table 13-2, the mass of ²³⁵U in the fuel volume exposed by the accident, and power-related factors. The mass and power-related factor data are summarized in Table 13-3. The mass of fuel contained in a 1-inch square by 5 mil thick volume that is exposed by the fuel plate damage is 0.117 and 0.248 grams of ²³⁵U for the HEU and LEU fuel elements, respectively. It is conservatively assumed that the damage occurs at the location of the peak power density. Power distribution data from detailed three-dimensional MCNP models of the reference cores for HEU and LEU were utilized. The nuclear peaking factors used in the accident analysis are for the number-1 fuel plate with the largest local power density peaking factor in a reference HEU or LEU core at equilibrium xenon conditions. The power distribution for a reference core with equilibrium xenon conditions and critical control blade position is most appropriate since the inventory subject to release in the accident corresponds to a very long irradiation history prior to the accident. The reference cores

assumed elements with a mixture of burnups that are typical for MURR operations, control blades that are banked, and a typical loading of samples in the center flux trap and reflector. The "additional allowable factor" is included to account for changes to the plate power peaking that might occur due to adjustments in the fuel management, experiment loading effects, and control blade skewing relative to the reference core. The HEU value of 1.062 has been used historically at MURR. The LEU value of 1.014 is the largest change to the plate 1 peaking factor calculated from a number of alternate LEU cores that also had equilibrium xenon, but skewed control blades (within the limits of the Technical Specifications) and/or an empty central flux trap. The total nuclear peaking factor is used to conservatively estimate the specific activity of fission products at the location of the fuel plate damage.

TABLE 13-3
DATA FOR CALCULATING FISSION PRODUCT SOURCE TERM
IN FUEL HANDLING ACCIDENT WITH HEU AND LEU FUEL ELEMENTS

	HEU	LEU
Fissile Loading		
Fuel volume: 1 in ² × 5 mils (cc)	0.0819	0.0819
²³⁵ U density in fuel meat (g/cc)	1.427	3.025
²³⁵ U mass (g)	0.117	0.248
Power-related Factors		
<i>Nuclear Peaking Factors</i>		
Fuel plate (hot plate average)	2.007 ¹	3.123 ²
Azimuthal Peaking Factor	1.069	1.049
Axial Peaking Factor	1.339	1.314
Additional allowable factor	1.062	1.014
Total Nuclear Peaking Factor	3.051	4.366

¹ Power-related Factors from Reference Core 4A (eq. Xe), Element 5, Plate 1. Yields largest local power density peaking factor in core.

² Power-related Factors from Reference Core 8A (eq. Xe), Element 5, Plate 1. Yields largest local power density peaking factor in core.

13.2.1.2.1 Occupational Dose

For calculating the dose as a result of the FHA, it is conservatively assumed that the noble gases in the exposed part of the fuel plate are released directly into the containment from the pool, while the radioiodine mixes uniformly into the 20,000 gallons of pool water. When the reactor and containment building ventilation systems are in operation, the evaporation rate from the reactor pool is approximately 80 gallons of water per day, or 0.055 gallons/minute. For the purpose of the FHA, the assumption is made that there is an evaporation rate of 4 gallons/minute of pool water containing the radioiodines released from the damaged portion of the fuel. The noble gases (krypton and xenon) and radioiodines released from the fuel into the containment are assumed to

uniformly mix into the containment building air volume of 225,000 ft³. None of the assumptions related to the pool evaporation rate or the exposure time for Operations personnel will be affected by the conversion to LEU fuel.

The external dose to a person due to submersion in an airborne concentration of radionuclides is computed using the Derived Air Concentration (DAC) factors reported in Table 1 of Appendix B of 10 CFR 20 (Ref. 13.25). However, four radionuclides in the fuel failure during operation accident (FFA) source term do not have DAC values published in 10 CFR 20. These are ⁸⁹Kr, ⁹⁰Kr, ¹³⁷Xe, and ¹³⁹Xe. In the current analyses of both the HEU and LEU fuel failure accidents, the DAC values for these "unlisted" radionuclides were calculated using data and methodologies described in Federal Guidance Report No. 12 (EPA-402-R-93-081) and reported in Reference 13.21. These DAC values have been accepted by the NRC.

For the occupational dose in the restricted area as a result of the FHA, it assumed that workers remain in the containment building for 5 minutes after the start of the accident, during which the workers would perform evacuation procedures. For the fuel failure during operation accident described in Section 13.2.5, an occupation time of 10 minutes is assumed because the workers will also need to secure the primary system. In the case of the FHA, however, the reactor is already in a shutdown mode, so there is no need for Operations personnel to secure the primary system. It is worth noting that the expected evacuation time for most occupants of the containment building is 2 minutes, instead of the conservative 5 minutes assumed in the dose calculations.

In the previous analysis of the dose consequences from the FHA performed in References 13.1 and 13.2, the reduction in the concentration of radionuclides in the containment air due to radioactive decay was neglected. However, some of the radionuclides considered in the analysis have half-lives on the order of minutes or even seconds. To eliminate unnecessary conservatism in the calculation of the dose, radioactive decay during the interval of exposure was included in the current analysis of the FHA. The time-averaged airborne concentrations of the noble gas and iodine radionuclides in the containment air over the 5-minute interval were assumed when calculating the occupational dose in the restricted area.

The occupational dose to a worker in the containment for 5 minutes following the accident was calculated to be 447 mrem for the HEU FHA, and 827 mrem for the LEU FHA. These doses are well within the published regulatory occupational limit of 5,000 mrem (5 rem) for the total effective dose equivalent (TEDE). These dose values are also lower than the occupational dose of 1,180 mrem calculated for the fueled experiment failure accident (Ref. 13.22).

13.2.1.2.2 Public Dose

To develop what would clearly be a worst-case scenario, the FHA analysis assumes that there is some leakage of the air from the isolated containment building and the outside atmosphere. It is highly probable that there will be no positive pressure differential between the inside of the containment building and the outside atmosphere, and consequently there will be no air leakage from the building to the outside environment, and consequently no radiation dose to members of the general public in the unrestricted area. Nonetheless, the assumption is made that an atmospheric pressure drop of 0.7 inches of Hg (0.33 psi) occurs at the onset of the FHA. The

resulting pressure differential will result in an average leak rate of 5.2 scfm over a period of 16.5 hours before the containment building pressure is equalized with the atmospheric pressure. The air from the containment leaks into the surrounding laboratory building at an average rate of 5.2 scfm, which then mixes with the large volume of laboratory building air and is discharged from the facility through the exhaust stack at a rate of approximately 30,500 scfm. This causes a significant reduction in the radionuclide concentration exhausting from the facility, which is further reduced by atmospheric dispersal. Assuming an individual outside the exclusion zone remains stationary (i.e., does not move further away) during the entire 16.5-hour period of exposure, calculations were performed to compute the dose to individuals at various distances from the containment building. The most conservative (worst-case) meteorological conditions were assumed to obtain the maximum public dose.

The concentration of noble gas and iodine radionuclides in the containment building air, which is then released to the environment, can be calculated in the same manner as described in the previous section. The FHA assumes 20 gallons of pool water containing radioiodines from the damaged portion of the fuel plate evaporate into the containment building air over a 5-minute interval (4 gallons/minute \times 5 minutes). However, based on the normal conditions inside the containment, the additional water vapor from 20 gallons of evaporated pool water will result in a relative humidity of 100% and inhibit any further evaporation of contaminated pool water into the containment air during the 16.5 hours following the accident. Consequently, the air leaking from the containment to the environment during the 16.5 hours of the public dose calculation is assumed to have the same concentration of radioiodines and radioactive noble gases as are present 5 minutes after the accident occurs, with further reductions due to radioactive decay and mixing with the laboratory building ventilation flow.

It is assumed that 100% of the noble gases in the containment air are released to the environment. Experimental data measured in the containment mockup facility at Oak Ridge National Laboratory (ORNL) have shown that 75% of the radioiodine in the containment air is deposited in the containment, so that only 25% of the airborne radioiodine would be released to the environment. However, for the purposes of the public dose calculations performed in this work, the more conservative NRC-accepted value of 50% reduction of radioiodines from plate-out and deposition was assumed, so that only 50% of the radiodines is released to the environment.

The point of maximum dose for a member of the general public in the unrestricted area under the worst-case meteorological conditions was found to be 760 meters north of the containment building. 10 CFR 20 Appendix B Effluent Concentration Limits were used. For the four "unlisted" noble gas nuclides for which data are not provided in 10 CFR 20 (Kr-89, Kr-90, Xe-137 and Xe-139), Effluent Concentration Limits were calculated using the data and methodology contained in Federal Guidance Report (FGR) No. 12, "External Exposure to Radionuclides in Air, Water, and Soil," for submersion isotopes.

The calculated dose for the general public resulting from the HEU FHA is 0.0083 mrem. For the LEU FHA, the public dose is calculated to be 0.0153 mrem. The dose to the general public from the fueled experiment failure accident, was calculated in Reference 13.22 to be 0.0112 mrem. Since the public dose for the LEU FHA is greater than the fueled experiment failure accident, the FHA will be classified as the MHA following conversion to LEU.

13.2.1.2.3 Additional Analysis

At the request of the regulator, an analysis was also performed to confirm that containment integrity is not required when handling irradiated fuel with a decay time of greater than 60 days. This analysis was previously performed by MURR for a damaged HEU fuel element in response to a "request for additional information" in the NRC review of the previous SAR (Ref. 13.26). The same fuel damage as occurs in the FHA analysis is assumed with a decay time of 60 days and the exposure time for Operations personnel in the containment is assumed to be 60 minutes following the fuel damage.

The occupational dose for this accident scenario with HEU and LEU fuel was calculated using the same power-related factors as used in the FHA analysis above and specific activity data derived from the same models as the FHA, but accounting for the longer post-irradiation decay interval before the accident. The specific activity data for irradiated HEU and LEU fuel after 60 days post-irradiation cooling are provided in Table 13-2. By this point, most of the radioiodines and radioactive noble gases in the irradiated fuel element will have decayed by orders of magnitude due to their shorter half-lives. The remaining noble gases in the exposed portion of the fuel meat are assumed to be released directly into the containment and form a uniform concentration in the containment volume. Additionally, 80 gallons of pool water contaminated with the remaining radioactive I-131 from the exposed fuel are assumed to evaporate during the 60-minute exposure time and form a uniform airborne concentration in the containment. This is a conservative assumption, since under normal conditions the pool evaporation rate in the containment structure is 80 gallons of water per day. The calculated occupational dose to a worker present in the containment for one hour with a breached HEU fuel element with 60 days of decay is 1.10 mrem. This is somewhat higher than the occupational dose of 0.79 mrem that was calculated in Reference 13.2 due to differences in the power-related factors and the methodology used to calculate the irradiated core fission product inventory. For the LEU fuel, the occupational dose from this accident is calculated to be 1.98 mrem. The calculated occupational dose for this accident scenario is well within the published regulatory limit for both HEU and LEU fuel.

Finally, it is noted that the nominal design thickness of the cladding on the LEU plate 1 is 17.5 mil, which is thicker than the 15 mil cladding on the HEU fuel plates. The thicker cladding would decrease the likelihood of fuel release from the mishandling accident. However, no credit was taken for the thicker cladding on the LEU fuel plate.

13.2.2 Insertion of Excess Reactivity

13.2.2.1 Introduction

Insertion of uncontrolled and/or unanticipated positive reactivity to either a critical reactor or during a reactor startup is one of the nine (9) postulated accident-initiating scenarios required to be analyzed for potential radiological consequence per the NUREG-1537 guidelines (Refs. 13.8, 13.9). Following the guidance provided in NUREG-1537, two different accident scenarios for an insertion of positive reactivity were evaluated for the selected LEU core (CD35 element design) and the results are compared against those for the current HEU core. First, several positive step reactivity insertions, based upon the various maximum reactivity limits given in the MURR Technical Specifications (TSS), were considered. Second, a continuous ramp insertion of positive

reactivity, based on the simultaneous continuous withdrawal of MURR's four shim control blades and the regulating blade, was analyzed. The exact mechanisms or events that could cause these reactivity insertions can vary, but could include an inadvertent rapid insertion or removal of an experiment from the center test hole, reactor or equipment malfunction, or operator error.

The analyses were performed using the PARET/ANL code (Ref. 13.10). PARET/ANL is a 1-dimensional reactor transient analysis code that models plate, pin and nested tube fuel geometries. The collection of fuel meat, cladding, and associated coolant is called a "channel" in PARET/ANL. An average channel is typically used to represent the core and bulk reactivity feedback effects from the transient, while one or more "peak" channels are used to represent those components (e.g., a fuel plate) which are expected to reach the highest temperature as a result of the transient. There is no heat transfer between the channels in PARET/ANL, but the channels are coupled through reactivity feedback effects, i.e., the reactivity feedbacks from each channel in the model are volume-weighted and summed to compute the total core reactivity and power as a function of time in the transient.

The user provides a description of the fuel geometry, steady-state thermal-hydraulic conditions, thermo-physical properties, and the transient initiating condition (e.g., insertion of reactivity) as a time-dependent table. The thermal conductivity and volumetric heat capacity of the plate materials can be supplied as input to PARET/ANL as temperature dependent functions. The coolant properties are generated by the code using built-in functions. A point-kinetics solution is used to calculate the overall core reactivity, total core power, and local heat generation rates as a function of time. The thermal-hydraulics models in PARET/ANL are used to compute the heat conduction, material temperatures (e.g., fuel meat, clad, coolant), and inherent reactivity feedbacks. Lastly, termination of the reactor transient from engineered safety systems (i.e., control blade scram) that are tripped from core power, coolant flow, or reactor period settings can be modeled.

13.2.2.2 Changes to Modeling Relative to Prior SAR Analysis

For the current HEU-fueled core, the accidental positive step reactivity addition accident scenarios were analyzed in the MURR SAR (Ref. 13.1) from an initial steady-state power level of 10 MW, and with coolant flow, pressure, and core inlet temperature conditions as specified in Table 13-4. The continuous ramp insertion of positive reactivity accident scenario was also analyzed from low power (1.0 W) and from a nominal steady-state power of 10 MW.

TABLE 13-4
KEY REACTOR PARAMETERS FOR REACTIVITY INSERTION ACCIDENTS
IN THE CURRENT MURR SAR

Parameter	Nominal Operating Value	Assumed Value in SAR Analysis
Reactor Power	10 MW	10 MW
Primary Coolant Flow Rate	3,800 gpm	3,600 gpm
Reactor Core Inlet Pressure	84 psia	75 psia ¹
Reactor Core Inlet Temperature	120 °F	130 °F

¹The LSSS pressurizer pressure at MURR is 75 psia.

During the review of the SAR as part of the MURR's license renewal application, the NRC made several requests for additional information - which included requests regarding the Reactivity Insertion Accidents (RIA). Among these, the NRC requested MURR to provide results based on initial conditions prior to the start of the accident that are more stringent than previously considered. This is a new development proposed to the MURR HEU safety basis and is based on regulatory exchanges and precedent.

These new initial conditions for the safety basis were incorporated during the preparation of this PSAR for the HEU to LEU fuel conversion and are documented in this Section. For the RIA analysis, the accidents were evaluated assuming the reactor is initially operating at the Limiting System Safety Settings (LSSS) conditions for the coolant flow rate and inlet temperature. For the reactor operating power at the start of the accident, the Limiting Conditions for Operations (LCO) for power was chosen over the LSSS power. The LCO on reactor power is an administratively established constraint on reactor operation. For reactor power, this constraint is 115% of the full licensed power, which is also the maximum limit for the automatic rod run-in set point. The initial conditions assumed for the RIAs in both HEU and LEU cores are compared in Table 13-3. These conditions are consistent with the requirements set forth in Chapter 13 of NUREG-1537, Part 2 (Ref. 13.9).

TABLE 13-5
INITIAL STEADY-STATE CONDITIONS FOR RIA ANALYSES BASED ON
REGULATORY REQUEST DURING HEU RELICENSING

Setting	HEU	LEU
Reactor Power, MW (115% of Full Power)	11.5	13.8
Primary Inlet Temperature, °F	155	145
Primary Coolant Flow Rate, gpm	3200	3300
Pressurizer Pressure, psia	75	75
Pressurizer Level, inches	-16	-16

As part of the PSAR analysis, a review of the PARET/ANL models used in the MURR SAR analyses was conducted. The review found some modeling inconsistencies, which were corrected prior to performing the new analysis (Ref. 13.11). The PARET/ANL models were also enhanced to include depleted as well as fresh fuel plates. The HEU SAR analysis had only considered fresh fuel plates. The depleted fuel plates will have a lower local heat flux compared with the fresh plates. However, the thermal conductivity is known to degrade especially for LEU with fuel irradiation. Additionally, the growth of an oxide layer on the fuel plates during residence in the core, plus the restriction of the coolant channel gap due to the oxide layer and irradiation-induced dimensional changes, may cause fuel temperatures to be higher in the depleted fuel plates relative to the fresh fuel plates previously evaluated. Furthermore, a series of sensitivity studies were executed to analyze the potential impact of variations in parameters such as thermo-physical properties or core operating conditions.

In the HEU SAR analysis of the RIAs, primary coolant temperature and void feedback coefficients corresponding to the MURR TS limits of $-6.0 \times 10^{-5} \Delta k/k/^\circ\text{F}$ and $-2.0 \times 10^{-3} \Delta k/k/\%$ void, respectively, were employed. For this conversion PSAR, the reactivity feedback coefficients and reactor kinetics parameters (effective delayed neutron fraction [β_{eff}] and neutron lifetime [Λ]) were calculated for the MURR core loaded with HEU or LEU fuel using an MCNP5 core model instead of using the MURR TS values. Table 13-6 summarizes the calculated reactivity feedback coefficients that are used in the PARET/ANL analysis. As described in Section 4.5.3, the reactivity coefficients and kinetics parameters were calculated for three different core loadings of each fuel type (HEU or LEU): 1) all fresh fuel, 2) a typical mixed-burnup core loading at beginning-of-cycle (BOC) with no xenon, and 3) a typical mixed-burnup core loading at equilibrium-xenon conditions. For each fuel type, the smallest magnitude value calculated for each parameter was chosen for the current work, which is the conservative approach.

TABLE 13-6
REACTIVITY FEEDBACK COEFFICIENTS AND KINETICS PARAMETERS FOR MURR
CALCULATED WITH MCNP5

Parameter	HEU	LEU
Coolant Density Coefficient, $\$/\%$ -void	-0.301 ± 0.011	-0.304 ± 0.011
Coolant Temperature Coefficient, ^a $\$/^\circ\text{F}$	$-2.9 \times 10^{-3} \pm 5.2 \times 10^{-5}$	$-9.06 \times 10^{-4} \pm 5.27 \times 10^{-6}$
Fuel Temperature Coefficient $\$/^\circ\text{F}$	N/A	$-5.06 \times 10^{-4} \pm 2.89 \times 10^{-5}$
β_{eff} = Fraction of delayed fission neutrons	$0.783\% \pm 0.003\%$	$0.765\% \pm 0.002\%$
Λ (μs) = mean neutron generation time	49.5 ± 0.10	38.7 ± 0.03

^a This is the reactivity feedback for temperature changes of the coolant only. The effect of coolant density changes on reactivity due to temperature increase or decrease is accounted for in the coolant density coefficient.

In addition to inherent reactivity feedbacks from fuel and coolant temperature changes that occur during the transient, engineered safety systems are also available to terminate any transient initiated by an unanticipated positive insertion of reactivity. External reactivity control of the

MURR core is accomplished with four BORAL[®] shim blades that move in a water-filled gap between the reactor outer pressure vessel and the beryllium reflector. When any one of the various reactor trip settings is reached, a scram signal is sent and the control blades are dropped to insert a sufficiently large amount of negative reactivity and terminate the transient. The blades can travel from fully withdrawn to 80% inserted (a travel distance of 20.8 inches) in less than 0.70 seconds. This is equivalent to a blade insertion speed of 0.76 m/s. A dashpot mechanism slows the blade drop speed after the blades reach the 80% inserted position. There is a short delay time of 150 milliseconds from the time the scram signal is sent to the start of control blade motion.

The reactivity worth of the entire control bank was calculated with MCNP5 for HEU-fueled and LEU-fueled cores under different core burnup conditions. As shown in Section 4.5.1 and 4.5.2, the control bank worth for the LEU-fueled cores is less than for the HEU-fueled cores, but the total bank worth is still sufficiently large to compensate for any credible reactivity insertion accidents postulated for MURR. The reactivity worth inserted from the fully-withdrawn position (26 inches withdrawn) to the 80% inserted position as a function of time from the start of the control blade drop (assuming a blade drop rate of 0.76 m/s) was calculated and entered in the PARET/ANL models. For all accident analyses, the 80% inserted position is considered the full insertion position for the control bank. This conservative assumption corresponds to only 92% of the total control bank worth for both the HEU and LEU cores.

A comparison of the plate dimensions in the HEU and CD35 elements is provided in Table 13-7. While all the plates in the HEU fuel element have the same meat and clad thickness (20 mil meat and 15 mil clad, for a total plate thickness of 50 mil), the LEU fuel plates are not all identical. The CD35 meat and clad thicknesses were optimized to flatten the steady-state heat flux profile (Ref. 13.12).

The plate with the peak heat flux in the HEU cores is plate number-1, while the plate with the peak heat flux in the LEU cores is plate 23. Both of these plates are cooled on one side by a channel that is wider than the other side, and the wider channel is heated on only one side, as it is bounded by either the inner pressure vessel (HEU) or the outer pressure vessel (LEU). A majority of the heat generated by fission in the fuel plate will conduct out the (cooler) side of the plate that is cooled by the one-sided heated channel. This effect was modeled in the PARET/ANL analysis.

In the MURR HEU SAR, calculations were performed with version 5.0 of the PARET/ANL code. The latest version of PARET/ANL v.7.5 (controlled source code file PARETANL_7.5_r82_160809) was used for this analysis. Unlike the earlier versions of the program, this newer version of the code does not require that all fuel plates in the channels be modeled with the same dimensions. Thus, each of the channels can be modeled with plate dimensions, oxide layer thickness, coolant channel thickness, and thermo-physical parameters that are appropriate for the geometry and burnup conditions of the plate. A drawing of a PARET/ANL channel showing the fuel plate and coolant is provided in Figure 13.1. The materials represented in the model are the fuel meat, cladding (zirconium interlayer, if present, and 6061-Al), any oxide layer, which forms on the surface of the fuel plate during operation, and water coolant.

Table 13-7 also shows that all internal coolant channels (the gap between fuel plates) in the HEU element are nominally 80 mil thick. There is a wider coolant channel that is nominally 110 mil

thick on the concave side of HEU plate number-1 (distance from the plate surface to the inner pressure vessel wall), and a channel that is nominally 90 mil thick on the convex side of HEU plate number-24 (distance from the plate surface to the outer pressure vessel wall). The internal coolant channel thicknesses in the LEU element were varied as part of the fuel design optimization. These channels are nominally either 93 or 92 mil, with an average interior coolant channel thickness for the LEU element of 92.4 mil. The coolant channels on the concave side of LEU plate number-1 and the convex side of LEU plate number-23 are both nominally 95.5 mil.

TABLE 13-7
NOMINAL HEU AND LEU FUEL PLATE DIMENSIONS

Element Component	HEU	LEU (CD35)
Fuel plates per element	24	23
Fuel meat length (inches)	24.0	24.0
Fuel meat width, varies by plate (inches)	1.703 to 4.052	1.690 to 4.048
Unfueled width of plate in coolant channel (mil)	70 [#]	70 [#]
Plate 1 meat thickness (mil)	20	9
Plate 2 meat thickness (mil)	20	12
Plate 3 meat thickness (mil)	20	16
Plate 4-22 meat thickness (mil)	20	20
Plate 23 meat thickness (mil)	20	17
Plate 24 meat thickness (mil)	20	N/A
Plate 1 clad thickness (mil) – Al + Zr*	15	17.5
Plate 2 clad thickness (mil) – Al + Zr*	15	16
Plate 3 clad thickness (mil) – Al + Zr*	15	14
Plate 4-22 clad thickness (mil) – Al + Zr*	15	12
Plate 23 clad thickness (mil) – Al + Zr*	15	16
Plate 24 clad thickness (mil) – Al + Zr*	15	N/A
Average plate meat thickness (mil)	20	18.87
Average plate clad thickness (mil) - Al + Zr*	15	12.67
Coolant channel 1 thickness – plate 1 to inner pressure vessel wall (mil)	110	95.5
Interior coolant channel thickness (mil) – with exception of channels 6-19	80	93
Interior coolant channel 6-19 thickness (mil)	80	92
Average interior coolant channel thickness (mil)	80	92.4
Coolant channel 25 (HEU)/24 (LEU) thickness – plate 24 (HEU)/23(LEU) to outer pressure vessel wall (mil)	90	95.5

[#] Total unfueled width on each end of plate is 145 mil. 75 mil of plate extends into side plate.

*Zr interlayer exists only in LEU. The nominal Zr interlayer thickness is 1 mil.

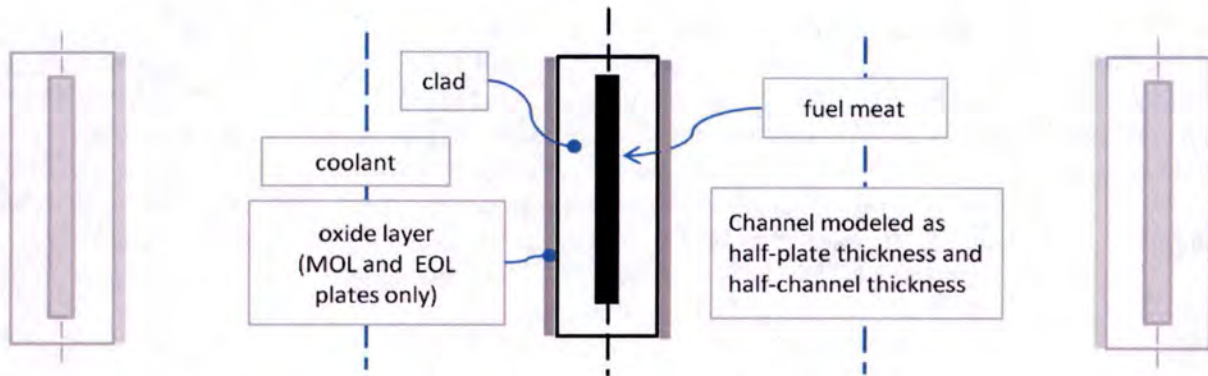


FIGURE 13.1
PARET/ANL FUEL PLATE/COOLANT CHANNEL

In the current analysis, up to four fuel plate/coolant channels will be modeled to represent the MURR core plus the fuel plates most likely to have peak fuel temperatures. The channels to be modeled will be 1) an average channel representing the core, 2) a beginning-of-life (BOL, unirradiated) fuel plate with the peak heat flux of all fresh fuel plates in the core, 3) an end-of-life (EOL) plate with the peak heat flux of all EOL plates in the core, 4) and a middle-of-life (MOL) plate with the peak heat flux of all MOL plates in the core. Appropriate degradation of the U-10Mo thermal conductivity with fuel burnup, the formation of an oxide layer on irradiated fuel plates, and reduction of the coolant channel thickness due to oxide growth, fuel swelling, and fuel creep were modeled in the MOL, EOL, and average fuel channels. A detailed discussion of the modeling of the effect of fuel burnup on thermal conductivity in the RIA analysis is provided in Reference 13.11.

The fuel plate/channel dimensions for the average and peak plates in the HEU and LEU core PARET/ANL models are summarized in Table 13-8. The dimensions for the average channel in the core were calculated using the average values for the nominal design data for all fuel plates in the element (e.g., fuel meat width, plate width, fuel meat thickness, cladding thickness, and interior coolant channel thickness). The oxide layer thickness on the convex surface of HEU plate number-1 or the concave surface of LEU plate number-23 is estimated from a version of the Griess correlation (Ref. 13.13) that was modified to take into account the specific operating conditions of the MURR (Ref. 13.14). These plate surfaces were chosen for predicting the oxide layer thicknesses because they will have the highest temperature, and so, a thicker oxidation layer than the surface on the other side of the plate.

TABLE 13-8
FUEL PLATE/CHANNEL DIMENSIONS IN PARET/ANL MODEL

Dimension	Average Plate/Channel		Peak Plate/Channel	
	HEU	LEU	HEU Plate 1	LEU Plate 23
Meat width (in)	2.877	2.868	1.703 ¹	4.048 ¹
Plate width (in)	3.017 ²	3.008 ²	1.843 ²	4.188 ²
Meat thickness (mil)	20	18.87	20	17
Zr interlayer thickness (mil)	N/A	1	N/A	1
6061-Al thickness (mil)	15	11.67	15	15
Plate thickness (mil)	50	44.22	50	49
Oxide layer thickness formed on surface of fuel plate (mil) ^{3,4}	0.0 (@ 0 MWd) 0.36 (@ 72.0 MWd ⁵)	0.0 (@ 0 MWd) 0.59 (@ 85.9 MWd ⁵)	<u>BOL</u> : 0.0 <u>MOL</u> : 0.34 (@ 65 MWd) <u>EOL</u> : 0.54 (@ 150 MWd)	<u>BOL</u> : 0.0 <u>MOL</u> : 0.63 (@ 96 MWd) <u>EOL</u> : 0.93 (@ 180 MWd)
Coolant channel thickness, C (mil) ⁶	C ₀ = 80.0 ⁷ C (72.0 MWd) = 75.2	C ₀ = 92.4 ⁷ C (85.9 MWd) = 88.5	<u>BOL</u> : C ₀ = 80.0 ⁸ <u>MOL</u> : C (65 MWd) = 75.7 <u>EOL</u> : C (150 MWd) = 70.0	<u>BOL</u> : C ₀ = 93.0 ⁹ <u>MOL</u> : C (96 MWd) = 88.7 <u>EOL</u> : C (180 MWd) = 85.0

¹ Peak heat flux data were calculated in a 5 mm stripe along the vertical edge of the fuel meat adjacent to the unfueled portion of the fuel plate (next to fuel element side plate).

² Includes 70 mil unfueled portion of fuel plate along both vertical edges of the plate that extends to the element side plate.

³ Oxide thickness estimated as a function of core residence time from Griess correlation modified based on measured data for HEU fuel plates in MURR (Ref. 13.14).

⁴ Convex surface of HEU plate 1 or concave surface of LEU plate 23. These are the surfaces of the plates that will have the highest temperatures, and so, the thicker oxidation layer.

⁵ Average burnup of all elements in reference mixed-burnup core.

⁶ Coolant channel thickness assumed to reduce linearly with burnup due to combined effects of fuel swelling and oxide layer formation. Total combined effect is 10 mil at 150 MWd for HEU element, so that $C = C_0 - 10 \cdot B / 150$, where C and C₀ are the channel thickness in mil, C₀ is the nominal channel thickness for an unirradiated element, and B is the element burnup in MWd. For the LEU element, the total combined effect is 8 mil at 180 MWd.

⁷ Average of all interior coolant channels in unirradiated element.

⁸ Nominal thickness of coolant channel on convex side of HEU plate 1 in unirradiated element.

⁹ Nominal thickness of coolant channel on concave side of LEU plate 23 in unirradiated element.

Furthermore, during irradiation the coolant channel will become constricted relative to the fresh element coolant channel due to oxide growth, fuel swelling, and irradiation-induced fuel creep. For HEU fuel elements, the current acceptance criteria for the elements during irradiation limit this constriction to a maximum of 10 mils. For the LEU fuel, it was determined in Reference 13.14 that the total coolant channel restriction for channels bounded by two fuel plates will be no more than 8 mils due to these effects. The channel restriction is assumed to increase linearly, reaching 10 mils at the expected HEU element discharge burnup of 150 MWd and 8 mils at the expected LEU element discharge burnup of 180 MWd.

PARET/ANL is a 1-D code, and uses a user-supplied axial heat source profile for each channel to compute the thermal-hydraulic conditions and temperatures. It is assumed that while the reactivity insertion will affect the total core power, the power shape relative to the steady-state power distribution will not be affected by the transient. Detailed, 3-dimensional power distribution data in MURR cores loaded with HEU or LEU fuel were calculated using MCNP5 as part of the steady-state safety analyses for a number of reference cores (Ref. 13.12). Reference cores that represent the typical operating conditions at MURR were selected for the accident analyses. These so-called Cores 3A (HEU) and 7A (LEU) are loaded with eight elements with a mixture of burnup, the flux trap is loaded with experiments typical for MURR operations, and the four control blades are banked at the same axial position. Tally results from the MCNP model for these reference cores were used to calculate the plate heat flux in radial (plate), axial, and azimuthal directions in all eight elements in the MURR core. For the peak BOL, MOL, and EOL channels in the PARET/ANL models, the 1-D axial heat source was calculated for the plate and azimuthal strip in the core that generates the highest local heat flux. For the average channel in the PARET/ANL models, the axial heat source description was calculated from a volume-weighted average of the power density of all plates in the core.

Table 13-9 compares the steady-state peak heat fluxes calculated by core neutron physics and assumed in the PARET/ANL modeling for the RIAs in HEU and LEU cores that are typical for MURR operations. The values calculated by MCNP are taken from the results of an MCNP5 (Ref. 13.15) model for a typical mixed-burnup core loaded with HEU or LEU fuel at beginning-of-cycle (BOC) conditions and normalized to the LCO power of either 11.5 MW for HEU or 13.8 MW for LEU. The peak heat flux (by plate, axial level, and azimuthal position) was computed from an f7 tally in the MCNP5 calculation, and assuming an even power split between the concave and convex surfaces of the fuel plate. The axial heat source for the PARET/ANL model was based on the detailed power distributions calculated by MCNP5, but taking into account thermal-hydraulic and neutronics effects that reduce the heat that must be removed by the coolant in the peak channel. As described above, the plate with the peak heat flux in the HEU and LEU cores is cooled on each side by coolant channels that are of differing thicknesses and conditions, so that a smaller fraction of the heat generated in the plate will be conducted into the peak coolant channel. Since PARET/ANL assumes a radially-symmetric fuel plate and channel, this effect was accounted for by reducing the axial heat source for the peak channels by the fraction of heat conducted out the cooler side of the fuel plate during steady-state operations. This avoids unnecessary conservatism in the analysis. This modeling is described in more detail in Reference 13.11. Furthermore, based on calculations performed in Reference 13.18, it was assumed that 6.0% and 3.6% of the energy produced in the HEU and LEU cores, respectively, is deposited outside the

primary coolant system, thus reducing the heat that must be removed from the fuel plate by the primary coolant system.

TABLE 13-9
PEAK STEADY-STATE HEAT FLUX (W/CM²) IN HEU AND LEU CORES

Plate	HEU Core (Core 3A)		LEU Core (Core 7A)	
	Calculated by MCNP ¹	PARET/ANL Model for RIA ²	Calculated by MCNP ³	PARET/ANL Model for RIA ⁴
BOL	213.1	183.0	242.4	225.5
MOL	176.3	152.7	219.7	204.6
EOL	134.2	116.6	196.1	182.7

¹ Calculated from MCNP5 f7 tally for typical mixed-burnup core at BOC conditions. Assumes total reactor power of 11.5 MW and an even power split between the concave and convex surfaces of plate.

² Calculated heat flux multiplied by fraction of energy conducted towards the hottest surface of the fuel plate. For the HEU fuel at steady-state, the hottest surface of fuel plate 1 is the convex side of the plate. The power split fractions to the convex surface are 45.68%, 46.07%, and 46.22% for the BOL, MOL, and EOL plates, respectively. Also assumes 6.0% of total reactor power is deposited outside the reactor core.

³ Calculated from MCNP5 f7 tally for typical mixed-burnup core at BOC conditions. Assumes total reactor power of 13.8 MW and an even power split between the concave and convex surfaces of plate.

⁴ Calculated heat flux multiplied by fraction of energy conducted towards the hottest surface of the fuel plate. For the LEU fuel at steady-state, the hottest surface of fuel plate 23 is the concave side of the plate. The power split fractions to the concave surface are 48.25%, 48.27%, and 48.33% for the BOL, MOL, and EOL plates, respectively. Also assumes 3.6% of total reactor power is deposited outside the reactor core.

The peak heat fluxes from the MOL and EOL LEU plates are roughly 9% and 19% less, respectively, than the peak heat flux from the BOL LEU plate in the reference core. However, there is a significant degradation of the U-10Mo thermal conductivity that occurs with irradiation (up to 35% reduction of the thermal conductivity at EOL, as shown in Table 2.2 of Reference 13.11). This, in addition to the formation of an oxide layer on the irradiated plate surface, were anticipated to result in higher fuel temperatures for the irradiated LEU fuel plates compared to the fresh LEU plate. It is less likely that the irradiated HEU plates will have higher fuel temperatures than the fresh HEU plates because the heat flux reduction in the HEU EOL plate relative to the BOL plate is much larger (36%) than the degradation of the UA_{fx} thermal conductivity from BOL to EOL (25%).

13.2.2.3 Accident Initiating Events and Scenarios

The following reactivity insertion accidents will be evaluated in the LEU reference core:

(1) *Rapid Step insertion of positive reactivity accident.*

- 0.60% $\Delta k/k$ step insertion of reactivity in a core operating at full power. This is the TS limit for a) total reactivity worth of *all unsecured experiments* in the reactor, b) reactivity worth of *any secured removable experiment*, and c) total reactivity worth of *all experiments in the center test hole*.

- 0.25% $\Delta k/k$ step insertion of reactivity in a core operating at full power. This is the TS limit for the reactivity worth of any *unsecured experiment*.
 - 0.10% $\Delta k/k$ step insertion of reactivity in a core operating at full power. This is the TS limit for the reactivity worth of any *moveable experiment*.
- (2) *Continuous blade withdrawal accident*. 0.03% $\Delta k/k$ /second ramp insertion of reactivity from full power. This is the TS limit for the reactivity insertion rate from control blade withdrawal.
- (3) *Startup accident*. 0.03% $\Delta k/k$ /second ramp insertion of reactivity from low power (1.0 W). This will simulate a blade withdrawal accident at startup without operator intervention.

For the HEU core, only the results from the 0.6% $\Delta k/k$ step reactivity insertion accident will be presented in this section since it has already been noted in the SAR that this accident results in the most severe consequence (highest fuel temperature) of all the RIA accidents analyzed. Furthermore, the full set of step and ramp insertion accidents identified above were previously evaluated for the HEU core (Ref. 13.16) and it was observed that the 0.6% $\Delta k/k$ step insertion accident resulted in the highest fuel temperature.

Table 13-10 provides a summary of the steady-state conditions that will be assumed for a "Base Case" for each RIA. The base case assumes the initial steady-state conditions summarized in Table 13-5, unless noted otherwise. These conditions are the initial conditions requested by the regulator during the HEU relicensing and are more challenging than the initial conditions assumed in the HEU SAR analysis. Table 13-10 also summarizes parameter variations that will be modeled in a series of branch cases to cover potential non-conservative variations of thermo-physical properties or core operating conditions that may affect the severity of the accidents. No hot channel factors will be applied in the reactive insertion accident analysis.

TABLE 13-10
 CONDITIONS FOR BASE AND BRANCH CASES FOR REACTIVITY INSERTION
 ACCIDENTS

Base Case	<p>Analyses of the step reactivity insertion (0.6%, 0.25%, and 0.10% $\Delta k/k$) and blade withdrawal (0.03% $\Delta k/k/s$) accidents will be initiated from steady-state at the conditions given in Table 13-5.</p> <p>The LEU core startup accident will be initiated from these same conditions, except the initial core power will be 1.0 Watt with the blades fully inserted (-4.2% $\Delta k/k$, or -5.49\$).</p>
BRANCH CASES FOR REACTIVITY INSERTION ACCIDENTS	
Branch01	<p>Decrease the U-10 Mo thermal conductivity by 20% in all LEU fuel plates. For the LEU fuel, this will yield a thermal conductivity of the EOL plate number-23 that is roughly half of that for the unirradiated U-10Mo.</p> <p><i>Rationale: Thermal conductivity of U-10 Mo degrades with burnup. The measurement data by Burkes et al. in Reference 13.17 indicate that at the peak burnup expected in the MURR fuel plates ($\sim 3 \times 10^{21}$ fissions/cm³); the lower-bound of the experimental data for the thermal conductivity is 50% of the fresh U-10Mo thermal conductivity.</i></p> <p><i>This branch case will not be run for the HEU fuel as the lower bound data for the UAl_x thermal conductivity was selected from the available data (see Section 2.1.1 of Reference 13.11).</i></p>
Branch02	<p>Increase the oxide layer thickness on the MOL and EOL fuel plates.</p> <p><i>Rationale: The oxide layer thickness can be estimated using a correlation that depends on the hours the fuel plates are resident in the core and the fuel plate surface temperature. The correlation developed by Griess et al. in Reference 13.13 is for fuel plates in ATR. This was modified based on measurements at MURR for HEU fuel plates (Ref. 13.14), which reflects the effect of the water chemistry (pH) of the MURR primary coolant and the MURR HEU fuel plate surface temperature. This "modified Griess correlation" was evaluated over the life of the fuel plate at the peak plate surface temperature for the core at equilibrium-xenon and nominal operating conditions. If the correlation is evaluated using the peak plate surface temperature at steady-state conditions that are at the most conservative values of the normal operating band for MURR, the oxide thickness is estimated to be up to 18% thicker for HEU fuel plates, and 23% thicker for LEU fuel plates.</i></p>

Branch03	<p>Coolant channel restriction with burnup will be limited to 5 mil in Branch03, and no coolant channel restriction with burnup will be assumed in Branch03b.</p> <p><i>Rationale: The formation of an oxide layer on the fuel plates, irradiation-induced fuel swelling, and fuel creep will cause the coolant channels between fuel plates to become constricted with fuel burnup. Acceptance criteria for the elements limit this constriction to 10 mil and 8 mil, respectively, for the HEU and LEU fuel elements. This branch case assesses the impact on the accident consequences if the coolant channel restriction is less than the assumed limit.</i></p>
Branch04	<p>Initiate the reactivity insertion accident from different steady-state conditions for the coolant inlet temperature, coolant flow rate, and system pressure. Branch04f (HEU and LEU) assumes the pressurizer pressure is 90 psia and pressurizer level of +4 inches.</p> <p><i>Rationale: The system pressure assumed in the Base Case was for a pressurizer pressure of 75 psia (60.7 psig) and a pressurizer level of -16 inches (LSSS for pressure). Branch04f assesses the impact of using a pressure that is above the normal operating band for MURR.</i></p>
Branch05	<p>Perform the analyses of the step insertion of reactivity and blade withdrawal accidents for Mode II operating conditions (half of the full licensed power and single coolant pump in operation).</p> <ul style="list-style-type: none"> • HEU: initiate accident from reactor power = 5.75 MW (115% of full power for Mode II) and at LSSS flow (1,600 gpm), temperature (155 °F), and pressure (75 psia pressurizer pressure, -16 inch water level). • LEU: initiate accident from reactor power = 6.90 MW (115% of full power) and at LSSS flow (1,650 gpm), temperature (145 °F), and pressure (75 psia pressurizer pressure, -16 inch water level). <p>For the startup accident in the LEU core, the initial conditions for this branch case will be a steady-state core power of 1.0 Watt and LSSS conditions for the coolant flow rate, inlet temperature, and pressure.</p> <p><i>Rationale: This repeats a case performed by MURR in response to the RAI's during the HEU relicensing.</i></p>

Branch06	<p>The step reactivity insertion accident was modeled in the MURR SAR and the Base Case analysis with an insertion time of 10^{-5} seconds. Branch cases will be run with the reactivity insertion occurring in 10^{-3} (Branch06a) and 10^{-1} (Branch06b) seconds.</p> <p><i>Rationale: The step insertion of 0.6% $\Delta k/k$ represents the ejection of the TS limit total worth of all unsecured experiments. For this ejection to occur in 10 microseconds (or even 1 millisecond) is extremely rapid, and beyond any realistic scenario for the ejection of unsecured experiments in MURR. An ejection time of > 0.1 second is more realistic.</i></p>
Branch07	<p>The blade withdrawal and startup accidents will be modeled with the stainless steel regulating blade withdrawn concurrently with the shim blades. The TS limit for the reactivity insertion from regulating blade withdrawal is 0.015% $\Delta k/k/s$. For the purpose of this analysis, the reactivity insertion rate from regulating blade withdrawal was assumed to be 0.025% $\Delta k/k/s$, giving a combined reactivity insertion rate of 0.055% $\Delta k/k/s$. The TS limit for the total worth of the regulating blade is 0.6% $\Delta k/k$, so that the reactivity addition from the regulating blade withdrawal will last for only the first 24 seconds (0.6/0.025) of the accident analysis. After this, the TS limit for the shim blade withdrawal of 0.03% $\Delta k/k/s$ will apply for the remainder of the accident analysis.</p> <p><i>Rationale: The RAI's for the MURR HEU relicensing requested justification for not including the regulating blade withdrawal in the startup accident. Administrative procedures prohibit the simultaneous withdrawal of both the shim blades and the regulating blade. Nonetheless, this scenario was analyzed in MURR's response to the RAI.</i></p>
Branch08	<p>The startup accident will be evaluated in Mode III/natural circulation conditions initiated from a steady-state power of 50 kW, a coolant inlet temperature of 100 °F (same as the pool temperature), and atmospheric pressure (14.3 psia at the MURR site; 21.02 psia at the bottom of the fuel element).</p> <p><i>Rationale: Low power operations will be used for startup physics testing of the LEU core. Note that this accident will be analyzed only for the reference core loaded with all-fresh LEU fuel (reference core 5B1 identified in Reference 13.12).</i></p>

13.2.2.4 Accident Analysis and Consequences

As explained in Section B-5.10 of Reference 13.4 (“Regulatory Safety Analysis Acceptance Criteria for Loss-of-Coolant Accidents”), the acceptance criteria for both HEU and LEU fuel are met if the peak fuel temperature of each fuel is shown to remain below the fuel blister threshold temperature for that fuel. Section 13.2.3.2 of Reference 13.1 indicates that during fabrication every HEU fuel plate is tested to 900 °F (482 °C), which is taken to be the “no fuel plate blister verification temperature” for fresh HEU fuel in this reference. Section 2.6 of Reference 13.4

indicates that, based on a two-standard-deviation lower-bound fit of the data of Reference 13.6, this is a reasonable temperature limit to apply to irradiated HEU fuel as well.

Section 2.6 of Reference 13.4 used the nominal fuel blister threshold temperature data of monolithic fuel provided by Reference 13.7 to conclude that the LEU fuel temperature safety limit vs. peak fission density at the lower bound of the 95% confidence interval (-2σ) of the blister threshold temperature can be represented as $T_{\text{blister, 95\%CI, lower}}$ in the following equation:

$$T_{\text{blister, 95\% CI, lower}} = \begin{cases} 6.72 \times 10^6 \times F_D^{-0.1974} & \text{for } F_D \geq 1.5 \times 10^{21} \\ 450 & \text{for } F_D < 1.5 \times 10^{21} \end{cases} \quad (13-1)$$

where F_D is the fission density, fissions/cm³.

13.2.2.4.1 HEU Core Step Reactivity Insertion Accident Results

The results for the reference core loaded with HEU fuel are presented in Table 13-11. The reference core selected for this analysis (Core 3A) has eight elements with a mixture of burnups, which are typical for MURR operations. The loading of experiments in the center flux trap and reflector are also typical for MURR operations. Results are presented for the accident initiated from the initial conditions specified in Table 13-5. It is conservatively assumed that the bank of four control blades was inserted at scram from the fully withdrawn position (26 inches withdrawn).

The step insertion of 0.6% $\Delta k/k$ reactivity in the critical, steady-state core results in a sharp reactor power rise from 11.5 MW to nearly 38.1 MW in the mixed-burnup reference core before the transient is curtailed by negative reactivity feedback effects from changes in the coolant conditions (density and temperature). The transient is terminated by reactor scram at 0.151 seconds after the reactivity insertion. The peak HEU fuel temperature reached in the accident is predicted to be 221.3 °C in a fresh plate number-1 in fuel element position 5. The steady-state heat flux profile for this plate normalized to a core power of 10 MW is provided in Figure 4.33. As described in Section 13.2.2.2 above, the effect of the uneven heat conduction between the two radial surfaces of the fuel plate and the fission energy deposited outside the primary coolant system were taken into account in the analysis. The peak fuel temperatures in the MOL and EOL plates in this core are predicted to be 220.9 °C and 196.8 °C, respectively.

Several branch cases were run to estimate the effect of potential non-conservative variations of the core operating conditions on the severity of the accident in the HEU core. In the Branch02 case, the oxide layer thickness on the MOL and EOL plates was increased by 18% relative to the Base Case. An oxide layer thickness of 0.54 mil on an EOL plate in the plate number-1 position had previously been estimated from a modified Griess correlation (Ref. 13.14) based on fuel elements in a core operating at the nominal conditions for MURR. However, if the MURR consistently operated at the limits of the normal operating band, the oxide layer thickness on an EOL plate in the plate number-1 position is estimated to be 0.63 mil (18% thicker). The peak reactor power reached during the accident increases only 0.07 MW in this branch case relative to the Base Case, while the increased oxide thickness results in a modest 2.4 °C increase in the peak fuel temperature

in the MOL plate (up to 223.3 °C from 220.9 °C in the Base Case) and a 2.6 °C increase in the peak fuel temperature in the EOL plate (up to 199.4 °C from 196.8 °C in the Base Case).

TABLE 13-11
PEAK REACTOR POWER AND PEAK FUEL TEMPERATURE FOR 0.6% $\Delta K/K$ STEP
INSERTION OF REACTIVITY IN HEU REFERENCE CORE

Initial Conditions			
Power _{ss} (MW)		11.5	
T _{inlet} (°F)		155	
Flow (gpm)		3200	
P _{pressurizer} (psia)		75	
Pressurizer level (in)		-16	
Results of Accident Analysis		Reactor Power, MW	Peak Fuel Temperature, °C (Plate)
Base Case		38.08	221.3 (BOL)
Branch02	Increase oxide layer thickness by 18%	38.15	223.3 (MOL)
Branch03b	No coolant channel restriction with burnup	38.36	225.9 (MOL)
Branch04f	Pressurizer pressure = 90 psia; Pressurizer level = +4 inches	38.07	227.3 (BOL)
Branch05	Mode II LSSS Operating Conditions	20.63	202.6 (BOL)
Branch06b	t _{insertion} = 0.1 s	34.86	218.8 (BOL)

In the Base Case, the coolant channel restriction at EOL due to irradiation effects was set at the MURR acceptance criteria of ≤ 10 mil. In the Branch03b case it was assumed that coolant channels remain at their nominal gap (i.e., there is no channel restriction with burnup). Under these conditions, the peak power is 0.28 MW higher relative to the Base Case. The peak fuel temperature reached in the BOL and MOL plates during the accident increase by 1.7 °C and 5.0 °C,

respectively. Without the reduction of the coolant channel gap from burnup-related effects, the EOL channel receives a greater fraction of the coolant flow rate than in the Base Case, so that the temperature increase of the EOL plate in this branch case is only 1.1 °C.

Branch04f was evaluated to assess the impact of the coolant pressure on the accident consequences. In this branch case, the pressurizer pressure is increased from the Base Case value of 75 psia with a pressurizer water level of -16 inches, which corresponds to the LSSS condition of low pressure for the primary system. For this branch case, the pressurizer pressure was assumed to be 90 psia and a pressurizer water level at the upper end of +4 inches. This value was set as a conservative upper limit for the pressurizer based on HEU and LEU cores over the range of interest including LSSS conditions. Consequently, the pressure in this branch case is well above the pressure at the high-end of the normal operating band for MURR. Increasing the pressurizer pressure to this maximum value causes a negligible 0.01 MW decrease in the peak power, but a 6.0 °C increase in the predicted peak fuel temperature during the accident (227.3 °C versus 221.3 °C for the Base Case). This behavior was not expected (decreased power but increased fuel temperature) and warranted further investigation.

Under steady-state conditions, the coolant in the peak channel remains sub-cooled throughout the accident. Under the conditions of the Base Case in the 0.6% $\Delta k/k$ step reactivity insertion accident, there is some nucleate boiling in the peak coolant channel that occurs briefly during the power excursion. Nucleate boiling of this sort in the coolant channel has a beneficial effect because it increases the heat transfer coefficient from the fuel plate surface to the coolant, which, in turn, reduces the peak fuel temperature resulting from the reactivity insertion accident. However, when the coolant pressure is increased in the Branch04f case, this increases the saturation temperature of the coolant so that there is a lesser amount of nucleate boiling in the coolant channel that takes place during the accident. This, in turn, effectively reduces the heat transfer from the fuel plate surface to the coolant.

Figure 13.2 illustrates this effect by presenting results for an LEU reference core for the heat transfer coefficient in the peak MOL fuel plate channel calculated by PARET/ANL at the time near when the fuel reaches its peak temperature. The behavior for the HEU reference core is similar. The peak heat flux and peak fuel temperature in this case occurs in axial node 10. It can be seen that the plate-to-coolant heat transfer coefficient increases significantly in this axial range. This is due to the nucleate boiling that occurs in the coolant channel. However, the increase in the heat transfer coefficient is not as much in the Branch04f case because the higher coolant pressure results in a higher coolant saturation temperature, so that there is less nucleate boiling in the coolant channel. Consequently, since the heat transfer coefficient at the location of the peak heat flux is smaller in Branch04f relative to the Base Case, there is a corresponding increase in the predicted peak fuel temperature during the accident under these conditions.

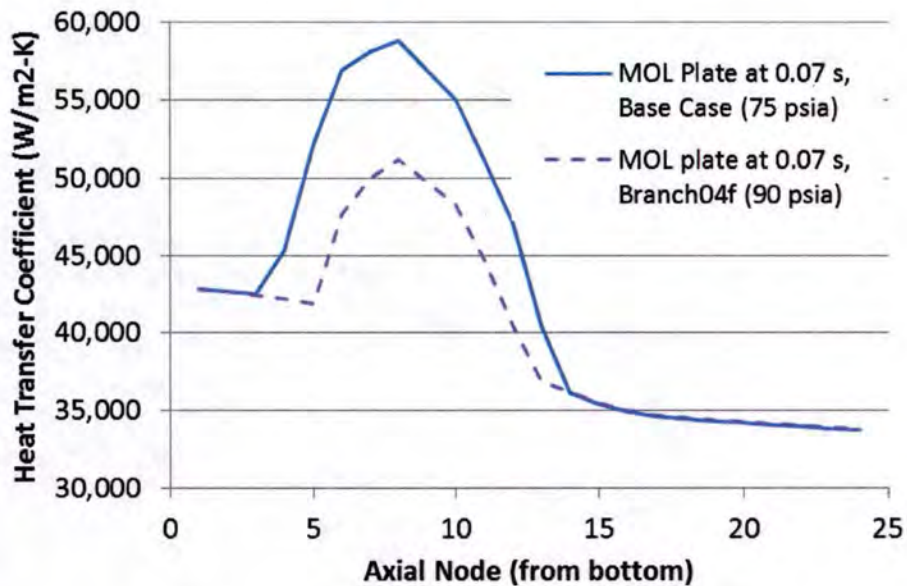


FIGURE 13.2
HEAT TRANSFER COEFFICIENT FROM MOL PLATE SURFACE TO PRIMARY COOLANT CHANNEL 70 MS AFTER 0.6% $\Delta k/k$ STEP REACTIVITY INSERTION IN LEU REFERENCE CORE INITIATED FROM LSSS CONDITIONS ON TEMPERATURE AND FLOW RATE

In Branch05, the steady-state conditions in the analysis were set to the LSSS coolant inlet temperature and coolant flow rate for Mode II operations of MURR. Under these conditions, the coolant inlet temperature is 155 °F (68.3 °C) just as in the Base Case, but the core coolant flow rate (single coolant pump in operation) is reduced to 1,600 gpm and the total steady-state reactor power is 5.75 MW. In this case, the peak transient power is only 20.63 MW and the peak fuel temperature reached during the transient is 202.6 °C. The predicted peak fuel temperature from the 0.6% $\Delta k/k$ RIA is nearly 20 °C lower in this case compared with the Base Case for Mode I (full-power) operations.

The last branch case evaluated the impact of the insertion time for the 0.6% $\Delta k/k$ reactivity in the accident. The time needed to eject the unsecured experiments from the core was conservatively set to 10 μ s in the Base Case. In the Branch06b case, the ejection time was increased to 0.1 seconds, which is a more realistic time for the ejection of the unsecured experiments. This adjustment decreased the peak power reached during the accident by more than 3 MW and the peak fuel temperature reached during the transient is 2.5 °C lower compared to the Base Case.

Table 13-12 summarizes the peak fuel temperatures predicted for the BOL, MOL, and EOL plates following the 0.6% $\Delta k/k$ step RIA in the reference HEU core operating at initial conditions corresponding to most extreme license conditions. The peak UAl_x fuel temperature calculated among all the cases considered is 227.3 °C in a fresh fuel plate. For the MOL and EOL fuel plates, the peak predicted UAl_x temperatures among all the cases are 225.9 °C and 199.4 °C, respectively.

Among all of the cases considered, the peak UAI_x fuel temperature was 227.3 °C for the 0.6% $\Delta k/k$ step RIA in the reference HEU core initiated from the LCO for reactor power, the LSSS for coolant inlet temperature and primary coolant flow rate, and a primary system pressure that is above the maximum pressure of the normal operating band in MURR.

Analysis presented in the SAR showed that in the HEU core the 0.6% $\Delta k/k$ step reactivity insertion accident is the most limiting in terms of peak fresh fuel temperature reached during the accident. In analysis performed here, modeling enhancements were made to improve the accuracy of the PARET/ANL predictions relative to the SAR analysis. For example, depleted MOL and EOL plates were included in the PARET/ANL model, as well as improvements to the heat source description that removes unnecessary conservatisms and more accurately reflects the heat conduction from the fuel plates into the hottest coolant channels in the core. Even when depleted MOL and EOL plates are included in the PARET/ANL analysis for mixed-burnup reference core, the peak HEU fuel temperature still occurs in the fresh, BOL plate. For an accidental step insertion of 0.6% $\Delta k/k$ in the HEU core (0.77\$ inserted), the peak HEU temperature is well below the fuel and cladding temperature limit of 530 °C specified in Reference 13.8. Reference 13.8 appears to be making a determination based on the analysis of fresh fuel, since the lower bound of the 95% confidence interval (-2σ) blister threshold temperature for UAI_x at all burnups relevant to MURR is 482 °C (Ref. 13.6). For the MURR analysis presented here, the peak HEU temperature is below both of these temperatures.

TABLE 13-12
PEAK FUEL TEMPERATURE (°C) FOR 0.6% $\Delta K/K$ STEP INSERTION OF REACTIVITY
IN HEU REFERENCE CORE OPERATING AT THE MOST EXTREME LICENSE
CONDITIONS

	Plate	BOL	MOL	EOL
Base Case		221.3	220.9	196.8
Branch02	Increase oxide layer thickness by 18%	221.5	223.3	199.4
Branch03b	No coolant channel restriction with burnup	223.0	225.9	197.9
Branch04f	Pressurizer pressure = 90 psia; Pressurizer level = +4 inches	227.3	220.9	196.7
Branch05	Mode II LSSS Operating Conditions	202.6	193.8	172.2
Branch06b	$t_{insertion} = 0.1$ s	218.8	217.6	194.1

13.2.2.4.2 LEU Core Step Reactivity Insertion Accident Results

Results for the 0.6% $\Delta k/k$ step RIA in a reference core loaded with LEU fuel are presented in Table 13-13. The reference core selected for this analysis (Core 7A) has eight elements with a mixture of burnups, which are typical for MURR operations. The loading of experiments in the center flux trap and reflector are also typical for MURR operations. Results are presented for the accident initiated from the initial conditions specified in Table 13-5. It is conservatively assumed that the bank of four control blades is inserted at the scram from the fully withdrawn position (26 inches withdrawn). The reference core selected for this analysis (Core 7A) has eight elements with a mixture of burnups, which are typical for MURR operations. The loading of experiments in the center flux trap and reflector are the same as assumed in the HEU reference core and are typical for MURR operations. Results are presented for the accident initiated from the license extreme initial conditions summarized in Table 13-5.

The step insertion of 0.6% $\Delta k/k$ reactivity in the critical, steady-state core results in a sharp reactor power rise from the LCO power (115% of full licensed power) of 13.8 MW to 46.7 MW before the transient is curtailed by negative reactivity feedback effects from changes in the fuel temperature and coolant conditions (density and temperature). The transient is terminated by reactor scram at 0.151 seconds after the reactivity insertion. The predicted maximum steady-state LEU fuel temperature is in an EOL plate at 167.5 °C, and reaches a peak of 289.4 °C in the accident. The steady-state heat flux profile for this plate normalized to a core power of 12 MW is provided in Figure 4.34. As described in Section 13.2.2.2 above, the effect of the uneven heat conduction between the two radial surfaces of the LEU fuel plate and the fission energy deposited outside the primary coolant system were taken into account in the analysis. The peak fuel temperatures in the MOL and BOL fuel plates are 289.2 and 256.7 °C, respectively.

Figure 13.3 plots the time-dependent results for the 0.6% $\Delta k/k$ step reactivity insertion accident in Core 7A. The assumed steady-state reactor power at the start of the accident is 13.8 MW and the overpower trip setting of 15 MW is reached at just 0.6 milliseconds after the start of the transient. This is followed by a 150-millisecond delay before the reactor scram occurs. Prior to the reactor scram which will shut down the reactor and terminate the accident, the reactor reaches a peak power of 46.7 MW at 0.040 seconds after the reactivity insertion. This power burst is then curtailed due to inherent reactivity feedback effects. The maximum fuel meat temperature in the fuel plates increases due to the energy generated by the transient, reaching a peak temperature in the BOL plate at 52 milliseconds after the start of the accident, and at 69 milliseconds and 79 milliseconds in the MOL and EOL plates, respectively, before heat conduction from the fuel meat to the surrounding clad and coolant decreases the fuel temperature. The time to reach the peak temperature is longer for the burned plates because the lower thermal conductivity and oxide layer for these plates relative to the unirradiated fuel plate inhibits heat conduction.

TABLE 13-13
 PEAK REACTOR POWER AND PEAK FUEL TEMPERATURE
 FOR 0.6% $\Delta K/K$ STEP INSERTION OF REACTIVITY IN LEU REFERENCE CORE

Initial Conditions			
Power _{ss} (MW)		13.8	
T _{inlet} (°F)		145	
Flow (gpm)		3300	
P _{pressurizer} (psia)		75	
Pressurizer level (in)		-16	
Results of Accident Analysis		Reactor Power, MW	Peak Fuel Temperature, °C (Plate)
Base Case		46.69	289.4 (EOL)
Branch01	Thermal Conductivity Decrease K_{U10-Mo} by 20%	46.68	297.9 (MOL)
Branch02	Increase oxide layer thickness by 23%	46.77	297.4 (EOL)
Branch03b	No coolant channel restriction with burnup	46.84	290.9 (MOL)
Branch04f	Pressurizer pressure = 90 psia; Pressurizer level = +4 inches	46.68	293.8 (MOL)
Branch05	Mode II LSSS Operating Conditions	25.41	241.1 (MOL)
Branch06b	t _{insertion} = 0.1 s	41.47	285.2 (EOL)

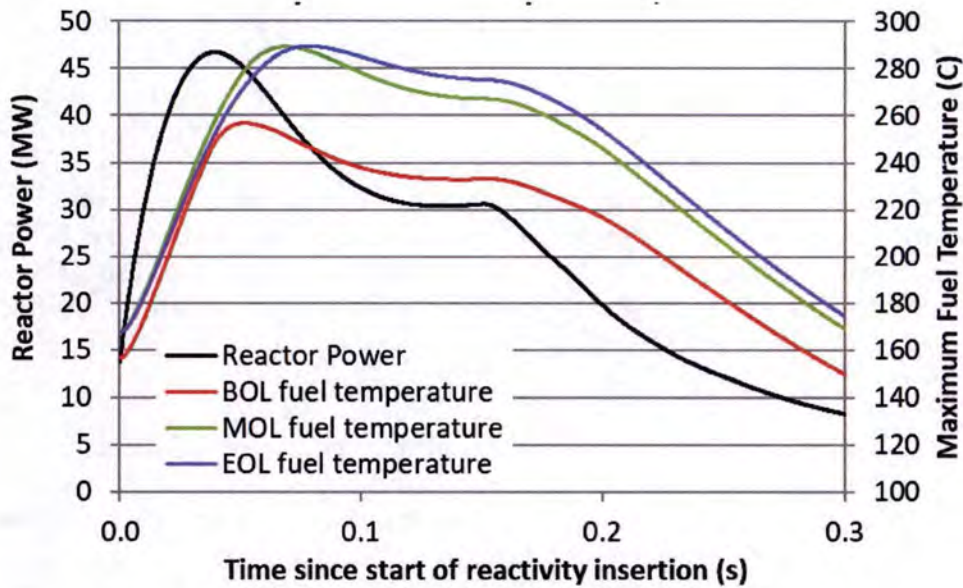


FIGURE 13.3
 REACTOR POWER AND MAXIMUM FUEL TEMPERATURES
 FOR 0.6% $\Delta K/K$ STEP REACTIVITY INSERTION IN LEU CORE 7A

The delay time of 150 milliseconds from the time that the scram signal is sent to the start of the blade drop is the same as used in References 13.1 and 13.16 for the previous RIA analyses. A shorter time of 75 milliseconds is used for the LOCA and LOFA analyses in Sections 13.2.3 and 13.2.4 respectively, based on improved measurements of the safety system trip functions timing performed at MURR in May and June of 2014. The longer delay time of 150 milliseconds will yield more conservative results for the accident analysis and was retained for the modeling of the RIAs in the current work.

Several branch cases were run to estimate the effect of potential non-conservative variations of the thermo-physical properties or core operating conditions on the severity of the accident. In the Branch01 case, the thermal conductivity of the U-10Mo was reduced by 20% from that used in the Base Case. This takes into account the experimental uncertainty in the U-10Mo thermal conductivity measurements conducted in Reference 13.17. The predicted peak reactor power from the reactivity insertion is negligibly decreased by this modeling change. However, the predicted peak fuel temperatures are higher because of the lower thermal conductivity. The peak fuel temperatures in the MOL and EOL fuel plates are 297.9 °C and 297.7 °C, respectively, which is an increase of about 8.5 °C relative to the Base Case.

In the Branch02 case, the oxide layer thickness on the MOL and EOL plates was increased by 23% relative to the Base Case to account for the impact of core operating conditions on the oxide thickness. An oxide layer thickness of 0.93 mil on the concave surface of an EOL plate in the plate 23 position had previously been estimated from a modified Griess correlation (Ref. 13.14) based on fuel elements in a core operating at nominal conditions. If the MURR consistently operated at

the limits of the normal operating band, the oxide layer thickness on the fuel plates is estimated to be 1.14 mil on the concave surface of the EOL plate in the plate 23 position (23% thicker). While there is only a 0.08 MW increase in the peak reactor power relative to the Base Case, the increased oxide thickness results in a 8.0 °C increase in the peak fuel temperature in the limiting EOL plate.

In the Base Case, the coolant channel restriction at EOL due to irradiation effects was set at the anticipated MURR acceptance criteria for LEU elements of ≤ 8 mil. In the Branch03b case it was assumed that coolant channels remain at their nominal gap (i.e., there is no channel restriction with burnup). Under these conditions, the peak power is 0.15 MW higher relative to the Base Case and the peak fuel temperature reached in the limiting plate during the accident is 1.5 °C higher, occurring in an MOL plate.

The background for the Branch04f case to assess the impact of variations in the coolant pressure on the accident consequences was described above in Section 13.2.2.4.1. As for the HEU fuel, setting the coolant pressure above the normal operating band has a negligible effect on the peak reactor power. However, when the coolant pressure in the LEU core was increased the peak fuel temperatures in the BOL, MOL, and EOL fuel plates increased by 6.8, 4.6, and 2.9 °C, respectively, relative to the Base Case. At the higher pressure, the saturation temperature of the coolant increases so that there is less nucleate boiling in the coolant channels adjacent to the peak plates during the accident. Thus, there is less heat transfer from the fuel plate to the bulk coolant, and the fuel temperatures are higher.

In Branch05, the effect of the 0.6% $\Delta k/k$ step reactivity insertion in the MURR in Mode II operations was evaluated. The steady-state conditions in the analysis were set to the Mode II LSSS coolant inlet temperature and coolant flow rate. Under these conditions, the coolant inlet temperature is 145 °F (62.8 °C), and the core coolant flow rate (single coolant loop) is 1,650 gpm. The LCO steady-state reactor power is 6.9 MW (115% of 6 MW) and the overpower trip setting is 7.5 MW (125% of 6 MW). In this case, the peak transient power is only 25.41 MW and the peak fuel temperature reached during the transient is 241.1 °C in the MOL fuel plate. The predicted peak fuel temperature from the 0.6% $\Delta k/k$ RIA is nearly 50 °C lower in this case compared with the Base Case for Mode I (full-power) operations.

The last branch case evaluated the impact of the insertion time for the reactivity in the accident analysis. The 0.6% $\Delta k/k$ reactivity inserted in this accident represents the TS limit on the total positive worth of all experiments in the center flux trap (CFT). Therefore, the accident postulates the ejection of the experiments in the CFT, which may be distributed along the 24-inch axial length of the fuel in the core. The 10 microsecond ejection time in the MURR SAR analysis (Ref. 13.1) represents an extremely rapid time frame for this to occur. Assuming the experiments travel the entire fuel length of 24 inches in 10 microseconds, the average velocity of the experiment ejection is 200,000 feet/second. In Branch06b, the reactivity insertion time in the model was increased from 10 microseconds to 0.1 seconds, which would be consistent with an average ejection speed of 20 fps. The longer insertion time decreases the peak accident power by more than 5 MW before the transient is curtailed by the negative reactivity feedbacks. The peak fuel temperature is 4.2 °C lower relative to the Base Case.

TABLE 13-14
PEAK FUEL TEMPERATURE (°C) FOR 0.6% ΔK/K STEP INSERTION OF REACTIVITY
IN LEU REFERENCE CORE OPERATING AT THE MOST EXTREME LICENSE
CONDITIONS

	Plate	BOL	MOL	EOL
Base Case		256.7	289.2	289.4
Branch01	Thermal Conductivity Decrease κ_{U10-Mo} by 20%	265.2	297.9	297.7
Branch02	Increase oxide layer thickness by 23%	256.9	296.0	297.4
Branch03b	No coolant channel restriction with burnup	257.5	290.9	290.6
Branch04f	Pressurizer pressure = 90 psia; Pressurizer level = +4 inches	263.5	293.8	292.3
Branch05	Mode II LSSS Operating Conditions	224.9	241.1	239.5
Branch06b	$t_{insertion} = 0.1$ s	250.1	283.5	285.2

Table 13-14 summarizes the peak fuel temperatures predicted for the BOL, MOL, and EOL plates in the reference LEU core operating at the more challenging initial conditions following the 0.6% Δk/k step RIA for all cases. Among all the branch cases considered, the peak calculated U-10Mo fuel temperature is 297.9 °C in an MOL fuel plate. For the BOL and EOL fuel plates, the peak predicted UAl_x temperatures among all the cases are 265.2 °C and 297.7 °C, respectively. It is noted that these peak temperatures all occur for the Branch01 case in which the fuel thermal conductivity was set below the burnup-dependent best-estimate value based on measurement uncertainties.

For the LEU MURR core Base Case, the peak fuel temperatures as a result of the 0.6% Δk/k step reactivity insertion were calculated to be 257 °C in plate number-23 of a BOL element and 289 °C in plate number-23 of the MOL and EOL elements. Preliminary blister temperature data for irradiated U-Mo monolithic were used to formulate fuel temperature safety limits that are burnup dependent and specific to MURR fission densities. A formulation of the fuel temperature safety limit as a function of peak fission density is provided in Equation 13-1, above. The safety limit is 450 °C for plate number-23 in the BOL and MOL fuel elements, and 398 °C for plate number-23 in the EOL element. Therefore, the margins to the safety limits are calculated to be 193 °C, 152 °C, and 109 °C for the BOL, MOL, and EOL fuel elements, respectively. Based on these preliminary measurement data for the U-Mo fuel blister temperature, there is significant margin between the safety limit and the peak fuel temperature calculated in the most limiting LEU reactivity insertion accident.

Plate number-23 in BOL, MOL, and EOL elements was modeled in the step reactivity insertion accident analysis. Among the 23 fuel plates in the LEU element, this plate was selected because it was judged prior to the accident analysis to have the smallest margin to the fuel temperature safety limit. This judgment was based on 1) plate number-23 has the highest heat flux among the plates in the LEU element throughout its life (as can be seen in Figure 13.4) and 2) the high discharge burnup in plate number-23 relative to the other plates in the element results in a lower thermal conductivity for the U-10Mo. It should be noted that the heat flux values plotted in Figure 13.4 are based on the reactor operating at the full-licensed power of 12 MW with all heat from fission deposited in the fuel meat (i.e., fraction of heat deposited outside the core is neglected) and assuming that there is an equal power split for the heat from the fuel meat conducting out the concave and convex sides of the fuel plate. Even so, this data illustrates the relative heat flux among the plates in the LEU element at different stages of the element lifetime. Both the thermal conductivity of the U-10Mo and the fuel temperature safety limit decrease as the fuel burnup increases. Plate number-1 and -2 each have a higher U-10Mo burnup at EOL than plate number-23 (3.4×10^{21} fissions/cm³ in plate number-1 and 2.8×10^{21} fissions/cm³ in plate number-2, compared with 2.6×10^{21} fissions/cm³ in plate number-23), but it can be seen from Figure 13.4 that throughout the life of the element the local heat flux for each of these two plates is substantially lower than that of plate number-23.

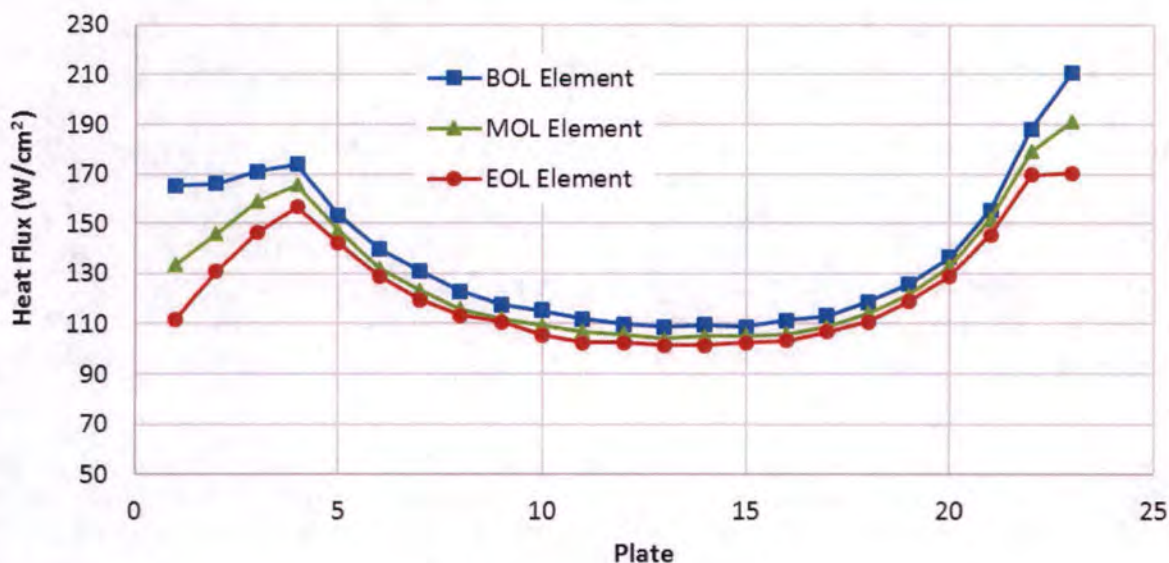


FIGURE 13.4
PEAK LOCAL HEAT FLUX CALCULATED BY MCNP5 FOR PLATES IN BOL, MOL,
AND EOL ELEMENT IN LEU REFERENCE CORE OPERATING AT 12 MW

To confirm that plate number-23 does have the smallest margin to the safety limit, additional plates that could potentially be more limiting were modeled for the 0.6% $\Delta k/k$ step reactivity insertion accident. Results are presented in Table 13-15. Plate number-1 was selected because it has the highest discharge burnup of all plates, and so the lowest U-10Mo thermal conductivity relative to

other plates and the smallest safety limit. Plate number-4 was selected because it has the highest heat flux among the plates near the center flux trap and also has a full-thickness fuel meat (20 mils). Plate number-22 was selected because the heat flux on this plate calculated by MCNP5 is the second highest among the plates in the element (plate number-23 being the highest) and also because plate number-22 has a full-thickness meat (20 mil).

TABLE 13-15
RESULTS FOR SELECTED PLATES IN 0.6% $\Delta K/K$ STEP REACTIVITY INSERTION
ACCIDENT IN LEU REFERENCE CORE OPERATING AT THE MOST EXTREME
LICENSE CONDITIONS

Plate	BOL				EOL			
	1	4	22	23	1	4	22	23
Meat thickness (mil)	9	20	20	17	9	20	20	17
Peak Local Burnup (fissions/cm ³)	0	0	0	0	3.4E+21	1.8E+21	2.1E+21	2.6E+21
U-10Mo Thermal Conductivity Relative to Fresh Fuel	1.0	1.0	1.0	1.0	0.57	0.72	0.70	0.65
Oxide Layer Thickness on Plate Surface (mil)	0	0	0	0	0.93	1.07	0.94	0.93
Plate Heat Flux Conducted into Coolant Channel at Steady-State (W/cm ²)	177.0	192.7	208.4	225.9	119.7	173.7	188.2	182.7
Peak Fuel Temperature (°C)	227	246	252	257	216	290	299	289
Fuel Temperature Safety Limit (°C)	450	450	450	450	378	426	417	398
Margin to Safety Limit (°C)	223	204	198	193	162	136	118	109

The U-10Mo thermal conductivity for the EOL plates was calculated based on the peak fuel burnup for each plate using the formulation described in Section 2.2.1 of Reference 13.4. The thickness of the oxide layer on the plate surface was calculated based on the plate surface temperature and using a version of the Griess correlation, which was modified to take into account the specific operating conditions of the MURR. For plate number-23 at EOL, an oxide thickness of 0.93 mil was previously calculated. At steady-state conditions, the plate surface temperature for plate

number-1 is lower than that of plate number-23, so 0.93 mil was used as a conservative value. The peak plate surface temperatures for plate number-4 and -22 are approximately 4.5 °C and 0.5 °C higher than the surface temperature of plate 23. Using the modified Griess correlation, the oxide layer thicknesses on plate number-4 and -22 at EOL were calculated to be 1.07 mil and 0.94 mil, respectively. The peak heat flux for each plate conducted into the coolant channel in the PARET/ANL model was calculated assuming that the core is operating at a steady-state power of 115% of the full licensed power (13.8 MW), and with 3.6% of the heat deposited outside of the core (Ref. 13.18). Additionally, a larger fraction of the heat generated in plate number-1 and -23 will conduct to the concave or convex surfaces of the fuel plate, respectively, due to the wider, one-sided heated coolant channel adjacent to that plate surface. For plate number-4 and -22, it was conservatively assumed that there is equal heat conduction to each coolant channel surrounding the fuel plate. At BOL, plate number-23 has the highest heat flux conducted into the coolant channel in the PARET/ANL model, but it is observed that at EOL the heat flux conducted into the coolant channel is 3% higher for plate number-22 than for plate number-23.

For the BOL element in the reference core, the peak fuel temperature following the step reactivity insertion of 0.6% $\Delta k/k$ is highest for plate number-23, 257 °C. The margin to the fuel temperature safety limit for this plate is 193 °C. For the EOL element, it can be seen that following the step reactivity insertion, plate number-4 has a peak fuel temperature that is slightly higher than that calculated for plate number-23 (290 °C versus 289 °C). Although the heat flux from plate number-4 is 5% lower than plate number-23 and the thermal conductivity is 10% higher than plate number-23, the thicker fuel meat and thicker oxide layer in plate number-4 result in a slightly higher fuel centerline temperature. The calculated peak fuel temperature for plate number-22 is 10 °C higher than plate number-23 following the step reactivity insertion accident. This is because of the higher heat flux and thicker fuel meat. However, the higher burnup of plate number-23 results in a lower fuel temperature safety limit relative to plate number-22. Consequently, the margin to the safety limit is shown to be the smallest for plate number-23 among all plates and burnup states in the reference core following the 0.6% $\Delta k/k$ step reactivity insertion accident.

Lastly, the effects of smaller step reactivity insertion accidents of 0.25% $\Delta k/k$ and 0.10% $\Delta k/k$, representing the MURR TS limits for the maximum worth of a single unsecured and moveable experiment, respectively, were also evaluated. The results for the peak fuel temperature are summarized in Table 13-16. The peak fuel temperature from the 0.25% $\Delta k/k$ and 0.10% $\Delta k/k$ step insertion accidents are much lower than that from the 0.6% $\Delta k/k$ RIA.

TABLE 13-16
PEAK FUEL TEMPERATURE FOR 0.25% $\Delta K/K$ AND 0.10% $\Delta K/K$ STEP REACTIVITY
INSERTIONS IN LEU REFERENCE CORE AT THE MOST EXTREME LICENSE
CONDITIONS

Reactivity Inserted	Peak Fuel Temperature
0.60% $\Delta k/k$	289.4 °C (EOL Plate)
0.25% $\Delta k/k$	204.8 °C (MOL Plate)
0.10% $\Delta k/k$	182.7 °C (MOL Plate)

13.2.2.4.3 LEU Core Blade Withdrawal Accident

The second class of reactivity accidents analyzed to assess the impact of fuel conversion is a ramp reactivity insertion accident resulting from continuous control blade withdrawal initiated from the reactor operating at steady-state. Even though the reactivity addition resulting from the simultaneous withdrawal of all four shim control blades follows the typical differential rod worth curve behavior (with reduced worths at the beginning and end of blade withdrawal, as shown in Figure 4.7), it was conservatively assumed that the maximum value for reactivity addition from control blade withdrawal allowed by the MURR TSs occurs during the analysis of this accident. It was also previously found that the maximum rate of reactivity addition from blade withdrawal in the LEU core is less than the TS requirement. Thus, a conservative positive ramp reactivity insertion at the rate of 0.03% $\Delta k/k$ /second in the LEU core was considered.

Table 13-17 summarizes the results of the analysis of this accident scenario in the reference mixed-burnup core loaded with LEU fuel. The blade withdrawal accident is initiated from the same steady-state conditions as the step reactivity insertion accident assumed in Section 13.2.2.4.2, above. In the Base Case, the overpower trip setting of 15 MW is reached 2.20 seconds after the beginning of blade withdrawal, followed by a scram at 2.35 seconds that terminates the accident and safely shuts down the reactor. The peak power reached during the blade withdrawal accident is 15.10 MW, and the peak fuel temperature in the Base Case is predicted to be 176.6 °C and occurs in the MOL plate. This is just 8.8 °C above the maximum fuel temperature in the plate of 167.8 °C at steady-state, compared with a 121.9 °C fuel temperature rise for the peak plate in the 0.6% $\Delta k/k$ step reactivity insertion accident.

In addition to the Base Case, a series of branch cases were also run to assess the impact of potential non-conservative variations on thermo-physical properties and reactor operating parameters. All cases predict essentially the same peak reactor power for the blade withdrawal accident (about 15.1 MW), with the exception of the Branch05 case for the reactor operating in Mode II conditions at 115% of half-nominal power (the LCO setting). The reason for this is that the reactivity feedback effects do not introduce enough negative reactivity to curtail the transient prior to the scram, so that the reactor power steadily increases until the time of reactor scram. The cases Branch01, Branch02, Branch03b, and Branch05 for the blade withdrawal accident all show similar behavior for the peak fuel temperature relative to the Base Case as seen for the 0.6% $\Delta k/k$ step insertion accident. See Section 13.2.2.4.1 for explanations of these behaviors. Unlike the step reactivity insertion accident, increasing the coolant pressure (Branch04f case) has no effect on the peak fuel temperature predicted for the blade withdrawal accident. This is because the mild accident conditions of the blade withdrawal accident do not result in any nucleate boiling in the peak coolant channels.

In Branch07, the simultaneous withdrawal of the regulating blade along with the four shim blades was evaluated. This is an unlikely accident scenario. Simultaneously withdrawing the regulating blade with any of the shim blades is prohibited by administrative procedure at MURR. Additionally, inadvertently performing this type of control system withdrawal is highly unlikely, as the two blade types are controlled by separate switches. Nonetheless, this accident scenario was analyzed and was found to have a negligible effect on the predicted peak fuel temperature.

In all cases, the peak fuel temperature occurs in either an MOL or EOL plate. However, the temperatures are substantially lower than for the step insertion accident, and well below the U-10Mo fuel temperature safety limit.

TABLE 13-17
PEAK REACTOR POWER AND PEAK FUEL TEMPERATURE FOR BLADE
WITHDRAWAL ACCIDENT IN LEU REFERENCE CORE

Initial Conditions			
Power _{ss} (MW)			13.8
T _{inlet} (°F)			145
Flow (gpm)			3,300
P _{pressurizer} (psia)			75
Pressurizer level (in)			-16
		Reactor Power, MW	Peak Fuel Temperature, °C (Plate)
Base Case		15.10	176.6 (MOL)
Branch01	Thermal Conductivity Decrease κ_{U10-Mo} by 20%	15.11	180.5 (MOL)
Branch02	Increase oxide layer thickness by 23%	15.11	180.9 (EOL)
Branch03b	No coolant channel restriction with burnup	15.10	178.5 (MOL)
Branch04f	Pressurizer pressure = 90 psia; Pressurizer level = +4 inches	15.10	176.6 (MOL)
Branch05	Mode II LSSS Operating Conditions	7.52	149.6 (MOL)
Branch07	Withdraw Reg. blade simultaneous with Shim blades for first 24 seconds	15.13	176.6 (MOL)

13.2.2.4.4 LEU Core Startup Accident

A second type of ramp reactivity insertion accident that has the potential for creating conditions that can lead to core damage is the startup accident. Typical reactor startups are very controlled activities with the control blade withdrawal done in small incremental steps. Also, blade withdrawal is stopped at predetermined control blade heights prior to reaching the critical control blade position. This is done to take measurements of core multiplication data and predicting the next step in the control blade withdrawal sequence in the approach to critical.

The startup accident postulates that all the control blades are withdrawn simultaneously (in gang) until the reactor passes through the critical state without any automatic or manual (operator) action to halt the uncontrolled blade withdrawal. Once the reactor passes through the critical state, the power increase is very rapid during such a transient. Furthermore, since the power level and temperatures remain extremely low during the majority of the transient, no major reactivity feedback mechanisms exist to affect the reactor response to the transient, except for during the very end of the transient. Thus, the entire reactivity effect seen by the core is due to the withdrawal of the control blades in the startup accident.

A positive ramp reactivity insertion at the rate of $0.03\% \Delta K/K / \text{sec}$, corresponding to the MURR TS limit on the maximum rate of reactivity insertion for all four shim control blades operating simultaneously, was introduced, starting with a subcritical power level of 1.0 w and a shutdown reactivity value of $-4.2\% \Delta K/K$ (this corresponds to -5.49% for the reference LEU core). The coolant inlet temperature, flow rate, and pressure are assumed to be the same as in the other accident analyses (see Table 13-5). In the analysis of this accident, no automatic or manual reactor scram is assumed to occur. Branch cases such as those evaluated for the other accident scenarios were also executed. Furthermore, a case with the reactor operating in natural circulation mode, which is unique to the startup accident, was also executed. The fuel loading corresponding to a typical mixed-burnup core (reference core 7A) was assumed for the startup accident analyses, with the exception of the branch case for natural circulation conditions which used all-fresh fuel that will be loaded during startup physics testing. The results for all cases are summarized in Table 13-18. The predicted reactor power and peak fuel temperature are reported at 150 seconds after the start of the blade withdrawal, unless otherwise noted.

TABLE 13-18
PEAK REACTOR POWER AND PEAK FUEL TEMPERATURE
FOR STARTUP ACCIDENT IN LEU REFERENCE CORE

Initial Conditions			
Power _{ss} (W)		1.0	
T _{inlet} (°F)		145	
Flow (gpm)		3300	
P _{pressurizer} (psia)		75	
Pressurizer level (in)		-16	
		Reactor Power at 150 seconds, W	Peak Fuel Temperature, °C (Plate)
Base Case		11.65	62.8 (ALL)
Branch01	Thermal Conductivity Decrease K_{U10-Mo} by 20%	11.65	62.8 (ALL)
Branch02	Increase oxide layer thickness by 23%	11.65	62.8 (ALL)
Branch03b	No coolant channel restriction with burnup	11.65	62.8 (ALL)
Branch04f	Pressurizer pressure = 90 psia; Pressurizer level = +4 inches	11.65	62.8 (ALL)
Branch05	Mode II LSSS Operating Conditions	11.65	62.8 (ALL)
Branch07	Withdraw Reg. blade simultaneous with Shim blades for first 24 seconds	1.86 kW @ 140 seconds	62.8 (EOL)
Branch08	Natural Circulation: atmospheric pressure, T _{inlet} = 100 °F, Power = 50 kW, period scram, all-fresh core	90.2 kW @ 7.484 seconds	63.8 (BOL)

Throughout the first 150 seconds of the accident, there is no discernable effect on the peak fuel temperature relative to the initial conditions at the start of the accident, which remains essentially the same as the coolant inlet temperature because of the very low power level. For the startup accidents evaluated for the mixed-burnup reference Core 7A, there is no difference in the temperature for the peak BOL, MOL, and EOL plates in the core (thus, the location of the peak fuel temperature in the table is reported as "ALL"). Likewise, all of the branch cases, with the exception of Branch07 and Branch08, have a negligible effect on the predicted reactor power of 11.65 W that is reached 150 seconds into the accident. Since the reactor power level and temperatures remain very low during the majority of the transient, no major reactivity feedback mechanisms exist to affect the response to the transient. No reactor trips were modeled in the startup accident analysis. At 150 seconds after the start of the blade withdrawal, the reactor period is 4.8 seconds. The 8-second minimum reactor period trip would automatically scram the reactor and terminate the accident at about 145 seconds after the start of the blade withdrawal. Modeling this reactor trip would limit the calculated reactor power to less than 6 W.

In Branch07, the startup accident is analyzed with the regulating blade being simultaneously withdrawn with the four shim blades. The TS limit for the reactivity insertion from regulating blade withdrawal is 0.015% $\Delta k/k/s$. For the purpose of this analysis, the reactivity insertion rate from regulating blade withdrawal was assumed to be 0.025% $\Delta k/k/s$, giving a combined reactivity insertion rate of 0.055% $\Delta k/k/s$. The TS limit for the total worth of the regulating blade is 0.6% $\Delta k/k$, so that the reactivity addition from the regulating blade withdrawal will last for only the first 24 seconds (0.6/0.025) of the accident. After this, the TS limit for the shim blade withdrawal of 0.03% $\Delta k/k/s$ was assumed for the remainder of the accident.

The additional reactivity insertion from the uncontrolled withdrawal of the regulating blade along with the shim blades has a significant effect on the reactor power level in the startup accident, as can be seen in Table 13-18 and Figure 13.5. The critical state is reached in Branch07 at 120 seconds, when the reactor power level is 4.2 W and the reactor period is 12.6 seconds. If the shim blades continue to be withdrawn at the TS limit, the calculated reactor power after 140 seconds is 1.86 kW with a reactor period of 0.9 seconds. However, as the results in Table 13-18 show, if the transient is terminated at 140 seconds or earlier (due to the 8-second minimum period trip, for example) the fuel temperature increase from the accident is negligible (less than 0.1 °C).

In Branch08, the startup accident is modeled with the reactor operating at a steady-state, critical power level of 50 kW and cooled by natural circulation. It is envisioned that low-power startup physics testing of the MURR loaded with eight fresh LEU elements and natural circulation cooling will be conducted at the time of reactor conversion. Thus, this accident was analyzed for the initial power distribution in reference Core 5B1. Furthermore, the reactor overpower trip setting of 62.5 kW is assumed to fail (125% of full power for this operating mode), but the minimum reactor period trip setting of 8 seconds was applied in the analysis.

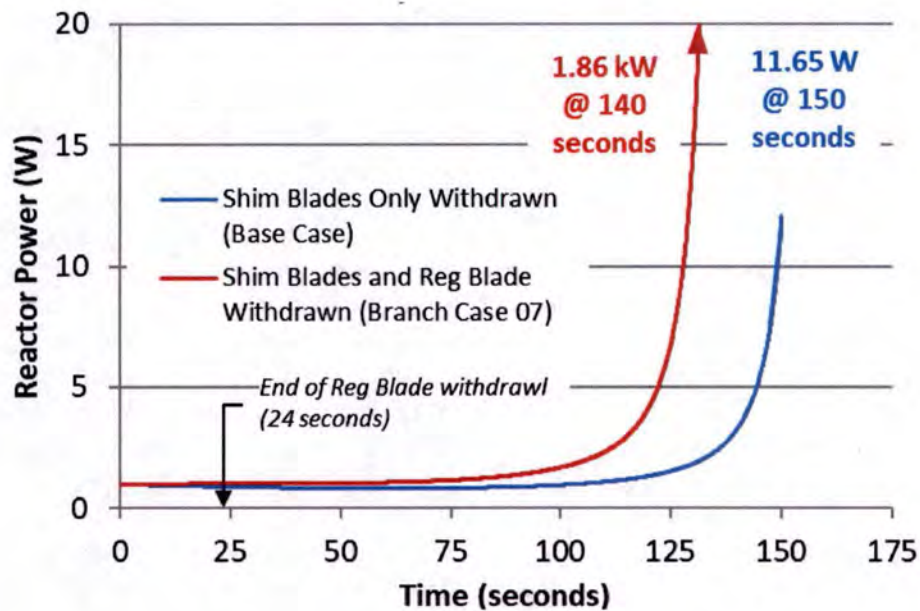


FIGURE 13.5
REACTOR STARTUP ACCIDENT IN LEU CORE 7A

For the natural circulation mode of operation, the reactor pressure vessel head is removed and the blank flange is opened, which is located about 4.5 feet above the inverted loop at the end of the 12-inch diameter primary coolant pipe upward extension. This allows for the lower density heated water in the core to flow up the pressure vessel into the pool, while higher density pool water can be drawn into the open flange and down into the inverted loop. The water will continue to flow down to below the bottom of the core and then flow up the pressure vessel into the core. The flow continues as it started with the heated coolant flowing through the pressure vessel and exiting back into the 20,000-gallon pool. The coolant inlet temperature in this analysis is assumed to be 100 °F, and the pressure at the top of the fuel meat in this case is assumed to be 20 psia (Ref. 13.27).

The PARET/ANL manual recommends performing accident analyses for cores cooled by natural circulation in two steps. First, a steady-state case is run to compute the coolant flow rate through the core due to buoyancy effects (parameter IFLOW=4). This was done and a flow rate that is more than a factor of 100 less than the steady-state flow rate under normal operating conditions was computed. The manual then recommends using this steady-state flow as a constant value in a "forced-flow" calculation in PARET/ANL (IFLOW=1) for analyzing the effects of the transient in the core cooled by natural circulation. This will be conservative, as the coolant flow rate through the core during the transient will naturally increase as the reactor power increases due the blade withdrawal and the coolant temperature rises.

The results of the Branch08 accident analysis are shown in Figure 13.6. In this case, the control blades are assumed to be at the critical position for the core when the blade withdrawal begins rather than the deeply sub-critical state assumed in the other startup accident analyses. From the

steady-state power of 50 kW, the control blade withdrawal results in a gradual increase in the reactor power. The power reaches 62.5 kW at 3.82 seconds, but the reactor is not tripped in the analysis until the 8-second minimum period trip set point is reached at 7.33 seconds after the start of the blade withdrawal. Subsequently, the reactor is safely shut down with a peak power during the accident of 90.2 kW. The maximum fuel temperature in the core increases from 58.7 °C at steady-state in the core operating at 50 kW with natural circulation to a peak of 63.8 °C, a rise of just 5.1 °C.

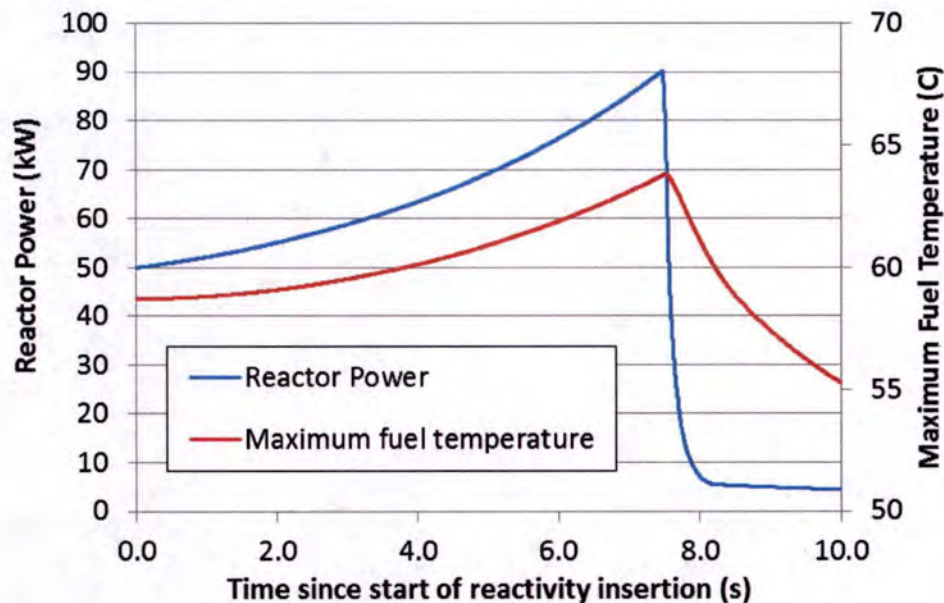


FIGURE 13.6
REACTOR STARTUP ACCIDENT IN LEU CORE 5B1 IN NATURAL CIRCULATION
MODE

Finally, the initial core with all-fresh LEU fuel will contain a mixture of standard fuel elements and transition fuel elements with borated side plates to serve as reactivity hold-down (Ref. 13.19). The presence of the borated side plates will cause a slight reduction in the peak local heat flux in the all-fresh startup core relative to the Core 5B1, which contained only standard elements. Consequently, the results calculated here provide an upper bound on the expected peak fuel temperature for the startup accident in the fresh LEU core.

13.2.2.5 Conclusions

The insertion of excess reactivity in the HEU-fueled and LEU-fueled MURR has been analyzed to assess the impact of a rapid step insertion of positive reactivity and the impact of a continuous control blade withdrawal accident. The accidents were initiated from challenging initial conditions that represent the license extremes for operation.

For the most limiting accident of a 0.6% $\Delta k/k$ step insertion of reactivity the peak HEU UAl_x fuel meat temperature modeled during the reactivity transient was 221 °C (430 °F) in a fresh fuel plate in a reference core that is typical for MURR operations, and 227 °C (441 °F) in various cases with uncertainties. Throughout the accident, the peak fuel temperature in the HEU core remains well below the measured blister threshold temperature for UAl_x fuel.

For the same RIA accident in a reference core loaded with LEU fuel, the estimated peak U-10Mo temperatures were 257 °C (494 °F), 289.2 °C (552.6 °F), and 289.4 °C (553.0 °F) in the limiting plates in fresh, middle-of-life, and end-of-life elements, respectively. In various cases with uncertainties, the peak U-10Mo temperature in the limiting plate rose to 298 °C (568 °F). A fuel temperature safety limit based on preliminary blister measurement data that is burnup-dependent and specific to expected MURR fission densities has been formulated. The peak fuel temperatures in BOL, MOL, and EOL elements in the LEU core remain below the safety limit by at least 109 °C.

The results indicate that fuel conversion to a proposed U-10Mo monolithic fuel will result in no damage to fresh or depleted fuel plates for any of the reactivity insertion accidents postulated for MURR.

13.2.3 Loss of Primary Coolant

13.2.3.1 Accident Initiating Events and Scenarios

Historically, the most serious accident considered in the safety analyses of most reactors is the postulated loss of coolant accident from the primary coolant system, frequently initiated, in theory, by the double-ended rupture in a section of main coolant piping. The use of Engineered Safety Features (ESFs) greatly helps to mitigate the effects of this type of accident; however, the consequences of such an accident should still be considered.

Section 13.2.3, "Loss of Primary Coolant," of Chapter 13, Accident Analyses, of the University of Missouri Research Reactor (MURR) Safety Analysis Report (SAR) Reference 13.1 demonstrates for the HEU core that for all credible Loss of Primary Coolant Accidents (LOCAs) unacceptable consequences to people and the environment would not occur. For the conversion of the MURR core from HEU fuel to LEU fuel it is necessary to provide an analogous demonstration for the LEU core that is to replace the HEU core and to demonstrate adequate safety margins for the LEU core. Also, the performance of the two cores must be compared using consistent modeling assumptions.

A LOCA is an accident in which water (liquid or vapor) is lost from the primary system. Such accidents not only include a rupture of a reactor main inlet or outlet pipe, but also the loss of coolant through the rupture of a valve or smaller pipe in which the amount of coolant lost is relatively small. However, a depressurization accident in which only nitrogen is lost from the pressurizer is not considered to be a LOCA. This accident would be classified as a Loss-Of-primary-coolant Flow Accident (LOFA) because the loss of pressure would initiate a trip of the primary pumps along with a scram. Similarly, a loss of site electric power leading to a primary flow coastdown would also be classified as a LOFA. LOFAs are discussed in Section 13.2.4.

Section C.2 of Appendix C describes the MURR facility and the modeling of it with the RELAP5 code. Figure C.1 of this appendix shows a diagram of the MURR primary system loop. As explained in this appendix and as the figure shows, the reactor pressure vessel is immersed in a large open pool of water. The location modeled for a double-ended rupture of a main coolant pipe to occur is between the pool wall and either isolation valve: V507B (inlet) or V507A (outlet). The double-ended break at each valve is indicated in the figure by a pair of light green arrows. These locations are modeled because they are outside of the pool boundary and the closing of the adjacent isolation valve does not impede the flow of water from the reactor pressure vessel.

A LOCA could also be initiated by a rupture of the diaphragm in either of the two flow control diaphragm valves, valves 540A and 540B. This LOCA happened in the MURR facility on April 12, 2008. The location of this break is indicated in Figure C.1 by a light green arrow and the words "8-inch break" near the V540 valve in the figure, where two parallel paths in the primary loop are combined into a single equivalent path in the model. There is another light green arrow labeled "2" break" next to this arrow. It represents the rupture of the 2-inch line that connects the pressurizer (labeled "Fixed Pressure Source" in the figure) and the main coolant path. All four LOCAs are simulated with the RELAP5/MOD3.3 code Reference 13.3 in an accident analysis report Reference 13.4. In summary the four LOCAs considered are:

1. Cold leg LOCA – double-ended 12-inch diameter break at the core side of primary coolant isolation valve V507B (cold leg isolation valve).
2. Hot leg LOCA – double-ended 12-inch diameter break at the core side of primary coolant isolation valve V507A (hot leg isolation valve).
3. Cold leg LOCA – 8-inch diameter breach in the 8-inch cold-leg piping at one of the two flow control diaphragm valves.
4. Cold leg LOCA – 2-inch diameter breach in the 2-inch cold-leg piping that connects the pressurizer to the 8-inch cold leg piping.

The results presented in Appendix B of the Reference 13.4 report show that by a considerable margin the first LOCA is much more severe in terms of potential for fuel damage than any of the other three. Therefore, this LOCA is considered in some detail in the next subsection.

Table 13-19 provides the sets of initial conditions assumed in the RELAP5 LOCA simulations. These represent full licensed power and the Limiting Safety System Settings (LSSS) values for primary coolant inlet temperature, primary coolant flow rate, primary system pressure, and pool temperature. The pressurizer level is set at the scram set point. The HEU RELAP5 simulation set in the table is the one used in the LOCA and LOFA analyses during the 2015 relicensing of the MURR. See the response to question 6.b provided in the Reference 13.5 response to Request for Additional Information.

TABLE 13-19
INITIAL CONDITIONS ASSUMED IN THE RELAP5 SIMULATIONS

Parameter	HEU	LEU
Reactor Power, MW	10	12
Primary Inlet Temperature, °F	155	145
Primary Coolant Flow, gpm	3200	3300
Primary System Pressure, psig	60.7 ¹	
Pressurizer Level, inches	-16	
Anti-Siphon Tank Pressure, psig	36	
Anti-Siphon Tank Temperature, °F	120	
Pool Temperature, °F	120	

¹ For the analyses this pressure is the assumed nitrogen gas pressure of the pressurizer and the pressurizer water level is as indicated.

13.2.3.2 Accident Analysis and Consequences

The temperature safety limits for HEU and LEU fuel based on blister temperature data are discussed in Section 13.2.2.4, above. These temperature limits will be applied for the LOCA analysis. Furthermore, as discussed in Section B-5.10 of Reference 13.4, the regulatory safety acceptance criteria for LOCAs also require that there is no significant difference in the radiation levels between the uncovered HEU and LEU cores. However, this requirement is not applicable because the MURR LOCAs do not uncover the core and the analysis shows that they leave at least five feet of water above the core.

The fuel management scheme for the HEU core was modeled in a fuel cycle simulation. A reference core was selected from this simulation such that, at the beginning of a cycle, two of the eight fuel elements are fresh with 0 MWd of burnup, two have 65 MWd, two have 81 MWd, and two have 142 MWd. In this scheme, the end-of-life burnup is at 150 MWd. The LEU fuel management scheme is similar. The representative LEU core has two elements each at 0, 77, 96, and 170 MWd and with the end-of-life burnup at 180 MWd. The analysis in Appendix B of Reference 13.4 considered all four burnups for both HEU and LEU cores.

Burnup has the potential to reduce the coolant channel gap thickness in the burned elements due to fuel swelling and/or the formation of an oxide layer on the fuel plate surface. This can redistribute coolant from the more burned elements to the less burned elements. In the RELAP5 simulations, this flow redistribution tends to improve the predicted performance of the fresh pair of elements and degrades the predicted performance of the most burned pair of elements. As explained in Section C.2.2.10 of Appendix C of this report, appropriate channel gap thickness reductions were conservatively considered. For HEU core, where the fresh element is limiting, assuming no flow redistribution is both reasonable and conservative. For the LEU core, a channel

reduction of up to 8 mils was considered. All LEU cases were analyzed with and without channel gap reductions in order to determine the most conservative result. In the HEU analysis performed in Appendix B of Reference 13.4, no channel reduction due to burnup was assumed. In Appendix B of Reference 13.4, the LEU fuel is analyzed both with no channel reduction due to burnup and with the maximum channel reduction due to burnup of 8 mils at 180 MWd and with reductions that are linearly proportional to the MWd for values less than 180 MWd. All of these reductions are for internal channels that are formed between pairs of fuel plates. For end channels, which are the ones bounded by only one fuel plate, half of the reduction was assumed. In the Appendix B analysis of Reference 13.4, a full element of each of the four burnups for each core was simulated with the RELAP5 code.

The peak fuel temperature during the double-ended cold leg LOCA for the HEU core occurs in plate number-2 of element 5, which is a fresh element. The steady-state heat flux profile for this plate normalized to a core power of 10 MW is provided in Figure 4.35. It was previously calculated for a core with HEU that 6.0% of the reactor power is deposited outside the primary coolant system. (Ref. 13.18) Consequently, the steady-state HEU core power in the RELAP5 model of the LOCA is 9.4 MW. Since the radial geometry of all plates and coolant channels is represented in the RELAP5 model, any uneven heat conduction into the coolant channels adjacent to the two radial surfaces of the HEU fuel plate is accounted for directly in the RELAP5 analysis.

Figure 13.7 shows the peak centerline temperature history of the hottest node of the hottest fuel plate (plate number-2 of element 5) during the accident. The fuel temperature is plotted for axial node 3 (which is just below the core midplane). The four vertical lines, which extend through all four subplots, are to indicate the times of transient initiation, scram, anti-siphon system activation, and peak fuel temperature. This peak is 510 °F (266 °C) and occurs at 1.44 seconds after the start of the transient. The peak HEU temperature is well below the fuel and cladding temperature limit of 986 °F (530 °C) specified in Reference 13.8. Reference 13.8 appears to be making a determination based on the analysis of fresh fuel, since the lower bound of the 95% confidence interval (-2σ) blister threshold temperature for UAl_x at all burnups relevant to MURR is 900 °F (482 °C) (Ref. 13.6). For the analysis of the LOCA presented here, the peak HEU temperature is below both of these temperatures. The anti-siphon system is described in Section C.2.2.5 of Appendix C.

Figure 13.7 also shows the RELAP5 defined heat transfer mode for both surfaces of this fuel plate node. RELAP5 uses heat transfer mode numbers to define heat transfer regimes. The RELAP5 manual defines modes 0 through 8 verbatim as follows:

- Mode 0 Convection to noncondensable-steam-water mixture or superheated liquid
- Mode 1 Convection at supercritical pressure or superheat wall with negative heat flux due to superheated gas
- Mode 2 Single-phase liquid convection at subcritical pressure, subcooled wall and low void fraction
- Mode 3 Subcooled nucleate boiling

- Mode 4 Saturated nucleate boiling
- Mode 5 Subcooled transition boiling
- Mode 6 Saturated transition boiling
- Mode 7 Subcooled film boiling
- Mode 8 Saturated film boiling

When non-condensable gases are present, RELAP5 uses the same mode numbers, but adds 20 to each mode number. At about 1 second, the anti-siphon system valve opens and injects air, which is a non-condensable gas, into the reactor vessel. Shortly thereafter, all of the mode numbers increase by 20. This is shown by the numbers on the right scale of the heat transfer mode subplot, which apply when the curve in the plot is dashed instead of solid. It is important to note that Modes 4 and 24 correspond to saturated nucleate boiling and that 5 and 25 correspond to subcooled transition boiling, which is the start of CHF. Although the plot has continuous solid or dashed lines, only integer values of mode can exist. Connected lines were used only to make the plot easier to read.

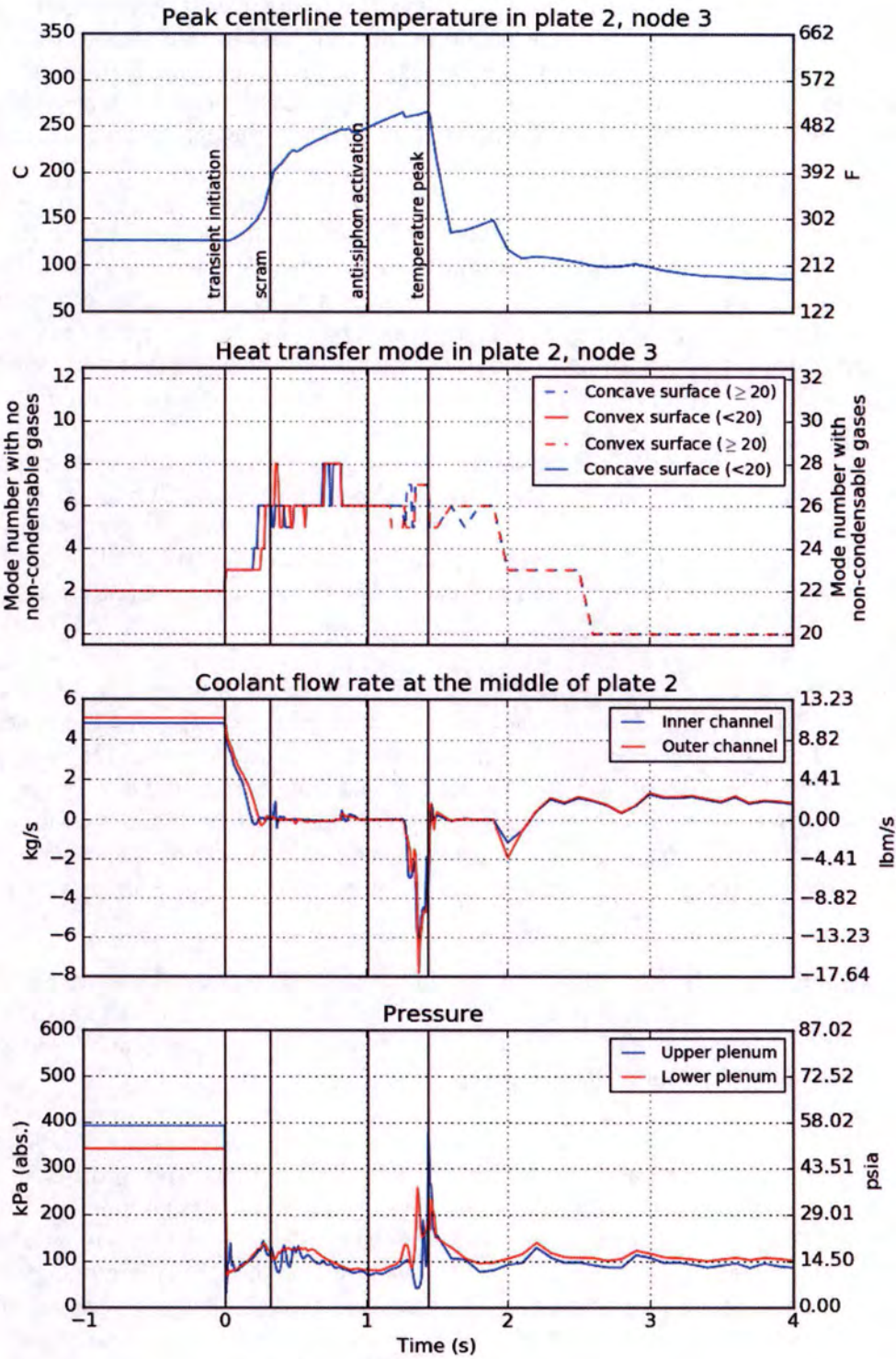


FIGURE 13.7
HEU ELEMENT 5 DOUBLE-ENDED COLD-LEG LOCA RESULTS

The heat transfer mode subplot of Figure 13.7 shows that both sides of the fuel plate reach CHF before the scram at 0.3255 seconds and remain in the poor heat transfer modes of 5 (or 25) or above until beyond the peak fuel temperature, which is achieved at 1.260 seconds. It is important to observe that it is not a return to very good heat transfer, Mode 4 or 24, that caused the fuel temperature to stop rising and decline significantly, but rather the activation of the anti-siphon system 0.260 seconds earlier.

As the coolant flow rate subplot shows, the coolant flow rates on both sides of the fuel plate are essentially zero until the air injected by the anti-siphon system temporarily pushes the flow on either side of the channel upward, which corresponds to a significant negative flow pulse. The inner channel is on the concave side of the fuel plate and the outer is on the convex side. The pressure subplot shows that the pressure pulse, which is produced by the anti-siphon system activation, arrives in the lower plenum before reaching the upper plenum, as it should.

Because the pumps are running at their initial steady-state speed until they are tripped at 1.0 seconds after the start of the transient, at first glance, one would expect that both the pump and the core flow to remain essentially the same and near their initial values. However, this does not happen because of cavitation in the outlet leg. The top of the outlet riser (pipe 102, node 1 in Figure C.2 of Appendix C) during most of the first second of the transient the pressure is in a severe vacuum.

The reason for this severe vacuum is that the pressure at both ends of the break is the atmospheric pressure of 14.3 psia. Fluid is drawn toward and out of the primary loop through both ends of the break. The fluid in the core is being pulled from two directions. One end of the break is pulling from the inlet side of the core and the pump is pulling on the outlet side of the core. As Figure C.1 of Appendix C indicates, the break is at the lowest point in the primary loop. The top of the outlet riser is 18.626 feet higher. The difference in gravity head plays an important role here. A stagnant 18.626 feet column of liquid water would have a pressure at the top that is about 8 psi lower than that at the bottom.

The very low pressure at the top of the riser caused by the break enables the water there to boil at the temperature that normally occurs there. Thus, the coolant boils and generates vapor in the outlet leg at the outset of the transient. This causes the core flow rate to precipitously drop as vapor is generated between the core outlet and the pump inlet.

For the LEU core cold leg double-ended LOCA the peak fuel temperature occurs in plate number-3 of fuel element 5, which is a fresh element. The steady-state heat flux profile for this plate normalized to a core power of 12 MW is provided in Figure 4.37. It was previously calculated for a core with LEU that 3.6% of the reactor power is deposited outside the primary coolant system (Ref. 13.18). Consequently, the steady-state LEU core power in the RELAP5 model of the LOCA is 11.57 MW. Since the radial geometry of all plates and coolant channels is represented in the RELAP5 model, any uneven heat conduction into the coolant channels adjacent to the two radial surfaces of the fuel plate is accounted for directly in the RELAP5 analysis.

The peak fuel temperature during this accident, 578 °F (303 °C), occurred in a fresh element, element 5, in axial node 3 of plate number-3. Flow redistribution among fuel elements due to burnup is not included in this RELAP5 analysis. The minimum margin to the fuel temperature safety limit (lower 95% confidence interval of the U-10Mo blister threshold temperature) is a ΔT of 297 °F (147 °C) in this case. However, the calculated minimum margin to the fuel temperature safety limit is smaller when flow redistribution due to burnup is included. For this situation, the minimum margin to the fuel temperature safety limit is a ΔT of 239 °F (115 °C). This occurred in a maximum-burned element, element 8, at 1.48 seconds after the start of the transient, in axial node 3 of plate number-22. The steady-state heat flux profile for this plate is provided in Figure 4.36. For this latter case, the peak fuel temperature is 4 °F lower, at 574 °F (301 °C), than when flow redistribution among the elements due to burnup is not included. The results for this simulation, which are analogous to those for the HEU core, Figure 13.7, are provided in Figure 13.8.

13.2.3.3 Cold Leg Double-Ended LOCA Analysis Used for Recent HEU Relicensing

The HEU peak fuel temperature results used for the relicensing of the MURR and provided in the Reference 13.5 in the response to Request for Additional Information question 6.b differ from those presented in Figure 13.7. In Reference 13.5 the peak fuel temperature for the cold-leg break LOCA is given as 413.9 °F (212.2 °C), which is considerably less than the 510 °F (266 °C) presented here. As indicated in Section B-5.13 of Reference 13.4, the earlier analysis used for relicensing assumed that there is a coolant channel gap thickness reduction due to burnup with 10 mils of channel reduction at 150 MWd. The current HEU analysis, as described above, assumes no channel gap thickness reduction due to burnup. This reduction increases the initial flow in the limiting fresh element by 10%, which reduces the initial and peak fuel temperatures. Also, as described in some of the subsections of Section B-5.0 of Reference 13.4, there are other changes that were made to the RELAP5 simulation model used to obtain the Figure 13.7 results that are not included in the analysis for the Reference 13.5 submittal. These are perhaps less significant, but include a revised main inlet coolant check valve model and an improved post-scrum power history. In addition, because of modeling difficulties, the analysis was performed without the anti-siphon system activated in the HEU LOCA analysis that predicted 413.9 °F as the peak temperature. In all of the other HEU and LEU LOCA analyses for this conversion PSAR, the simulation includes the activation of the anti-siphon system.

13.2.3.4 Conclusions

The consequences of a loss of coolant due to a break in a section of primary coolant piping, including a double-ended rupture of the largest diameter coolant pipe, have been analyzed. Ruptures in sections of the in-pool primary coolant piping, as well as ruptures at different locations relative to the reactor pool and the inlet and outlet isolation valves, have been considered. The four LOCAs listed in Section 13.2.3.1 have been simulated with the RELAP5 code for both fuels. These four included the cold-leg double-ended LOCA, which is the most severe. This analysis assumes the same loss-of-coolant initiating event and scenario for the proposed LEU-fueled reactor as previously postulated for the licensed HEU core. The safety analysis demonstrates that the fuel temperatures are below the safety limit for the LEU fuel so that fuel integrity is maintained. None

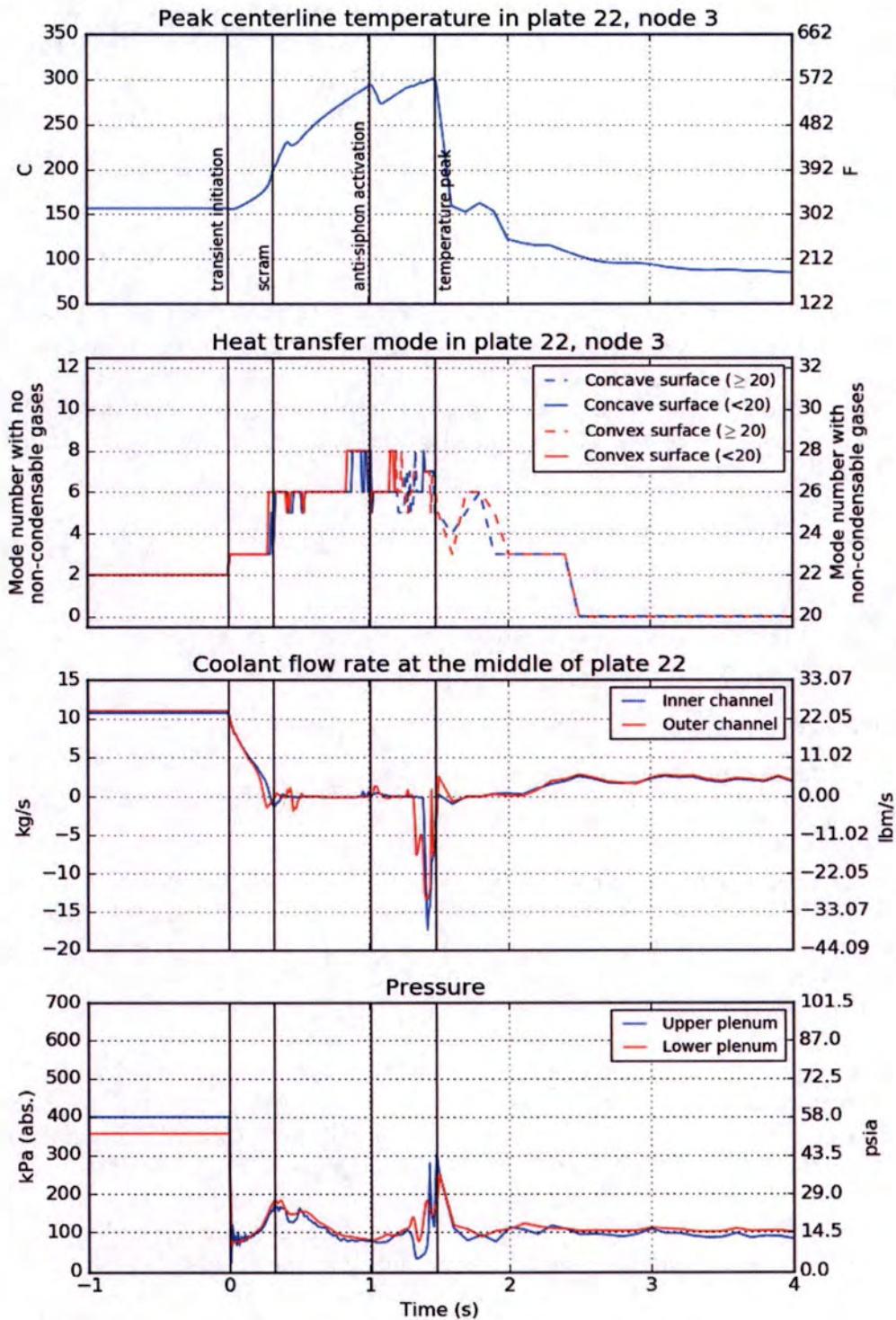


FIGURE 13.8
 LEU ELEMENT 8 DOUBLE-ENDED COLD-LEG LOCA RESULTS
 (WITH FLOW REDISTRIBUTION DUE TO BURNUP)

In conclusion, the MURR possesses sufficient redundant safety features to prevent core damage as a result of the double-ended rupture of the largest diameter primary coolant piping, or ruptures at other locations in the primary system, and requires no additional emergency core cooling system for core protection in the event of a LOCA.

13.2.4 Loss of Primary Coolant Flow

13.2.4.1 Accident Initiating Events and Scenarios

Section 13.2.4 ("Loss of Primary Coolant Flow") of Chapter 13, Accident Analyses, of the MURR SAR Reference 13.1 demonstrates for the HEU core that for all credible Loss of Primary Coolant Flow (LOFAs) unacceptable consequences to people and the environment would not occur. For the conversion of the MURR core from HEU fuel to LEU fuel it is necessary to provide an analogous demonstration for the LEU core that is to replace the HEU core and to demonstrate adequate safety margins for the LEU core. Also, the performance of the two cores must be compared using consistent modeling assumptions.

A loss of flow accident (LOFA) for the primary coolant system can be initiated by any one, or a combination, of the following anomalies:

- (a) Loss of facility electrical power (or coolant circulation pump power);
- (b) Inadvertent closure of coolant loop isolation valve(s);
- (c) Inadvertent loss of pressurizer pressure;
- (d) Locked rotor in a coolant circulation pump; and
- (e) Failure of a coolant circulation pump coupling.

Any of these five anomalies is considered to be possible for the MURR facility, but a loss of flow (by any means) without an accompanying reactor scram is not considered credible because of the redundancy in the reactor safety system. Because the MURR is a downward flow reactor, the analysis must consider such challenging design features as flow stagnation and reversal that will occur during the accident.

The LOFA caused by a loss of pressure in the primary coolant system pressurizer can be initiated by anomalies such as a break in any of the piping penetrations near the top of the pressurizer, a failure of the pressurizer relief valve, or pressurizer nitrogen vent valve V545 failing in the open position. All of these pressurizer scenarios result in loss of pressure in the pressurizer, which causes a primary loop depressurization through the 2-inch diameter line that connects the pressurizer to an 8-inch pipe in the primary loop, as shown in Figures C.1 and C.2 of Appendix C. The cold leg LOCA caused by a 2-inch break in the pressurizer line that was included in the LOCA analysis and is item 4 in the list of LOCAs in Section 13.2.3.1, from a simulation perspective, is nearly the same as the accident (c) LOFA above. The key differences are that 1) in the LOFA nitrogen is lost, but not coolant, and 2) in the LOCA the 2-inch break is about 12 feet closer along the 2-inch connecting pipe to the main 8-inch primary header pipe than is the pressurizer.

The system depressurization accident (c) LOFA will cause the anti-siphon system to be activated and inject air into the top of the primary loop. Since there is no coolant lost in the case of the LOFA the long-term pressures may be a little higher than in the 2-inch break LOCA, as would be the long-term coolant temperatures. The higher long-term coolant temperatures should cause the long-term fuel temperatures to be a little bit higher, as well. Thus, the peak fuel temperature history for the accident (c) LOFA is expected to be essentially the same as for the cold-leg 2-inch break LOCA. Since this LOFA by no means rivals the most limiting of the four LOCAs that are list in Section 13.2.3.1, it was not analyzed. However, accidents (a), (b), and (d) were explicitly simulated with RELAP5.

The unique aspect of accident (a) is that the both the primary coolant circulation pumps and the pool pump coastdown at the outset of the accident. For accident (b) there is no reason to assume that both isolation valves will close simultaneously since they are independently controlled. Thus, accident (b) represents two separate accidents, one for the inadvertent closing of the inlet isolation valve, valve V507B in Figure C.1 of Appendix C, and one for the inadvertent closing of the outlet isolation valve, valve V507A in Figure C.1 of Appendix C. Intuitively, the case of both of the isolation valves closing simultaneously should be slightly worse than only one valve closing. In the model, the flow area of valve V507A is reduced on a linear ramp and goes from its fully open to fully closed position in 4.9 s. Valve V507B has the same behavior, except that it takes 5.0 seconds to fully close. Closing either valve stops the flow. Therefore, for modeling efficiency, in the simulation of accident (b) both isolation valves were assumed to close simultaneously.

When accident (d) occurs, the flow of one of two parallel primary coolant pumps is suddenly lost. The RELAP5 model represents both primary coolant circulation pumps as a single pump. In the model, the speed of this pump was reduced to 60% of its initial speed in 0.001 s. Figure 6.4 of Reference 13.4 provides a plot of primary pump flow vs. time as predicted by RELAP5 for this transient. Both HEU and LEU cores are represented. Both assume an initial pump flow rate of 3,700 gpm and an initial core inlet temperature of 125 °F (51.7 °C). The flow initially decreases rapidly and, as the figure shows, is about 63% of its initial value at 1.5 seconds and remains nearly constant until 2.0 s, where the plot ends. A flow value greater than 50% is to be expected since the flow area of the primary loop has not been halved or even reduced. Measured data was taken at MURR on May 26, 2014, in which one of the two parallel primary coolant circulation pumps was stopped. The measurements indicate 3,823 gpm through the pumps with both of the primary coolant circulation pumps operating and 2,420 gpm, or 63.3%, with only one of the primary pumps operating. The measurements were taken with the in-pool heat exchanger valves closed. Had they been open during the measurements, as is the case for both accident (d) and the RELAP5 simulations of it, the measured flow through the primary pumps would have been slightly higher than the measured 63.3% value because of the reduced hydraulic resistance caused by the flow path through the in-pool heat exchanger loop that is parallel to the core flow path.

Accident (e) is similar to accident (d) in that in both accidents the flow of one of two parallel pumps is lost. In either case, backflow through the failed pump is avoided by a check valve at the pump outlet. In both cases, the failure of the pump is assumed to be essentially instantaneous and therefore results in a very quick drop in the combined flow of the two pumps. Thus, the peak fuel

temperature simulation results for accident (d) should bound or be the same as those of accident (e).

The initial reactor conditions assumed for all three LOFAs are the same as those used for the RELAP5 simulation of the LOCA analysis and are provided in Section 13.2.3.1 in Table 13-19.

13.2.4.2 Accident Analysis and Consequences

As explained in Section B-6.1 of Reference 13.4 ("Regulatory Safety Analysis Acceptance Criteria for Loss-of-Flow Accidents"), the acceptance requirement for LOFAs is that the temperature margin between the peak fuel temperature and the fuel temperature safety limit has not significantly decreased to the point of potential fuel damage as a result of the reactor conversion.

The analysis of the LOFAs in Reference 13.4 is analogous to the analysis of the LOCAs in this reference. As described in Section 13.2.3.2 above for the LOCAs, for the LOFAs four burnup states were explicitly simulated with the RELAP5 code for each core (HEU or LEU), the HEU analysis assumed no flow redistribution among fuel elements due to burnup, and the LEU analysis was performed twice: once with flow redistribution due to burnup and once without. The RELAP5 simulation model of the MURR facility used for the LOFA analyses is the same as the one described in Appendix C and used for the LOCA analyses.

As indicated in Section B-6.2 of Reference 13.4, the most limiting LOFA for the HEU core is accident (a) listed in the previous section, which is the LOFA caused by a loss-of-site power. The peak fuel temperature, 299 °F (148 °C), occurred in element 5, which is a fresh element, at 22.3 seconds after the start of the transient, in axial node 3 (just below the core midplane) of plate number-24. The analysis assumed no flow redistribution due to burnup. The temperature history at the location of the peak is provided in Figure 13.9.

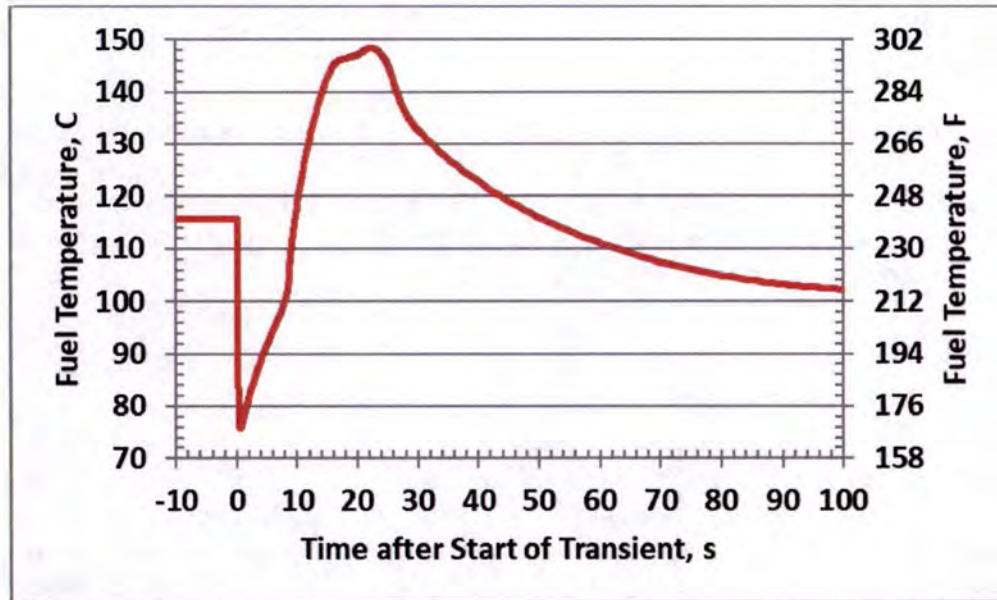


FIGURE 13.9

HEU CORE PEAK FUEL CENTERLINE TEMPERATURE AT LIMITING LOCATION FOR LOSS-OF-SITE POWER (NO FLOW REDISTRIBUTION DUE TO BURNUP)

As indicated in Section B-6.2 of Reference 13.4, the most limiting LOFA for the LEU core is accident (d) listed in the previous section, which is the LOFA caused by the locked rotor (i.e., seizure) of one of two primary pumps. The RELAP5 simulation that assumed no flow redistribution due to burnup yielded the most limiting LEU LOFA result, as explained in the last paragraph of Section B-6.2 of Reference 13.4. The smallest margin to the fuel temperature safety limit in this case, was a ΔT of 418 °F (232 °C), which occurred in element 8, which is an end-of-life element with 170 MWd of burnup, in axial node 3 of plate 23. It is noted that the peak fuel temperature in this element, 339 °F (171°C), occurred in axial node 3 of plate 22 at 0.34 s after the start of the transient. The locations of the peak fuel temperature and the smallest margin to the fuel temperature safety limit are different because of differences in the peak fuel burnup in each plate, which affects the burnup-specific safety limit. Figure 13.10 shows the peak fuel temperature history at the node of the peak fuel temperature.

13.2.4.3 Limiting LOFA Analysis Used in Recent HEU Relicensing

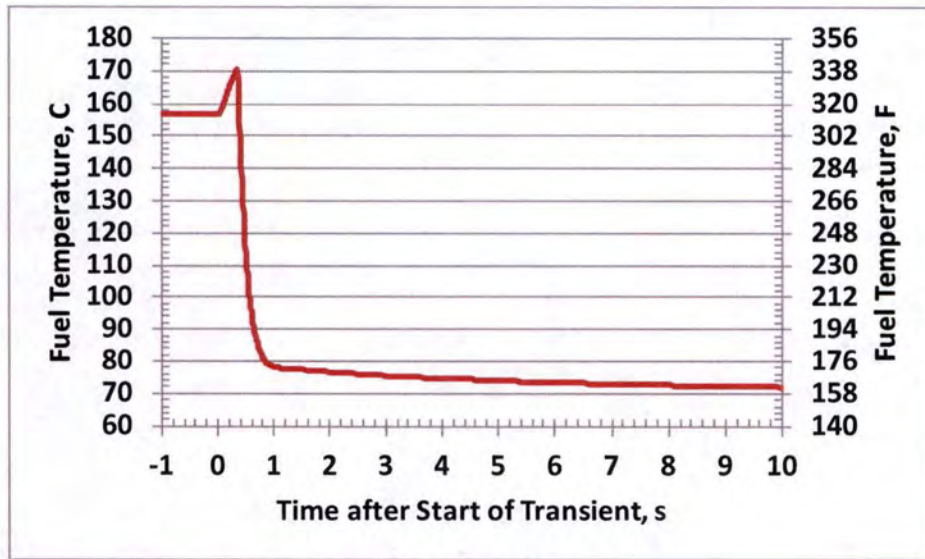
The limiting LOFA for the relicensing of the MURR as provided in Reference 13.5 in the response to the Request for Additional Information question 6.b has a peak fuel temperature of 292.3 °F (144.6 °C). The LOFA that was simulated by RELAP5 for the relicensing is the transient that is initiated by both main isolation valves inadvertently and simultaneously tripping. This is accident (b) in Section 13.2.4.1. Subsequent to relicensing, in Reference 13.4, the model has been updated as discussed in Section 13.2.3.3. As explained in Section B-5.13 of Reference 13.4, the LOFA results were also slightly impacted by the addition of a missing primary coolant pump trip that occurs when either main isolation valve starts to close. These changes caused the temperature for accident (b) to increase. However, the temperature remained lower than that for the most limiting

LOFA in Reference 13.4, which is LOFA accident (a), loss-of-site-power, with a peak fuel temperature of 299 °F (148 °C).

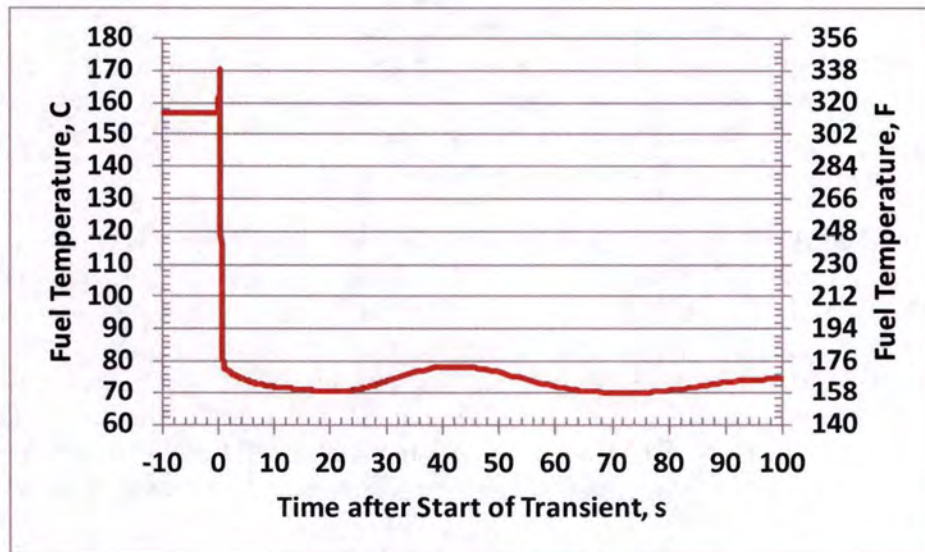
As indicated in Section B-5.13 of Reference 13.4, and briefly described in Section 13.2.3.3, there are significant differences between the currently used RELAP5 models and those used for the Reference 13.5 relicensing. However, the peak fuel temperature predicted for the relicensing LOFA and the peak for the one plotted in Figure 13.9 differ by only several degrees Fahrenheit because LOFAs tend to be mild.

13.2.4.4 Conclusions

The safety acceptance requirement is that the temperature margin between the peak fuel temperature and the fuel blister threshold temperature has not significantly decreased to the point of potential fuel damage as a result of the reactor conversion. The most limiting LOFA for the LEU core is accident (d) listed in Section 13.2.4.1, which is the LOFA caused by the locked rotor (i.e., seizure) of one of two primary pumps. For this transient the predicted smallest margin to the fuel temperature safety limit is a ΔT of 418 °F (232 °C) and the predicted peak fuel temperature is 339 °F (171°C). Thus, the safety acceptance requirement has been met.



Plot (a) 0 to 10 s.



Plot (b) 0 to 100 s.

FIGURE 13.10

LEU CORE PEAK FUEL CENTERLINE TEMPERATURE AT PEAK TEMPERATURE LOCATION FOR SEIZURE OF ONE PUMP (NO FLOW REDISTRIBUTION DUE TO BURNUP)

13.2.5 Fuel Failure During Operation Accident

The analyses of the reactivity insertion and loss of coolant/loss of flow accidents showed that no fuel damage is expected if these accidents were to occur. Consequently, there is no anticipated

release of radioactive material as a result of these postulated accidents which would contribute to a radiation dose for MURR Operations personnel or any person outside of the MURR containment. Nonetheless, the fuel failure during operation accident (FFA), which postulates the release of radioactive material by cladding failure during reactor operation, was analyzed to compute the radiation doses to workers and the general public.

Previous modeling and analyses of the FFA were described in detail for the HEU- and LEU-fueled cores in References 13.1 and 13.20, respectively. Subsequent to those reports, the radioactive source term and methodology for calculating the dose consequences were revised as part of a response to regulatory request for additional information (RAI). Summary descriptions of the accident scenario, analysis, and consequences are provided here.

The FFA was previously labeled as the MHA for MURR since it led to general public dose consequences worse than those resulting from any other credible accident (Ref. 13.1). However, based on the analyses performed as part of the aforementioned RAI, the fueled experiment failure accident was found to result in a dose for members of the general public in the unrestricted area of 0.011 mrem (Ref. 13.22). Since this accident has a greater dose consequence than the HEU FFA (which is described below) and fuel handling accident (which is described in Section 13.2.1), the fueled experiment failure accident was classified as the MHA. However, the calculated public dose for the LEU fuel handling accident is greater than that for the fueled experiment failure accident, so it is anticipated that this accident will be classified as the MHA following conversion (see Section 13.2.1). It is noted that the fueled experiment failure accident will not be affected by the LEU conversion, and so is not evaluated here.

In the FFA for the MURR, it is assumed that some accidental condition has caused fuel plates in the operating core to melt. The conditions that lead to this event are considered immaterial to the analysis. The FFA for the HEU fuel assumes that four number-1 fuel plates in four separate elements melt. The number-1 plates are in the peak power density region of the HEU core. Likewise, for the LEU core, the FFA assumes that four number-1 fuel plates in four separate elements melt. While the number-23 fuel plates are in the peak heat flux region of the LEU core, the higher power density that exists in the number-1 fuel plates will lead to a larger source term of fission products per gram of fuel, and is therefore considered the conservative basis for this accident scenario.

The potential energy release from the melting of four number-1 fuel plates could occur as a possible metal-water reaction (Ref. 13.28). While hydrogen would be formed, it is highly unlikely that in a water environment a hydrogen deflagration reaction would occur. The amount of material which would be involved in a metal-water reaction under the conditions of four (4) number-1 fuel plates melting is not predictable as the amount is dependent upon many conditions. For purposes of calculation, it is conservatively assumed that all the aluminum in the plates involved in the accident react with water. In the HEU fuel assembly, the aluminum in the four number-1 fuel plates is 426 grams. In the LEU fuel assembly, the aluminum in the four number-1 fuel plates is 314 grams aluminum. The aluminum is assumed to react according to the following equation:



The energy release per kg of aluminum is 15.16 MW-sec. The amount of energy released from the aluminum-water reaction is 6.5 and 4.8 MW-sec in the HEU and LEU cores, respectively. This amount of heat would easily be transferred to the adjacent fuel elements and primary coolant in the core. Additionally, any steam that would form in the vicinity of the molten area would also assist in dissipating the heat. Since the FFA would result in a negligible release of energy to the primary coolant system, the introduction of pressure surges, which could lift the primary relief valves, are not considered credible.

The whole-core radioactive material source term for the FFA was calculated by assuming the same conservative power history and burnup as used in the FHA. The whole-core inventory of radioiodines and noble gases for the HEU and LEU cores are summarized in Table 13-1.

The source term for the FFA is based on the fraction of the whole-core inventory of radioactive material that is contained in the fuel plates that are assumed to be damaged in the accident. Table 13-20 summarizes the basic data used to calculate the fractions of the HEU and LEU core inventories released in the FFA. The release fraction is calculated based on the fuel meat mass in the four number-1 plates that are assumed to melt and on a number of power-related factors. The ^{235}U mass data were derived from the nominal plate loading and data for the reference HEU and LEU cores evaluated in Reference 13.12. Power distribution data from detailed three-dimensional MCNP models of these reference cores were also utilized. The fuel plate nuclear peaking factor used in the accident analysis is for the number-1 fuel plate with the largest plate-average power density peaking factor in a reference HEU or LEU core at equilibrium xenon conditions. The power distribution for a reference core with equilibrium xenon conditions and critical control blade position is most appropriate since the inventory subject to release in the accident corresponds to a very long irradiation history prior to the accident. The reference cores assumed elements with a mixture of burnups that are typical for MURR operations, control blades that are banked, and a typical loading of samples in the center flux trap and reflector. The "additional allowable factor" is included to account for changes to the plate power peaking that might occur due to adjustments in the fuel management, experiment loading effects, and control blade skewing relative to the reference core. The HEU value of 1.062 has been used historically at MURR. The LEU value of 1.014 is the largest change to the plate 1 peaking factor calculated from a number of alternate LEU cores that also had equilibrium xenon, but skewed control blades (within the limits of the TSS) and/or an empty central flux trap. Lastly, the plate fuel loading variation hot-channel factor is applied to account for potential increases in the as-built ^{235}U loading in the fuel plate, which will cause a corresponding increase in the fission product inventory in the plate. The HEU value of 1.03 was specified in Table 4-14 of Reference 13.1. The LEU value is based on an assumed ± 1 mil thickness tolerance for the U-10Mo fuel foils. Plate 1 of the LEU design has a nominal meat thickness of 9 mil, so that the maximum as-built ^{235}U loading in plate 1 is 11.1% (1/9) greater than the nominal loading of 18.09 g. Applying all these factors results in a whole-core fission product release fraction for the FFA of 3.11% and 2.28% for the HEU and LEU cores, respectively. The release of radioisotopes of krypton, xenon, and iodine are the major sources of radiation exposure to personnel in the containment building and will, therefore, serve as the basis for the source term for the dose calculations.

TABLE 13-20
 FRACTIONAL RELEASE OF WHOLE-CORE RADIOACTIVE SOURCE FROM FUEL
 FAILURE ACCIDENT IN HEU AND LEU CORES.

	HEU	LEU
Fissile Loading		
Plate 1 ²³⁵ U mass (g)	████	18.09
²³⁵ U mass in four plates (g)	████	72.36
Core ²³⁵ U mass (g)	████	11,204
Power-related Factors		
<i>Nuclear Peaking Factors</i>		
Fuel plate (hot plate average)	2.018 ¹	3.138 ²
Additional allowable factor	1.062	1.014
<i>Engineering Hot-Channel Factors</i>		
Plate fuel loading variation	1.03	1.111
Overall product	2.207	3.535
Fractional release of fission product inventory	3.11%	2.28%

¹ Power-related Factors from Reference Core 4A (eq. Xe), Element 1, Plate 1.
 Yields largest plate-average power density peaking factor in core.

² Power-related Factors from Reference Core 8A (eq. Xe), Element 1, Plate 1.
 Yields largest plate-average power density peaking factor in core.

The FFA is assumed to occur with the primary coolant system operating, resulting in a quick dispersal of all fission products from the melted fuel plates throughout the system. It is conservatively assumed that 100% of the radioiodine and noble gas fission products from the affected plates are instantaneously and uniformly dispersed within the 2,000-gallon primary coolant system volume. There is a low leakage rate of coolant from the primary coolant system into the reactor pool, providing a path for Operations personnel in the containment building to be exposed to radioactive material from the FFA. This leakage is typically less than 40 gallons per week. However, for the purpose of the FFA analysis, a conservative leakage rate of 80 gallons per week (7.9×10^{-3} gpm) from the primary system to the pool was assumed.

13.2.5.1 Occupational Dose

For calculating the occupational dose to Operations personnel as a result of the FFA, it is assumed that workers remain in the containment building for 10 minutes after the start of the accident, during which the workers would secure the primary coolant system and perform evacuation procedures. During this 10-minute interval, the radioiodines that transfer from the primary coolant system into the pool are conservatively assumed to instantaneously and uniformly mix into the

20,000 gallons of bulk pool water. For the purpose of the FFA, the assumption is that a total of 40 gallons of pool water containing the radioiodines released from the fuel evaporates over 10 minutes into the containment building. This is the same evaporation rate as assumed for the FHA. The radioiodines are then assumed to uniformly mix into the containment building air volume of 225,000 ft³. The noble gases (krypton and xenon) released from the primary coolant system over the 10-minute interval are assumed to pass immediately through the pool water and enter the containment building air volume, ignoring their significant solubility in water. None of the assumptions related to the leakage rate of primary coolant to the pool, the pool evaporation rate, or the exposure time for Operations personnel will be affected by the conversion to LEU fuel.

The objective of the analysis is to present a worst-case dose assessment for a person who remains in the containment building for 10 minutes following the FFA. Figure 13.11 illustrates the calculated airborne concentration of radioiodines and noble gases in the containment from the start of the HEU FFA analysis to when the primary coolant system is secured at 10 minutes after the fuel failure. In the previous analyses of the dose consequences from the FFA performed in References 13.1 and 13.20, the reduction in the average concentration during the accident due to radioactive decay of the radionuclides was neglected. However, some of the radionuclides considered in the analysis have half-lives on the order of minutes or even seconds, which are provided in parentheses for each nuclide shown in Figure 13.11. To eliminate unnecessary conservatism in the calculation of the occupational dose, radioactive decay during the 10-minute interval was included in the current analysis of the FFA. Figure 13.11 shows that for long-lived noble gases such as Xe-133 (half-life of 5.2 days), the airborne concentration increases linearly as the contaminated primary system coolant leaks into the reactor pool/containment, whereas for shorter-lived nuclides such as Xe-137 (half-life 3.8 minutes), the airborne concentration begins to decrease after about six (6) minutes due to the effects of radioactive decay. The airborne concentrations of radioiodines (all of which have $t_{1/2} \gg 10$ minutes) increase monotonically but non-linearly due to the combined effects of primary-to-pool leakage and pool-to-containment evaporation. The time-averaged airborne concentrations of the noble gas and iodine radionuclides in the containment air over the 10-minute interval are assumed when calculating the occupational dose in the restricted area. The DAC values assumed for the FFA analysis are the same as assumed for the FHA in Section 13.2.1.2.1.

Table 13-21 summarizes the results of the dose to Operations personnel calculated for the HEU and LEU FFA. The results show that the occupational doses are well within the published regulatory occupational limit of 5 rem for the total effective dose equivalent (TEDE) for both HEU and LEU cores. Furthermore, the occupational doses are a factor of 9 and 31 lower than the calculated values previously reported in Reference 13.20 for the FFA in HEU and LEU cores, respectively. This is primarily because 1) more realistic DAC values were adopted in this analysis for the unlisted nuclides, 2) the reasonable modeling of radioactive decay during the 10-minute interval of the exposure to workers, and 3) the LEU analysis now corresponds to the same basis of four number-1 plates as in the HEU analysis. The occupational dose resulting from the FFA in the LEU core is slightly less than for the HEU core. Although the whole-core fission product inventory is about 20% larger for the LEU core due to the required power uprate, the fraction of the fission product inventory contained in the damaged fuel plates is about 25% lower for the LEU core.

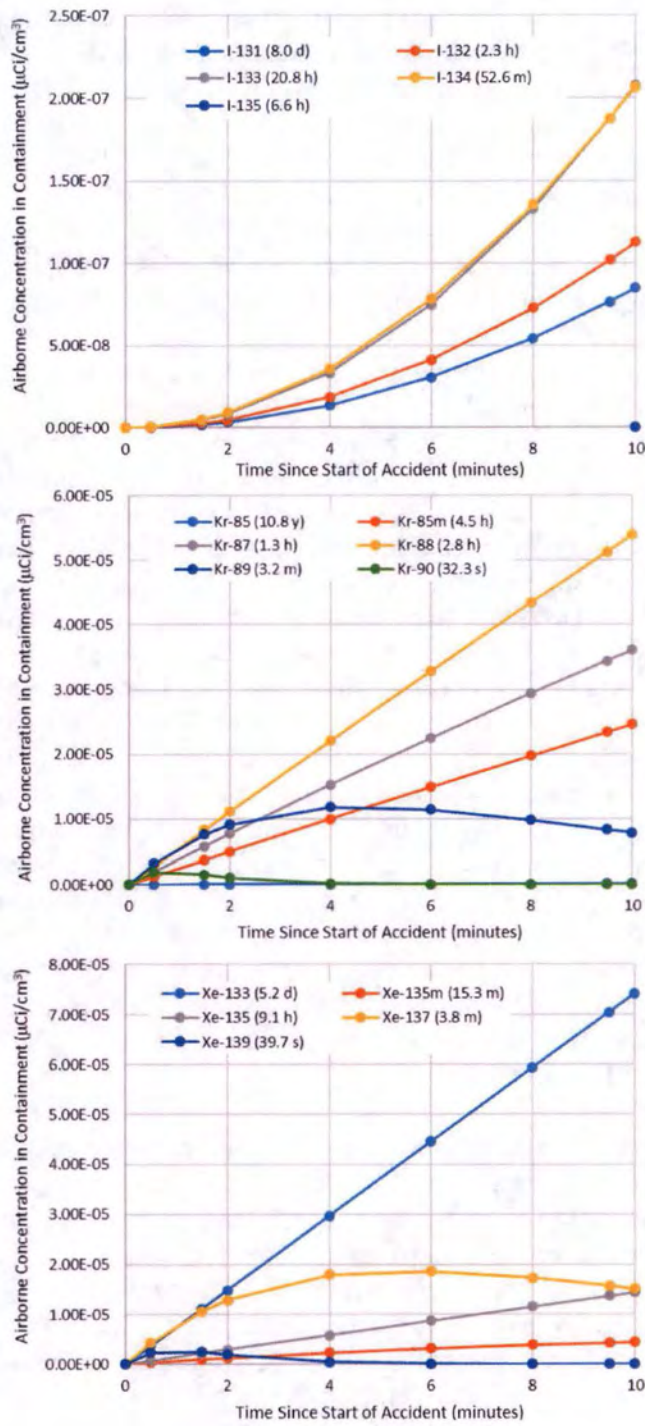


FIGURE 13.11
 AIRBORNE CONCENTRATION OF RADIONUCLIDES
 IN THE CONTAINMENT BUILDING FOLLOWING THE START OF THE HEU FFA

TABLE 13-21
10-MINUTE OCCUPATIONAL DOSE FROM RADIOIODINES AND NOBLE GASES IN
CONTAINMENT FROM FFA

	HEU	LEU
Total Effective Dose Equivalent (TEDE) from Radioiodines, mrem	0.27	0.25
Deep Dose Equivalent from Noble Gases, mrem	14.31	12.86
Total Effective Dose Equivalent (TEDE), mrem	14.59	13.11
Annual Occupational Limit, mrem	5,000	5,000

It is also worth noting that the expected evacuation time for most occupants of the containment building is 2 minutes, instead of the conservative 10 minutes assumed in the dose calculations. In the event that the worker evacuates the building sooner than the assumed 10 minutes, the worker will receive a much smaller dose due to two effects. First, there will be a 5-fold reduction in dose simply due to the shorter occupancy time (2 minutes vs. 10 minutes). Additionally, Figure 13.11 shows that the airborne concentrations of all but the most short-lived radionuclides in the containment air increase from the onset of the FFA. Consequently, the average concentration of radionuclides to which the worker is exposed will be reduced for shorter occupancy times. The combination of these two effects reduces the dose to Operations personnel who evacuate within 2 minutes by a factor of about 16 compared with those who remain in the containment for 10 minutes.

13.2.5.2 Public Dose

The dose to a member of the general public in the unrestricted area is calculated for the FFA in much the same manner as for the FHA in Section 13.2.1.2.2. Prior to evacuation, Operations personnel will secure the primary system so that there is no further leakage of contaminated primary coolant into the reactor pool. Consequently, the airborne concentration of noble gases in the containment air at 10 minutes after the start of the accident, with further reductions due to radioactive decay and mixing with the laboratory building ventilation flow, is what is assumed to leak into the environment. It is conservatively assumed that 100% of the noble gases in the containment air are released to the environment.

The airborne concentration of radioiodines in the containment depends on the evaporation rate of the water from the pool. For the purpose of the FFA, the conservative assumption is that 40 gallons of pool water containing radioiodines released from the melted fuel plates evaporate into the containment building air over 10 minutes, which is twice the amount of water vapor which would be needed to saturate the containment air at normal conditions of temperature and relative humidity. Thus, it can be assumed that there will be no further evaporation of pool water into the containment air, and so no further increase in the airborne radioiodine concentration in the containment, during the remainder of the accident evaluation. As for the FHA, the NRC-accepted

value of 50% reduction of radioiodines from plate-out and deposition was assumed, so that only 50% of the radioiodines is released to the environment.

The point of maximum dose for a member of the general public in the unrestricted area under the worst-case meteorological conditions was found to be 760 meters north of the containment building. 10 CFR 20 Appendix B Effluent Concentration Limits were used. For the four "unlisted" noble gas nuclides for which data are not provided in 10 CFR 20 (Kr-89, Kr-90, Xe-137 and Xe-139), Effluent Concentration Limits were calculated using the data and methodology contained in FGR No. 12 for submersion isotopes.

Table 13-22 summarizes the calculated TEDE for members of the general public for the HEU and LEU FFA cases. For the HEU FFA, the calculated maximum dose to a member of the general public in the unrestricted area is negligibly small, only 1.9×10^{-4} mrem. For the same accident with LEU fuel, the dose to a member of the public remains negligible, only 1.7×10^{-4} mrem.

TABLE 13-22
MAXIMUM DOSE IN THE UNRESTRICTED AREA
FOR 16.5 HOURS FOLLOWING THE FFA.

	HEU	LEU	LEU (Primary coolant system not secured)
TEDE, mrem	0	0	0.003

The public dose was also calculated for the case in which contaminated primary system coolant continues to leak into the pool at the conservative rate of 80 gallons per week (0.48 gallons per hour) throughout the accident, which would occur if Operations personnel were unable to secure the primary coolant system before evacuating the facility. Because the noble gases in the primary coolant are assumed to move directly through the pool and uniformly disperse in the containment air, the concentrations of noble gases in the containment building in this scenario would continue to increase throughout the 16.5-hour period of the accident analysis, except for isotopes with very short half-lives. While the concentration of radioiodines in the reactor pool would also continue to increase in this scenario, continued evaporation of the pool water containing the radioiodine would be inhibited because the containment air would already be supersaturated by the 40 gallons of water that are assumed to evaporate in the first 10 minutes after the start of the accident. The resulting maximum dose to members of the general public in the unrestricted area in this unlikely scenario is only 0.003 mrem.

10 CFR 20 provides a guideline for the TEDE to members of the general public of less than 100 mrem annually, and 2 mrem/hour. The calculated maximum TEDE for a member of the general public resulting from the FFA is well below the annual limit, and is also below the hourly dose limit. Additionally, this dose assumes very conservative atmospheric conditions and a conservative burnup of the core to produce the radioactive inventory that was used to calculate the

dose. Lastly, the dose to the general public can be greatly mitigated with the order of a site evacuation by MURR.

13.2.6 Experiment Malfunction

There are no changes to this section due to conversion.

13.2.7 Loss of Electrical Power

There are no changes to this section due to conversion.

13.2.8 External Events

There are no changes to this section due to conversion.

13.2.9 Mishandling or Malfunction of Equipment

There are no changes to this section due to conversion.

THIS PAGE INTENTIONALLY LEFT BLANK

CHAPTER 14

TECHNICAL SPECIFICATIONS

THIS PAGE INTENTIONALLY LEFT BLANK

14.0 TECHNICAL SPECIFICATIONS

No changes to this chapter are expected due to conversion. Changes to the Technical Specifications can be found in Appendix A.

THIS PAGE INTENTIONALLY LEFT BLANK

CHAPTER 15

FINANCIAL QUALIFICATIONS

THIS PAGE INTENTIONALLY LEFT BLANK

15.0 FINANCIAL QUALIFICATIONS

No changes to this chapter are expected due to conversion.

THIS PAGE INTENTIONALLY LEFT BLANK

CHAPTER 16

OTHER LICENSE CONSIDERATIONS

THIS PAGE INTENTIONALLY LEFT BLANK

TABLE OF CONTENTS

16.0	OTHER LICENSE CONSIDERATIONS	16-1
16.1	Prior Use of Reactor Components	16-1
16.1.1	Fuel and Fuel Cladding.....	16-1
16.1.2	Primary Coolant System Pressure Boundary	16-1
16.1.3	In-Pool Components Receiving High Neutron Fluence	16-1

16.0 OTHER LICENSE CONSIDERATIONS

16.1 Prior Use of Reactor Components

16.1.1 Fuel and Fuel Cladding

This section will not be required since with LEU conversion the only fuel that will be used is new unirradiated LEU fuel elements.

16.1.2 Primary Coolant System Pressure Boundary

A calculation of the reactor pressure vessel structural integrity including the effects of neutron fluence during the years of operation since MURR went critical in 1966 has been performed for the HEU core. As of the January 4, 2017 relicensing of MURR HEU operations, the pressure vessel has a predicted remaining lifetime in excess of 10 years. The lifetime of the vessel under LEU operations will require re-evaluation for the future conversion SAR to be submitted. Failure of either pressure vessel is not a safety problem, but would result in an unscheduled maintenance period to replace the vessels. MURR currently has a spare inner and outer pressure vessel. If operation at 12 MW with LEU will require replacing either, or both, pressure vessels significantly earlier than under HEU operations, then additional spare pressure vessels will be need to be machined from material that has been purchased.

16.1.3 In-Pool Components Receiving High Neutron Fluence

The analysis of the dose to the pool liner performed to answer one of the NRC requests for additional information questions will be recalculated for the LEU core operating at 12 MW.

CHAPTER 17

DECOMMISSIONING

THIS PAGE INTENTIONALLY LEFT BLANK

17.0 DECOMMISSIONING

No changes to this chapter are expected due to conversion.

THIS PAGE INTENTIONALLY LEFT BLANK

APPENDIX A

TECHNICAL SPECIFICATIONS

FOR

**THE UNIVERSITY OF MISSOURI RESEARCH
REACTOR**

**FACILITY OPERATING LICENSE No. R-103
DOCKET No. 50-186**

THIS PAGE INTENTIONALLY LEFT BLANK

TABLE OF CONTENTS

A.0	SAFETY LIMITS AND LIMITING SAFETY SYSTEM SETTINGS.....	A-1
A.1	SAFETY LIMITS	A-1
A.2	LIMITING SAFETY SYSTEM SETTINGS.....	A-2
A.3	LIMITING CONDITIONS FOR OPERATIONS	A-4
	A.3.1 Reactor Core Parameters.....	A-4
A.4	SURVEILLANCE REQUIREMENTS	A-5
	A.4.1 Reactor Core Parameters.....	A-5
A.5	DESIGN FEATURES.....	A-5
	A.5.1 Reactor Core and Fuel	A-5

A.0 SAFETY LIMITS AND LIMITING SAFETY SYSTEM SETTINGS

The Technical Specifications represent the administrative controls, equipment availability, operational conditions and limits, and other requirements imposed on reactor facility operation in order to protect the environment and the health and safety of the facility staff and the general public in accordance with 10 CFR 50.36.

The Technical Specifications are normally divided into the following six sections:

- Section 1 - Definitions
- Section 2 - Safety Limits (SL) and Limiting Safety System Settings (LSSS)
- Section 3 - Limiting Conditions for Operations (LCO)
- Section 4 - Surveillance Requirements
- Section 5 - Design Features
- Section 6 - Administrative Controls

Specific limitations and equipment requirements for safe reactor operation and for dealing with abnormal situations are called specifications. These specifications, typically derived from the facility descriptions and safety considerations contained in the Safety Analysis Report (SAR), represent a comprehensive envelope of safe operation. Only those operational parameters and equipment requirements directly related to preserving that safe envelope are listed in the Technical Specifications. Procedures or actions employed to meet the requirements of these Technical Specifications are not included in the Technical Specifications. Normal operation of the reactor within the limits of the Technical Specifications will not result in off-site radiation exposure in excess of 10 CFR 20 guidelines.

Only those specifications that have been changed as a result of conversion from HEU to LEU are included here. Changes are noted by strikethrough of text that is related to HEU operations and underlining text related to LEU operations.

Specifications in Sections 2, 3, 4 and 5 provide related information in the following format shown:

- Applicability - This indicates which components are involved;
- Objective - This indicates the purpose of the specification(s);
- Specification(s) - This provides specific data, conditions, or limitations that bound a system or operation. This is the most important statement in the Technical Specifications; and
- Bases - This provides the background or reasoning for the choice of specification(s), or references a particular section of the SAR that does.

A.1 SAFETY LIMITS

Applicability:

This specification applies to the reactor fuel.

Objective:

The objective of this specification is to define the maximum reactor fuel element temperature that can be permitted to ensure that the integrity of the fuel cladding is maintained to guard against an uncontrolled release of radioactivity.

Specification:

- a. The temperature of a reactor fuel element shall not exceed ~~986 °F (530 °C)~~ the fuel temperature safety limit for any operating condition.

Bases:

- a. Maintaining the integrity of the fuel cladding requires that the ~~cladding fuel~~ fuel remain below the blistering temperature of ~~986 °F (530 °C)~~. A burnup-dependent fuel temperature safety for U-10Mo monolithic fuel is formulated based on blister threshold temperature data. For all operating conditions that avoid either a Departure from Nucleate Boiling (DNB), or exceeding the Critical Heat Flux (CHF), or the Onset of Flow Instability (OFI), fuel ~~cladding~~ fuel temperatures remain substantially below the fuel ~~blistering~~ blistering temperature safety limit (~~NUREG-1313~~).

A.2 LIMITING SAFETY SYSTEM SETTINGSApplicability:

This specification applies to the set points for the reactor safety system channels monitoring reactor power level, primary coolant flow rate, reactor inlet water temperature and pressurizer pressure.

Objective:

The objective of this specification is to assure that automatic protective action is initiated to prevent a safety limit from being exceeded.

Specification:a. Mode I Operation

Reactor Power Level (12 MW)	125% of full power (Maximum)
Primary Coolant Flow Rate	1,625 <u>1,675</u> gpm each loop ⁽¹⁾ (Minimum)
Reactor Inlet Water Temperature	155 <u>145</u> °F (Maximum)
Pressurizer Pressure	75 Psia (Minimum)

⁽¹⁾ Both primary coolant system loops are required to be in operation for Mode I.

b. **Mode III Operation**

Reactor Power Level (50 kW)	125% of full power (Maximum)
-----------------------------	------------------------------

Bases:

- a. The limiting safety system settings (LSSS) are set points which, if exceeded, will cause the reactor safety system to initiate a reactor scram. The LSSS were chosen such that the true value of any of the four safety-related variables, i.e., reactor power level, core flow rate, reactor inlet water temperature and pressurizer pressure will not exceed the operating limits under the most severe anticipated transient. Section 4.6.4 of the conversion PSARSAR and Amendment No. 36 presents analyses analysis to show that the LSSS for Mode I and H operation meet this criterion.
- b. For Mode III operation, the high power scram set point of 125% of full power will occur at 62.5 kW, thus, there is a margin of 87.5 kW between the LSSS and the operating limit of 150 kW.

A.3 LIMITING CONDITIONS FOR OPERATIONS

General: Limiting Conditions for Operations (LCOs) are those administratively established constraints on equipment and operational characteristics that shall be adhered to during operation of the facility. The LCOs are the lowest functional capability or performance level required for safe operation.

A.3.1 Reactor Core Parameters

Applicability:

This specification applies to the reactor core and fuel elements used in the reactor core.

Objective:

The objective of this specification is to assure that the reactor can be controlled and shut down at all times and that the fuel elements are operated within acceptable design considerations thus ensuring fuel element integrity is maintained.

Specification:

- a. The reactor shall not be operated using fuel in which anomalies have been detected or in which the dimension reduction of any coolant channel between the fuel plates exceeds ~~ten~~ eight (408) mils below the minimum of the fuel element acceptance criteria.

Bases:

- b. Specification 3.1.d assures that fuel elements which have been inspected and found to be defective are no longer used for reactor operation. Specification 5.3.c restricts the peak fissions per cubic centimeter burnup to $< 3.4 \times 10^{21}$, which results in less than 9% swelling of the fuel plates. A 9% swelling of a fuel plate would roughly equate to an increase in plate thickness of 4 mils. Assuming a worst-case scenario where two adjacent fuel plates swell towards the same coolant channel gap, this would cause a decrease in the nominal coolant channel gap of 8 mils. (Note: Nominal coolant channel gaps are either 92 or 93 mils, with a lower fabrication tolerance of 84 or 85 mils, respectively.) ~~Specification 5.3.c restricts the peak fissions per cubic centimeter burnup to values that have been correlated to result in less than 10% swelling of the fuel plates. 10% swelling of a fuel plate would roughly equate to an increase in plate thickness of 5 mils. Assuming a worst case scenario where two adjacent fuel plates swell towards the same coolant channel gap, this would cause a decrease in the nominal coolant channel gap of 10 mils (Note: Nominal coolant channel gap is 80 mils, with a lower fabrication tolerance of 72 mils).~~

A.4 SURVEILLANCE REQUIREMENTS

A.4.1 Reactor Core Parameters

Applicability:

This specification applies to the surveillance requirements of the reactor core parameters.

Objective:

The objective of this specification is to verify reactor core parameters which are directly related to reactor safety.

Specification:

- a. ~~One out of every eight (8) fuel elements that have reached their end-of-life shall be inspected for anomalies.~~ LEU fuel elements will have the element with the highest burnup from each pair of elements introduced into the core inspected for anomalies at the middle-of-life burnup (90 MWd) and when this element has reached the end-of-life.

Bases:

- b. The specified fuel element inspections along with the continuous primary coolant system fission product monitoring and the weekly radiochemical analysis of the primary coolant provide for the detection of anomalies resulting from reactor operation and reduces the possibility of fission product release to the primary coolant system. Inspecting the fuel elements at the end of their life has the added advantage of allowing for the decay of the fuel elements and, thus, reduction of exposure to personnel.

A.5 DESIGN FEATURES

A.5.1 Reactor Core and Fuel

Applicability:

This specification applies to the reactor core and fuel elements.

Objective:

The objective of this specification is to specify the general reactor core configuration and to assure that the fuel elements are of a type designed for use in the reactor.

Specification:

The following design features apply to the reactor core and fuel:

- a. The peak burnup for ~~UAl₄ dispersion~~ monolithic U-10Mo alloy fuel in MURR shall not exceed a calculated ~~2.3×10^{21}~~ 3.4×10^{21} fissions per cubic centimeter.

- b. Each reactor fuel element shall contain ~~2423~~ fuel-bearing plates with a nominal active length of 24 inches and a nominal plate thickness of ~~0.050~~0.044 inches for plates 1-22, and 0.049 inches for plate 23. The nominal distance between the fuel plates shall be ~~0.080~~0.092 inches for coolant channels 6-19 and 0.093 inches for coolant channels 1-5 and 20-23. Plate nominal cladding thickness shall be a minimum of ~~0.015~~0.012 inches, including the Zr interlayer.
- c. The fuel material shall be ~~aluminide dispersion UAlx~~monolithic U-10Mo alloy nominally enriched to ~~93~~19.75% in the isotope uranium-235.
- d. Each reactor fuel element shall have a maximum uranium-235 loading of ~~775~~1,507 grams.

Bases:

Specification 5.3.c restricts the peak fissions per cubic centimeter burnup to values that have been correlated to result in less than ~~109%~~ swelling of the fuel plates. ~~† Preliminary data has been found that fuel plate swelling at these fission densities less than 10% has no detrimental effect on fuel plate performance (Ref.: Change No. 4 to Facility License No. R-103, Change No. 6 to Facility License No. R-103, and Application dated September 12, 1986 with supplements).~~ † Preliminary data has been found that fuel plate swelling at these fission densities less than 10% has no detrimental effect on fuel plate performance (Ref.: Change No. 4 to Facility License No. R-103, Change No. 6 to Facility License No. R-103, and Application dated September 12, 1986 with supplements).

- e-g. The MURR reactor fuel elements are one of a configuration (~~aluminide UAlx dispersion~~monolithic U-10Mo alloy fuel system) ~~successfully and extensively used for many years in test and research reactors~~which is currently being qualified for use in test and research reactors in the US. Specifications 5.3.e, 5.3.f, and 5.3.g require fuel content, materials and dimensions of the fuel elements to be in accordance with the design and fabrication specifications (Ref. Section 4.2.1 of the conversion PSAR).

THIS PAGE INTENTIONALLY LEFT BLANK

APPENDIX B

**RADIOLOGICAL IMPACT OF AR-41
DURING NORMAL OPERATIONS**

THIS PAGE INTENTIONALLY LEFT BLANK

B.0 RADIOLOGICAL IMPACT OF AR-41 DURING NORMAL OPERATION

As discussed in Section 11.1.1.1.1, Ar-41 from the Pneumatic Tube System, argon-41 (^{41}Ar) is produced in the pneumatic tube (p-tube) system, the thermal column and the beamports, with approximately 98% of the ^{41}Ar production from the p-tube system. MCNP calculations show there will be an approximately 5% increase in thermal flux (≤ 1.0 eV) in the graphite reflector region where the p-tube terminus is located when a conversion to low-enriched uranium (LEU) fuel and an uprate in power to 12 MWs is performed (See Tables 4-15 and 4-16). This will increase the operational radiation doses in the unrestricted area listed in Table B-4 minimally from 0.5 mrem/y to 0.525 mrem/y to an individual located 150 meters from the facility (Emergency Planning Zone) and from 3.0 mrem/y to 3.15 mrem/y to an individual 760 meters from the facility (nearest resident).

THIS PAGE INTENTIONALLY LEFT BLANK

APPENDIX C

THERMAL-HYDRAULIC TRANSIENT ANALYSIS

THIS PAGE INTENTIONALLY LEFT BLANK

TABLE OF CONTENTS

C.0	Thermal-Hydraulic Transient Analysis.....	C-1
C.1	Introduction.....	C-1
C.2	Methodology for Transient Analysis of the Reactor System.....	C-1
C.2.1	RELAP5 Application.....	C-1
C.2.2	Modeling of the MURR.....	C-2
C.2.2.1	Reactor Pressure Vessels	C-2
C.2.2.2	Primary Coolant Loop.....	C-3
C.2.2.3	Secondary Coolant Loop.....	C-8
C.2.2.4	Bulk Reactor Pool and Pool Coolant Loop.....	C-9
C.2.2.5	Anti-Siphon System	C-11
C.2.2.6	In-Pool Heat Exchanger Loop	C-12
C.2.2.7	Fuel Elements.....	C-16
C.2.2.8	Plant Protection System	C-25
C.2.2.9	Reactor Inlet Check Valve, V502	C-30
C.2.2.10	Core Flow Redistribution Due to Burnup.....	C-31
C.2.2.11	Mode III (Natural Convective) Operation	C-33

LIST OF FIGURES

Figure C.1 Diagram of MURR Primary System Loop	C-4
Figure C.2 Primary System Pipe Sizes in the MURR RELAP5 Model	C-7
Figure C.3 Detailed RELAP5 Model of the MURR Bulk Reactor Pool and Pool Coolant Loop	C-10
Figure C.4 Anti-Siphon System Air Volume.....	C-13
Figure C.5 In-Pool Heat Exchanger Data Provided by Reference C-7.....	C-15
Figure C.6 RELAP5 Model of the Circulation Loop Between the Reactor Core and the in-Pool Heat Exchanger.....	C-16
Figure C.7 HEU Reactor Core Element Nodal Structure	C-18
Figure C.8 LEU Reactor Core Element Nodal Structure.....	C-19
Figure C.9 Comparison of RELAP5 and PLTEMP/ANL Maximum Fuel Temperatures.....	C-22
Figure C.10 Trip 1: Core Outlet Pressure	C-26
Figure C.11 Trips 2 and 3: Primary Flow	C-26
Figure C.12 Trip 4: Core Inlet Pressure.....	C-27
Figure C.13 Trip 5: Core Pressure Drop.....	C-27
Figure C.14 Trip 7: Core Outlet Isolation Valve Starts to Close.....	C-27
Figure C.15 Trip 8: Core Inlet Isolation Valve Starts to Close	C-28
Figure C.16 Trip 99: Site Electric Power is Lost.....	C-28
Figure C.17 Core Inlet Check Valve V502.....	C-31
Figure C.18 RELAP5 Model for Mode III Analysis	C-35

LIST OF TABLES

Table C-1 Components of the Pool Coolant Loop Thermal-Hydraulics Model.....	C-11
Table C-2 Anti-Siphon System Model Volumes	C-14
Table C-3 Inner and Outer Radii of Fresh Fuel Plates, inches	C-20
Table C-4 Relative Power Post Scram.....	C-24
Table C-5 Plant Protection System Setpoints	C-28
Table C-6 Element Burnup and Channel Reduction.....	C-32

REFERENCES

- C-1. J. C. Posey, "Release of Fission Products from Miniature Fuel Plates at Elevated Temperature," Proceedings of the Intl. Meeting on Research and Test Reactor Core Conversions from HEU to LEU Fuel, ANL/RERTR/TM-4, Argonne National Laboratory, November 1982.
- C-2. T. Shibata, *et al.*, "Release of Fission Products from Irradiated Aluminide Fuel at High Temperatures," Proceedings of the Intl. Meeting on Research and Test Reactor Core Conversions from HEU to LEU Fuel, ANL/RERTR/TM-4, Argonne National Laboratory, November 1982.
- C-3. *Guidelines for Preparing and Reviewing Applications for the Licensing of Non-Power Reactors, Standard Format and Content*, NUREG-1537, Part 1, United States Nuclear Regulatory Commission, February 1996.
- C-4. *Guidelines for Preparing and Reviewing Applications for the Licensing of Non-Power Reactors, Standard Review Plan and Acceptance Criteria*, NUREG-1537, Part 2, United States Nuclear Regulatory Commission, February 1996.
- C-5. J. A. Stillman, *et al.*, *Accident Analysis for Conversion of the University of Missouri Research Reactor (MURR) for Highly-Enriched to Low-Enriched Uranium*, ANL/GTRI/TM-14/5, Revision 1, Argonne National Laboratory, February 2017.
- C-6. The RELAP5/MOD3.3 Code Manual, Nuclear Systems Analysis Division, Information Systems Laboratories, Inc., Rockville, Maryland and Idaho Falls, Idaho, Prepared for the Division of Systems Research, Office of Nuclear Regulatory Research, U. S. Nuclear Regulatory Commission, Washington, DC 20555, March 2006.
- C-7. *MURR Hazards Summary Report*, University of Missouri Research Reactor Facility, July 1965.
- C-8. Arne P. Olson and Kalimullah, *A User's Guide to the PLTEMP/ANL Code*, Version 4.1, ANL/RERTR/TM-11-22, Nuclear Engineering Division, Argonne National Laboratory, Argonne, IL, April 6, 2011.
- C-9. E. E. Feldman, *et al.*, *Technical Basis in Support of the Conversion of the University of Missouri Research Reactor (MURR) Core from Highly-Enriched to Low-Enriched Uranium – Steady-State Thermal-Hydraulic Analysis*, ANL/RERTR/TM-12-37, Rev. 1, Argonne National Laboratory, January 2013.
- C-10. A. P. Olson, *A Users Guide to the PARET/ANL Code*, ANL/RERTR/TM-11-38, Version 7.5, Argonne National Laboratory, August 14, 2012.

C.0 Thermal-Hydraulic Transient Analysis

C.1 Introduction

The potential for fuel damage has been evaluated for various accidents and transients postulated for the University of Missouri Research Reactor (MURR). Data has been collected on fuel performance after exposure to elevated temperatures. This post-irradiation testing is performed by annealing plates. Inspection follows to determine whether blistering has occurred. Hence, this process is known as a 'blister test'. Historically this test has been established as a basis for retention of fission products (Refs. C-1 and C-2). Consequently, blister temperature data have been used to establish fuel temperature safety limits for fuel being operated in reactors (Refs. 13.8 and 13.9).

A substantial portion of the information provided in this appendix is from the reference J. A. Stillman, et al., *Accident Analyses for Conversion of the University of Missouri Research Reactor (MURR) from Highly-Enriched to Low-Enriched Uranium*, ANL/GTRI/TM-14/5, Revision 1 (Ref. C-5).

The computer code RELAP5/MOD3.3 (Ref. 13.3) was used to perform the thermal-hydraulic transient analyses needed to determine the peak fuel plate temperatures reached for each of the accidents analyzed.

C.2 Methodology for Transient Analysis of the Reactor System

C.2.1 RELAP5 Application

RELAP5 is a light- and heavy-water reactor transient analysis code developed by the Idaho National Laboratory (INL) for the U.S. Nuclear Regulatory Commission (NRC) and is now maintained by Information Systems Laboratories, Inc. (Ref. 13.3). It is capable of analyzing a wide variety of thermal-hydraulic transients in nuclear and non-nuclear systems involving mixtures of steam, water (light/heavy), non-condensables, and solute. RELAP5 is one of the most widely used system codes for analyzing reactor accidents/transients. The U.S. Department of Energy (DOE) has utilized RELAP5 to analyze design basis accidents for the Advanced Test Reactor (ATR) and High Flux Isotope Reactor (HFIR) in their respective Safety Analysis Reports (SARs). RELAP5 has also been applied to the analysis of the High Flux Beam Reactor (HFBR), the National Institute of Standards and Technology Reactor (NBSR), and the Massachusetts Institute of Technology Reactor (MITR). The MURR fuel element and reactor design is closest in design to the ATR, but can also be related to other research reactor designs and fuel element geometries (Material Test Reactor plate-type).

RELAP5/MOD3.3, the current version of the code system, was developed with the objective of creating a code version suitable for the analysis of postulated accidents in water reactor systems, including both large- and small-break loss of coolant accidents (LOCAs) as well as a full range of operational transients. The hydrodynamic model in RELAP5/MOD3.3 is a one-dimensional, transient, two-fluid model for flow of a two-phase steam-water mixture. The non-equilibrium transient two-fluid model is represented by the conservation equations of mass, momentum, and energy for each phase. The steam phase can contain non-condensable components and the water

phase can have a solute component. Special process models are available to handle choked flow, abrupt area changes, and counter-current flow.

Metal components are modeled by heat structures with internal heat generation. Heat transfer within the structures is by one-dimensional heat conduction. A full boiling curve is implemented in the code for modeling heat transfer between heat structures and the coolant. Reactor power and decay power can be calculated by a point kinetics model with reactivity feedback. A tabular input of power vs. time also can be used. In RELAP5/MOD3.3, a hydraulic system is constructed by connecting fluid components, such as pipes, valves, pumps, etc., in series or in parallel. Geometric data is required for the interconnecting components. Heat structures are defined with the heat transfer surface facing the coolant in a hydraulic component. Time varying boundary conditions can be specified in terms of fluid flow rate or the thermodynamic state of the fluid. Control system components are available in RELAP5/MOD3.3 to model system dynamic behavior, such as component trips and the evaluation of system variables.

C.2.2 Modeling of the MURR

The fuel region is cooled by a pressurized primary coolant system which, at 10 MW for HEU core and 12 MW for LEU core, circulates a nominal 3,750 gpm (14,195 lpm) of light-water coolant through the reactor pressure vessels. The reflector region, the control blade region, and the center test hole are cooled by pool water which is drawn through these regions and circulated through the pool coolant system at a nominal flow rate of 1,200 gpm (4,542 lpm). The heat from the pool and primary coolant systems is transferred to a secondary coolant system by means of separate pool and primary heat exchangers. The heat is then dissipated to the atmosphere through a cooling tower.

The RELAP5/MOD3.3 model of the MURR simulates the transport of heat and coolant in both the primary and pool coolant systems. The reactor pressure vessels, the primary coolant loop, the bulk reactor pool, and the pool coolant loop are represented by a series of hydrodynamic volumes. Fuel plates in the core region are represented by heat structures. Steady-state and decay power are controlled as time-dependent variables in RELAP5/MOD3.3.

The discussion of the MURR model below is grouped into eleven sub-sections: the reactor pressure vessels, the primary coolant loop, the secondary coolant loop, the bulk reactor pool and pool coolant loop, anti-siphon system, in-pool heat exchanger loop, the fuel elements, the plant protection system, reactor inlet check valve, core flow redistribution due to burnup, and Mode III (natural convective) operation. A component number, as defined in the RELAP5/MOD3.3 input file, is used to identify each hydrodynamic volume and heat structure modeled.

C.2.2.1 Reactor Pressure Vessels

Two cylindrical reactor pressure vessels provide a fixed geometry for the reactor fuel region consisting of eight (8) fuel elements having identical physical dimensions placed vertically around the annulus formed between the pressure vessels.

The pressure vessels, including the reactor core assembly, the fuel element support matrix, and the reflector support assembly are supported from the bottom of the reactor pool in circular sections, which also serve as part of the primary and pool coolant piping.

C.2.2.2 Primary Coolant Loop

Parallel flow paths in the MURR primary coolant loop are modeled by combining them into a single effective flow path. This applies to the split in the primary coolant loop into two branches through the two primary coolant pumps and two primary coolant heat exchangers. This simplification does not have a significant effect on the RELAP5/MOD3.3 analysis since the parallel flow paths are thermally and hydraulically similar. Additionally, after the first several seconds of the loss-of-coolant transients, the primary coolant piping with parallel flow paths are no longer involved in flow through the core because the core isolation valves fully close within 10 seconds in depressurization transients.

Figure C.1 provides a schematic representation of the MURR primary coolant system loop. In the figure the elevations are represented to scale, but the piping lengths, in general, are not to scale. The solid red rectangle on the left side of the figure represents the reactor annular core. When operating, the flow goes downward through the core to the lower plenum. From there the flow follows the piping that is shown in black through the hot-leg exit isolation valve V507A and on to the primary coolant pumps. (Although the figure shows a gap to avoid overlapping the V507B valve, the piping from the V507A valve to the pump is continuous.) In the plant there are two parallel pump paths, each with its own pump and check valve. After the check valves the two parallel paths rejoin for 7 feet before dividing into two paths again, each with a heat exchanger followed by a V540A or V540B diaphragm valve. Then these two parallel paths merge and follow a path to core inlet isolation valve V507B. In the simulation model, the two essentially identical parallel pump paths are combined into a single equivalent path, as are the two heat exchanger paths. After inlet isolation valve V507B, the primary piping enters the pool and the flow goes through check valve V502 to the upper plenum, which connects to the top of the reactor pressure vessel above the core. A description of this check valve and the key parameters used in modeling it with RELAP5 are provided below in Section C.2.2.9.

The upper plenum, reactor core, and lower plenum are contained within the pressurized primary coolant annular volume located between the inner and outer reactor pressure vessels, which are not explicitly labeled in Figure C.1. The shaded area in the figure labeled near the top "Inside of the Pool" indicates the pool water, which surrounds the outer reactor pressure vessel and piping adjacent to the vessel. The pool water also flows down through the inner pressure vessel. The surface of the pool is at atmospheric pressure, which is taken to be 14.3 psia. The reactor safety systems and pool water limit the loss of coolant due to a primary loop breach that occurs within the pool boundary. Isolation valves V507A and V507B close after a substantial drop in core outlet pressure occurs in order to minimize the potential for loss of coolant from the reactor pressure vessels during a LOCA. As Figure C.1 shows, the piping exiting the lower plenum rises back up to near the top of the pressure vessels before turning back downward. This "inverted loop" piping arrangement is to minimize the loss of coolant from the reactor pressure vessels should the reactor exit pipe break outside the pool.

The "Fixed Pressure Source" labeled in the middle of Figure C.1 is the plant pressurizer, which is attached via 2-inch piping to Loop 'A,' which is one of the two parallel heat exchanger paths. In the model, the two paths are combined into a single path, which has the hydraulic diameters of each path and the combined flow areas of the two paths. The pressurizer is attached to the combined path in the model. Pressurizer isolation valve V527, located along the 2-inch line, is also shown in the figure.

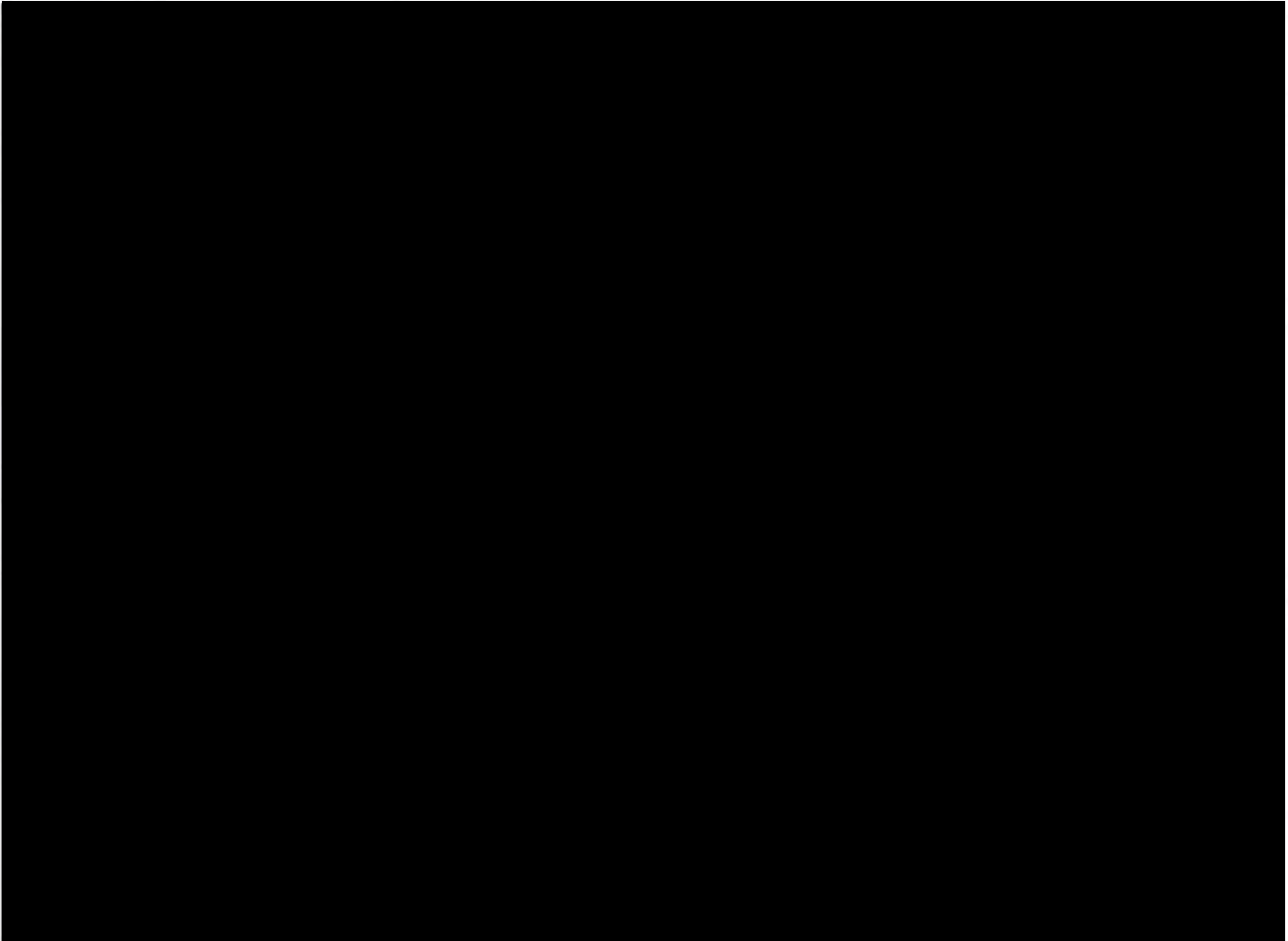


FIGURE C.1
DIAGRAM OF MURR PRIMARY SYSTEM LOOP

A primary loop breach that occurs within the pool results in a depressurization and ejection of primary coolant from the pressurized system to the open pool. The primary loop breaches of greater concern are the ones that occur outside of the pool, especially those that occur between the exterior of the pool wall and either of the two main isolation valves (V507B and V507A). The six light green vertical arrows in Figure C.1 indicate locations in the model where pipe breaks can be simulated. Although not shown in the figure, at each arrow there is a fixed-pressure air sink at 14.3 psia that is separated from the pipe at that location by a closed valve whose full open diameter matches the pipe to which it is attached – 12, 8, or 2 inches. (All of these pipes are Schedule 40.)

In a LOCA simulation one or more of these closed valves are assumed to instantaneously go to its full open position, connecting the pipe to the adjacent fixed-pressure sink modeling a fully ruptured pipe.

Because all of these accidents are initiated by a depressurization of the primary loop, the automatic actions taken by the plant protection system are the same in each instance. A reactor scram is promptly initiated, the primary coolant pumps are tripped, the two parallel redundant anti-siphon isolation valves (V543 in Figure C.1) are opened, the two primary loop isolation valves (V507A and V507B) are closed, the two parallel redundant valves to the in-pool heat exchanger (V546 in Figure C.1) are opened, and the pressurizer isolation valve V527C (V527 in Figure C.1) is closed. The scram rapidly reduces the reactor power to decay heat levels, while the closing of valves V507A, V507B, and V527C is designed to minimize the loss of coolant from the plant.

The anti-siphon system contains compressed air that is injected into the top of the hot leg inverted loop by opening valves V543A and V543B, V543 in Figure C.1. In the event of a hot-leg break immediately upstream of valve V507A, this compressed air is designed to evacuate the down-flow portion of the hot leg leading to valve V507A and prevent the siphoning of water from the reactor pressure vessels. Similarly, check valve V502 (Check Valve V502 in Figure C.1) on the primary inlet pipe riser is designed to limit siphoning from the cold-leg side of the reactor pressure vessels.

The in-pool heat exchanger is designed to facilitate decay heat removal from the core to the pool in a loss-of-flow accident when isolation valves V507A and V507B are closed. The system is designed so that when these isolation valves are closed and the in-pool heat exchanger valves are open, water can circulate by natural circulation between the core and this heat exchanger. After the flow coasts down, the buoyancy due to core heat causes the core flow direction to reverse. Heated coolant from the core travels upward and is cooled in the in-pool heat exchanger, which is immersed in the pool, and then travels downward and returns to bottom of the core via the reactor normal outlet plenum. However, the air injected into the primary loop by the opening of the anti-siphon valves during a LOCA and water vapor (until it condenses) can collect at the top of the in-pool heat exchanger and severely impede or stop the natural circulation of water between the core and the in-pool heat exchanger. Thus, the long-term decay heat removal in the LOCA is largely through the reactor pressure vessel walls. The in-pool heat exchanger is more useful during LOFAs and during normal reactor shutdowns.

Heat removal through the pressure vessel walls is enhanced by forced pool flow over the outer surfaces of the reactor pressure vessels, specifically in the island tube at the core center and in the control blade channels that surround the core. This flow is driven by the pool pump, which is not tripped as a result of a LOCA. The control blade channels do not extend significantly above the core. Hence, virtually the entire outer convex surface of the outer reactor pressure vessel above the core is cooled by free convection from the wall surface to the pool water. This free convection can be very effective in transferring decay heat to the pool water. Also, when there is no net flow through the reactor core, recirculation among the core coolant channels, with upward flow in the warmer channels and downward flow in the cooler channels, may substantially facilitate heat removal.

During normal operation the V546 valves at the top of the in-pool heat exchanger are closed and stop the flow through this heat exchanger, which is shown in red in Figure C.1. Then the primary flow follows the path shown in black in the direction of the arrows.

The two primary coolant circulation pumps are horizontal, centrifugal, single-stage pumps that are direct-connected to 125-HP drive units through flexible couplings. These pumps are modeled as a single pump with the characteristics of the combined pumps supplying approximately 3,750 gpm (14,195 lpm) with sufficient discharge head to overcome system pressure drop losses.

Figure C.1 has been revised to form Figure C.2, which shows the primary loop piping dimensions in considerable detail. In Figure C.2 a form of shorthand was used to represent the dimensions of each piping path. For example, alongside the core outlet riser pipe, the piping dimension is given as "100(2-3), 12" diam., 9.834". The 100 is the RELAP5 component (pipe) number. The "(2-3)" implies that these are nodes 2 and 3 of RELAP5 component 100. The "12" diam." implies that this is a 12-inch diameter pipe. All of the pipes in the primary loop are Schedule 40 pipes unless otherwise noted. Therefore, one can deduce from a table of pipe schedules that this pipe has an outside diameter of 12.75 inches and a wall thickness of 0.406 inches. Hence, the inside diameter and the flow area can be calculated. The "9.834" in the dimension implies that the length of the two nodes taken together is 9.834 feet long. If the change in elevation is not given in the figure, the component is assumed to be vertical or horizontal. When this is not the case, the elevation change is the " Δh " dimension. For example, the reactor outlet plenum has the label "501 (br), 0.6048 ft², 6.437', $\Delta h = -5.937$ ". "501" is the component number in the RELAP5 model. The "(br)" implies that it is a branch component in RELAP5. (A branch in RELAP5 is a single volume in RELAP5 with up to nine built-in junction points for connecting other volumes to the branch.) The "0.6048 ft²" is the flow area. "6.437'" is the length of the node that is used for calculating the volume of the node. The elevation change in the normal flow direction is 5.937 feet downwards. The magnitude of the elevation change is less than the volume length because in the plant the inlet pipe is below the top of the volume. Contrary to the figure, in the RELAP5 model the inlet pipe is connected to the top of the branch rather than at 0.500 feet below the top. However, in the model the change in elevation is only 5.937 feet. Thus, in the model, the elevation change and the nodal volume are correctly represented, but the flow traverses the entire length of the volume rather than only the lower 5.937 feet of it. This slight modeling approximation is deemed minor and in line with other modeling approximations.

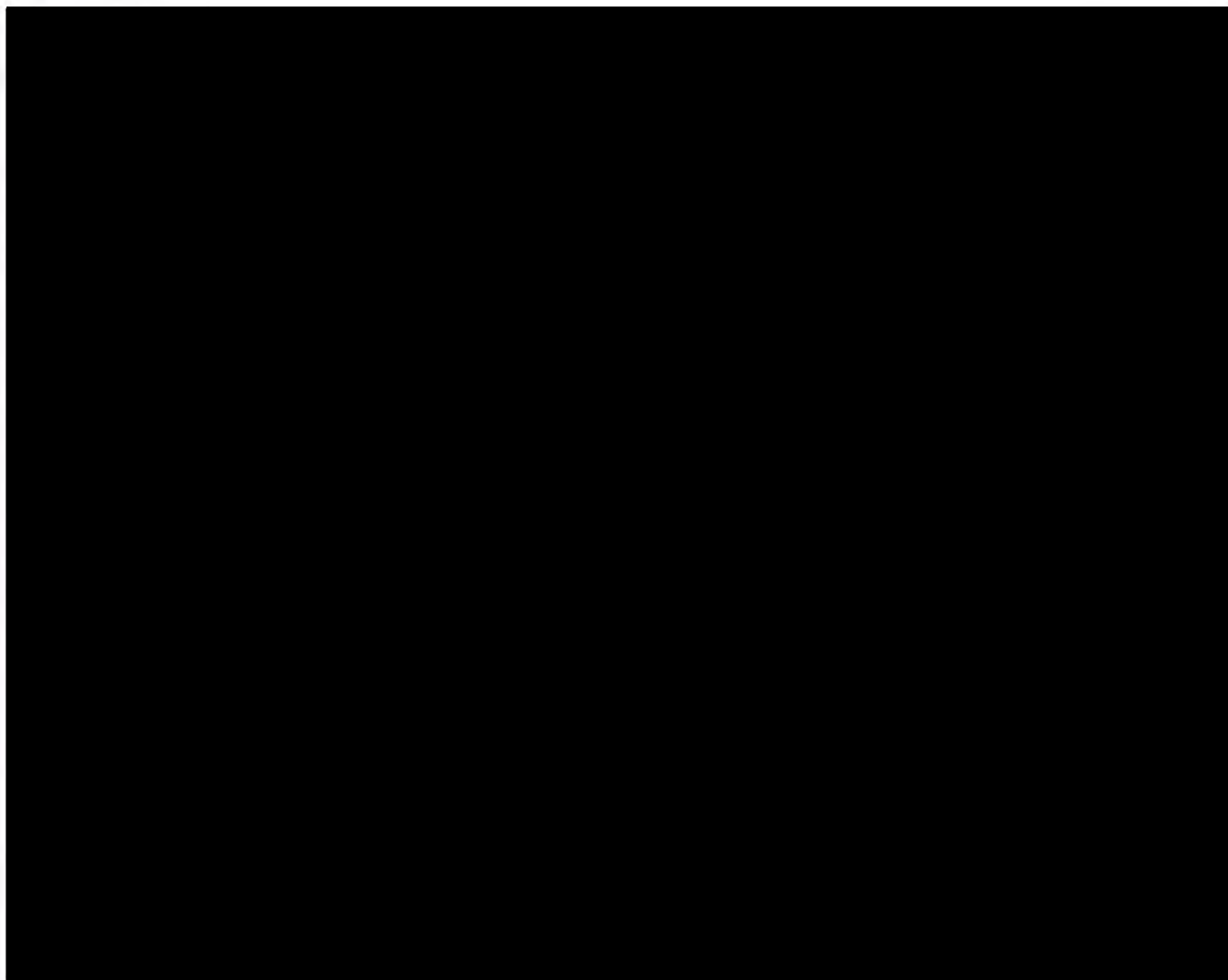


FIGURE C.2
PRIMARY SYSTEM PIPE SIZES IN THE MURR RELAP5 MODEL

In Figure C.2, the point where one piping segment ends and an adjacent one begins is sometimes marked by a black or blue line. A line to mark the transition is not used where there is an obvious change in direction. There are only four blue marker lines and they are thicker than the black ones. These are to indicate where one path in the plant splits into two or two merge into one. Hence, there is a blue line upstream of the pump to note the transition from a 12-inch pipe to two 8-inch pipes. The pipe dimension "2 × 8" diam." signifies two Schedule 40 8-inch pipes in parallel. There is another blue line where the two pump paths merge, followed by another where the path in the plant splits for the two parallel heat exchanger paths. The fourth blue line is after the valves that are downstream of the heat exchangers. Of course, there is only one pressurizer in the plant, which is represented as a fixed pressure source in the model and is connected to only one of two parallel paths, Loop A in the plant. The horizontal path downstream of valve V507A, which is interrupted by valve V507B in the figure, is a total of 31.832 feet in length, as indicated in the figure. In the RELAP5 model the heat transfer between the pool and the components immersed in it is explicitly represented.

C.2.2.3 Secondary Coolant Loop

The primary coolant heat exchangers are plate-type with all surfaces in contact with the reactor coolant constructed of stainless steel. . At a maximum of 1,600 gpm (6,057 lpm) of secondary water flow and an inlet water temperature at 87 °F (31 °C), one heat exchanger is capable of removing 17×10^6 BTU/h of heat from 1,800 gpm (6,814 lpm) of primary coolant water and returning it at 140 °F (60 °C). Two heat exchangers are installed for design power operation.

During normal reactor operation, heat is removed from the primary coolant system by the two parallel primary-loop heat exchangers and from the pool coolant system by a third exchanger. The water flowing on the secondary sides of these three heat exchangers transfers the heat to a cooling tower where the heat is dissipated to the atmosphere. In the RELAP5 model the two primary-loop heat exchangers are represented as a single component. In the model both the primary and the pool heat exchangers are represented as counter flow heat exchanges in which the initial steady-state flow rate on the secondary side is fixed and approximately equally to the primary-side flow rate. These secondary-side flow rates were reduced to relatively low values over the first five seconds of the transient so that excessive heat removal would not follow the scram.

For much of the analysis, a trial-and-error method was used to obtain the inlet temperatures to the secondary sides of the heat exchangers that produced the desired cold-leg temperatures for the primary and pool loops, which in the RELAP5 models were observed at the first primary-side node after the heat exchanger. RELAP5 was executed multiple times to calibrate the steady-state solution by adjusting the secondary side inlet temperatures (nodes 910 and 751 of the heat exchangers) until the desired cold-leg loop temperatures were obtained (node 1 of pipe 115 and node 5 of pipe 700). To obtain the desired primary exit coolant temperature, one would use a guessed value for each of the two secondary-side inlet temperatures during the model initialization process. If the desired heat exchanger primary exit temperatures were not achieved, the initialization process was repeated with new guessed values. This typically required several iterations in which a null transient was executed for 1,000 seconds for each iteration. The null transient solution that produced the desired inlet temperatures was restarted, another 100 seconds of null transient was executed to smooth out any discontinuity that was introduced by the restart, and then the transient was initiated.

The above initialization process is cumbersome, time-consuming, and takes a fair amount of human interaction. A better method is to include a proportional-integral (PI) control in the RELAP5 model for each of the two secondary inlet temperatures that is to be obtained. The model calculates the difference between the desired and predicted primary-side exit temperature – at node 1 of pipe 115 for the primary loop inlet temperature (Figure C.2) and at node 5 of pipe 700 for the tank temperature. Based on this error and the integral of it, the PI controller adjusts the secondary-side inlet temperature – (RELAP5 time-dependent) volume 910 for the reactor loop heat exchanger and (RELAP5 time-dependent) volume 751 for the pool-loop heat exchanger – until the desired primary-side outlet temperature is obtained. Logic was included in the controllers to prevent them from functioning and changing the secondary-side inlet temperatures during the simulation of the transient itself. It took some experimentation to find effective controller constants. With the PI controllers in place, the RELAP5 model initialization and null transient was accomplished in less than 200 seconds and a steady-state condition was clearly demonstrated before 200 seconds. Because the initialization could be completed in a single 200-second RELAP5 execution, the

transient was initiated at 200 s and typically execution was continued for 100 more seconds and the problem was terminated at 300 seconds. These 100 seconds of transient simulation was usually more than enough to show that the peak fuel temperature had been achieved and that the most severe conditions had occurred.

C.2.2.4 Bulk Reactor Pool and Pool Coolant Loop

The bulk reactor pool is an aluminum-lined structure 10 feet (3 m) in diameter and 30 feet (9.1 m) deep containing approximately 20,000 gallons (75,708 l) of light water.

The pool coolant loop is modeled by a single effective flow path combining the two pool coolant pumps and pool coolant heat exchanger. This simplification does not have a significant effect on the RELAP5 analysis since the parallel flow paths are thermally and hydraulically similar. The interaction of the pool with the reactor pressure vessels, control rod gap, and the graphite reflector is explicitly modeled. A detailed representation of the RELAP/MOD3.3 model of the bulk reactor pool and pool coolant loop is shown in Figure C.3. The specific components used to define the pool coolant loop are described in Table C-1. As Figure C.3 and the table indicate parallel pipes 705, 715, and 725, respectively, represent the downward flow through the center flux trap, the flow through the control blade channel, and the flow through the reflector. The fourth parallel path, pipe 735, represents the flow through reflector plenum natural convection valve V547 (Butterfly Valve), which is always open. It should be noted that although the total pool coolant flow rate is 1,200 gpm (4,542 lpm) in MURR, a more conservative pool coolant flow rate of 1,100 gpm (4,164 lpm) was used in the analysis.

In the original MURR design, valve V547 would be closed during normal operation and would open upon loss of forced pool loop flow. Then this opened valve would allow natural circulation of pool coolant into the lower plenum (lower reflector tank cylinder) and up through the reflector elements, the control blade gaps, and the center test hole (flux trap). To ensure compliance with the Institute of Electrical and Electronic Engineers Standard 279 (IEEE-279), Single Failure Criterion, this valve is presently left open. Operational experience has shown that valve V547 can be left in the open position while increasing normal pool flow to provide sufficient cooling to these regions. Since the Butterfly Valve is left open at all times, it is modeled in RELAP5/MOD3.3 as an open pipe.

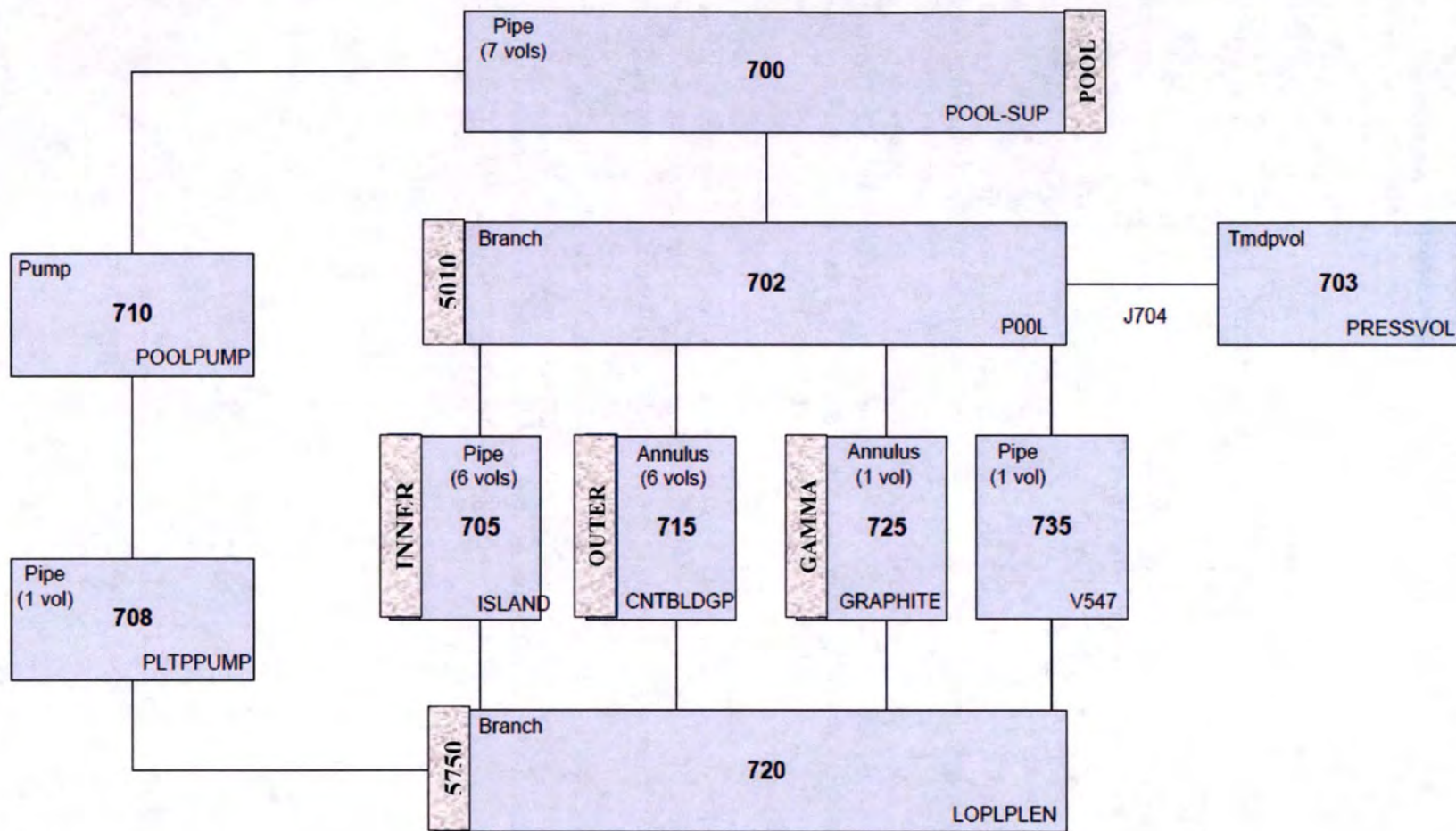


FIGURE C.3
 DETAILED RELAP5 MODEL OF THE MURR BULK REACTOR POOL AND POOL COOLANT LOOP

TABLE C-1
COMPONENTS OF THE POOL COOLANT LOOP THERMAL-HYDRAULICS MODEL

Number	Type	Description
700	Pipe	Pipe component from pool coolant pump to the pool. This pipe has 7 axial segments. The fourth one is attached to the heat structure that represents the pool heat exchanger.
702	Branch	Branch component as input for through-core components. This branch component is sized to represent the significant pool volume.
703	Time-dependent volume	Time dependent volume which establishes the pool surface at atmospheric pressure.
704	Single junction	Junction between the modeled open atmosphere and the pool surface.
705	Pipe	Pipe component representing flow through the center test hole, or flux trap. Heat transfer from the innermost reactor core coolant channels of the reactor core, through the inner pressure vessel wall to the flux trap is represented in the RELAP5 model.
708	Pipe	Pipe component from the lower plenum to the pool coolant pump.
710	Pump	Pump component establishing pool flow.
715	Annulus	Pipe component representing flow through the control blade gap external to the pressure vessels. Heat transfer from the outermost reactor core coolant channels through the outer pressure vessel wall to the control blade channels is represented in the RELAP5 model.
720	Branch	Branch collecting flow from the various through-core or bypass elements.
725	Annulus	Pipe component representing flow through the sample positions in the graphite reflector. In the RELAP5 model all of the power deposited outside of the reactor core is deposited here.
735	Pipe	Pipe component modeled as straight path since valve V547 is locked open.

C.2.2.5 Anti-Siphon System

The function of the anti-siphon system is to prevent the loss of water from the reactor core in the event of a rupture in the primary coolant system piping external to the reactor pool. The anti-siphon system functions as a backup system to the various safety instrumentation and equipment (e.g., pressure sensors, pump and valve interlocks, etc.) all of which ensures that the reactor core does not become uncovered during a LOCA. A rupture of the primary coolant system, followed by a loss of pressure, causes the anti-siphon system to admit a fixed volume of air to the high point of the reactor outlet piping, thus breaking any potential siphon which may have been created by the pipe rupture. As shown in Figure C.1, the RELAP5/MOD3.3 model incorporates a pressurized air volume at the appropriate point in the primary coolant system for injection upon detection of low pressure in the primary coolant loop.

Figure C.4 provides a sketch of the anti-siphon system. In the lower left there are two 4-inch valves, V543A and V543B, which connect to opposite sides of a 12-inch primary coolant pipe extension

above the inverted loop. This connection point is 10 inches below the lower horizontal header of the in-pool heat exchanger that also connects to the end pipe extension. As can be seen in Figure C.4, the two valves connect to two 4-inch pipes that merge into a single 4-inch pipe, which joins a $\frac{3}{4}$ -inch pipe just above the "refuel level". The $\frac{3}{4}$ -inch pipe is 45 inches long. After two 90° bends it connects to a closed 25-gallon tank that is filled with air. When the anti-siphon valves are open and the air volume has depressurized, water can enter and replace some of the air in the anti-siphon system. The right edge of the figure shows a dry well with a level sensor to measure the water level in the anti-siphon system and a venting line and valve through which the water can be forced out by adding air to the 25-gallon tank. The added volume for the level detection and venting is less than 4 gallons.

In the RELAP5 model valves V543A and V543B are combined into a single V543 valve. This valve connects to the middle of branch 406, as indicated in Figure C.2 and described in Section C.2.2.2 above. The valve area is that of two 4-inch valves. The air volume has been approximated by a series of three connected volumes, as indicated in Table C-2. As the table indicates, the first volume, which is furthest from the valve, is the 25-gallon tank and is nominally 16 inches in diameter and 30 inches long, the second volume is the $\frac{3}{4}$ -inch Schedule 40 pipe, and the third volume is the combined volume of the 4-inch pipes and the drywell. The volume of the 4-inch pipes in the third volume is about three times that of the drywell. Thus, merely adding the drywell volume to volume of the 4-inch pipes to form a single volume is a reasonable approximation. The air volumes were calculated from available drawings. In the model, the lengths of the first and third volumes are oriented vertically and the length of the second volume is oriented horizontally.

C.2.2.6 In-Pool Heat Exchanger Loop

The in-pool heat exchanger consists of ten vertical finned aluminum tubes that are approximately 5 feet long. Each tube has 14 internal vertical fins and 28 external vertical fins. The ten tubes are connected in parallel by two 6-inch diameter Schedule 40 curved header pipes, which are located in two parallel horizontal planes. The tubes are arranged along the header pipes in a 90° arc with a radius of curvature of 3.5 feet.

Figure C.5 provides data used in the MURR Hazards Summary Report (Ref. C-7) in modeling the in-pool heat exchanger and some of their derived quantities, such as areas and film coefficients. The dimensional data was used in the current analysis. In the RELAP5 model, the ten parallel tubes were represented by a single tube that was scaled to represent all ten tubes. The fins were included by increasing the heat transfer areas in the model. Figure C.6 shows the RELAP5 model of the circulation loop between the reactor core and the in-pool heat exchanger. This figure adds details that could not fit in Figure C.2. In Figure C.2 the two horizontal header pipes and the vertical finned tube are shown as red rectangles.

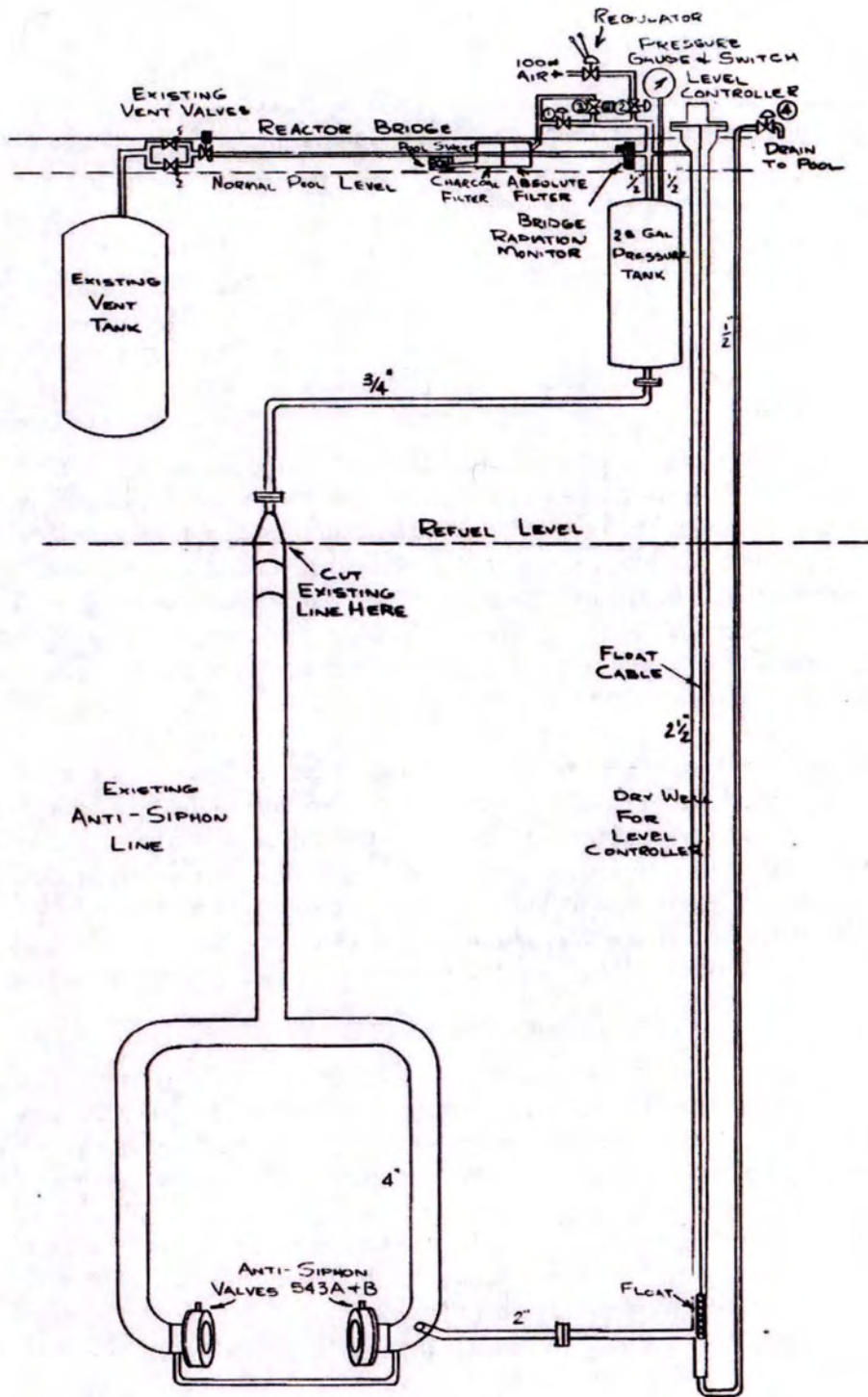


FIGURE C.4
ANTI-SIPHON SYSTEM AIR VOLUME

TABLE C-2
ANTI-SIPHON SYSTEM MODEL VOLUMES

Number	Description	Length, ft	Diameter, ft	Area, ft ²	Volume, ft ³
1	25-gallon tank	2.5	1.305	1.338	3.345
2	3/4-inch pipe	3.75	0.06867 (0.824 inch)	0.003704	0.014
3	4-inch pipe & drywell	10.0	0.5079	0.2026	2.026
Total		16.25			5.385 (40.28 gal)

Since the header pipes for the in-pool heat exchanger are 6-inch Schedule 40 pipes, the outside diameter is 6.625 inches, the wall thickness is 0.280 inches, and the inside diameter is 6.065 inches. The top header is 7 feet long. The bottom header is 8 feet long. There is an additional 26 inches of 6-inch pipe that connects the lower header to the vertical 12-inch diameter extension of primary piping that extends up 2.5 feet above the inverted loop. In the heat exchanger, all of the flow approaches the first tube, and about a tenth of the flow goes into the first tube. Nine-tenths of the flow continues through the header to the second tube, and a tenth of the flow goes into that tube. Flow continues in a like manner to all ten tubes.

An analogous situation exists at the lower (exit) header where the flows from each of the ten tubes combine and exit through the end of the header after the last tube in the flow path is reached. The flow behavior in the headers can only be approximated unless all ten vertical finned tubes are explicitly represented. As an approximation, since there is only one vertical tube in the model, each header was assumed to be half as long. Thus, the top 6-inch horizontal pipe was assumed to be 3.5 feet long and the bottom one was assumed to be 4 feet long plus the additional 26 inches in length, for a total of 74 inch = 6.167 feet. The flow areas of the two horizontal headers are each 0.2006 ft².

Although the inside diameter of each finned tube is 1.712 inches, its hydraulic diameter is only 0.4528 inches. This is because the hydraulic diameter is defined as four times the flow area divided by the wetted perimeter. If there were no internal fins, the hydraulic diameter would be the inside diameter. However, the fins reduce the flow area and increase the wetted perimeter.

Hydraulic resistances are important in flows driven by natural convection. The form- or K-losses are indicted in blue in Figure C.6. These losses can be a result of such things as elbows. The RELAP5 code uses built-in form losses where abrupt changes in area are indicated in the code input. These are in addition to the K-losses shown in the figure. Some of the locations of the K-losses are designated by blue circles. There is a 7.02-inch orifice near the top of the riser pipe, which is shown in the figure between node 3 of pipe 100 and the bottom of branch 101. It is modeled by RELAP5's abrupt area change model.

- Top horizontal header pipe:
 - Pipe center line is 62.5 inches above the bottom header center line
 - Pipe diameter 6 inches
 - Curvature radius 3.5 ft
 - Length of horizontal curved pipe 7 ft
 - Distance from center line of 6-inch riser pipe going to valve 546 center line is 1 inch
- Bottom horizontal header pipe:
 - Pipe center line is 30 inches above the center line of the 12-inch horizontal primary pipe going into the top of the pressure vessel
 - Pipe diameter 6 inches
 - Curvature radius 3.5 ft
 - Length of horizontal curved pipe 8 ft
 - 26-inch long horizontal straight piece of 6-inch pipe connects the 8-foot curved pipe to the 12-inch diameter vertical natural convection extension above the inverted loop
- Heat Exchanger tubes:
 - Tube OD 1.90 inches
 - Tube ID 1.712 inches
 - Number of tubes 10
 - Finned length 4.5 ft
 - External Fins:
 - Number 28
 - Thicknesses 0.05 inches
 - Height 0.5 inches
 - Internal Fins:
 - Number 14
 - Thicknesses 0.05 inches
 - Height 7 - 0.5 inches
 - 7 - 0.375 inches
 - Internal Net Flow Area 0.01389 ft^2
 - Internal Equivalent Diameter 0.0377 ft^2
 - Total Outside Surface Area $2.831 \text{ ft}^2/\text{ft}$.
 - For water at 180 °F with the finned tube properties the inside film coefficient is 396 BTU/hr - ft^2 - °F
 - The average value for the outside of the finned tube was 146.5 BTU/hr - ft^2 - °F
 - So the over-all heat transfer coefficient is 55 BTU/hr - ft^2 - °F

FIGURE C.5
IN-POOL HEAT EXCHANGER DATA PROVIDED BY REFERENCE C-7

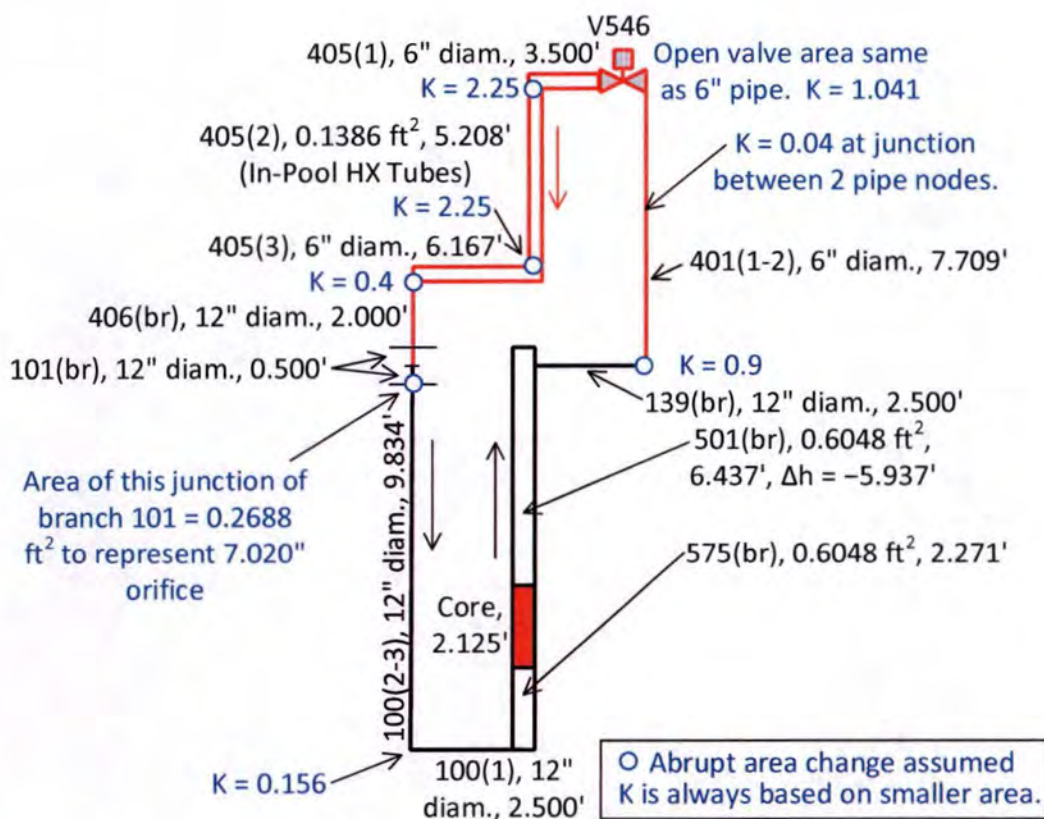


FIGURE C.6

RELAP5 MODEL OF THE CIRCULATION LOOP BETWEEN THE REACTOR CORE AND THE IN-POOL HEAT EXCHANGER

The improved heat transfer due to the fins was taken into account in the RELAP5 model by multiplying the heat transfer area without fins by a factor of 2.00 for the inside area and by a factor of 4.00 for the outside area. These values are obtained from the added fin surface area and the heat transfer efficiency as described in Section 5.3.2.10 of Ref. C-5. RELAP5 provides a parameter, which it calls a "fouling factor", which can be used to facilitate these heat transfer area increases. The heat transfer area and the film coefficient appear together as a product in the RELAP5 model. This product is multiplied by the RELAP5 fouling factor. When no value of fouling factor is provided in the input, the default value of 1.0 is used by the code.

C.2.2.7 Fuel Elements

In the RELAP5 model a single fuel element is scaled up by a factor of eight to represent all eight elements in the MURR core. In this element model all fuel plates and coolant channels are explicitly represented. Each channel has eight times the flow area of that of its single channel counterpart and each fuel plate has eight times the fuel, heat transfer area, and power of its single element counterpart. Figure C.7 and Figure C.8 provide the nodal structures for the HEU and LEU elements, respectively, as represented in their respective RELAP5 models. The blue areas of these

two figures are coolant. The pink areas are fuel plates. The yellow areas are the aluminum inner and outer reactor pressure vessel walls. The concave side of the inner pressure vessel wall is cooled by the coolant flow through the flux trap. This flux trap coolant flow is shown as a dotted blue region. Similarly, the coolant flow that cools the convex surface of the outer pressure vessel wall is also shown as a dotted blue region. The upper part of this region is the reactor pool, the middle part is the control blade channels, and the bottom part is the reactor tank, as indicated in these figures. The coolant region numbers in these dotted regions, 705, 702, 715, and 720, correspond to the coolant regions in Figure C.3. The coolant nodes shown in the dotted regions of Figure C.7 and Figure C.8 are the ones that are boundaries of the inner and outer vessel walls. The succession of coolant nodes shown in these two figures for the control blade channel of the RELAP5 model can be misleading. Hydraulically, pool volume 702 is connect to the first node of Pipe 715, 715(1), which is not shown, and this node is hydraulically connected to the second node of Pipe 715, 715(2), which is shown. Similarly, the sixth node of Pipe 715, 715(6), which is not shown, is hydraulically connected in between volumes 715(5) and 720, which are shown. This arrangement was created because Volumes 702 and 720 serve as upper and lower headers, respectively, for the four parallel paths 705, 715, 725, and 735.

For the HEU core, all 24 fuel plates and 25 coolant channels of the highest power element are explicitly modeled. Each fuel plate is divided into four axial nodes. The first and last node are each 7.75 inches long and the middle two nodes each are 5.0 inches long, for a total plate length of 25.5 inches. The fuel meat and its two cladding layers, one on each side, are explicitly represented in each node. Thus, in the analysis $4 \times 24 = 96$ fuel centerline temperatures are predicted as a function of time for each transient analyzed. In this model the geometry of the 0.75 inches of unfueled length at either end of the fuel plate is lumped in with the first and last nodes of the fuel plate and the power generated in the top and bottom nodes are each smeared over 7.75 inches instead of 7.00 inches. This conserves the total power generated in the fuel plate but reduces the heat flux in these two nodes to 90.3%. The middle two nodes have higher heat fluxes than do the other two. All of the power of each fuel plate is distributed among the four axial nodes of the plate.

The LEU plates were modeled in the same manner. For both fuel types the aluminum clad and the fuel meat are explicitly represented as distinct layers. For the LEU fuel, the nominal 1-mil thick zirconium interlayer between the fuel meat and 6061-Al clad is explicitly represented. The radii of the fresh HEU and LEU fuel plates used in the RELAP5 models are provided in Table C-3. Additionally, for both fuel types the oxidation layer on each surface of the burned fuel plate is explicitly represented as a distinct layer. The oxide thickness is zero mils for the fresh fuel and increases linearly with MW days with a maximum of 0.54 mils for the HEU fuel at 150 MWd and 0.93 for the LEU fuel at 180 MWd.

plate channel	Pool	Control Blade Channels				Reflector Tank	channel plate
	702	715(2)	715(3)	715(4)	715(5)	720	
	5011	5243	5253	5263	5273	5751	
25		526(1)	526(2)	526(3)	526(4)		25
24		6240	6490	6740	6990		24
24		525(1)	525(2)	525(3)	525(4)		24
23		6230	6480	6730	6980		23
23		524(1)	524(2)	524(3)	524(4)		23
22		6220	6470	6720	6970		22
22		523(1)	523(2)	523(3)	523(4)		22
21		6210	6460	6710	6960		21
21		522(1)	522(2)	522(3)	522(4)		21
20		6200	6450	6700	6950		20
20		521(1)	521(2)	521(3)	521(4)		20
19		6190	6440	6690	6940		19
19		520(1)	520(2)	520(3)	520(4)		19
18		6180	6430	6680	6930		18
18		519(1)	519(2)	519(3)	519(4)		18
17		6170	6420	6670	6920		17
17		518(1)	518(2)	518(3)	518(4)		17
16		6160	6410	6660	6910		16
16		517(1)	517(2)	517(3)	517(4)		16
15		6150	6400	6650	6900		15
15		516(1)	516(2)	516(3)	516(4)		15
14		6140	6390	6640	6890		14
14		515(1)	515(2)	515(3)	515(4)		14
13		6130	6380	6630	6880		13
13		514(1)	514(2)	514(3)	514(4)		13
12		6120	6370	6620	6870		12
12		513(1)	513(2)	513(3)	513(4)		12
11		6110	6360	6610	6860		11
11		512(1)	512(2)	512(3)	512(4)		11
10		6100	6350	6600	6850		10
10		511(1)	511(2)	511(3)	511(4)		10
9		6090	6340	6590	6840		9
9		510(1)	510(2)	510(3)	510(4)		9
8		6080	6330	6580	6830		8
8		509(1)	509(2)	509(3)	509(4)		8
7		6070	6320	6570	6820		7
7		508(1)	508(2)	508(3)	508(4)		7
6		6060	6310	6560	6810		6
6		507(1)	507(2)	507(3)	507(4)		6
5		6050	6300	6550	6800		5
5		506(1)	506(2)	506(3)	506(4)		5
4		6040	6290	6540	6790		4
4		505(1)	505(2)	505(3)	505(4)		4
3		6030	6280	6530	6780		3
3		504(1)	504(2)	504(3)	504(4)		3
2		6020	6270	6520	6770		2
2		503(1)	503(2)	503(3)	503(4)		2
1		6010	6260	6510	6760		1
1		502(1)	502(2)	502(3)	502(4)		1
	5010	5020	5030	5040	5050	5750	
	705(1)	705(2)	705(3)	705(4)	705(5)	705(6)	
		Flux Trap					

FIGURE C.7
HEU REACTOR CORE ELEMENT NODAL STRUCTURE

plate	channel	Pool	Control Blade Channels				Reflector Tank	channel	plate
		702	715(2)	715(3)	715(4)	715(5)			
		5011	5243	5253	5263	5273			
24			525(1)	525(2)	525(3)	525(4)		24	
23			6230	6480	6730	6980		23	
22			524(1)	524(2)	524(3)	524(4)		22	
21			6220	6470	6720	6970		21	
20			523(1)	523(2)	523(3)	523(4)		20	
19			6210	6460	6710	6960		19	
18			522(1)	522(2)	522(3)	522(4)		18	
17			6200	6450	6700	6950		17	
16			521(1)	521(2)	521(3)	521(4)		16	
15			6190	6440	6690	6940		15	
14			520(1)	520(2)	520(3)	520(4)		14	
13			6180	6430	6680	6930		13	
12			519(1)	519(2)	519(3)	519(4)		12	
11			6170	6420	6670	6920		11	
10			518(1)	518(2)	518(3)	518(4)		10	
9			6160	6410	6660	6910		9	
8			517(1)	517(2)	517(3)	517(4)		8	
7			6150	6400	6650	6900		7	
6			516(1)	516(2)	516(3)	516(4)		6	
5			6140	6390	6640	6890		5	
4			515(1)	515(2)	515(3)	515(4)		4	
3			6130	6380	6630	6880		3	
2			514(1)	514(2)	514(3)	514(4)		2	
1			6120	6370	6620	6870		1	
			513(1)	513(2)	513(3)	513(4)			
			6110	6360	6610	6860			
			512(1)	512(2)	512(3)	512(4)			
			6100	6350	6600	6850			
			511(1)	511(2)	511(3)	511(4)			
			6090	6340	6590	6840			
			510(1)	510(2)	510(3)	510(4)			
			6080	6330	6580	6830			
			509(1)	509(2)	509(3)	509(4)			
			6070	6320	6570	6820			
			508(1)	508(2)	508(3)	508(4)			
			6060	6310	6560	6810			
			507(1)	507(2)	507(3)	507(4)			
			6050	6300	6550	6800			
			506(1)	506(2)	506(3)	506(4)			
			6040	6290	6540	6790			
			505(1)	505(2)	505(3)	505(4)			
			6030	6280	6530	6780			
			504(1)	504(2)	504(3)	504(4)			
			6020	6270	6520	6770			
			503(1)	503(2)	503(3)	503(4)			
			6010	6260	6510	6760			
			502(1)	502(2)	502(3)	502(4)			
		5010	5020	5030	5040	5050	5750		
		705(1)	705(2)	705(3)	705(4)	705(5)	705(6)		
		Flux Trap							

FIGURE C.8
LEU REACTOR CORE ELEMENT NODAL STRUCTURE

TABLE C-3
INNER AND OUTER RADII OF FRESH FUEL PLATES, INCHES

Plate	HEU		LEU	
	Inner	Outer	Inner	Outer
1	2.7700	2.8200	2.7555	2.7995
2	2.9000	2.9500	2.8925	2.9365
3	3.0300	3.0800	3.0295	3.0735
4	3.1600	3.2100	3.1665	3.2105
5	3.2900	3.3400	3.3035	3.3475
6	3.4200	3.4700	3.4395	3.4835
7	3.5500	3.6000	3.5755	3.6195
8	3.6800	3.7300	3.7115	3.7555
9	3.8100	3.8600	3.8475	3.8915
10	3.9400	3.9900	3.9835	4.0275
11	4.0700	4.1200	4.1195	4.1635
12	4.2000	4.2500	4.2555	4.2995
13	4.3300	4.3800	4.3915	4.4355
14	4.4600	4.5100	4.5275	4.5715
15	4.5900	4.6400	4.6635	4.7075
16	4.7200	4.7700	4.7995	4.8435
17	4.8500	4.9000	4.9355	4.9795
18	4.9800	5.0300	5.0715	5.1155
19	5.1100	5.1600	5.2075	5.2515
20	5.2400	5.2900	5.3445	5.3885
21	5.3700	5.4200	5.4815	5.5255
22	5.5000	5.5500	5.6185	5.6625
23	5.6300	5.6800	5.7555	5.8045
24	5.7600	5.8100		

The arc length of the fuel meat is the 45° arc length at the centerline radius of the fuel meat reduced by 0.492 inches. This reduction provides room for two 0.150-inch thick side plates and 0.040 inches between the side plates of adjacent elements. Where the fuel plate is inserted into each grooved side plate there is an unfueled region between the edge of the side plate and the edge of the fuel meat, which is nominally 0.070 inches. For practical assembly tolerances, the current HEU

aluminide fuel elements require that the fuel plate arc length be slightly smaller than the arc length between the bottom of the groove of one side plate and the bottom of the groove of the corresponding opposite side plate. Therefore, for both fuel types the nominal fuel plate arc length is reduced by an additional 0.012 inches, and this is taken as a reduction in the fuel-meat portion of the plate. (This can be thought of as a 0.006-inch gap between the edge of the fuel plate and the bottom of the groove for each side plate.) Combining these dimensions yields $2 \times 0.150 + 0.040 + 2 \times 0.070 + 0.012 = 0.492$ inches.

For the RELAP5 input, the heat transfer area at each surface of each fuel node is calculated as $2 \times \pi \times r \times L \times F$, where, r is the radius at the surface (water-oxide or water-aluminum interface), L is the node length (7.75 or 5.00 inches), and F is the ratio of the plate arc length to the 360° arc length. F is taken to be the ratio $(\pi/4 \times r_{\text{avg}} - 0.492 \text{ inches}) / (2\pi \times r_{\text{avg}})$, where r_{avg} is the average of the plate inner and outer radii. Technically, r should be used in place of r_{avg} in the calculation of F . However, the difference in the resultant heat transfer area is virtually insignificant. Having only one value of F for both surfaces of each plate, regardless of oxide thickness, reduces the opportunity for input error. In the RELAP5 input for the fuel node heat transfer areas, values of $L \times F$ were provided.

Steady-state fuel centerline temperatures obtained with the RELAP5 model for end-of-life (EOL) LEU Core 7A fuel element 8 were compared with those obtained with the PLTEMP/ANL code (Ref. C-8). A beta version of PLTEMP/ANL v 4.2 of October 30, 2013 (SVN revision 65) which includes speedup improvements, extended Groeneveld 2006 CHF table, channel-dependent hot channel factors, and an improved double search algorithm was used in the analysis. In the PLTEMP/ANL analysis the 24-inch length of the fuel meat was represented as 24 1-inch long axial nodes. This enabled a much finer distribution of axial power generation in each fuel plate than in the RELAP5 simulation. In the comparison, the reactor power was 12 MW and the primary inlet coolant temperature and flow rates were 125 °F (51.7 °C) and 3,700 gpm (14,006 l/m), respectively.

Among the four axial nodes in the RELAP5 model, node 3 (where node 1 is at the top of the core) produces the highest fuel centerline temperature in each of the 23 fuel plates in the fuel element. This can be observed in Figure 5.17 of Ref. C-5 where the RELAP5 plate-to-plate centerline temperature distribution for the LEU case under consideration is plotted for each axial node. Node 3 in the RELAP5 model covers the axial range from 12 to 17 inches from the top of the fuel meat, which corresponds exactly to nodes 13 through 17 in the PLTEMP/ANL model. The middle of node 3 in the RELAP5 model corresponds to the middle of node 15 in the PLTEMP/ANL model.

Figure C.9 compares the temperatures at this elevation for all 23 fuel plates of element 8 for LEU Core 7A. The same power, flow, and inlet coolant temperature assumptions were made in both calculations. Both calculations include the azimuthal peaking factors. The RELAP5 code input model is based on the input model used in the MURR steady-state thermal-hydraulic analysis technical basis document (Ref. C-9), but was adapted to the conditions and assumptions used in the RELAP5 analysis. RELAP5 provides the temperature at the centerline of the fuel meat. PLTEMP/ANL provides the maximum fuel temperature regardless of where its exact location is relative to the centerline. This difference should have only a very minor effect on the temperature comparison in this work. The largest difference between node 3 of the RELAP5 solution and node

15 of the PLTEMP/ANL solutions is 2.89 °F (1.61 °C) and occurs in plate 6. In all instances, the PLTEMP/ANL temperature is greater than the RELAP5 temperature.

The bars shown in Figure C.9 show the range of temperatures from minimum to maximum among the five PLTEMP/ANL nodes that correspond to node 3 in the RELAP5 model. The maximum PLTEMP/ANL temperature in the figure, 294.82 °F (146.01 °C), occurs in plate 22 at node 17, which is the lowest of the five axial nodes in PLTEMP/ANL that correspond to node 3 in the RELAP5 model. The RELAP5 temperature for node 3 of plate 22 is 290.23 °F (143.46 °C). Thus, the PLTEMP/ANL and RELAP5 maximum/centerline temperature predictions are in close accord and the adverse effect on temperature of combining five 1-inch axial nodes in the PLTEMP/ANL model to form one 5-inch node in the RELAP5 model is extremely small, i.e., a few degrees Fahrenheit.

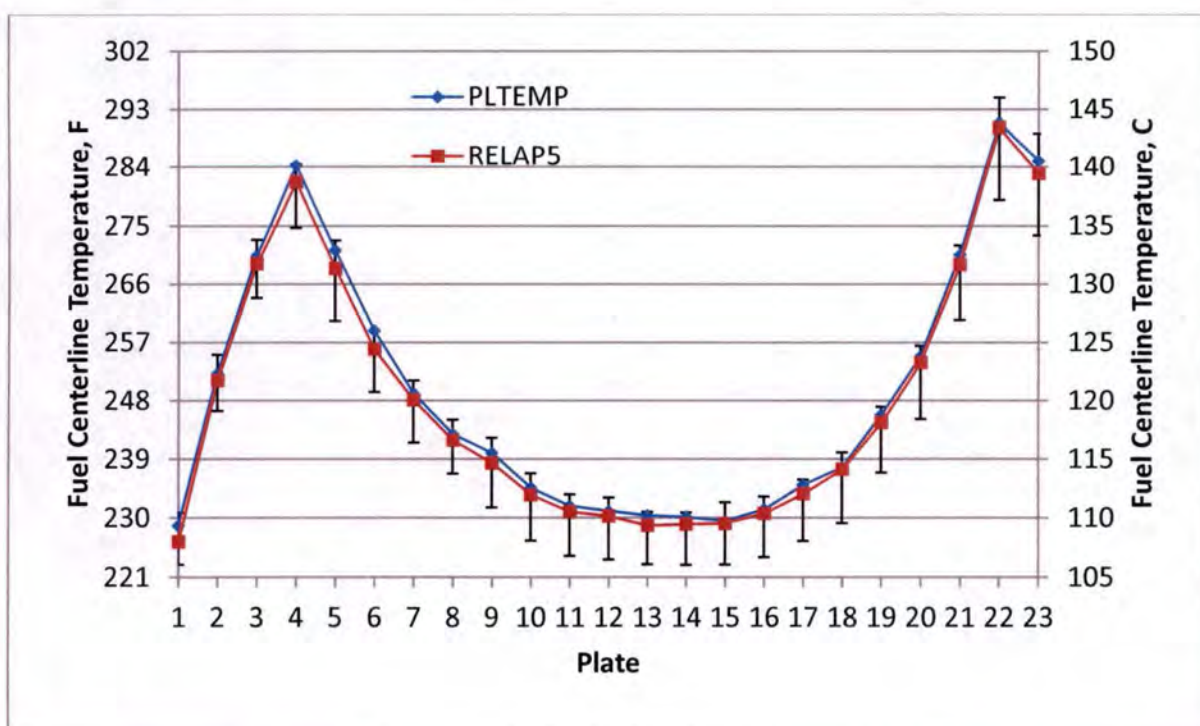


FIGURE C.9
COMPARISON OF RELAP5 AND PLTEMP/ANL MAXIMUM FUEL TEMPERATURES

The post-scrum power history was recalculated with the PARET/ANL code (Ref. C-10). This was done for two reasons. First, separate analyses were performed for the HEU Core 3A and LEU Core 7A to account for the effect of the different fuel types on the post-scrum power vs. time. The second reason was to account for the effect of photoneutrons coming from the interaction of fission-product gammas with the beryllium reflector. The operating history prior to scrum in the PARET/ANL model was assumed to be 120 days at full power. The reactor power with time after scrum with the increased delayed neutron fraction from the photoneutrons was compared with the power with time after scrum without photoneutrons. As a result of that comparison, the relative power after scrum calculated by PARET/ANL was conservatively increased by 2% to account for

the effect of photoneutrons, plus a small calculational uncertainty. With the 1.02 multiplier, the post-scrum power vs. time was not allowed to exceed the steady-state reactor power. The values of relative power as a function of time for these new analyses are listed in Table C-4, where time = 0.0 s corresponds to when the control blades start to move.

TABLE C-4
RELATIVE POWER POST SCRAM

HEU		LEU	
Time, s	Power	Time, s	Power
0.0000	1.0000	0.0000	1.0000
0.0023	1.0000	0.0020	1.0000
0.0053	0.9735	0.0052	0.9715
0.0113	0.8596	0.0117	0.8470
0.0203	0.6986	0.0214	0.6868
0.0292	0.5858	0.0311	0.5869
0.0501	0.4295	0.0505	0.4632
0.1010	0.2783	0.1023	0.2938
0.2000	0.1643	0.1998	0.1796
0.3023	0.1235	0.3007	0.1338
0.4017	0.1071	0.4017	0.1149
0.5010	0.1008	0.5027	0.1079
0.6004	0.0985	0.7015	0.1039
0.6998	0.0972	1.0144	0.0997
0.7992	0.0959	1.9923	0.0902
1.0161	0.0934	3.0029	0.0833
2.0102	0.0847	4.9915	0.0741
3.0043	0.0787	6.0022	0.0706
4.0286	0.0740	7.0128	0.0678
5.0228	0.0703	8.0235	0.0653
6.0171	0.0673	9.0017	0.0633
7.0113	0.0647	10.0120	0.0614
8.0056	0.0625	20.0230	0.0506
9.0301	0.0606	30.0010	0.0451
10.0240	0.0590	40.0120	0.0414
20.0280	0.0491	50.0230	0.0387
30.0030	0.0440	60.0020	0.0366
40.0070	0.0406	70.0130	0.0349
50.0120	0.0381	80.0250	0.0335
60.0180	0.0361	90.0040	0.0324
70.0230	0.0345	100.0200	0.0314
80.0280	0.0333	200.0100	0.0263
90.0040	0.0322	300.0000	0.0240
100.0100	0.0313	399.9900	0.0226
200.0100	0.0263	499.9900	0.0215
300.0100	0.0240	599.9900	0.0206
400.0100	0.0226	700.0100	0.0199
500.0100	0.0215	800.0100	0.0192
600.0200	0.0206	900.0100	0.0186
700.0200	0.0199	1000.0500	0.0181
800.0000	0.0192	1300.0500	0.0168
1000.0500	0.0181	1700.1500	0.0155
		2000.0500	0.0148
		2300.0500	0.0141
		2500.0500	0.0137

C.2.2.8 Plant Protection System

The choice of an HEU or LEU core does not affect the configuration of the plant protection system. A systematic review of the MURR plant protection system as it affects the RELAP5 models under consideration was performed. The current trip values for pressure and pressure drop will change with an LEU core. The six trips of concern for operation with the current HEU core are as follows:

- Trip 1 – core outlet pressure (PT-944A & PT-944B) ≤ 26.0 psig
- Trips 2 and 3 – primary flow (FT-912A&E, FT-912G&H) \leq limiting safety system setting (LSSS) flow, which is 3,200 gpm of water at 155 °F. (The actual plant trips are set conservatively slightly higher than the LSSS conditions.)
- Trip 4 – pressure at the junction of the two primary heat exchanger loops (PT-943) ≤ 57.5 psig
- Trip 5 – pressure drop between valves V507B and V507A (DPS-929) ≤ 24.8 psia
- Trip 7 – core outlet isolation valve V507A starts to close
- Trip 8 – core inlet isolation valve V507B starts to close

The same six trips are to be used for the LEU core, but some of the trip values would need to be adjusted. The LSSS flow for the LEU core is 3,300 gpm of water at 145 °F.

The trip numbers are how they are labeled in the RELAP5 model and the instrument numbers correspond to how they are labeled in the MURR facility. The first four trips are indicated in blue near the bottom of Figure C.1. More specific details, including delay times, are provided for these six trips in Figure C.10 through Figure C.15, respectively. A concerted effort was undertaken to obtain accurate upper limits for delay times. In these six figures the value to the left of the “|” symbol is the additional delay time prior to taking the action to the right of the “|”. For example, in Trip 1 when the core pressure drop drops to 26.0 psig, there is a 0.8 s delay to de-energize relays 2K13 and 2K28. There is a 0.0 s delay after the opening of these relays, before a scram signal is sent. Then after a 0.075 s delay the control blades start to drop. All of the actions listed in the six trips are the start of the action. Isolation valves V507A and V507B, for example, require a few seconds before they start closing and take a few additional seconds to go from fully open to fully closed. All of the trip values shown in Figure C.10 through Figure C.13 are the values for the MURR facility, but not necessarily for the RELAP5 models.

Trip 6 is based on the liquid level in the pressurizer, which is not included in the above list because the liquid level in the pressurizer is not part of the RELAP5 model. This trip closes valve V527C, labeled V527 in Figure C.1, which isolates the pressurizer from the main coolant line. This valve is also closed by either of the primary coolant isolation valves (V507A and V507B) starting to close (Trips 7 and 8). In RELAP5 model the timing of the closing of the V527C valve is important because the pressurizer is treated as a constant pressure source rather than a volume that loses pressure as the transient progresses. Thus, if this valve is not closed in a timely manner, inappropriately higher pressures can be predicted for the core, which, in turn, affect the temperatures predicted in the core. The decreasing pressurizer level and pressure are not modeled. Thus, Trip 1 closes valves V507A and V507B, which, in turn, closes valve V527C via Trip 7 or

Trip 8. The effect on the peak fuel temperature for the most severe accident, the double-ended pipe break at the inlet isolation valve, should be insignificant because in this accident the peak fuel temperature is reached within 2 s.

The plant protection system provides protection for the plant when site electric power is lost. When the RELAP5 model of the MURR facility was developed, Trip 99, as shown in Figure C.16, was incorporated into it. The particular trip number, 99, was created for modeling convenience and has no relationship to any trip in the MURR facility.

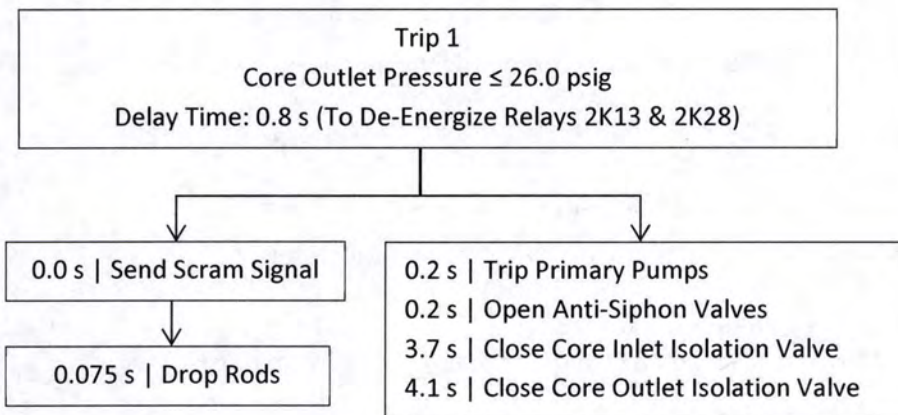


FIGURE C.10
TRIP 1: CORE OUTLET PRESSURE

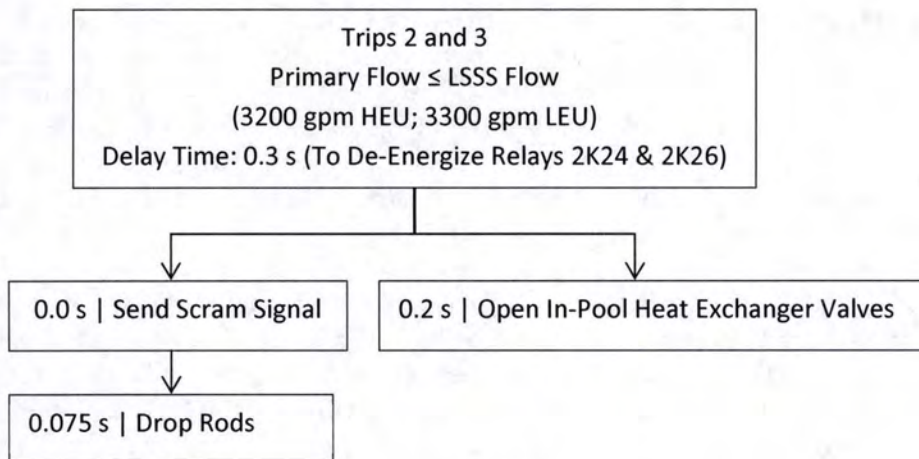


FIGURE C.11
TRIPS 2 AND 3: PRIMARY FLOW

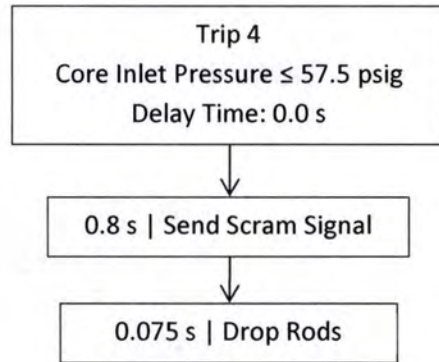
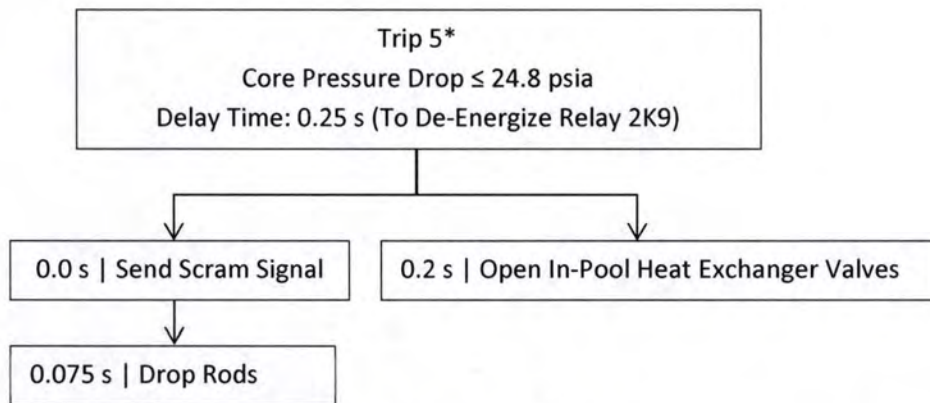


FIGURE C.12
TRIP 4: CORE INLET PRESSURE



*In the RELAP5 model this trip is not active during the hot-leg LOCA.

FIGURE C.13
TRIP 5: CORE PRESSURE DROP

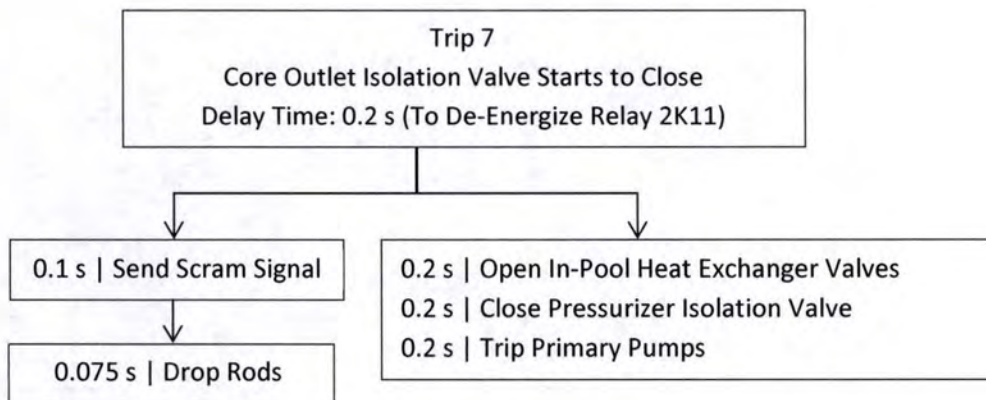


FIGURE C.14
TRIP 7: CORE OUTLET ISOLATION VALVE STARTS TO CLOSE

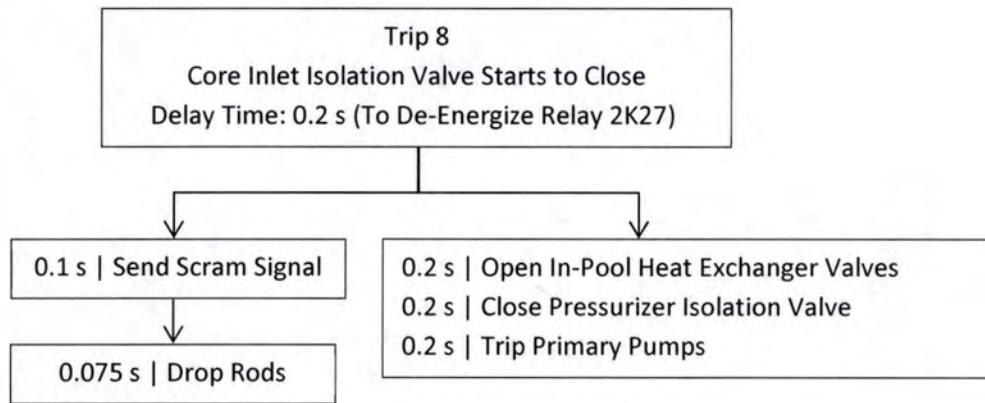


FIGURE C.15
TRIP 8: CORE INLET ISOLATION VALVE STARTS TO CLOSE

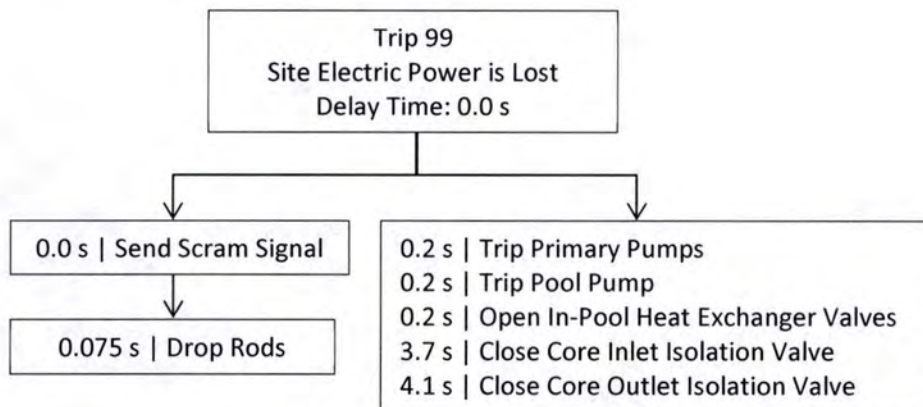


FIGURE C.16
TRIP 99: SITE ELECTRIC POWER IS LOST

TABLE C-5
PLANT PROTECTION SYSTEM SETPOINTS

Trip Number	Measured Item	RELAP5 Model Variable	MURR Facility Set point	RELAP5 Trip Values
1	Core outlet pressure, psia	p-102070000	40.3 psia (26.0 psig)	40.3 psia
2 & 3 (HEU)	Primary flow, lbm/s	mflowj-116000000	3,200 gpm (436 lbm/s)	380 lbm/s
2 & 3 (LEU)	Primary flow, lbm/s	mflowj-116000000	3,300 gpm (451 lbm/s)	400 lbm/s
4	Core inlet pressure	p-132010000	71.8 psia (57.5 psig)	60 psia
5	Core pressure drop	cntrlvar-20	24.8 psi	12 psi

The most effective way to limit the peak fuel temperature is to minimize the time it takes from the start of the event until the control blades start to drop. The trip sequence that moves the control blades the quickest during a cold-leg LOCA is Trip 5. The combination of 0.25 s to de-energize the relay, 0.0 s to send the signal to drop the blades, and 0.075 s before the blades start to move, implies that the plant protection system internal built-in scram delay is 0.325 s. Since the pressure drop across the core drops to the trip point within a few ten-thousands of a second after the cold-leg pipe ruptures, this trip is the one that causes the scram. In the hot-leg LOCA, the break at the outlet should temporarily increase the pressure drop across the core and thereby delay the activation of Trip 5. However, because of what may be an artifact of the simulation, there may be a temporary dip or oscillation in pressure drop across the core that causes the core pressure drop to reach the trip setting. Therefore, the trip logic in the model is constructed so that whenever there is a pipe break upstream of valve V507A, Trip 5 is rendered inactive.

In the current RELAP5 models for the HEU and LEU cores, all of the trips on the above bullet list are explicitly represented in the model. The quicker response time of Trip 5 compared to Trips 1 and 4 is due the vintage of the electronic components used in Trips 1 and 4.

The fourth column of Table C-5 summarizes the MURR facility set points for the four trips in Figure C.10 through Figure C.13. The third column provides the corresponding variable name in the RELAP5 models. "p-102070000" is the pressure at the 7th node of pipe 102 of Figure C.2. "mflowj-116000000" is the junction flow rate at V540 in Figure C.1. "p-132010000" is the pressure at branch 132 of Figure C.2. "cntrlvar-20" is "p-135010000" - "p-102070000", where "p-135010000" is the first node of pipe 135 of Figure C.2. The locations of all of these trip variables are shown in light blue in Figure C.1.

The last column in the table shows the values in the RELAP5 models, which were used for both HEU and LEU cores. Three considerations were taken into account in establishing the values. The first is that in the LEU core the pressures and pressure drops may be different than in the HEU core due to differences in hydraulic resistant between the two core. Thus, different trip values need to be established for the LEU core after the conversion to LEU has been completed. The second consideration is that since in the model one element is being scaled up to represent all eight, the MURR facility set points may not apply to the model if core channel reduction due to burnup is included in the modeling. In the LEU EOL case with no reduction in channel gap thickness, for example, the appropriate initial value for the total RELAP5 model flow rate is 3,300 gpm (451 lbm/s), but when maximum channel gap thickness due to burnup of 8 mils is assumed the corresponding flow rate is 3,080 gpm (421 lbm/s). The third consideration is that the initial flow rate in the plant is to be the LSSS value, which coincides with the trip value. Starting the transient with the flow trip set could be problematic.

A simple defensible approach to specifying trip values for the RELAP5 model is to set most of them artificially low. This may seem to be needless conservative, but in practice it is only very slightly conservative because in the simulations of the most limiting transient, the double-ended cold-leg LOCA, the trip pressures and pressure drops decrease extremely rapidly. Even with the Trip 5 pressure drop set point at 12 psi, the scram is reached at 0.3255 s, which is only 0.0005 s longer than the 0.325 s delay time. Therefore, the values in the last column of Table B-2 were used

in all of the HEU and LEU RELAP5 cases. These trip values guaranteed that each is always considerably less than its corresponding initial state-state RELAP5 model predicted value.

Trip 1 is the only trip that was set at the MURR facility set point rather than at an artificially low value. This trip has a 0.875-s delay before the rods start to drop, which is much longer than the 0.325-s delay of Trip 5, which is active in the modeling of all accidents except for the hot-leg LOCA. Trip 1 is the only trip in the model that activates the anti-siphon system. The precise timing of this activation was not expected to have a significant impact on the peak fuel temperature results. However, as the results for the most severe LOCA show, the pulse of air from the anti-siphon system provides a sudden jolt of upward core flow that cools the limiting fuel plate and limits the peak fuel temperature. For the LEU simulation that produced the smallest margin to fuel failure, at the limiting location the peak fuel temperature is 300.6 °C 0.01 s before the peak of 301.1 °C is reached. At the outset of the transient, the Trip 1 pressure decreases 34 psi during the first 0.01 s. Thus, even if a lower Trip 1 set point increases the Trip 1 time by 0.01 s, which is an excessively large increase, the predicted temperature would increase less than 0.6 °C.

C.2.2.9 Reactor Inlet Check Valve, V502

Figure C.17 shows a cross-sectional view of check valve V502 oriented as it is in the MURR facility. A spare flapper disc and swing arm were weighed and found to be 55 pounds together. From the figure it is estimated that 1) the flapper disc is at a 5° angle to the horizontal when fully closed and is at 55° relative to the horizontal when fully open, 2) the pivot is 10.2 inches from the center axis of the 12-inch diameter hole through the valve, and 3) the disc diameter is 15.1 inches. The moment of inertia of the disc about its diameter is $mD^2/16$, where m is the mass of the disc and D is the diameter of the disc. The parallel axis theorem indicates that the moment of inertia about the pivot, I , which is X away from the centroid should be $I = mD^2/16 + mX^2$. If $m = 55$ lbm, $D = 15.1$ inches, and $X = 10.2$ inches, then $I = 45.2$ lbm-ft². In the RELAP5 model, the moment length of the flapper was taken to be 10.2 inches (0.85 feet) and the disk radius was taken to be the inside radius of a 12-inch Schedule 40 pipe, 0.4974 feet.

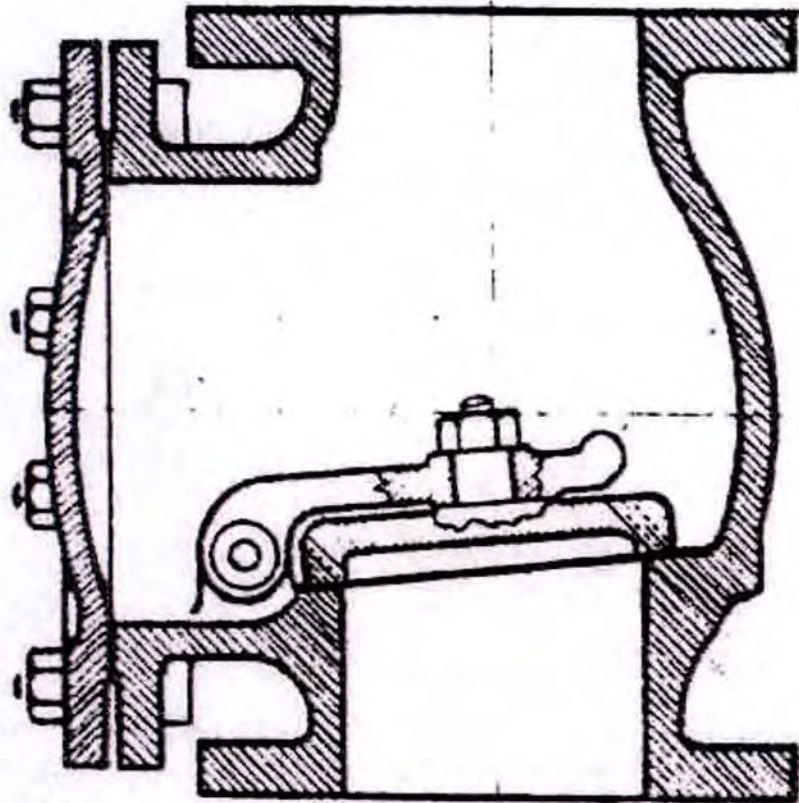


FIGURE C.17
CORE INLET CHECK VALVE V502

C.2.2.10 Core Flow Redistribution Due to Burnup

Burnup can cause 1) oxide to form on the fuel plate surfaces and 2) the fuel meat to swell, resulting in fuel plate swelling. If the oxide growth and fuel plate swelling cause coolant channels to become thinner, coolant flow in the affected coolant channels will be reduced. In a core with elements of differing burnups, if coolant channels are restricted due to burnup, flow will be redistributed from the more burned elements to the less burned ones. Table C-6 provides the element burnups and assumed potential channel reduction at maximum burnup for both the HEU and the LEU core. As the table shows, all channel thicknesses are linearly reduced with element burnup with a maximum internal channel reduction of 10 mils at 150 MWd for the HEU core and 8 mils at 180 MWd for the LEU core. The channel reduction of the end channels were assumed to be half those of the internal channels. Thus, an LEU internal channel in an element with 170 MWd of burnup would be reduced by $170/180 \times 8.00$ mils = 7.56 mils and an end channel in the same element would be reduced by half of this amount. However, these channel reductions are extremes that are based on administrative controls and may not be achieved. Little, if any, channel reduction due to burnup is expected for the HEU core. For the final results, the LEU analysis was performed twice: once with the maximum prescribed channel reductions and once with no channel reduction due to burnup. For the LEU analysis of each transient, the temperature margin to fuel failure is based on the more limiting of each pair of results.

TABLE C-6
ELEMENT BURNUP AND CHANNEL REDUCTION

	HEU	LEU
Burnup, MWd		
Elements 1 & 5	0	0
Elements 2 & 5	81	96
Elements 3 & 7	65	77
Elements 4 & 8	142	170
At End of Life		
Burnup, MWd	150	180
Channel Reduction, mils		
Internal	10	8
End	5	4

All of the final LOCA/LOFA results for the HEU core, which are provided in Table B-5.3 of Ref. C-5 for the LOCAs and in Table B-6.1 of Ref. C-5 for the LOFAs, are based on no channel reduction due to burnup. The HEU results obtained in this manner indicate that for each of the seven transients considered, the limiting element, which is the one with the highest peak fuel temperature, is always a beginning-of-life (BOL) one. In general, flow redistribution reduces the peak fuel temperatures of the BOL element and increases those of the EOL elements. Because, as provided in Table B-5.3 of Ref. C-5, for the most severe transient, the double-ended cold-leg LOCA, the peak HEU fuel temperature is only 294 °F (145 °C) for the EOL element versus 510 °F (266 °C) for the BOL element, it is unlikely that an analysis with flow redistribution would cause the EOL element to yield a peak temperature greater than 510 °F. Moreover, the focus of the analysis in this report is the LEU core.

A way to visualize the channel reduction due to burnup in an element is to assume that the centerline arc of each fuel plate remains at a fixed radius while the concave radius of the plate gets shorter and the convex one gets longer by the same amount. Given the dimensions of each coolant channel of each fuel element in a core, it is a simple matter to determine the total flow area of each element and its total wetted perimeter. The hydraulic diameter of the element was taken to be four times the total flow area divided by the sum of the wetted perimeters of all of the individual channels.

Since the elements appear in burnup pairs with each element of the pair at about the same power, each pair was assumed to form a single parallel hydraulic path. Although coolant temperature has at most a second order effect on the flow distribution among the paths, the average coolant temperature of each path was determined as the average of the inlet and outlet temperatures for the path. The power produced by each path was included in the model so that these average temperatures could be determined. This was accomplished by assuming that the power produced

by the path is $\dot{m} C_P \Delta T$, where \dot{m} is the path flow rate, C_P is the specific heat capacitance, and ΔT is the coolant temperature rise.

The hydraulic network has one unknown flow rate for each of the four parallel paths. In addition, the pressure drop that is common across all four flow paths from the inlet to the outlet of the network is also unknown. There are four pressure-drop-versus-flow relationships - one for each path. A fifth equation is obtained by recognizing that the sum of the four path flow rates is equal to the known total flow rate.

The pressure drop across each path, ΔP , is assumed to be a result of wall friction and is represented as:

$$\Delta P = f_i L/D_i \rho_i V_i^2/2. \quad (C-1)$$

Here, f_i is the path Moody friction factor as obtained from the transcendental Colebrook equation, L is the 25.5-inch length of the fuel plates, ρ_i is the path coolant density, and V_i is the path coolant velocity. The Colebrook equation also needs a value of plate absolute roughness, which was taken to be 63 microinches. It also needs the Reynolds number, which is $\rho_i V_i D_i / \mu_i$, where μ_i is the coolant viscosity. The flow rate of each path was needed to determine the average temperature rise of each path. The average temperature of each path was used to determine the coolant specific heat capacity, viscosity, and density for the path. These properties were approximated by polynomial curve fits. All of the required functional relationships were represented in a spreadsheet where a simultaneous solution to the entire set of equations was obtained. Subsequently, when computer automation was added to prepare the RELAP5 input files, execute them, and post-process their results, the spreadsheet representation was replaced by programming implemented via the Python scripting language.

In the above pressure drop relationship, the form-, or K-losses, are ignored. As explained in Chapter 13 of Ref. C-9, these losses are very small compared to the wall friction ones and have a very minor effect on flow distribution among the channels of a particular element. Similarly, they should have a very small effect on the distribution among the eight elements of the core.

For the RELAP5 model the flow rate of the MURR element of interest was multiplied by a factor of 8. In effect there were eight copies of the element of interest in the RELAP5 model. Therefore, the total core flow rate in the RELAP5 model may not match the total core flow rate in the reactor. However, this is not a problem because the thermal-hydraulic conditions in the model element during the first few seconds of the transient, which is when the peak fuel temperature occurs in most transients, including the most limiting one, are correct.

C.2.2.11 Mode III (Natural Convective) Operation

Mode III is operation at a maximum power level of 50 kW with the reactor vessel head removed. The only time that the MURR has operated in Mode III was during initial fuel criticality and physics testing for the two different HEU fuel element designs that have been used in the reactor. Similar testing is expected following conversion to LEU fuel. A 12-inch diameter flange is removed to provide an opening above the top of the inverted loop in the reactor outlet leg. Cooling of the core is accomplished by natural circulation with pool water entering the opening in the outlet

leg, traveling backwards down the outlet leg, up through the core, and back to the pool through the open top of the reactor vessel.

The existing RELAP5 model of the MURR facility was adapted to do a plate-by-plate and channel-by-channel Mode III analysis. As shown in Figure C.18, the plant model of Figure C.2 was greatly reduced to include only the reactor vessel, the core, and some of the reactor vessel outlet piping. It should be noted that, although not shown in Figure C.18, the 7.02-inch diameter flow orifice shown in Figure C.6 is included in the model. The pool model and the heat transfer through the vessel wall and through the outlet piping to the pool were eliminated. Because during Mode III operation water enters at the top of the end pipe, a pressure and temperature boundary condition was added there. Similarly, another pressure boundary condition was added at the top of the reactor vessel where the reactor vessel cover was removed.

The distance from the top of the end pipe to the bottom of the outlet pipe is represented in the model as 15.167 feet. In Figure C.1, the end pipe is shown in black as a vertical pipe in the model and, based on differences in elevation, is 2.333 feet long. This is also the single volume 407, which is shown as "407(1)" in Figure C.18. As indicated in both Figure C.2 and in Figure C.18, this is followed by model branch 406, which is 2.000 feet long. Branch 101, which is 1.000 feet long and is shown in the figure as a 0.500-foot red segment and a 0.500-foot black segment, is next. This branch connects to the two vertical parts of pipe 100, which together is 9.834 feet long. The sum of 2.333, 2.000, 1.000, and 9.834 is 15.167 feet. The reactor vessel is 10.833 feet long. This length is the sum of the lower plenum, the core, and outlet plenum lengths, which are 2.271, 2.125, and 6.437 feet long, respectively. Note that in Figure C.18, the elevation change of the upper plenum is its full 6.437 length, rather than the 0.500 foot shorter elevation change from the bottom of the plenum to branch 139 of Figure C.2. In Figure C.18 D1 is the water depth at the top of the open vessel and D2 is the water depth at the top of the end pipe. Thus, $D1 - D2$, the elevation increase from the top of the vessel to the top of the end pipe is $15.167 - 10.833 = 4.334$ feet.

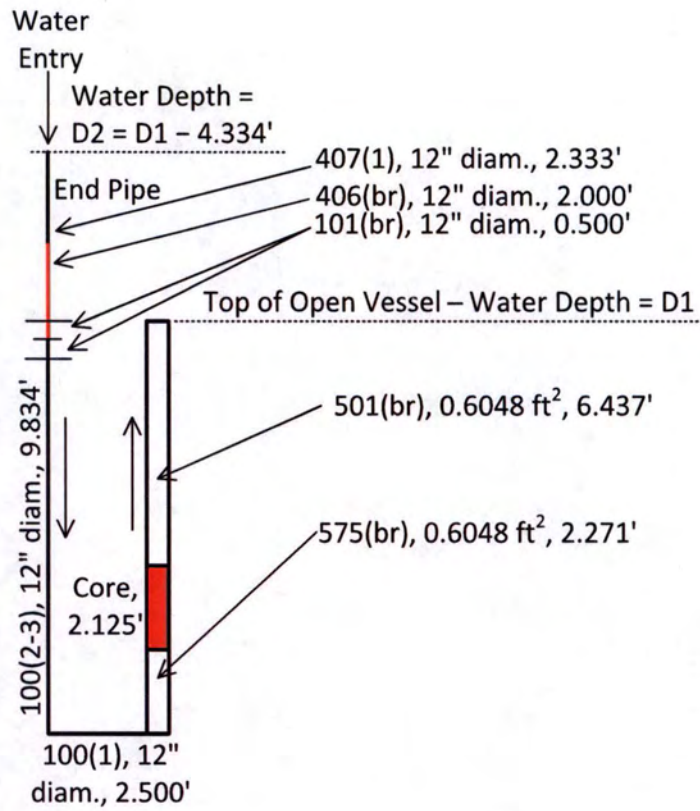


FIGURE C.18
RELAP5 MODEL FOR MODE III ANALYSIS